FACULTY OF ENGINEERING AND APPLIED SCIENCE
INSTITUTE OF SOUND AND VIBRATION RESEARCH

RAPID ACOUSTIC ASSESSMENT OF EXHAUST SYSTEMS DURING ENGINE ACCELERATION

by

Daniel Cornelius van der Walt

A Thesis submitted for the Degree
of Doctor of Philosophy

University of Southampton

September 2002

UNIVERSITY OF SOUTHAMPTON

ABSTRACT

FACULTY OF ENGINEERING AND APPLIED SCIENCE
INSTITUTE OF SOUND AND VIBRATION RESEARCH

Doctor of Philosophy

RAPID ACOUSTIC ASSESSMENT OF EXHAUST SYSTEMS
DURING ENGINE ACCELERATION

by Daniel Cornelius van der Walt

This study describes new computational and experimental procedures to evaluate the acoustic performance of exhaust systems under the practical operating conditions of a vehicle. The aim was to facilitate rapid acoustic optimisation.

An advanced experimental technique has been developed which incorporates order analysis methods to acquire precise estimates of the forward and backward travelling complex wave amplitudes at appropriate positions along the exhaust system from the variable harmonic pressure data. However, capturing such data at regular engine speed intervals requires reliable in-duct pressure records. The contamination of the acoustic pressure field by flow-induced noise make this a formidable challenge. Effective procedures are described to yield precise and reliable estimates of the acoustic performance of an exhaust system. The advantages of the new transient approach (compared to existing procedures, based on constant engine speed conditions) in producing a comprehensive set of rapid results to assess the acoustic properties of a silencer component were demonstrated.

Corresponding predictions were calculated by adapting existing validated linear acoustic code (APEX) to follow the changing flow conditions during normal engine operation. The new prediction code was applied to the design procedure of an exhaust system, illustrating the potential advantage of facilitating the rapid optimisation of the acoustic performance as opposed to a procedure based on tail-pipe orifice noise emission.

ACKNOWLEDGMENTS

I would like to acknowledge the advice of my supervisors, Prof. P. A. Nelson and Prof. P.O.A.L. Davies. I am grateful for their support during the completion of this thesis. In particular, I should like to thank Prof. P.O.A.L. Davies for his inspiration and encouragement throughout the project. His guidance during the preparation of the thesis is sincerely appreciated. Without his continued communication and feedback, this work would not have been possible because the author was an external student living in South Africa.

I should also like to thank Dr P. Steenackers and Dr J. P. Janssens of BOSAL International and Dr K. R. Holland of the I.S.V.R. for their helpful ideas and informative discussions on the subject matter during my regular visits to Europe. I extend my appreciation to Dr M. Fisher of the I.S.V.R. for his advice, insight and criticism, which have helped to keep the work focused.

I should also like to thank Mr Karel Bos (1928), the Chairman of BOSAL, who gave me the opportunity to undertake the research. I appreciate the encouragement and interest of both Mr Karel Bos (1928) and his son Karel Bos (1961).

This work was conducted at the automotive research and development facility of BOSAL Africa in Pretoria. I should like to thank BOSAL for its financial support. Appreciation is due to Danie Barnard for the assistance he provided with the experimental work and Johan Makkink for preparing the prototype exhaust systems. I also want to acknowledge Toys McLeod for his inspiration during the project.

Finally, I should like to thank my wife for her enduring support and loyalty over the last four years.

INDEX

CHAPTER 1

INTRODUCTION

1.1 AIM AND OBJECTIVES

This thesis describes a new approach to the experimental and computational evaluation of the acoustic properties of an exhaust system for the practical operating conditions of a vehicle. The aim of the work was to facilitate rapid optimisation of acoustic performance by guiding appropriate modifications to the geometric detail of the system. This required the development and validation of advanced new measurement technology [1.1] that quantifies the acoustic contribution of individual silencer elements to the overall acoustic performance of an exhaust system on a running vehicle under the transient operating conditions experienced in practice. It also involved the choice and development of appropriate prediction software that can produce assessments of the relative acoustic performance of each silencer component and the overall acoustic performance of the system.

At present, tail-pipe orifice noise predictions and measurements are used, but these normally provide inadequate information to indicate the appropriate changes to individual elements under operational conditions. In addition, the current methods provide insufficient spectral information to identify flow noise sources distributed along the system. The objective of the new procedures was to overcome the limitation of current methods.

The new experimental approach [1.1] is designed to assess the acoustic performance of silencer components during engine acceleration (transient operating conditions). The new technique incorporates order analysis methods and a wave decomposition method to estimate the positively P^+ and negatively P^- travelling wave spectral components at the inlet and outlet of a silencer component or exhaust system from the measured pairs of pressure time-histories. Using the wave components $P^{\pm}$, one can calculate a comprehensive set of corresponding acoustic transfer or local characteristics that describe exhaust system acoustic performance.

Appropriate prediction software [1.1] was developed by extending validated linear acoustic code (APEX) [1.2] to describe the acoustic performance of a silencer component for the realistic speed range of an engine. The software takes into account fully the varying engine rotational frequency, temperature gradients and mass flow gradients generated under the transient operating conditions of an engine. Acoustic quantities were calculated in harmonic format (order component amplitude versus engine speed) to compare predicted results to measured results.

1.2 RATIONALE FOR THE RESEARCH

The automotive industry is placing more and more pressure on exhaust system suppliers to reduce development lead times. At the same time, increasing concerns about the environment place severe legislative constraints on drive-by and proximity targets. For these reasons, it has become essential to follow a rational design strategy for exhaust systems, based on predictive modelling, followed by experimental assessment of both the exhaust silencer components and the complete system to ensure rapid and cost-effective exhaust system development [1.2].

Currently, tail-pipe orifice noise emission is measured during controlled acceleration and deceleration of the engine on a chassis or engine dynamometer to evaluate and then refine the acoustic performance of a given exhaust system for the practical operating conditions of the engine [1.3, 1.4]. The results are generally presented in

the form of a Campbell diagram, which displays the frequency content of tail-pipe noise. Figure 1.1 below shows such a tail-pipe noise measurement, recorded for a full throttle run-up of the vehicle (fitted with a four-cylinder four-stroke engine) on a chassis dynamometer.

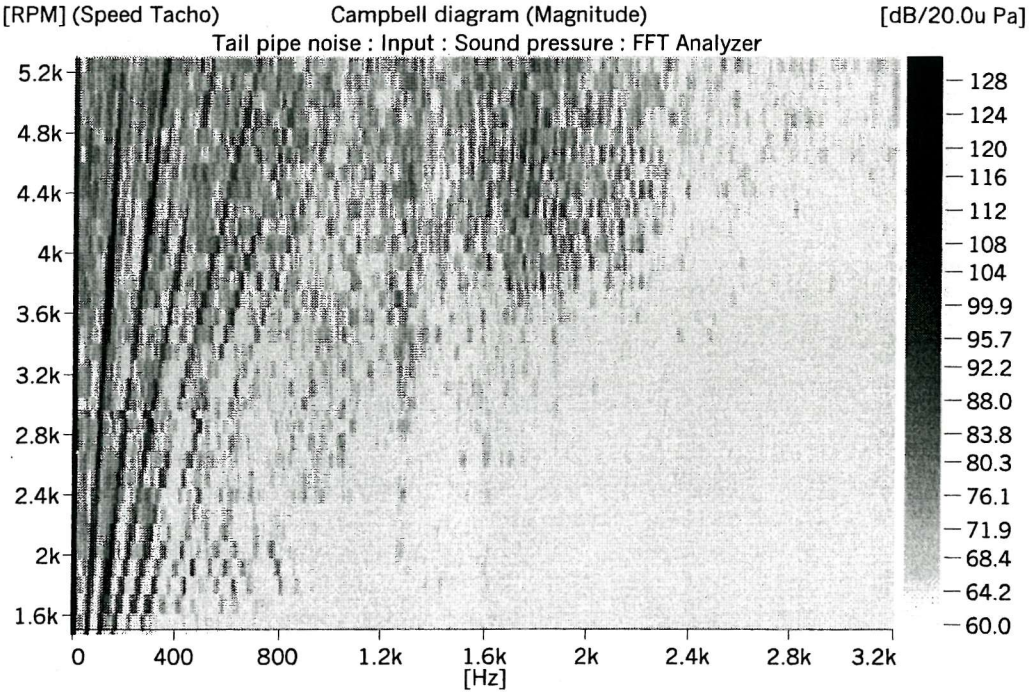

Figure 1.1 Campbell diagram of tail-pipe orifice noise emission recorded for a full throttle run-up of a vehicle (four-cylinder four-stroke engine) on a chassis dynamometer.

The radial straight lines that increase with frequency and engine speed can be identified as order noise, generated by the cyclic pulsating flow through the valves. The wave motion is periodic in nature and the exhaust noise signature consists of narrow-band components harmonically related to the firing frequency of the engine and expressed as multiples of the engine rotational speed. So, for example, for a four-cylinder four-stroke engine, the firing frequency occurs at twice the engine rotation frequency (2E). The signature also includes contributions by aerodynamic and flow noise, represented by the broad-band noise. These noises are caused by

turbulence and other flow-induced aeroacoustic sources at expansions, contractions, bends and the tail-pipe outlet [1.5].

Another important design consideration is that an exhaust system is assembled from a number of elements, including chambers and connecting pipes which interact dynamically. For passenger vehicles the chamber length may vary between 200 mm to 500 mm and chamber diameters between 80 mm to 200 mm. Connection pipe lengths are normally between 200 mm and 1000 mm and pipe diameters between 38 mm to 54 mm. A typical exhaust system normally consists of three silencers with an overall length of 4 metres. Provided the transverse dimensions of the system elements remain a fraction of a wavelength, the resulting motion remains substantially one-dimensional over most of the flow path. Experience suggests that the overall acoustic performance of such reactive systems is governed by system resonances which depend, amongst other factors, on the resonances of individual elements [1.4] conditioned by their mutual interaction. These resonances include quarter and half wavelength resonance frequencies that can be related to the effective lengths of the connecting pipes with their boundary conditions, while cavity resonances are related to the chamber volume, the connecting pipe length and diameter of each individual element. In order to optimise the acoustic performance of the design, it is essential to ensure that the resonance frequencies of these components do not coincide, but are well separated. It is essential to obtain a clear understanding of the contribution of each individual element to the overall acoustic performance of the exhaust system as a whole under practical operating conditions [1.2, 1.4]. Without such guidance, an assessment of tail-pipe noise measurements normally does not provide sufficient information to indicate the appropriate changes to each specific element that are required to optimise the acoustic performance of the complete exhaust system. Also, tail-pipe orifice noise emission cannot be used to identify flow noise sources distributed along the system.

Although there is extensive literature on the acoustic modelling of an exhaust system and its validation, only a few of the relevant papers describe experimental measurements on a running engine. A critical analysis of current experimental

techniques is provided in Chapter 2. Such techniques have normally been restricted to constant engine speed measurements [1.6 - 1.10]. Also, the time taken to obtain stable acoustic and temperature conditions for reliable measurements makes these approaches time-consuming and limits the practical application. Furthermore, although constant engine speed measurements may be sufficient to validate acoustic models, they do not normally reflect the practical operating conditions of the engine.

There are a number of reasons to promote transient measurements instead of constant engine speed measurements. The most obvious is that transient measurements reflect the practical operating conditions of the engine. Run-up and run-down of the vehicle are commonly experienced in practice and are therefore used extensively in the automotive industry to evaluate the acoustic performance of exhaust systems. The appropriate assessment of the acoustic performance of exhaust systems should therefore include the influence of engine speed and load, because the corresponding variation in gas temperature and mass flow has a controlling influence on the spectral characteristics of the sources of excitation and the acoustic response of the system.

A clear advantage of transient measurements is that they enable the production of a comprehensive record of the exhaust noise signature for the speed range of the engine, which is essential for the recognition of the narrow-band acoustic phenomena that are always present in the exhaust emission. Constant engine speed measurements often result in unrealistically high temperature gradients and even in overheating of the engine. Such factors can restrict the number of measurement intervals and thus fail to produce adequately continuous spectral descriptions. Therefore it is essential to capture information at regular engine speed intervals (during engine acceleration) that are small enough to provide sufficiently realistic descriptions of acoustic behaviour to identify all narrow-band characteristics.

In this study new measurement technology was developed. This technology evaluates the acoustic performance of individual exhaust silencer components by using pairs of flush wall-mounted pressure transducers at the inlet and outlet of each silencer box or

exhaust system under the practical operating conditions of the engine. Normally, the acoustic pressure field inside the exhaust system is contaminated by shear layer turbulence and flow-induced noise, due to the high flow velocities generated under the normal operating conditions of an engine [1.5]. These aeroacoustic mechanisms are associated with turbulent and vortical motion generated at discontinuities. Their presence may cause very low signal-to-noise ratios in the measured pressure-histories when the acoustic signal approaches the level of the flow-induced pressure fluctuations [1.11]. This makes obtaining the precise measurements required to identify the acoustic behaviour of an exhaust system a formidable challenge. The high sound pressure levels and temperature gradients generated under the transient operation of an engine represent some of the other difficulties that have to be considered in experimental measurements.

The development of the new transient measurement technique recommended in this study may facilitate the following potential applications:

- a faster and more practical method to evaluate the acoustic field inside running engine exhaust systems, compared to existing methods, for example, the impedance tube technique (probe traverse method);
- an appropriate method to validate hybrid predictions;
- facilities to identify flow-induced sources along the exhaust system by means of precise measurement of net power flux at either side of suspected flow noise sources;
- part of a rational design strategy that ensures rapid acoustic optimisation of the exhaust system under the actual operating conditions of an engine. This is particularly applicable when complicated silencer elements are to be assessed for which validated acoustic models do not exist.

1.3 CHAPTER OVERVIEW

Chapter 2 contains a review of existing methods used to predict the acoustic performance of exhaust systems, with the experimental techniques required to validate the models. The review focused on references to instances where the validation process is performed on running vehicles or engines. The review is critically analysed in terms of attributes relevant to the establishment of new advanced computational and experimental procedures to assess the acoustic properties of exhaust systems.

Chapter 3 contains a general discussion of the acoustic design of exhaust systems in terms of a rational design strategy. The exhaust noise signature is discussed to characterise the spectral content in relation to cyclic engine operations and system geometry. Then the linear acoustic modelling of the exhaust system and the principles that govern its acoustic behaviour are discussed. Taking all relevant factors into consideration, the last section of this chapter describes the appropriate additions and adjustments to existing linear acoustic code to adapt it for transient operating conditions.

Chapter 4 describes the development of a measurement technique to assess the acoustic properties of individual silencer elements on a cold flow test bench with variable harmonic excitation, giving a partial simulation of the acoustic conditions during engine acceleration. The chapter presents a detailed examination of the various order analysis methods that can be used to capture the variable harmonic pressure data. A procedure is also described to estimate the wave components $P^{\pm}$ from the pressure data recorded simultaneously at two pairs of flush wall-mounted transducers. After the optimisation of the signal processing parameters to obtain reliable results in the presence of mean flow, the most effective procedures are applied to measure the acoustic performance of a simple expansion chamber. Measurements are compared to predictions performed with a validated numeric code to verify the new technique.

Chapter 5 describes the application of the new measurement technique to the exhaust system of a 1.5 l, four-stroke four-cylinder engine. First, a method is described to estimate the signal-to-noise ratios from the measured pressure data, because it is not possible to record them physically. This was essential to explain certain discrepancies in the measurements. Next, the acoustic performance of a simple expansion chamber was assessed for the practical operating conditions of the vehicle to determine whether linear acoustic theory remains valid for running engines. The reliability of the measurements is discussed and the influence of exhaust gas temperature and velocity on acoustic behaviour is demonstrated. The last section of the chapter contains a discussion on constant speed engine measurements demonstrating the advantages of the new transient approach.

Chapter 6 describes the application of the new prediction code to assess and optimise the acoustic performance of a simple exhaust system for a full throttle run-up of the vehicle. The potential advantages of the new approach in facilitating rapid acoustic optimisation of the exhaust system (compared to an approach based on tail-pipe orifice noise emission) are demonstrated.

Chapter 7 contains a summary of the thesis. Findings and future applications of the new technology are also discussed.

CHAPTER 2

PREDICTIVE ACOUSTIC MODELLING OF EXHAUST SYSTEMS AND EXPERIMENTAL VALIDATION TECHNIQUES

2.1 INTRODUCTION

As was stated in Chapter 1, the aim of this thesis is to establish computational and experimental procedures to facilitate the rapid acoustic optimisation of exhaust systems for the practical operating conditions of the vehicle. Consequently, relevant literature was examined, searching for references that contain information on the acoustic assessment of automotive exhaust systems. Although extensive literature exists on the acoustic modelling and validation of exhaust systems, only a limited number of contributions are concerned with experimental procedures performed on a running engine. To place the work presented in this thesis in context, particular emphasis is placed on literature discussing the use of a running engine for the experimental validation of predicted acoustic behaviour. These references have been carefully studied to identify basic concepts that would be beneficial to this study. Drawbacks, limitations and disadvantages of current predictive modelling methods and experimental techniques are also highlighted.

There are basically three theoretical methods which are employed to model exhaust systems acoustically. For this reason the references were grouped under the following headings:

- Linear acoustic method
- Non-linear gas dynamic method
- Hybrid method

Section 2.2 describes the experimental procedures that have been used to validate linear acoustic theory on running engines. These include the impedance tube technique (probe traverse) and the wave decomposition method. Also included are methods to predict the radiated noise and insertion loss from the measured source impedance and a linear acoustic model of the exhaust system. The non-linear gas dynamic and hybrid models are discussed in Sections 2.3 and 2.4 respectively.

Section 2.5 presents a critical analysis of the results of the literature review and outlines the resulting conclusions and recommendations. The practical application of predictive acoustic modelling methods and experimental procedures are discussed in Section 2.6.

2.2 LINEAR ACOUSTIC THEORY

A large number of references can be found in the literature dealing with the linear acoustic modelling of exhaust systems. However, published literature describing experimental validation on a running engine is generally confined to sound radiation measurements [1.8] or single point pressure measurements at one or more positions along the exhaust system. Appropriate measurements describing the acoustic performance of exhaust systems and component elements under operational conditions have been almost exclusively been performed at the University of Southampton (ISVR). Hence, the list of references cited here may appear parochial. Nevertheless, these have been used as a starting point to formulate the requirements for a new approach.

2.2.1 Impedance tube technique (probe traverse)

Alfredson [1.6] published his thesis in 1970. His aim was to develop theoretical models for the design of reactive silencers. His thesis was also summarised in a paper by Alfredson and Davies [1.7]. In his thesis, theoretical models were developed for expansion chambers with extended inlet and outlet branches, dual tail-pipes and

concentric perforated resonators. The acoustic influence of the tail-pipe was included in Alfredson's models. Initial measurements performed on an engine indicated that the neglect of mean flow and incorrect boundary conditions were the most likely reasons for unreliable theoretical models, rather than the assumptions of linear acoustic theory [1.8]. Alfredson [1.6] determined that the tail-pipe boundary conditions could be described by the reflection coefficient magnitude and the phase angle between the incident and reflected waves at the open termination. It was also shown experimentally when mean flow was present that the reflection coefficient magnitude exceeded unity at low frequencies as predicted by Munt [2.1], although the reflection coefficient magnitude was still smaller than unity at higher frequencies. This provided a possible reason for previous unrealistic results when the somewhat smaller zero flow value of Levine and Schwinger [2.2] was normally assumed. Viscosity effects [1.6] were also included in the models.

The validation process was performed using a Rolls Royce K60 six-cylinder two-stroke diesel engine. The impedance tube technique was used to estimate the reflection coefficient magnitude and phase angle at the inlet and outlet sides of the exhaust system to define the overall acoustic performance. A pressure transducer was slowly traversed axially inside the exhaust system and the signals were recorded on tape as a function of position. The recordings were subsequently analysed to determine the standing wave pattern for sets of harmonic components with the engine running at a constant speed. A 10 Hz bandwidth filter was used, since it was found sufficiently wide to compensate for engine speed fluctuations. The pressure ratio, reflection coefficient magnitude and the phase angle between the reflected and incident waves were determined using the standing wave pattern. The technique was also shown to be valid in the presence of mean flow. The quasi-stationary linearised equations of energy and continuity, together with the isentropic state relations, were used to describe the acoustic performance of a sudden contraction and extended outlet. The quasi-stationary linearised equations of energy, continuity and momentum, together with the adiabatic state relations, were used to describe a sudden expansion and extended inlet.

2.2.2 Wave decomposition technique

Bhattacharya [2.3] developed a technique to analyse the acoustic field using measurements made anywhere along a duct by using a two-microphone decomposition method. Pairs of closely spaced wall-mounted pressure transducers were used to extract the wave components $P^{\pm}$ from simultaneous sound pressure measurements. The technique was compared to the (by then well-established) impedance tube technique on a test bench. A circular uniform pipe was used for the experiment and the system was excited with a single sinusoidal frequency signal from a speaker, while the flow in the duct varied between a Mach number $M = 0$ to $M = 0.26$. The wave components $P^{\pm}$ were translated along the duct, and when recombined, correlated closely with the observed pressure spectrum. The standing wave envelope of the duct acoustic field was then estimated using the magnitude and phase information. It was concluded that the two-microphone technique provided results as reliable as those obtained using the impedance tube technique.

The new technique was also applied to a four-cylinder engine converted to a single cylinder and driven by a 50 h.p. electric motor, with the intake system replaced by a straight uniform tube. Although experiments were initially planned for both the intake and exhaust ducts of a four-cylinder engine, motored experiments on the intake system were eventually chosen to minimise the uncertainties introduced by temperature gradients. The wave component $P^{\pm}$ Fourier spectra estimated with the two-microphone wave decomposition technique and hot wire anemometer measurements were compared at a constant engine speed. Greater discrepancies were observed at lower frequencies. These were attributed to the small separation distance of 76 mm of the two-microphone decomposition technique. However, the hot wire probe measurements showed considerably greater background noise because of the contamination caused by turbulence. Nevertheless, the results indicated the feasibility of the new approach as a method to obtain reliable results for practical situations.

Temple [1.9] studied the change in acoustic load on the source characteristics of an exhaust system for a running engine. Several exhaust systems were applied to the engine to obtain varying acoustic loads. A wave-decomposition method was used to extract the incident and reflected wave components $P^{\pm}$ from three water-cooled wall-mounted pressure transducers fitted upstream of the front muffler. Measurements were performed at four constant engine speeds between 2000 and 4500 r.p.m.. These measurements indicated that variation of the intermediate and the rear silencer had a greater effect on radiated noise, and variation of the front silencer had a greater effect on the source power delivered to the exhaust system. Large discrepancies were observed between measured and predicted insertion loss, presumably because the source characteristics were not known. However, the measurements did illustrate the strong influence of the exhaust system resonances and anti-resonances on the source characteristics.

Yaseen [1.10] studied the acoustic performance of silencer components on a running petrol engine. A four-microphone wave decomposition method was used to estimate the acoustic behaviour of the silencers by using pairs of flush wall-mounted water-cooled pressure transducers. Measurements were performed at five constant engine speeds between 2100 and 4500 r.p.m.. The incident and reflected wave components $P^{\pm}$ were calculated from the harmonic spectral components and the corresponding stable mass flow and temperature. Large differences were observed between the measured and predicted results for the front silencer and smaller differences for the rear silencer, where conditions were more steady.

2.2.3 Prediction of radiated noise from the measured source characteristics of an engine and a linear acoustic model of the exhaust system

A number of descriptions can also be found in the literature of methods to predict the radiated noise and insertion loss using the measured source impedance and a linear acoustic model of the exhaust system. However, these methods all assume constant

source characteristics independent of acoustic load, while the experimental evidence [1.9, 2.3] suggests that results are often unrealistic.

Prasad and Crocker [2.4] measured the source impedance of a Ford eight-cylinder engine using the standing wave method (impedance tube technique) and the transfer function method (two-microphone wave decomposition method). Experiments were conducted for five operating conditions of speed and load. The exhaust system was also excited with random noise by means of an acoustic driver attached to the exhaust system. The incident and reflected wave components $P^{\pm}$ were extracted using two wall-mounted pressure transducers. The complex reflection coefficient and normalised impedance were calculated from the measurements. Results were plotted against the non-dimensional wave number *ka*. Similar trends were recorded for the standing wave and transfer function methods. Measurements using the transfer function method indicated no significant influence of the source impedance under different load and speed conditions. The source impedance displayed the same trends for an operating and non-operating engine. However, it was reported that the standing wave method was both time-consuming and tedious.

Prasad and Crocker [2.5] published a second paper, describing a method to predict the insertion loss and radiated noise by incorporating the measured source impedance into a linear acoustic model. Experiments were again performed on a Ford eight-cylinder engine and measurements were only performed at one engine speed and load (2000 r.p.m.). Two exhaust systems consisting of a simple expansion chamber were investigated and modelled by means of linear acoustic theory. Insertion loss and radiated sound pressure were predicted using the four-pole matrix parameters, the radiation impedance and the measured source characteristics. Predicted and measured insertion loss and radiated noise produced improved agreement compared to an assumed value of zero or infinite impedance. It was also shown that the inclusion of actual flow and temperature conditions gave results that were more satisfactory.

Desmonds, Hardy and Auregan [2.6] used a least square method to characterise the source noise of an internal combustion engine. Measurements were performed on a 1.8 litre four-cylinder engine using only one external microphone, positioned close to the outlet of the exhaust system. The high sound pressure levels, temperature gradients, turbulence effects and corrosive atmosphere were mentioned as difficulties both in the experimental measurements and the theoretical interpretation of the results. The advantage of this method is that no in-duct measurements are required. Crankshaft frequency was also recorded using a photoelectric cell to obtain phase information. The exhaust temperature was measured every 0.5 metres along the system. In order to evaluate the source impedance, the exhaust system muffler was replaced by calibrated loads. In practice, different tube lengths were used. The first two measured harmonics of radiated noise were used to estimate the pressure and velocity at the inlet of the systems by means of the four-pole transfer matrix. The source characteristics were then determined by applying the least squares method on two configurations of the five tubes. The radiated sound pressure of the first and second harmonic of exhaust noise was then predicted and measured for two exhaust systems, the one a simple tube and the other consisting of one muffler. Fair agreement was only obtained for the first harmonic. No details were given of the experimental technique to measure the harmonic information.

2.3 NON-LINEAR GAS DYNAMIC METHOD

A number of papers have been published describing the unsteady flow in exhaust systems by means of one-dimensional non-linear gas dynamic numerical schemes. Although the theory was originally developed to predict the engine performance of internal combustion engines, it is now also applied to the modelling of the acoustic characteristics of an exhaust. Because the engine is also included in the model, it is claimed that insertion loss and radiated noise can be predicted. The wave action is formulated in time and normally analysed in discrete steps at appropriate time-intervals. However, a time-average model of the valve discharge coefficients is

used. Hence, the influence of the acoustic load of the exhaust system on the source characteristics is neglected.

Sapsford, Richards, Amlee, Morel and Chappell [2.7] published a paper in 1992 using a software programme, "WAVE", to optimise the acoustic behaviour of the exhaust system of a Chrysler 2.5 litre, twenty-four valve, V-six engine. The software code is based on one-dimensional fluid dynamic principles and a finite volume approach, dividing the system into sub-volumes where the equations of conservation of mass and energy are applied. Flow from one volume to another was calculated using the momentum equation. Previously established boundary conditions for flow ducts were used in the analysis. The engine was modelled by means of a self-contained and flexible thermodynamic cycle, including the effects of combustion rate, heat transfer and the engine valves.

Validation of the code was first performed for a perforated concentric resonator with speaker excitation. Prediction and measurement of transmission loss showed good agreement up to 3000 Hz. However, this validation of the modelling certainly does not apply to the behaviour with flow present [2.17] since this introduces major changes to the surface impedance. The rest of the paper [2.7] deals with the optimisation of an exhaust system in terms of engine performance and noise. A baseline matching was performed with a straight pipe to characterise pressure and temperature effects. Pressure, gas temperature and skin temperature were recorded at various positions on the exhaust system. Data were collected at 1 degree of crank angle and at different speeds for full load to validate the computer models. Predicted pressure time-history data and frequency spectra compared well with the measured data at 2400 and 4800 r.p.m. for a straight pipe. Satisfactory predictions were achieved for the original exhaust system for frequencies up to 500 Hz. A parametric study was conducted to optimise back pressure and acoustic performance. A-weighted overall radiated noise was predicted to evaluate the modification made to the exhaust system. It was stated that these predictions took approximate ten minutes per configuration. However, predictions were not compared to measurements.

Ferrari and Onorati [2.8] published a paper in 1994 with the aim of predicting the acoustic performance of silencers by means of a one-dimensional gas dynamic approach. Silencers were modelled with the quasi steady state boundary condition, while the wave action in the ducts was calculated by solving the hyperbolic conservation equations using three numerical techniques: the method of characteristics (MOC), the two-step Lax Wendroff (LW2) method and the MacCormack (MAC) method. Perfect gas was assumed with constant specific heat. It was stated that the MOC gave first order accuracy and the other two methods provided second order accuracy. The Flux Corrected Transport (FCT) technique was adapted to eliminate spurious overshoots due to steep gradients of the solution for the LW2 and MAC methods. Two variants of the FCT were used in the models: diffusion via smoothing, which did not completely erase the overshoot, and diffusion via damping, which eliminated the overshoot at the expense of reduction of the time step and increased computation time. End corrections and boundary conditions for the silencers were presented as determined by experimental and numerical research work. Eventually the end correction in [1.2] or the corrected ones in [2.13] were adopted. Radiated noise was calculated from the predicted volume velocity at the termination and converted to the frequency domain by means of a fast Fourier transform.

Measurements performed on a six-cylinder turbo charged diesel engine were used to validate the models. Pressure transducers were positioned upstream and downstream of the turbine and a microphone was placed at a distance of 0.5 metres at 45 degrees from the exhaust outlet. Straight pipes, expansion chambers, side branches and Helmholtz resonators were evaluated. Pressure time-histories and sound pressure spectra were measured and predicted downstream of the turbine at 1500 r.p.m. for null load. Measured and predicted radiated noise was also obtained for the same conditions. The agreement between experimental and predicted results was satisfactory up to 500 Hz. The LW2 and the MAC schemes provided similar spectral results, displaying more prominent peaks and troughs for higher harmonic

components with increased frequency (due to second order accuracy) compared to the MOC.

Onorati [1.3] published another paper in 1995 on the numerical modelling of the unsteady flow in the exhaust silencer of a small single-cylinder diesel engine. The (MAC) method with Total Variation Diminishing (TVD) and a new space time Conservation Element-Solution Element (CE-SE) technique was presented, providing a second order oscillation free solution. Measurements and predictions were performed on a variety of exhaust systems, including Helmholtz resonators and expansion chambers. Pressure versus crank angle data were recorded 130 mm from the exhaust valves and the radiated noise was recorded 0.5 metres at 45 degrees from the outlet. A single cylinder engine was operated at 3175 r.p.m. for 2/3 load. Predictions with the CE-SE technique showed the formation of a shock wave during the blow-down period in the front section of the exhaust system. Predicted and measured pressure time-history versus crank angle, frequency spectra, transfer functions across the silencer components and radiated noise showed satisfactory agreement. Some discrepancies were observed at high frequencies (700-1000 Hz). These discrepancies were attributed to flow noise. The predicted results of a simple perforated resonator with a porosity of 4.2 % was also compared to the predictions of a simple expansion chamber. The perforated resonator predictions displayed a significant increase in noise reduction, but this finding was not validated.

Payri, Torregrosa and Chust [2.9] published a paper describing a method to predict the radiated noise of an exhaust system by means of a non-linear flow calculation. The MAC predictor-corrector method was used for the study instead of the LW2 method because it is less dispersive and slightly faster. The MAC method was simplified to reduce computation time due to the smaller mesh spacing required for exhaust system modelling. Although it was mentioned that the boundary conditions developed for the MOC are not well suited for second order methods, it was still used for the proposed method. The source (engine) was modelled by applying the First Law of Thermodynamics for an open system, accounting for heat losses and

mass exchange. The relation between in-cylinder variables and the flow conditions in the ducts was obtained by assuming a quasi-steady flow at the valves. This relation was determined by the valve timing and the valve lift profile.

The model was validated by means of measurements on a single-cylinder spark ignition engine at 1500 r.p.m. for full load. The speed was chosen to ensure that flow noise was ignored in the calculations. Instantaneous pressure was recorded at a position 155 mm upstream from the outlet, and radiated noise was recorded 0.5 metres at 45 degrees from the outlet. For a straight pipe, the pressure peak was overestimated in the time domain. This was attributed to an error in the temperature calculations. The predicted volume velocity time-history displayed a clear steepening. Closer evaluation indicated that the steepening was not a shock wave. Fair agreement was found between the predicted and measured radiated noise, except below 100 Hz. Measurements were also performed for a simple expansion chamber, showing satisfactory agreement with predictions for in-duct pressure. Amplitude differences were attributed to an error in temperature calculations and the absence of end corrections. Measured radiated noise showed a similar trend compared to predictions with some discrepancies at low frequencies.

2.4 HYBRID METHOD

An alternative approach is the formulation of a hybrid time/frequency simulation for the prediction of the acoustic performance of the exhaust system [2.10]. The non-linear engine breathing characteristics are described in the time domain, and the acoustic performance of the exhaust system is described in the frequency domain. The hybrid system is then represented by a time-varying part coupled with a linear or acoustic part, as is illustrated in Figure 2.1 on page 20 [2.10]. The interface between the two parts is represented by a more realistic time-varying boundary condition, instead of the time average condition adopted for the non-linear gas dynamic method described in Section 2.3. Therefore, the influence of the acoustic load of the exhaust system on the source is now accounted for.

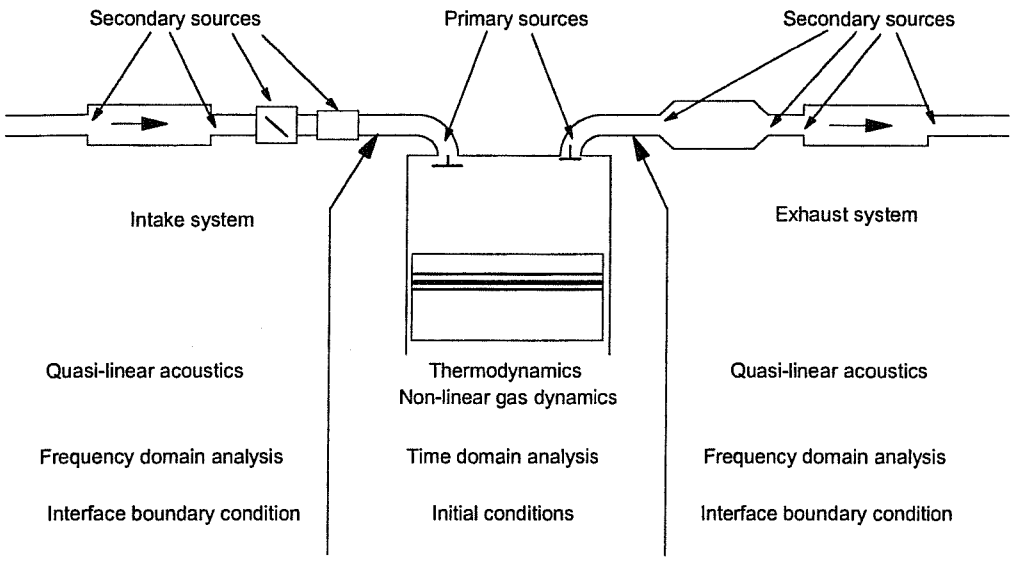

Figure 2.1 A hybrid prediction scheme with sources of excitation for engine breathing noise.

Such a hybrid method was described by Davies and Harrison [2.10] to predict the sound emission from a high performance petrol engine intake and exhaust system. The method coupled a time domain modelling of the combustion in the cylinders and associated valve and manifold gas flow with a frequency domain linear acoustic modelling of the intake and exhaust system. The boundary condition on the frequency domain side of the interface was described by the predicted pressure reflection coefficient which was Fourier transformed to give the corresponding cyclic reflection coefficient, at the appropriate times. This was then combined with the predicted source volume velocity through each open valve to give the fluctuating acoustic pressure at the corresponding valve, the remainder being closed. This procedure was performed for each cylinder and the predicted emissions were combined to give the final pressure spectrum, harmonically related to the engine firing frequency. Figure 2.2 compares some typical narrow-band results of the predicted and measured exhaust noise emissions. One notes that the agreement was poor above 500 Hz. It was reported that this was probably due to the inadequacies in the description of the valve flow time-histories, while the peak between 500 and 600 Hz was attributed to some defect in the acoustic modelling of the exhaust system.

Also, the validity of comparisons at low frequencies was doubtful due to the test cell "cut-off" around 150 Hz. However, fair agreement was obtained for the harmonics between 150 and 500 Hz.

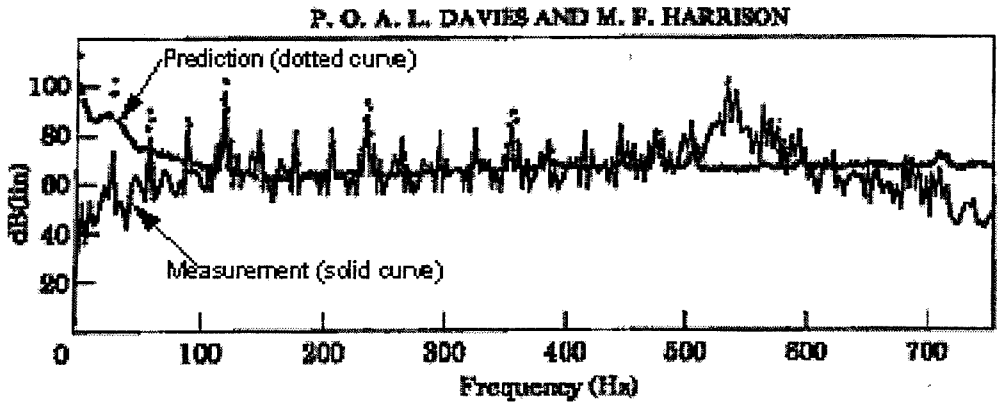

Figure 2.2 Exhaust noise emission at 3600 r.p.m.. Predictions by the hybrid method (dotted curve) compared with measurements (solid curve).

Payri, Desantes and Torregrosa [2.11] published a paper in 1995 presenting a calculation method to use the measured acoustic characteristics of a duct system as a boundary condition for a non-linear one-dimensional gas dynamic model of the engine. The method of characteristics was used to calculate the time domain model. The exhaust system was represented by the reflection and transmission coefficients at the front of the exhaust system, determined by measurement or linear acoustic theory. The response of the incident pressure wave was used as a boundary condition for the time domain calculations. Therefore, the interaction between the acoustic behaviour of the exhaust system and the acoustic source is taken into account.

A four-cylinder spark ignition engine was used to validate the model. The silencer transmission and reflection coefficients were determined experimentally at ambient conditions due to the complexity of the exhaust system. The wave number *ka* was adjusted to account for the hot running engine conditions. In-duct pressure measurements were recorded upstream and downstream of the silencer and at a distance of 0.5 metres from the outlet. In-duct pressure measurements versus crank

angle showed fair agreement with predictions for a straight pipe and when a silencer was present. Measurements of radiated noise showed good agreement with predictions for the first two harmonics for a straight pipe, and for the harmonics up to 500 Hz with a silencer.

Desantes, Torregrosa and Broatch [2.12] used the same method as that applied in [2.11] to predict the radiated exhaust noise of a four-cylinder spark ignition engine fitted with different exhaust systems. The complex amplitudes of the pressure waves incident on the muffler were calculated with one-dimensional flow equations by means of the method of characteristics. The paper also mentioned that transmission and reflection coefficients could be obtained using the elements of the scattering matrix or from experimental measurements. In-duct pressure measurements were performed at the inlet and outlet of the exhaust system. Predictions and measurements for a straight pipe and the one-muffler system discussed in [2.11] were repeated, except that the in-duct pressure results were presented in the frequency domain. Pressure measurements recorded upstream of the front muffler and radiated noise showed good agreement with predictions for the first four multiples of the firing frequency. Results for a two-muffler system also showed good agreements for in-duct pressure and less agreement for radiated noise. For a three-muffler system the in-duct pressure was overestimated for all the harmonic components except for the fundamental harmonic, radiated noise showed poorer agreement. The discrepancies were attributed to incorrect superposition of incident and reflected wave components and problems with temperature calculations.

2.5 DISCUSSION

This section takes a critical look at the various methods to predict the acoustic performance of exhaust systems and the experimental validation techniques. Drawbacks, limitations and advantages significant for the establishment of new measurement technology and prediction code are identified and discussed.

2.5.1 Impedance tube technique (probe traverse)

When one examines the impedance tube technique described in [1.6] critically, it can be argued that the stable temperatures at constant engine speeds do not represent the practical operating conditions of an engine. During normal engine operation the mass flow and temperature constantly change during the acceleration or deceleration of the engine speed. The variable temperature and mass flow have a controlling influence on the spectral characteristics of the exhaust noise signature. An open passage is also required to axially traverse the pressure transducer inside the exhaust system. For this reason, only straight-through silencers may be evaluated. To avoid the effect of changing the cross-sectional area of the connecting pipes due to the presence of the pressure transducer, only sufficiently large silencer components (for example, truck silencers) can be evaluated. The main disadvantage of the technique is inadequate description of the acoustic behaviour due to the restricted number of measurement intervals. The restriction in measurement intervals was probably due to the laboriousness performing measurements. Therefore, it can be concluded that this measurement method is time-consuming, labour-intensive and of limited practical application.

2.5.2 Impedance tube technique versus two-microphone wave decomposition method

Although the two-microphone wave decomposition method developed in [2.3] was only applied to an intake system on a motored engine, the results indicated the feasibility of the new approach to obtain reliable results for practical situations. In the context of the work to be undertaken, it is essential to point out the attributes of the two-microphone wave decomposition technique compared to the impedance tube technique.

Drawbacks of the impedance tube technique:

- It is enormously time-consuming.
- It interferes with the open boundary condition where an observer has to be stationed to conduct the traverse.
- There is jitter in the standing wave pattern, and the measurement of levels at the pressure minima.
- It is virtually impossible to maintain sufficient stable conditions at stationary engine speeds to execute traverse measurements.
- The signal-to-noise ratio at the pressure minima effects the results for each traverse measurement. However it will be shown later that this factor is only significant at the microphone position for the two-microphone technique, and can be optimised.
- The estimation of the standing wave patterns becomes more complex when axial temperature gradients are present, due to the relatively large distances involved and the corresponding influence on the wave attenuation and phase angle information.

Drawbacks of the two-microphone decomposition method:

- More than one-microphone separation distance may be required to cover a particular frequency range.
- A relative calibration of the microphones is essential to obtain meaningful results.
- When temperature gradients are present, it is essential to take proper account of the local velocity of sound c and Mach number M in the wave decomposition and translation calculations.
- Proper design of the microphone holders is essential to avoid the generation of noise.

Advantages of the two-microphone decomposition method:

- It offers considerable time saving compared to the impedance tube technique.
- Signal-to-noise ratios are only relevant at the microphone positions and not at the pressure minima as in the case of the impedance tube technique.
- Wall-mounted transducers cause minimal interference in the duct flow and acoustic field.
- Jitter in the standing wave pattern in the presence of mean flow is avoided with the two-microphone wave decomposition method, because the levels and positions of the standing wave minima are not required. With the wave decomposition method, the wave components $P^{\pm}$ are estimated simultaneously from a fixed pair of pressure transducers.
- With the wave decomposition method, the harmonics of the exhaust noise signature can be analysed in a single experiment. Then the wave components $P^{\pm}$ can be translated to any other position along the duct to determine its acoustic characteristics. The calculation can easily be performed with the aid of a computer programme. In contrast to this, with the microphone traverse method the data has to be analysed for each harmonic frequency at appropriate positions along the duct to obtain the standing wave pattern. It was reported [1.6] that the method was extremely time-consuming even when a mechanical traverse probe moving at a constant speed was employed and subsequent narrow-band analysis of the probe signals was recorded on tape.

Therefore, it can be surmised that the two-microphone wave decomposition method offers distinct advantages over the impedance tube technique, especially in an engine test situation.

2.5.3 Steady state (constant operating conditions) wave decomposition technique

Both Temple [1.9] and Yaseen [1.10] performed measurements at insufficiently close speed intervals to describe the acoustic behaviour of highly reactive exhaust systems adequately. Consequently, the results could not be used to describe narrow-band acoustic behaviour (for example, the connecting pipe resonances). The estimated acoustic quantities were calculated using harmonic pressure components recorded at different engine speed intervals. This made the interpretation of results difficult as the frequency components were represented by different mass flow and temperature conditions. Yaseen plotted the acoustic quantities against the dimensionless Helmholtz number *ka* to make them independent of the flow and temperature, but this only produced a small improvement. The limited data also prevented the presentation of individual order components. Instead, results were consolidated into frequency spectra. Equipment constraints and indeterminate measurement errors also resulted in inconclusive results.

2.5.4 Prediction of radiated noise from the measured source characteristics of an engine and a linear acoustic model of the exhaust system

The record [2.4 to 2.6] shows that methods to predict the radiated noise by means of the measured source characteristics of a running engine with a linear acoustic model of the exhaust system have not produced reliable results. The main reason for this is that the source characteristics of the engine are influenced [1.9] by the acoustic load of the exhaust system. Although it has been demonstrated that more realistic predictions can be obtained using measured instead of assumed values for the source impedance, the aim of this technique is to predict tail-pipe radiation noise, describing the overall performance of the exhaust system. The results give little insight into the acoustic contribution of individual components.

2.5.5 Non-linear gas dynamic method and hybrid method

In most cases single in-duct pressure measurements and tail-pipe orifice noise emission spectra have been used to validate non-linear and hybrid acoustic models. Low engine speeds were normally chosen to ensure neglect of aeroacoustic noise in the calculations. In some cases the wave components $P^{\pm}$ were measured using a wave decomposition method to describe the acoustic performance of a more complex exhaust system instead of modelling the wave components. In all the cases the aim was to predict the tail-pipe radiation noise. Consequently, one can conclude that these measurements describe the overall acoustic performance of the exhaust system. The results provide insufficient spectral data to guide the design process effectively.

2.5.6 Predictive acoustic modelling

This section contains a general discussion on the available modelling techniques. The aim is not to provide a detailed theoretical discussion of the different modelling techniques, but rather to indicate the limitations and advantages to exhaust signature management.

2.5.6.1 Linear acoustic theory

The prediction of the acoustic performance of exhaust systems by means of plane wave linear models [1.2] has reached a high stage of development if one takes into account the limitations imposed on linear acoustic theory by the acoustic assumptions [2.13]. In most cases acoustic theory has been validated on a bench test in the frequency domain for stationary conditions with random noise excitation. Insertion loss [2.14] and transmission loss measurements [2.15] have normally been measured directly. Wave decomposition methods [2.16, 2.17] have also been applied to calculate the wave components $P^{\pm}$ from in-duct sound pressure measurements at the inlet and outlet of the silencer component. Acoustic theory provides realistic predictions of the wave propagation in the exhaust system for complex components,

representing realistic silencers employed in the automotive industry [2.16, 2.17]. Another major advantage of linear acoustic theory is that calculations are performed in a very short time, normally in seconds.

Linear acoustic theory is based on a one-dimensional approach, where the excitation of higher order modes is neglected. The first circumferential acoustic mode propagates when the Helmholtz number *ka* exceeds 1.84 and the first radial mode propagates when the Helmholtz number *ka* exceeds 3.8 [2.18]. The limiting value of 1.84 corresponds to a frequency of about 1000 Hz in an exhaust system of normal dimensions. In most applications this is more than adequate since only the first three or four harmonic components of the pulsating wave motion are considered during the design process. Other prediction methods, for example, the non-linear gas dynamic and hybrid methods, are also based on the one-dimensional assumption.

Initial calculations of acoustic theory were based on simple attenuation equations, neglecting mean flow and viscosity effects [1.8]. Alfredson and Davies [1.6, 1.7] showed at an early stage that the neglect of mean gas flow can produce significant errors. The temperature gradient inside the exhaust system can also significantly alter the form of the wave propagation through the duct system [2.19, 2.20]. The local absolute gas temperature has a direct influence on the speed of sound. Therefore, knowledge of the gas temperature gradient is essential if realistic predictions are to be obtained.

Acoustic theory also assumes that the amplitudes of the pressure fluctuations remain below some limiting value so that steepening of the wave form can be ignored. Practical experience [1.6] shows that with plane wave conditions the limit lies between 0.01 and 0.1 bar. Although the fluctuating pressure amplitudes in the exhaust manifold normally exceed the acoustic limit by at least an order of the magnitude, it has been shown that below frequencies of 500 Hz and for levels below 160 dB, a wave must travel four to five metres before significant steepening occurs. The length of the exhaust manifold or down-pipe is too short for this to occur [2.21].

The validation of acoustic theory in noisy exhaust systems [1.6, 1.7] further justifies the application of linear acoustic theory in internal combustion engines.

2.5.6.2 Non-linear gas dynamic method

The non-linear gas dynamic method was originally developed to predict the engine performance of internal combustion engines in terms of volumetric efficiency, torque and power. The main advantage of the method is that the source characteristics of the engine are also included. Thus it is possible to predict the radiated noise at the tail-pipe outlet. This method also describes the non-linear effects due to the shape change of the finite amplitude waves in the front section of the exhaust system. However, the interaction between the response of the exhaust system and the source is not accounted for, because the system is represented by a time average model. Furthermore [1.3, 1.4], the general adoption of time averaged factors for flow coefficients and boundary conditions can produce inadequate predictions at higher frequencies.

Calculations were initially performed using the method of characteristics. A mesh spacing of one centimetre is necessary to obtain suitable frequency descriptions for an exhaust system which takes considerably more computation time. Second order methods were developed to reduce computation time. These included the LW2 and MAC methods. These methods produced spurious overshoots, due to steep gradients of the solution. Various techniques were adopted to reduce this effect. Examples of these techniques are the FCT technique with smoothing and damping, the TVD technique and the CE-SE technique (see Section 2.3). A disadvantage of the non-linear gas dynamic method is that it is often unable to handle complex geometries due to the absence of suitable boundary conditions. Therefore, it is not surprising that, in most cases, the validation of the models was performed using simple systems. This method is apparently less successful in calculating valid predictions of tail-pipe radiation noise above 200 Hz.

A number of studies reported on the validation for non-linear gas dynamic theory was performed under stationary bench test conditions. Onorati [2.22, 2.23] developed a full non-linear model for Helmholtz resonators, expansion chambers, extended inlet and outlet and other more complex silencers. Predicted and measured transfer functions across the silencers showed good agreement for zero flow. Dickey, Selamet and Novak [2.24] used a time domain computational approach to predict the acoustic performance of multiple pass silencers with perforated sections for the limiting case of low sound pressure levels and zero flow. Predicted and measured transmission loss correlated well for frequencies where the one-dimensional assumptions were valid. No details of the bench test set-up were provided.

2.5.6.3 Hybrid method

The hybrid method couples the non-linear gas dynamic modelling of the mass flow through the valves and the linear acoustic modelling of the exhaust system. The main incentive for using the method has been to obtain an acceptable computation time and to replace the time averaged boundary conditions and flow coefficients by more physically realistic time-varying ones. The hybrid method incorporates the advantages and overcomes the limitations of the non-linear gas dynamic method and acoustic theory. The interface between the time domain model of the engine and the frequency domain model of the exhaust system is represented by means of a boundary condition, normally in the front section of the exhaust system. Due to the cyclical nature of the exhaust noise signal, it can be Fourier transformed from the one domain to the other. A comparison between measured and predicted results shows that satisfactory agreement has now been extended to higher frequencies, compared to results obtained using non-linear gas dynamic modelling.

None of the predictive modelling methods described above (linear acoustic theory, the non-linear gas dynamic method and the hybrid method) includes quantitative estimates of the secondary sources depicted in Figure 2.1 on page 20. These sources

are related to high gas velocities in the exhaust system, associated with separating shear layers at duct discontinuities along the flow path.

2.6 PRACTICAL APPLICATION OF PREDICTIVE ACOUSTIC MODELLING METHODS

Linear acoustic theory is normally described by means of single parameter ratios to evaluate the overall acoustic performance of a silencer component (for example, transmission loss and pressure ratios). Single parameter ratios are also used to describe the acoustic properties at locations along the exhaust system (for example, acoustic power flux, acoustic impedance and reflection coefficients), while acoustic attenuation describes the transfer characteristics. Chapter 3 provides a detailed discussion on these acoustic quantities. They describe the relative passive acoustic performance, as the modelling of the source excitation is not included. Radiated noise and insertion loss can only be predicted using assumed or measured values for the source impedance. Although it has not previously been attempted, the prediction and measurement of the wave components $P^{\pm}$ at appropriate locations along the exhaust at regular engine speed intervals during a constant acceleration of the engine will provide a thorough evaluation of the acoustic behaviour of the exhaust system. This will also provide new detailed insight into the acoustic interaction between system components and the existence of any flow noise sources.

The non-linear gas dynamic method is less successful in providing valid predictions of radiated tail-pipe noise above 500 Hz [2.7, 2.8]. Apart from this, extensive computation time is required to perform the calculations. Hence, so far measurements are only performed at a limited number of speed intervals to validate the models. Measurements at between 30 to 50 regular engine speed intervals are required to describe the exhaust noise signature for the complete engine speed range. Normalisation of the actual frequency by the firing frequency will give an account of the harmonic order information. To gain insight into the behaviour of individual elements, it is necessary to estimate the wave components $P^{\pm}$ at appropriate locations

along the exhaust system by decomposing the predicted in-duct pressure. However, it appears that the excessive computation time that is required to perform the predictions makes this method impractical and unsuitable to facilitate rapid optimisation of design detail.

Although the hybrid method is in an early stage of development, good agreement has been found between measurements and predictions of radiated noise for frequencies below 500 Hz at multiples of the firing frequency. The validation procedure is the same as for the non-linear gas dynamic method, and so the same comments apply as discussed above. However, the hybrid method offers a considerable reduction of computation time and it is therefore possible to predict the exhaust noise signature at regular engine speed intervals in an acceptable amount of time. Performing the predictions in this format will closely represent the realistic engine operating conditions.

2.7 CONCLUSION

A study of the relevant literature has shown that both the impedance tube technique and the wave decomposition technique have been employed to validate linear acoustic theory on running engines. Complex acoustic ratios are normally used to describe the relative acoustic behaviour. The necessary time to obtain stable acoustic and temperature conditions for reliable measurements makes the impedance tube approach too time-consuming and limits its practical application. Furthermore, the restricted number of engine speed intervals normally adopted may produce inadequate identification of the acoustic behaviour. Also, constant speed measurements do not represent the realistic operating conditions of a vehicle.

Tail-pipe radiation noise and in-duct pressure measurements recorded at low stationary engine speeds are normally used to validate non-linear gas dynamic and hybrid models. These results describe the overall performance of the exhaust system and therefore provide insufficient spectral information to indicate the appropriate

modification to individual elements needed to optimise the acoustic performance of the exhaust.

Although the experimental methods discussed in this chapter provide a useful insight into the validity of theoretical models, they do not always give a corresponding insight into the wave motion of the pulsating exhaust gas flow signature throughout the speed range of an engine. The appropriate assessment of the acoustic performance should include the influence of the temperature and mass flow distribution for all the practical operating conditions of the engine. The spectral characteristics of exhaust noise and also the flow-induced aeroacoustic noise and its coupling with resonant acoustic feedback depend on the speed and load conditions of the engine. Therefore, it is essential to perform the measurements for the practical operating conditions of the engine to obtain a realistic description of acoustic behaviour.

Prediction of the acoustic performance of exhaust systems by means of plane wave linear models has reached a high stage of development, taking into account the limitations imposed on it by the acoustic assumption. The non-linear gas dynamic method provides less realistic predictions for radiated noise due to the adoption of unrealistic time average boundary conditions. An extension of the method to model the exhaust system has resulted in unacceptable computation time.

The hybrid method couples the non-linear gas dynamic modelling of the source and the linear acoustic modelling of the exhaust system. The evidence suggests that this method offers the most effective approach to predict the radiated noise due to reduced computation time with more realistic time-varying boundary conditions [1.2, 1.4, 2.10].

Although linear acoustic theory is not able to predict non-linear effects associated with high amplitude wave propagation (such as wave distortion and non-linear dissipation), it is preferable to other complicated methods due to its simplicity, low

computational cost and its ability to describe complex silencers. A study by Jones, van Moorhem and Voland [2.25] has also indicated that a linear acoustic model of the exhaust system and a non-linear modelling of the volume velocity at the exhaust valves appears to be adequate when compared to a full non-linear model. A more recent study by Payri, Torregrosa and Payri [2.26] compared a linear acoustic model of an engine and exhaust system against a full non-linear validated model. Non-dimensional pressure and mass velocity distribution along the exhaust system indicated that good agreement may be obtained in general.

Therefore, it can be concluded that linear acoustic theory offers the most effective method for the predictive modelling of the exhaust system to facilitate rapid acoustic optimisation. However, computational and experimental procedures to assess the acoustic performance of exhaust systems for transient operating conditions of a vehicle could not be found in the literature. These deficiencies are addressed in the chapters that follow.

CHAPTER 3

EXHAUST SYSTEM DESIGN

3.1 INTRODUCTION

Continuous efforts are made to improve engine performance and fuel economy in the automotive industry in order to satisfy customer expectations [3.1, 3.2]. Some of the concepts that have been introduced to achieve this objective include multi-valve engine configurations capable of high engine rotation speeds, and a reduction of vehicle mass to increase the power-to-weight ratio. There is also ongoing effort to refine the NVH (noise, vibration and harshness) characteristics of vehicles to increase comfort [1.2, 3.3, 3.4, 3.5 and 3.6]. The subsequent increase in exhaust flow velocities and space constraints present an enormous challenge to those who design and development exhaust systems. In the past, and in some cases still, an empirical method is followed during the design process. This is referred to as a "cut and try" or "build and test" approach. This approach is time-consuming and expensive and can often result in unacceptable development lead times. Therefore, the adoption of a rational design strategy based on validated acoustic modelling and experimental assessment is essential to ensure rapid exhaust system development [1.2]. Such a strategy may include the following steps:

- Step 1 : Assemble relevant input data
- Step 2 : Establish a design aim
- Step 3 : Initial design
- Step 4 : Assess acoustic performance
- Step 5 : Refine the design
- Step 6 : Build and validate prototypes

A schematic representation of such a rational design strategy is provided in Figure 3.1 on page 37, outlining the factors and actions involved in each step of this comprehensive operation. These steps may be subdivided into other sequences that relate to assessments based on past experience, style decisions based on market surveys, direct measurement, predictive calculations and so on. As is implied in Figure 3.1, acoustic design options may be severely restricted by other existing unrelated decisions, for example, the overall vehicle design layout.

However, the work in this thesis deals primarily with Step 4 ("Assess acoustic performance"), and includes the development of new advanced computational and experimental procedures. The purpose of these procedures is to allow a clear interpretation and identification of the individual contribution of each system element to the overall acoustic performance under operational conditions. This will facilitate rapid acoustic optimisation with the aim of reducing development lead times.

This chapter demonstrates some of the fundamental concepts governing the design of exhaust systems. In addition, the scope and extent of the research presented in this thesis is also specified where appropriate. The classification of internal combustion engine exhaust noise is described in Section 3.2. This is followed by a discussion of the acoustic behaviour of exhaust systems in Section 3.3. Reference is made to the acoustic modelling, acoustic resonances and acoustic performance of the exhaust system. The last section describes the appropriate additions and adjustments that have been made to existing linear acoustic code to enable it to be used under the transient operating conditions of an engine.

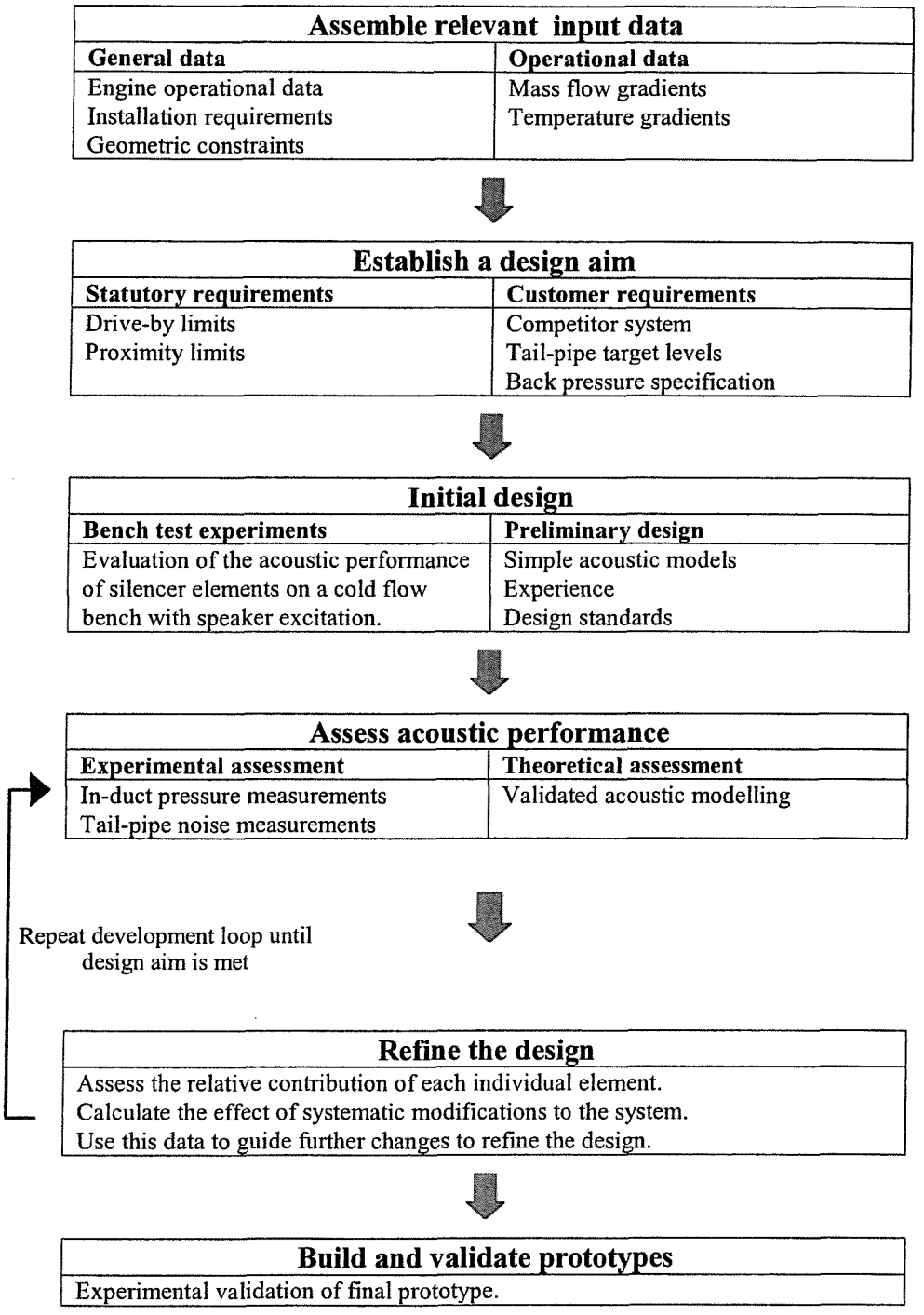

Figure 3.1 Example of a rational design strategy for exhaust system development and refinement.

3.2 INTERNAL COMBUSTION ENGINE EXHAUST NOISE

Exhaust noise is related to the cyclical operation of the engine and therefore includes both structural and acoustic noise sources. The structural sources are associated with the mechanical excitation of the silencers by engine vibration forces, transmitted from the engine as well as by fluctuating internal pressures. The acoustic sources are related to the cyclical pulsating flow through the valves. These include primary sources that are related to the periodic pressure pulses and secondary sources related to the high flow velocities in the exhaust system [1.5]. A further account of structural sources is excluded here as it falls beyond the scope of this thesis.

3.2.1 Primary source of exhaust noise

The primary source of exhaust noise is associated with the pulsating flow through the valves. In four-stroke engines the exhaust process is controlled by the valves, and in two-stroke engines the flow is controlled by the piston's moving past the exhaust port [3.7]. The cyclical wave motion is generated by the opening and closing of the valves or ports. Typically, for a four-stroke engine, the exhaust valve opens a few degrees before bottom dead centre during the expansion stroke, and closes a few degrees after top dead centre [3.8]. Therefore, the exhaust process occurs only about one third (240^0) of the total cycle time (720^0). The wave motion is essentially periodic and the time-history is readily Fourier transformed to analyse the exhaust noise signature in the frequency domain. The spectral content of the exhaust signal is dominated by a sequence of narrow-band components, harmonically related to the firing frequency of the engine. In four-cylinder four-stroke engines, the fundamental harmonic is twice the engine rotational frequency (2E) since combustion occurs every second revolution. In a six-cylinder engine, it is three times engine rotational frequency (3E), and so forth. Subsequently, the fundamental frequency for a two-stroke engine is twice that of a four-stroke engine as combustion occurs in each cylinder during every revolution of the engine.

Appropriate assessment of the acoustic behaviour of the exhaust system should include the influence of engine speed and load, since these two variables determine the gas temperature and mass flow distribution through the system. Accordingly, the acoustic performance of the exhaust system is evaluated during controlled run-up and run-down of the engine on an engine or chassis dynamometer. Tail-pipe radiation noise is normally measured and the results may be presented in a Campbell diagram, as displayed in Figure 3.2 on page 40; here the sound pressure levels are indicated by the grey colour scale. The spectral map is composed of narrow-band spectra captured at regular engine speed intervals. The radial straight lines that increase with frequency and engine speed can be identified as the harmonic components of the cyclical pulsating flow through the valves. These are usually classified into a sequence of harmonic orders related to the engine rotation frequency. The measurement shows the tail-pipe orifice noise emission of a four-cylinder four-stroke engine; hence, the fundamental order frequency is twice the engine rotation frequency (2E), the second order is four times the engine rotation frequency (4E), and so forth. Normally, only the first two or three orders are considered during the design process, as the higher orders are masked by the broad-band noise. The harmonic orders are frequently extracted from the Campbell diagram to facilitate interpretation of the results; the first four orders plotted against engine speed are displayed in Figure 3.3 on page 40. The tail-pipe noise signature describes the overall acoustic performance of the system and therefore provides insufficient information to indicate the appropriate changes to each specific element to guide the design process.

3.2.2 Secondary sources of exhaust noise

The secondary sources of exhaust noise are related to the high flow velocities in the exhaust system that result in the generation of flow-induced or aerodynamic noise [1.5]. These noise sources are associated with turbulent and vortical motion generated at duct discontinuities along the exhaust system, such as junctions, expansions, contractions and orifices [1.5]. The pulsating flow is often enhanced by the vortex noise and amplified by reverberation or acoustic feedback, producing

self-sustaining oscillations [3.9]. The sound generated by the vortices may also excite the acoustic resonances of the system [3.10, 3.11] (for example, multiples of the half wavelength resonance frequencies of the tail-pipe). Such flow-excited sources include discrete tones as well as acoustic energy distributed over a broad band [3.12].

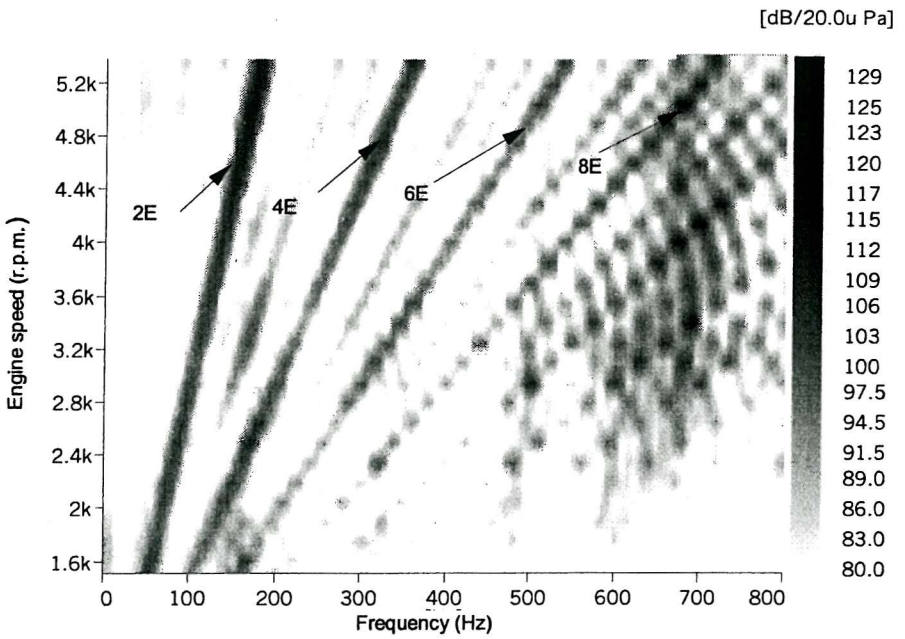

Figure 3.2 Campbell diagram of tail-pipe noise recorded for a full throttle run-up of a vehicle (fitted with a four-cylinder four-stroke engine) on a chassis dynamometer.

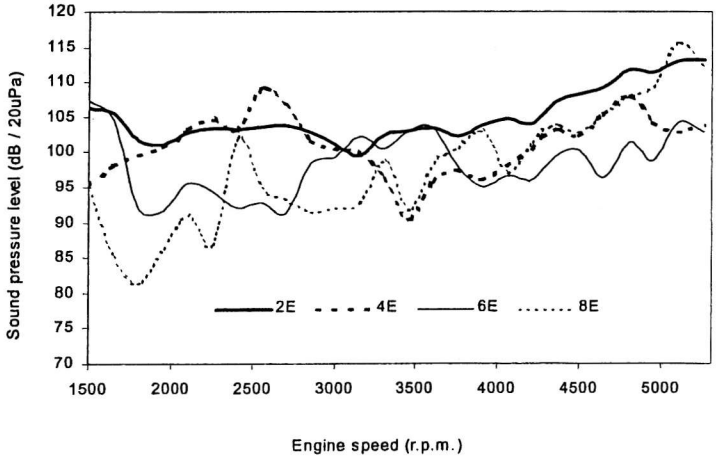

Figure 3.3 2E, 4E, 6E and 8E order components extracted from the Campbell diagram in Figure 3.2.

Therefore, the silencer can become a flow-excited sound generator rather than an attenuator, whose intensity may be the same or higher than the engine source at certain frequencies [1.5, 2.23].

The secondary sources of exhaust noise are exemplified by the broad-band noise in Figure 3.2 on page 40. Figure 3.4 below shows a 1/12 octave Campbell diagram of the sound pressure that was recorded inside the tail-pipe for a full throttle run-up of the vehicle.

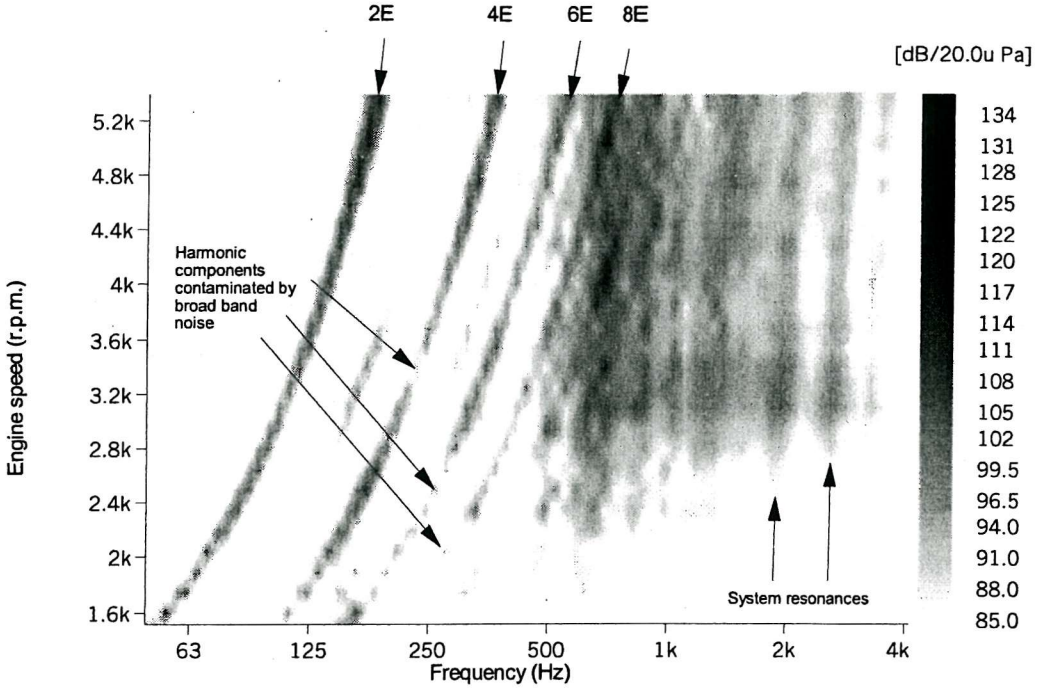

Figure 3.4 1/12 octave Campbell plot of sound pressure recorded inside the exhaust system tail-pipe during a run-up of the vehicle (fitted with a four-cylinder four-stroke engine) on a chassis dynamometer.

Performing the analysis in this manner facilitated the interpretation of the broad-band noise. One should note that the harmonic order lines are now hyperbolic rather than straight, due to the logarithmic frequency scale. The acoustic energy of the broad-band noise extends over the complete frequency span, with an increase in levels at frequencies above 400 Hz. The broad-band components arise from turbulence and flow-induced aeroacoustic sources associated with shear layers, flow

separations, wakes and vortex generation occurring at expansions, contractions, bends and other discontinuities distributed along the system [3.13]. One also notes that the broad-band levels show an increase at higher engine speeds, due to higher flow velocities. The increase in levels along the vertical straight lines indicate the system resonances. These are at a slight angle, resulting from the increase in temperature during the run-up.

It can also be observed that some of the order components are contaminated by the broad-band noise for sequences of specific frequencies, as indicated in Figure 3.4 on page 41. The order components normally approach the background noise at pressure minima associated with the axial distribution of the standing wave patterns inside the exhaust system. These minima may result in reduced signal-to-noise ratios [1.11]. Appropriate experimental procedures that identify the acoustic contribution of the order components at practically representative flow velocities are described in Chapter 4.

3.3 ACOUSTIC BEHAVIOUR OF EXHAUST SYSTEMS

3.3.1 Acoustic modelling of exhaust systems

Rational exhaust design involves a systematic tuning of the components based on realistic predictive numerical modelling of the gas dynamic and acoustic characteristics of the system [1.2]. Prediction software should facilitate rapid refinement of the acoustic performance of the system based on geometric modifications. As was concluded in Chapter 2, linear acoustic theory satisfies these requirements.

The acoustic behaviour of the exhaust system depends on the local sound propagation speed, $c(1 \pm M)$, where c and M are the local speed of sound and Mach number respectively. Therefore, apart from the geometry, a knowledge of the mass flow and temperature distribution throughout the system is required to model the acoustic

behaviour. The acoustic performance of the exhaust system can be described in terms of the wave component amplitudes $P^{\pm}$ at each discontinuity along the system. The open termination can be used as a reference plane to define the relative incident wave amplitudes, since the acoustic behaviour there is represented by its reflection coefficient [2.13]. A brief description of the acoustic propagation of wave energy through the exhaust system is provided in Appendix 3.1.

Acoustic predictions were performed using APEX (acoustic prediction of exhaust systems), a linear one-dimensional acoustic software programme [1.2, 2.13 and 2.16] developed by Prof. P.O.A.L. Davies at the University of Southampton. The programme provides the linear acoustic predictions of the pressure distribution and energy transport spectra throughout an exhaust system of specific geometry. Systems with complex geometries are modelled by means of a sequence of simple chambers. The programme takes full account of the flow velocity, temperature and static pressure distribution within the chambers and the complete system by establishing them initially before calculating amplitude spectra. The programme calculates the relative forward $P^{+}$and backward P^{-} travelling complex wave amplitudes at the inlet and outlet of each element for a specified frequency range and resolution. The acoustic behaviour of part or of the whole system can then be quantified in terms of the following single parameter descriptions (as set out in Figure 3.5 below).

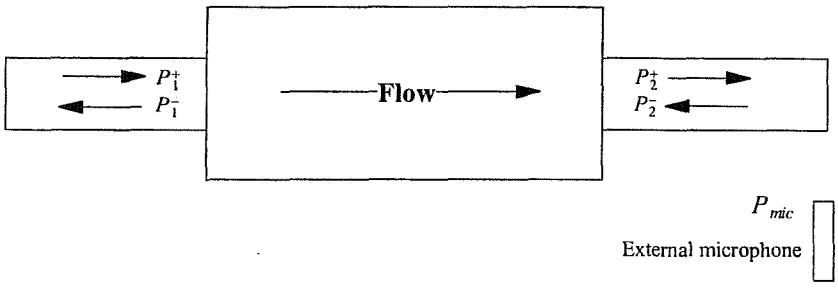

Figure 3.5 Simple silencer component indicating the direction of the forward P^{+} and backward P^{-} travelling wave components at the inlet and outlet.

The following single parameter descriptions define the acoustic spectral behaviour at a specific location along the axial direction x of the duct [2.13].

Reflection coefficient:

$$R_x = \frac{P_x^-}{P_x^+} . \tag{3.1}$$

Power reflection coefficient:

$$PR_x = \frac{|P_x^-|^2(1-M_x)^2}{|P_x^+|^2(1+M_x)^2}. \tag{3.2}$$

Acoustic impedance:

$$Z_x = P_x/u_x = \rho_x c_x\left[\frac{P_x^+ + P_x^-}{P_x^+ - P_x^-}\right]. \tag{3.3}$$

In these equations P is the fluctuating pressure and u is the fluctuating velocity at the axial position x, while ρ_o is the ambient density and c_o is the speed of sound.

The sound intensity I_x and hence the sound power flux per unit area is expressed by

$$I_x = \frac{1}{\rho_x c_x}(|P_x^+|^2(1+M_x)^2 - |P_x^-|^2(1-M_x)^2), \tag{3.4}$$

where the Mach number $M_x = u_x/c_x$. In this equation, u_x, c_x and ρ_x are the time averaged values of the flow velocity, speed of sound and density respectively at the axial position x.

The following single parameter descriptions may be used to define the acoustic spectral behaviour of individual elements, combination of elements or the system as a whole with the appropriate position of P_1^+ and P_2^+.

Attenuation:

$$AL_{1,2} = 20 \cdot \log\left|\frac{P_1^+}{P_2^+}\right| \text{ (dB).} \tag{3.5}$$

Pressure ratio or transfer function spectra:

$$H_{2,1} = 20 \cdot \log\left|\frac{P_2^+ + P_2^-}{P_1^+ + P_1^-}\right| \text{ (dB).} \tag{3.6}$$

The single parameter descriptions below define the acoustic behaviour of the system as a whole.

The transfer function between the inlet of the system and an external microphone is expressed by

$$\frac{P_{out}}{P_{in}} = 20 \cdot \log\left|\frac{P_{mic}}{P_1^+ + P_1^-}\right| \text{ (dB).} \tag{3.7}$$

The insertion loss is defined as the difference between the measured change in power flux at the same point in space before and after the insertion of an element between the measurement point and the source, provided that the impedance of both source and receiver remain invariant [1.2, 3.14]. The insertion loss is expressed by

$$IL = 10 \cdot \log\left(\frac{W_1}{W_2}\right) \text{ (dB),} \tag{3.8}$$

where W_1 is the received power before insertion of the element, and W_2 what is measured afterwards.

The transmission loss of a silencer element is defined as the difference in power flux between that incident on and that transmitted across it, in free space [1.2].

Transmission loss assumes anechoic termination and is expressed by

$$TL = 10 \cdot \log\left(\frac{S_1 \cdot I_1}{S_2 \cdot I_2}\right) \text{(dB)}, \tag{3.9}$$

where I_1 is the net incident intensity flux through cross-sectional area S_1, and I_2 is the transmitted intensity flux through cross-sectional area S_2.

3.3.2 Exhaust system acoustic resonances

The exhaust system consists of a sequence of silencer elements connected to each other by uniform lengths of pipe that extend from the exhaust valves to the open termination from where the sound radiates. Such systems are known to be highly reactive. Wave reflection occurs at each discontinuity so that the wave motion consists of forward P^+ and backward P^- travelling waves superposed on the mean flow to form standing waves. The acoustic behaviour of the exhaust system is therefore governed by system resonances that depend on the acoustic resonances of individual elements [1.2], with their coupled acoustic behaviour. The acoustic behaviour of the exhaust system and its elements is determined by its geometry, as well as by the temperature and mass flow distribution. Most of these resonances can be related to the length of the wave path through each element and the boundary conditions at the interfaces, as indicated in Figure 3.6 below.

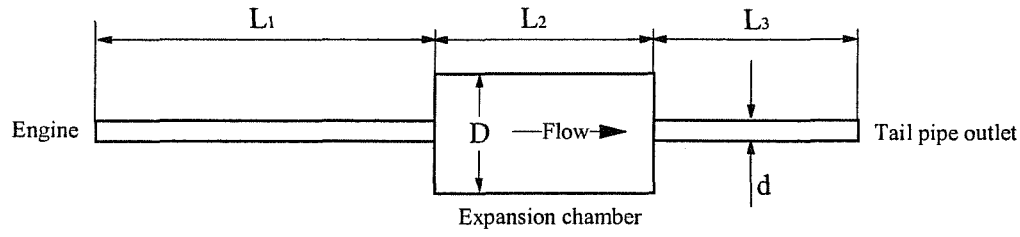

Figure 3.6 Schematic representation of a simple one-silencer exhaust system.

The front pipe of the exhaust system is represented by a pipe closed at the valves and open at the other end. This represents at a first approximation a quarter wavelength resonator. According to Seto [3.15], the resonance frequencies f_r are given by

$$f_r = \frac{n \cdot c_o}{4 \cdot L_1} \quad ; \quad n = 1,3,5, etc., \tag{3.10}$$

where c_o is the average speed of sound and L_1 is the length of the front pipe.

The connecting pipes and the tail-pipe are open at both ends and represent a half wavelength resonator. Hence, according to Seto [3.15], the resonance frequencies f_r are given by

$$f_r = \frac{n \cdot c_o}{2 \cdot L_3} \quad ; \quad n = 1,2,3, etc., \tag{3.11}$$

where L_3 is the length of the tail-pipe.

According to Peat, Callow and Bannister [3.5], each element that consists of a chamber and pipe can also be related to a cavity resonance f_r expressed by

$$f_r = \frac{c_o}{2 \cdot \pi} \sqrt{\frac{s}{V \cdot L_3}}, \tag{3.12}$$

where V is the chamber volume, s is the cross-sectional area of the tail-pipe and L_3 is the length of the tail-pipe and all transverse dimensions are a small fraction of the wavelength. Equations (3.10), (3.11) and (3.12) only provide an approximate answer, unless the appropriate end corrections are added to the length of the pipe [1.7, 2.13] to obtain the effective position of reflection.

The resonance frequencies f_r of the expansion chamber are related to the length of the chamber L_2. According to Beranek [3.14], the resonance behaviour is similar to the pipe open at both ends and occurs at

$$f_r = \frac{n \cdot c_o}{2 \cdot L_2} \quad ; \quad n = 1,2,3, etc.. \tag{3.13}$$

It turns out that the acoustic energy propagation is the highest at resonances and lowest at anti-resonances [1.2]. The optimum acoustic performance is established by means of systematic tuning of the connecting pipe lengths and the corresponding position of the silencers to ensure that resonances are well separated. Silencer elements may also include [2.16] flow reversals, cross-flows, perforations and absorption material that enhance their resistive performance. However, for the purpose of this study, for the sake of simplicity, only expansion chambers were considered.

3.3.3 Acoustic performance of a simple exhaust system

The most effective way to describe exhaust system acoustic performance is to evaluate the relative component wave amplitudes $P^{\pm}$ throughout the system. They can readily be used to describe the acoustic attenuation (see equation (3.5)) of the elements or system, or the relative change in acoustic power transmission (see equation (3.4)) along the system [2.13]. These acoustic quantities provide a simple and quantitative description of the acoustic characteristics of the exhaust system that give insight into the acoustic behaviour of the system. They also serve as a guide during the optimisation process to evaluate the effectiveness of geometric modifications.

On the other hand, the transfer function, where an external microphone is used (equation (3.7)), describes the system as a whole. However, without skilled interpretation, transfer functions provide little insight into the acoustic contribution of individual elements. Estimates of insertion loss (equation (3.8)) require the measured or calculated acoustic power of both a reference system W_1 and the system under investigation W_2. Therefore, it is assumed that the source impedance is known and invariant. However, the evidence shows [1.9] that the source impedance is normally effected when the system is modified due to the change in acoustic load. It is also

difficult to interpret insertion loss estimates, since the observed result is the relative combination of two systems. One also notes that the transmission loss index (equation (3.9)) represents the acoustic performance of the element in isolation, with an anechoic load. Therefore, standing waves normally present in the acoustic transmitted field [2.13] are neglected, since the reflection coefficient at the termination is zero (anechoic termination). The acoustic contribution of the tail-pipe resonance (equation (3.11)) and the cavity resonance (equation (3.12)) are disregarded. These resonances have a significant influence on the acoustic behaviour and are an essential design consideration in the development of any exhaust system.

One can conclude that either the relative acoustic attenuation or the normalised transmitted acoustic power flux normally provides the most useful and effective description of the acoustic performance since these two quantities identify both the attenuation and resonant behaviour of individual elements under specific operating conditions. Such dimensionless factors are independent of the source of excitation and represent the characteristic acoustic behaviour of the system.

To demonstrate the acoustic performance of individual elements and the system as a whole one can consider the simple exhaust system represented in Figure 3.7 below. The system consists of two elements that are both simple expansion chambers of different geometry, while each element consists of a chamber volume and tail-pipe.

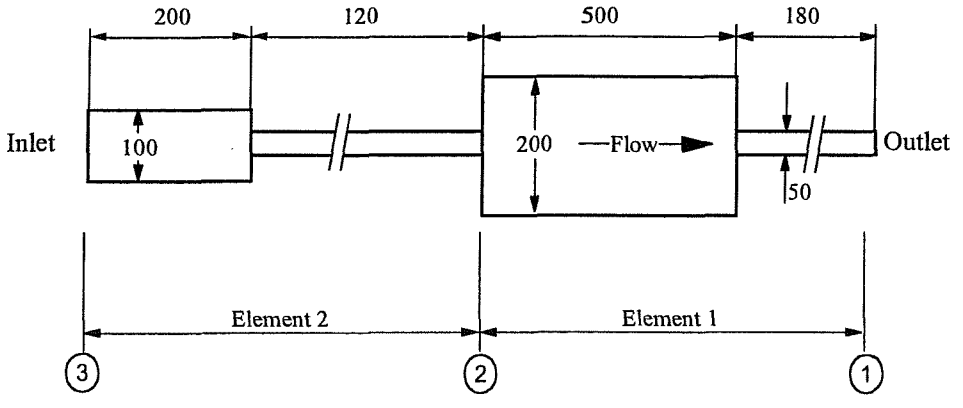

Figure 3.7 Schematic representation and geometric details of a simple exhaust system consisting of two elements (all dimensions are in millimetres).

Element 1 consists of a 200 mm diameter expansion chamber with a length of 500 mm and a tail-pipe with a length of 180 mm. The predicted attenuation spectrum $AL_{2,1}$ is shown in Figure 3.8 below. The calculation was performed assuming a constant temperature of 20^0 C (speed of sound = 342 m/s) and zero mean flow for the sake of simplicity, but does include appropriate end corrections at area discontinuities [1.2]. One notes that the acoustic performance of the element is the combination of the interacting contribution of the 500 mm long expansion chamber and the tail-pipe. The spectral behaviour is cyclical, displaying attenuation minima when the chamber and tail-pipe acoustic lengths are an integer multiple of half the acoustic wavelength as expressed by equations (3.11) and (3.13). The maximum attenuation of the expansion chamber occurs at frequencies f_c, when its length corresponds to an odd integer multiple of a quarter of the acoustic wavelength,

$$f_c = \frac{n \cdot c_o}{4 \cdot L} \quad ; \quad n = 1,3,5,etc., \tag{3.14}$$

where c_o is the speed of sound and L is the length of the chamber.

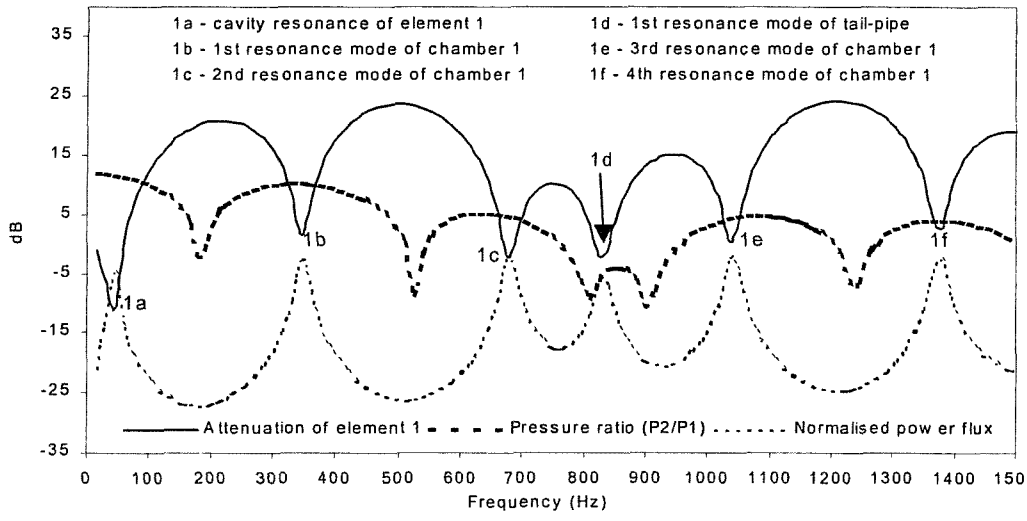

Figure 3.8 The predicted attenuation $AL_{2,1}$, transfer function $H_{2,1}$ and normalised power flux spectra at the inlet of element 1 (normalised to the incident power at the inlet of element 1) for the exhaust system in Figure 3.7 on page 49.

The chamber attenuation is always positive, while that for the tail-pipe attached to a chamber contraction is always negative. The relative amplitude of the attenuation maxima for the expansion [2.13] is related to the cross-sectional areas of the chamber and tail-pipe ratio, expressed by

$$\text{Attenuation level} = 20 \cdot \log\left(\frac{S_c}{S_p}\right) \text{(dB)}, \tag{3.15}$$

where S_c is the cross-sectional areas of the chamber, and S_p is the cross-sectional area of the tail-pipe. This gave a maximum attenuation of 24dB for the chamber of element 1. The negative contribution of the tail-pipe resonances reduced the overall attenuation performance. This is demonstrated by the fact that the maximum attenuation levels of the expansion chamber $AL_{2,1}$ were severely reduced by the first half wavelength resonance of the tail-pipe at 825 Hz (see symbol 1d in Figure 3.8 on page 50). One should, however, avoid coincidence of chamber and tail-pipe resonances to obtain improved acoustic performance. Compared to acoustic attenuation, the transfer function spectrum $H_{2,1}$ or P_2/P_1 that is also displayed in Figure 3.8 on page 50 does not characterise the acoustic performance of element 1. The peaks and troughs show no relation to the attenuation and resonance behaviour of element 1 indicated by the power flux and attenuation spectra predictions.

The boundary conditions of an element are also influenced by the wave reflection from consecutive elements along the exhaust system. One can easily demonstrate [1.2, 2.13] that all the elements interact acoustically with each other. The acoustic interaction between element 1 and element 2 is clearly demonstrated by the modification of the attenuation spectrum of element 2 $AL_{3,2}$ in Figure 3.9 on page 52 at the frequencies corresponding to the resonances of element 1. One also notes that the maximum attenuation was now reduced to 12dB with the 100 mm diameter chamber expansion. The first resonance (see symbol 2b in Figure 3.9 on page 52) of the 200 mm long chamber (element 2) occurred at 857 Hz and almost coincides with that of the tail-pipe (element 1). The first half wavelength resonance (see symbol 2c in Figure 3.9 on page 52) of the 120 mm long connecting pipe occurred at 1245 Hz.

Figure 3.10 on page 53 shows the overall or system attenuation $AL_{3,1}$, which is the combined acoustic contribution of element 1 and element 2. The trough at 45 Hz and the modification to the attenuation spectrum at 150 Hz are related to the cavity resonances (equation (3.12)) of element 1 and 2 respectively. These resonances may also be observed in the individual attenuation spectra predicted for element 1 $AL_{2,1}$ in Figure 3.8 on page 50 and element 2 $AL_{3,2}$ in Figure 3.9 below.

The transmitted normalised power flux associated with each element and the system is also plotted in Figures 3.8 to 3.10. One notes that the normalised power flux corresponds to the inverse of the attenuation in a fairly systematic way. Therefore, the power flux can also be used to identify the acoustic contribution of individual element to the overall acoustic performance of an exhaust system to guide the optimisation process.

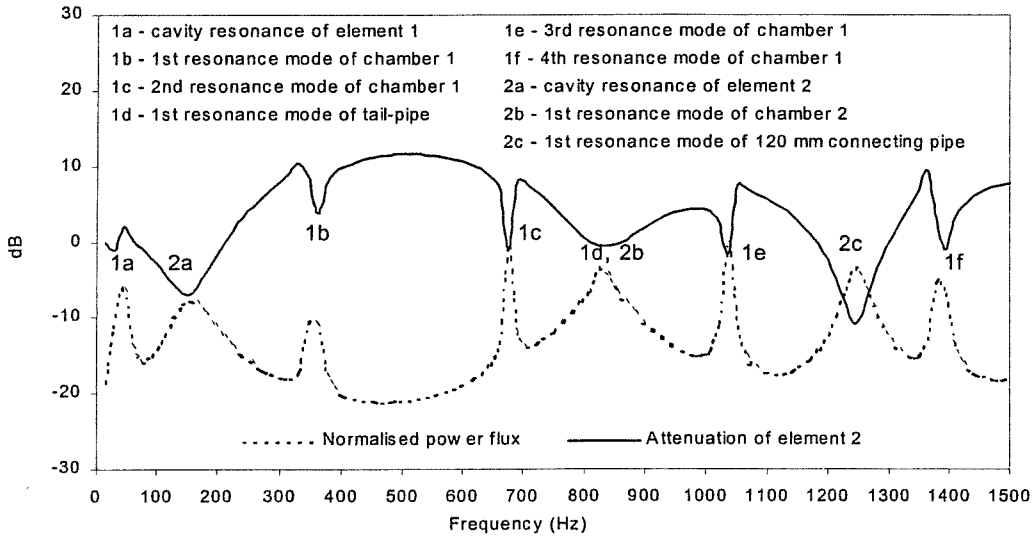

Figure 3.9 The predicted attenuation $AL_{3,2}$ and normalised power flux spectra at the inlet of element 2 (normalised to the incident power at the inlet of element 2) for the exhaust system in Figure 3.7 on page 49.

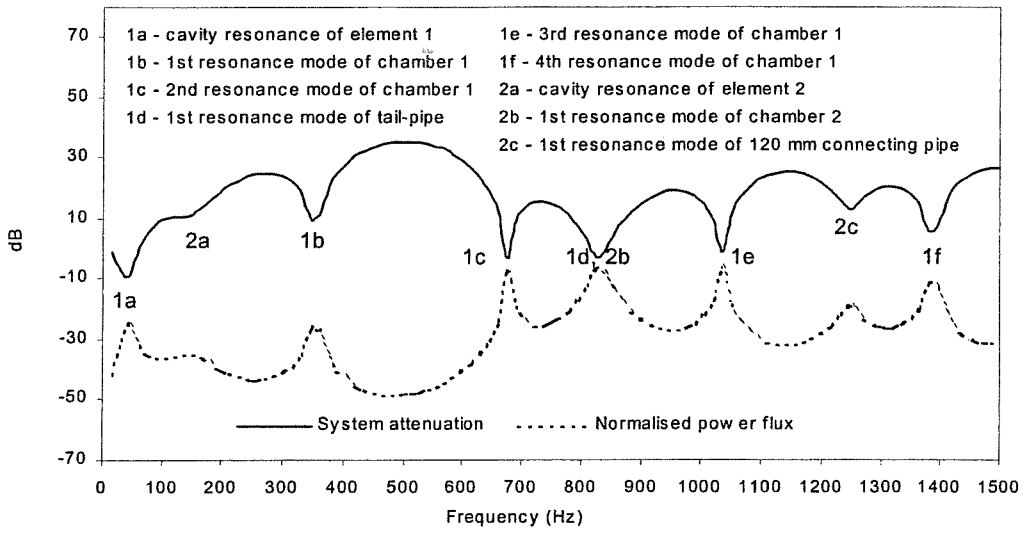

Figure 3.10 The predicted system attenuation $AL_{3,1}$ and normalised power flux spectra at the outlet of the system (normalised to the incident power at the inlet of the system) for the exhaust system in Figure 3.7 on page 49.

The overall development of the exhaust system is generally based on engine performance, fitment, structural dynamics, mechanical durability, thermal fatigue and industrialisation. Notwithstanding the design considerations for these functions, the author's experience has showed that the acoustic design and optimisation of the exhaust system still presents the main challenge to the overall development process. Although non-linear gas dynamic and hybrid predictive modelling techniques are becoming more popular, the use of linear acoustic theory is still widely used during the acoustic design process to rapidly optimise the acoustic performance of the exhaust system. Professional discussion [3.16] indicates that a non-linear gas dynamic programme used by the author's mother company yields longer calculation times which result in unacceptable development lead times if all analyses and calculations are based on such an approach. Although the hybrid method is faster, reliable results have normally been restricted to the first two harmonic components of exhaust noise emission (up to 600 Hz) [3.16]. For these reasons, linear acoustic theory is preferred because it facilitates the rapid production of reliable results.

To this end, the interpretation and identification of the acoustic resonances of exhaust systems form an essential part of current design strategies. The acoustic optimisation is then accomplished by means of a systematic modification of the geometry to ensure that the resonances are well separated. This process is currently performed with linear acoustic software equipped for constant engine conditions. The variable mass flow and temperature generated during a run-up of the vehicle require appropriate scaling of the results, which can prove to be time-consuming, and in some cases, unreliable, due to the acoustic interaction between system elements. It is the author's view that an extension of existing software equipped for the changing flow conditions during engine acceleration is required to enhance the potential of existing software as an effective design tool. This subject is covered in detail in the next section.

3.4 ACOUSTIC PREDICTION OF EXHAUST SYSTEMS FOR TRANSIENT OPERATING CONDITIONS

One essential part of this study is the development of computational procedures to assess the acoustic performance of an exhaust system for the practical operating conditions of an engine. In practice, this implies the controlled acceleration or deceleration of the engine, which is also referred to as transient operating conditions. Currently, the linear acoustic code APEX is restricted to the calculation of predictions for constant engine speed conditions. For example, the programme was used in its standard format to obtain the acoustic predictions for the controlled engine speed measurements performed by Temple [1.9] and Yaseen [1.10]. For transient operating conditions a sequence of calculations is required at regular closely spaced engine speed intervals. The mass flow and temperature gradients generated during acceleration or deceleration of the engine should also be included, because these have a controlling influence on the acoustic performance of the exhaust system. For this reason it was necessary to adapt the APEX code for the transient operating conditions of the engine. This was implemented in a specially developed Labview programme.

The objective was to predict the acoustic quantities of the order components for a run-up of the engine. A schematic presentation of the order components of a four-cylinder four-stroke engine is set out in Figure 3.11 below.

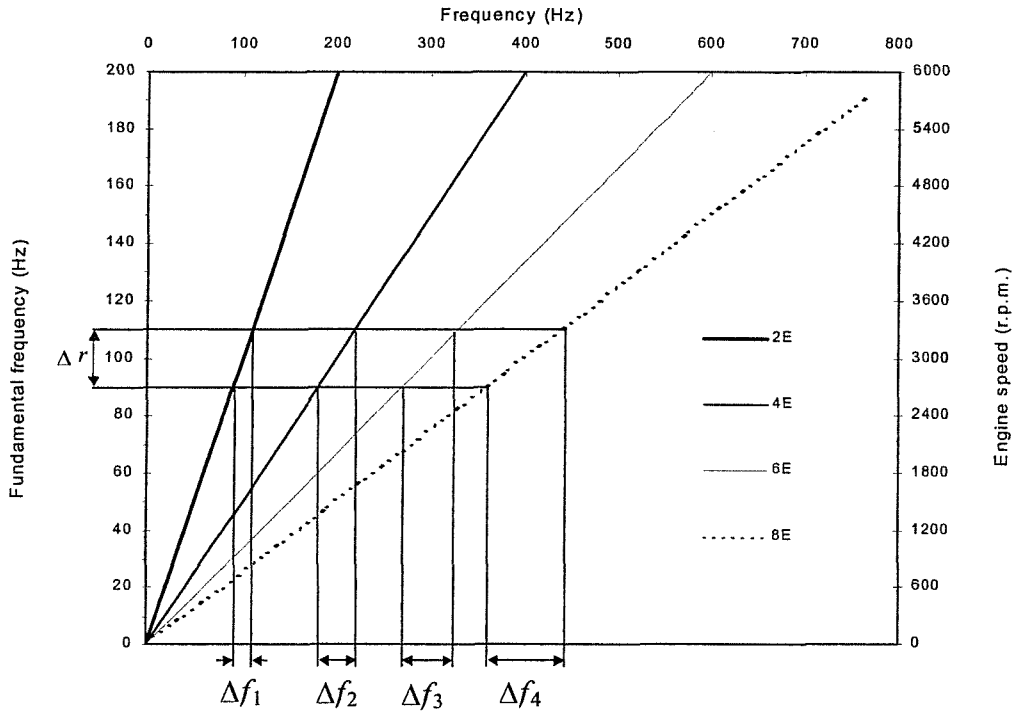

Figure 3.11 Schematic representation of the order components of a four-cylinder four-stroke engine, displaying the frequency range covered by each order (Δf_1 = 20 Hz, Δf_2 = 40 Hz, Δf_3 = 60 Hz and Δf_4 = 80 Hz) for a fundamental frequency interval Δr = 20 Hz (600 r.p.m.).

One notes that the frequency of each order F_K, and the frequency range Δf_K covered by each order for a particular measurement interval Δr are related to the order number K,

$$F_K = K \cdot F_1 \quad ; \quad K = 1, 2, 3, etc., \tag{3.16}$$

where F_1 refers to the fundamental frequency, in this case the 2E component.

Also, $\Delta f_K = K \cdot \Delta r \quad ; \quad K = 1, 2, 3, etc..$ (3.17)

To obtain transient results, it is necessary to calculate the wave components $P^{\pm}$ at the inlet and outlet of each element at closely-spaced engine speed intervals with the corresponding mass flow and temperature. This involves a large number of calculations (between 30 and 60 intervals depending on the engine speed interval Δr) that are time-consuming and impractical to perform manually. Therefore, it has been necessary to prepare an extensive software programme in Labview that performs the calculations in succession. The programme allows the user to specify the engine type, the engine speed range and the engine speed interval Δr. Next, the harmonic spectrum for each engine speed interval is calculated. The temperature and mass flow data for each engine speed interval may then be assumed or actual measured data may be imported into the programme. After the geometry of the exhaust system has been defined, the Labview programme executes the APEX code which calculates the wave components $P^{\pm}$ at the harmonic frequencies F_K for each individual engine speed interval. The order components are then extracted from the harmonic spectral matrix. A flow diagram of the Labview programme is shown in Figure 3.12 on page 57.

To demonstrate the acoustic behaviour for transient conditions, an acoustic prediction has been performed with the Labview programme for the exhaust system in Figure 3.7 on page 49. A typical run-up of a four-cylinder four-stroke engine was simulated. The transient condition was represented by 34 engine speed intervals from 1000 to 5950 r.p.m., giving an engine speed interval of 150 r.p.m. (Δr = 5 Hz). Table 3.1 on page 58 shows the harmonic frequencies, inlet and outlet temperatures and mass flow for each engine speed interval. Linear temperature and mass flow gradients were assumed for the speed range of the engine, and calculations were performed for the first four order components (2E, 4E, 6E and 8E). Figure 3.13 on page 59 shows the predicted system attenuation $AL_{3,1}$ for the first four orders plotted against engine speed.

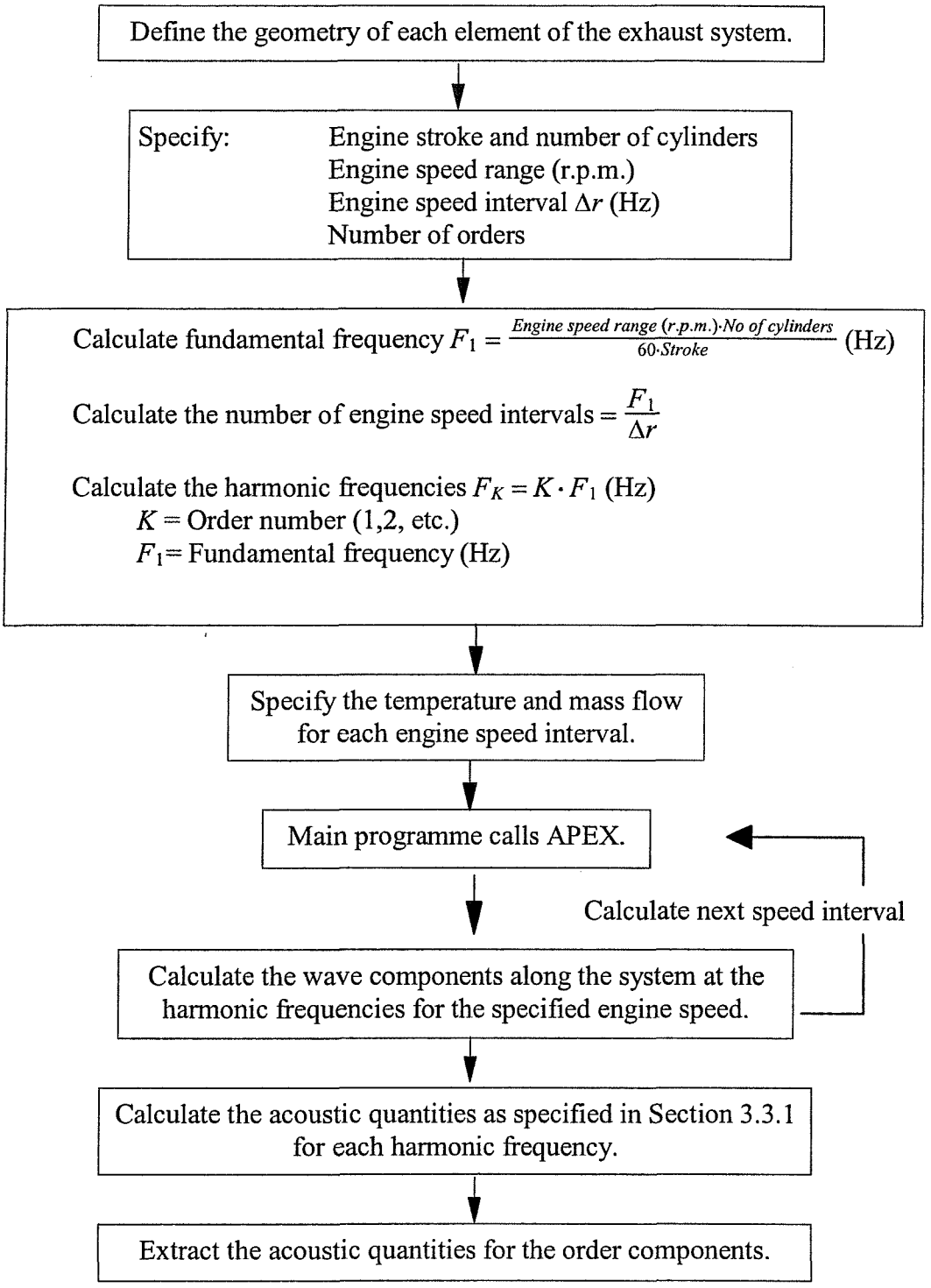

Figure 3.12 Flow diagram of the Labview software programme developed to predict the acoustic performance of silencer components for transient operating conditions.

Interval	Engine speed (r.p.m.)	2E (Hz)	4E (Hz)	6E (Hz)	8E (Hz)	Inlet Temp (^{o}C)	Outlet Temp (^{o}C)	Mass flow (kg/s)
1	1000	33	67	100	133	400	200	0.02
2	1150	38	77	115	153	409	206	0.022
3	1300	43	87	130	173	418	212	0.025
4	1450	48	97	145	193	427	218	0.027
5	1600	53	107	160	213	436	224	0.03
6	1750	58	117	175	233	445	230	0.032
7	1900	63	127	190	253	455	236	0.035
8	2050	68	137	205	273	464	242	0.037
9	2200	73	147	220	293	473	248	0.039
10	2350	78	157	235	313	482	255	0.042
11	2500	83	167	250	333	491	261	0.044
12	2650	88	177	265	353	500	267	0.047
13	2800	93	187	280	373	509	273	0.049
14	2950	98	197	295	393	518	279	0.051
15	3100	103	207	310	413	527	285	0.054
16	3250	108	217	325	433	536	291	0.056
17	3400	113	227	340	453	545	297	0.059
18	3550	118	237	355	473	555	303	0.061
19	3700	123	247	370	493	564	309	0.064
20	3850	128	257	385	513	573	315	0.066
21	4000	133	267	400	533	582	321	0.069
22	4150	138	277	415	553	591	327	0.071
23	4300	143	287	430	573	600	333	0.073
24	4450	148	297	445	593	609	339	0.076
25	4600	153	307	460	613	618	345	0.078
26	4750	158	317	475	633	627	352	0.081
27	4900	163	327	490	653	636	358	0.083
28	5050	168	337	505	673	645	364	0.086
29	5200	173	347	520	693	655	370	0.088
30	5350	178	357	535	713	664	376	0.09
31	5500	183	367	550	733	673	382	0.093
32	5650	188	377	565	753	682	388	0.095
33	5800	193	387	580	773	691	394	0.098
34	5950	198	397	595	793	700	400	0.1

Table 3.1 Engine speed, frequency of harmonic components, temperature and mass flow data for a typical run-up of a four-cylinder four-stroke engine.

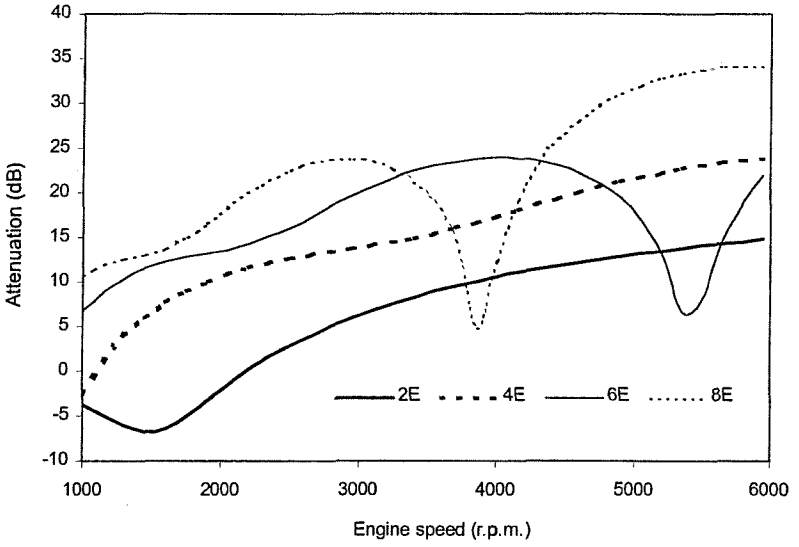

Figure 3.13 Predicted system attenuation $AL_{3,1}$ of the exhaust system in Figure 3.7 on page 49 for a typical engine run-up, showing the first four order components (2E, 4E, 6E and 8E) versus engine speed.

Here, each order covers a specific frequency range and frequency resolution as indicated in Table 3.1 on page 58. It is, however, essential to ensure that the frequency resolution for the highest order is adequate to demonstrate narrow-band acoustic characteristics. In this case, the engine speed interval of 150 r.p.m. ($\Delta r = 5$ Hz) gave a frequency resolution of $\Delta f_3 = 15$ Hz for the 6E component and $\Delta f_4 = 20$ Hz for the 8E component that appears to be sufficient to describe the 6E resonance at 5500 r.p.m. and the 8E resonance at 3800 r.p.m.. Alternatively, when the results are plotted on a frequency scale as shown in Figure 3.14 on page 60, one notes that the attenuation levels of the orders differ at overlapping frequencies.

This is particularly evident for the resonance above 500 Hz that occurs at 513 Hz for the 8E component and at 534 Hz for the 6E component. The amplitude variation and frequency shift of the orders at corresponding frequencies are caused by the variable mass flow and temperature generated during the simulated engine run-up. These results clearly demonstrate the influence of the variable gas flow properties on the acoustic behaviour of the exhaust system for transient engine conditions.

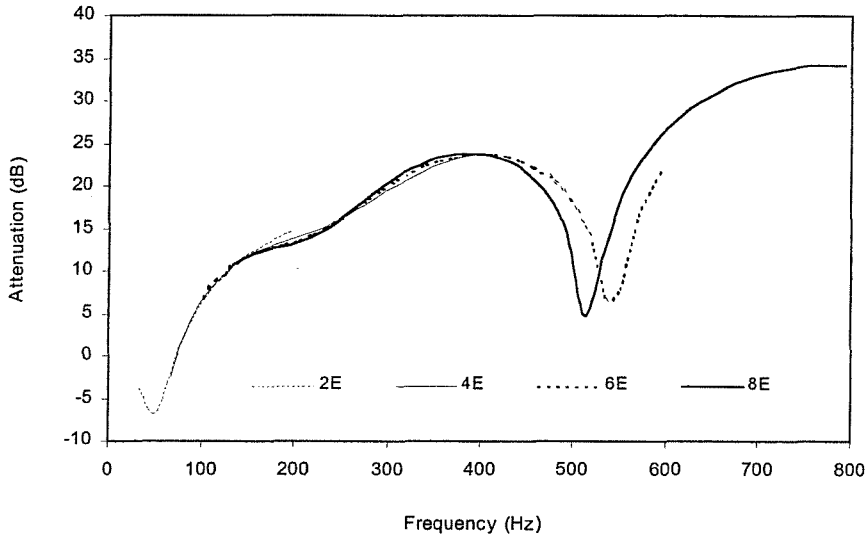

Figure 3.14 Predicted system attenuation spectra $AL_{3,1}$ of the exhaust system in Figure 3.7 on page 49 for a typical engine run-up, showing the order components (2E, 4E, 6E and 8E) on a frequency scale.

3.5 CONCLUSION

This chapter presented a brief outline of exhaust system design and focused on the assessment of the acoustic behaviour of the exhaust system. The acoustic behaviour of an exhaust system is determined by its geometry and the spectral distribution depends on the local speed of sound c and Mach number M. The acoustic performance is governed by system resonances related to the length of the wave path through each individual element. Evaluation of a simple exhaust system consisting of two expansion chambers also indicated that the elements interact dynamically with each other, as does the system [1.9] with the source of excitation. Therefore, it is essential to identify the contribution of each individual element to the overall system's acoustic performance. The author's experience suggests that the most effective way to describe exhaust system acoustic performance is to evaluate the relative component wave amplitudes $P^{\pm}$ throughout the system. To this end, attenuation and normalised power flux provide a simple description of the acoustic performance to facilitate rapid acoustic optimisation. Experience also indicates that

the acoustic optimisation of the exhaust system is accomplished by means of a systematic tuning of the geometry to avoid coincidence of system resonances.

However, it was necessary to make the appropriate additions and adjustments to existing validated linear acoustic code (APEX) to adapt it to follow changing temperature and flow conditions during engine acceleration. Preliminary acoustic predictions performed with the new software programme demonstrated the significant influence of the variable mass flow and temperature on the acoustic behaviour of the exhaust system for a constant acceleration run-up. For example, the variable gas dynamic conditions resulted in an amplitude variation and frequency shift of the harmonic components at corresponding frequencies. The new software was used to predict the acoustic performance of a silencer component for the practical operating conditions of a vehicle described in Chapter 5. It was also applied as part of a rational design strategy to facilitate the rapid acoustic optimisation of an exhaust system, as set out in Chapter 6.

APPENDIX 3.1

ACOUSTIC PROPAGATION OF WAVE ENERGY THROUGH THE EXHAUST SYSTEM

The modelling of the mainly periodic wave motion requires an analytical description of the mean and fluctuating fluid motion throughout the system by means of the equations of mass, momentum and energy transport based on fluid properties, geometry and boundary conditions. The transmission, reflection and dissipation of acoustic energy are determined by boundary conditions. Each spectral component of the forward travelling wave p^+ has a propagation speed of $c+u$ and the reflected component wave p^- has a speed of $c-u$, where c and u are the speed of sound and flow velocity respectively, both functions of time and axial position. The physical variables and fluid properties (such as density ρ, pressure p, velocity u with time average mean value u_o, kinematic viscosity ν, thermal conductivity k_T, ratio of specific heat γ) all depend on the local absolute temperature T of the flow. Therefore, the acoustic behaviour of an exhaust system depends on the local sound propagation speed $c(1 \pm M)$, where M is the Mach number u_o/c_o [1.2]. The plane wave propagation of wave energy in exhaust systems, based on the acoustic approximation, can be described by a linearised wave equation, as fully documented in [1.2, 2.13]. This is briefly summarised in what follows here.

A3.1.1 Acoustic wave propagation along flow ducts

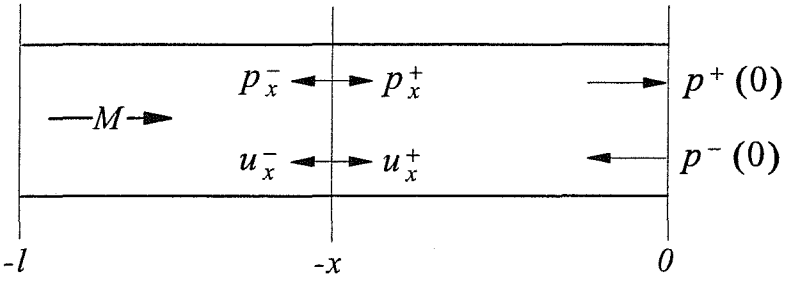

Figure A3.1.1 Uniform pipe with mean flow, u_o.

A uniform pipe of length l, radius a and mean flow at Mach number $M = u_o/c_o$ is shown in Figure A3.1.1. Dynamic equilibrium for fluctuations when $u(x,t) = u_o + u$, where u is the fluctuating, and u_o is the time average flow velocity, is expressed by

$$\rho_o[\partial/\partial t + u_o(\partial/\partial x)]u^+ = -\partial p^+/\partial x, \qquad \text{(A3.1.1)}$$

$$\rho_o[\partial/\partial t + u_o(\partial/\partial x)]u^- = -\partial p^-/\partial x, \qquad \text{(A3.1.2)}$$

where the subscript $_o$ refers to ambient values.

This is satisfied at any x for each spectral component of angular frequency w by

$$p^+(x,t) = p^+(0)\exp i(\omega t - k^+x), \quad p^-(x,t) = p^-(0)\exp i(\omega t + k^-x), \qquad \text{(A3.1.3a,b)}$$

$$u^+(x,t) = u^+(0)\exp i(\omega t - k^+x), \quad u^-(x,t) = u^-(0)\exp i(\omega t + k^-x), \qquad \text{(A3.1.4a, b)}$$

where k refers to the wave number and $\omega = 2\pi f$, while

$$k^+ = \omega/(c_o + u_o) \text{ and } k^- = \omega/(c_o - u_o). \qquad \text{(A3.1.5a, b)}$$

Also, one can easily show [2.13] that

$$p(x,t) = p_x^+ + p_x^-, \qquad \rho_o c_o u(x,t) = p_x^+ - p_x^-. \qquad \text{(A3.1.6a, b)}$$

The fluctuating pressure components are expressed by

$$p(x,t) = p^+(0)\exp i(Mk^*x)[\exp(-ik^*x) + r_o\exp(ik^*x)]\exp(i\omega t), \qquad \text{(A3.1.7)}$$

where $$k^* = (k^+ + k^-)/2 = (\omega/c_o)/(1-M^2) = k/(1-M^2). \qquad \text{(A3.1.8)}$$

This represents the combination of a progressive and interfering wave motion, with the node spacing defined by k^*.

With reference to Figure A3.1.1 the corresponding reflection coefficients are defined by

$$r_o = p^-(0)/p^+(0), \quad r_x = p_x^-/p_x^+ = (\zeta x - 1)/(\zeta x + 1). \qquad \text{(A3.1.9a, b)}$$

Impedances are defined by

$$Z_o = p(0)/u(0), \qquad Z_x = p_x/u_x = \rho_o c_o (p_x^+ + p_x^-)/(p_x^+ - p_x^-). \qquad \text{(A3.1.10a, b)}$$

Relative impedances are defined by

$$\zeta x = Z_x/\rho_o c_o = (1 + r_x)/(1 - r_x). \qquad \text{(A3.1.11a, b)}$$

The transmission coefficient is defined by

$$T_i = p_x^+/p_o^+, \qquad T_r = p_x^-/p_o^-. \qquad \text{(A3.1.12a,b)}$$

To include visco-thermal wave attenuation to first order, one replaces k by β, where $\beta = \omega/c_o + a(1 - i)$ and $a = (a \cdot c_o)^{-1}(\omega\nu/2)^{0.5}[1 + (\gamma - 1)\,\mathrm{Pr}^{-0.5}]$, where ν is the kinematic viscosity and Pr the Prandtl number [2.13]. Then

$$p(x,t) = p_x^+ + p_x^- \quad \text{and} \quad \rho_o c_o u(x,t) = d_x^+ p_x^+ - d_x^- p_x^-, \qquad \text{(A3.1.13a ,b)}$$

where $$d^\pm = [k + a(1 - i)]/[k \pm Ma(1 - i)]. \qquad \text{(A3.1.14)}$$

A3.1.2 Wave component transfer at discontinuities [1.2]

Given the geometry, M, T, p_2^+, p_2^-, to find p_1^+, p_1^- where mean variables are p_o, ρ_o, u_o, the acoustic fluctuations are p, ρ, u.

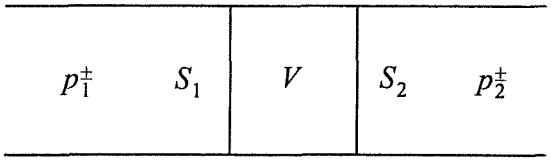

Figure A3.1.2 Control volume V and surfaces S.

Follow a sequence of analytical steps:

a) Identify and prescribe a relevant control volume V, with surface S.

b) For volume V, set out the integral relations describing:

   i) conservation of mass $\int_s \rho' u' dS = 0$, where $\rho' = \rho_o + \rho$, $u' = u_o + u$;

   ii) conservation of energy $\int_s [h' + (u')^2/2] dS$; with isentropic processes $\rho = p/c_o^2$, enthalpy, $h' = h_o + p/\rho_o + T_o s$ and with fluctuating entropy, $s = (-1/\rho_o T_o)\delta/(\gamma - 1)$, $\rho = (p + \delta)/c_o^2$;

   iii) momentum flux balance $\int_s [\rho'(u')^2 + p'] dS = \Sigma F = 0$, with fixed boundaries.

c) Subtract the terms relating to the mean motion from i), ii) and iii).

d) Discard fluctuating terms of order higher than first (acoustic approximation).

e) Express fluctuating velocity u, density ρ and pressure p in terms of the equivalent progressive component wave amplitude p^+ and p^-.

f) Satisfy all relevant conditions at fixed boundaries. With rigid boundaries the component of u' normal to it will be zero.

g) The result will be a set of three expressions expressing p_1^+ and p_1^- in terms of p_2^+, p_2^- and δ. With isentropic processes, $\delta = 0$, so that i) with either ii) or iii) are sufficient. Otherwise, eliminate δ first, to give two new equations in terms of p_2^+ and p_2^- alone.

h) Solve for p_1^+ and p_1^- in terms of p_2^+ and p_2^-.

i) Evaluate T_i, T_r, r_1, for a given $r_2 = p_2^-/p_2^-$.

A3.1.3 Plane wave reflection at an open unflanged pipe

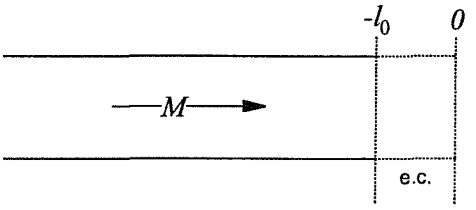

Figure A3.1.3 An open unflanged pipe and end correction (e.c.)

The end of the pipe in Figure A3.1.3 is at $-l_o$, where

$$r = R_M \exp i\theta = -R_M \exp(-2ikl_M).$$

With zero flow and plane waves, pipe radius a, $0 < ka < 1.8$:

a) with $ka < 0.5$, $l_o/a = 0.6133 - 0.1168(ka)^2$,

$0.5 < ka < 2$, $l_o/a = 0.6393 - 0.1104ka$;

b) $R_o \simeq 1 + 0.01336ka - 0.59079(ka)^2 + 0.33756(ka)^3 + 0.6432(ka)^4$.

With outflow at $M > 0$,

a) i) $l_M = l_o$, or ii) $l_M = l_o[1 - M^2]$, data inconclusive :

b) $R_M = R_o f(M)$ [2.1].

A more detailed description of the linear acoustic theory applicable to the work in this thesis is provided in Section 4.2, "Wave decomposition calculations" in Chapter 4.

CHAPTER 4

DEVELOPMENT OF A MEASUREMENT TECHNIQUE TO ASSESS THE ACOUSTIC PROPERTIES OF A SILENCER COMPONENT FOR TRANSIENT CONDITIONS

4.1 INTRODUCTION

The measurement of radiated tail-pipe noise with order analysis techniques is common practice in the automotive industry. However, a description of the evaluation of the acoustic behaviour of individual silencer components for the practical operating conditions of an engine has not yet been published, according to the author's knowledge. Essentially such an evaluation involves the estimation of the wave components $P^{\pm}$ inside the exhaust system while the engine is accelerating.

Swept-sine excitation was adopted by Holland and Davies [4.1] to measure acoustic power flux in flow ducts. They showed how swept-sine excitation improved reliability of the measurements in the presence of flow noise by improving the signal-to-noise ratio during the analysis of the data. This provided a useful basis for the measurement technology discussed here. However, some fundamental changes were required in the application of the method to measurements on a running engine. So, for example, the higher harmonics of exhaust noise require much faster sweep-rates. Therefore, the analysis for the proposed measurement technique was optimised to produce reliable results limited to the first four harmonics [1.1]. Furthermore, the high sound pressure levels as well as the variable mass flow and temperature gradients generated during the transient operating conditions of a vehicle

were some of the other issues that had to be considered in the experimental procedure.

Before performing tests on a running engine, a measurement technique was developed first on a bench test to simulate partly the acoustic conditions experienced during engine acceleration. Procedures are presented in Section 4.2 that describe the estimation of $P^{\pm}$ associated with one-dimensional wave motion for strongly reactive silencer elements. $P^{\pm}$ are calculated from the complex transfer function spectra acquired simultaneously at the inlet and outlet of a silencer component from two pairs of flush wall-mounted transducers. The bench test set-up for the experiment is described in Section 4.3. The variable sound pressure is captured using order analysis techniques; the basic principles of the fixed sampling rate method and order tracking are explained and demonstrated in Section 4.4. The estimation of the wave components from sound pressure measurements at practical representative flow velocities tends to be problematic due to poor signal-to-noise ratios [1.11, 4.1]. Therefore, it is essential to establish the most effective procedure for measurements in the presence of mean flow, as described in Section 4.5. Finally, in Section 4.6, the technique is applied to measure the acoustic quantities of a simple expansion chamber on a cold flow test bench with transient harmonic excitation. Measurements are compared to predictions calculated with a validated numerical code (APEX) to verify the measurement technique.

4.2. WAVE DECOMPOSITION CALCULATIONS

The wave decomposition method has been the subject of extensive study. The method was developed as a reliable and robust tool to validate the acoustic performance of silencer components for stationary bench test conditions. Bento Coelho [2.17] used the method to determine the incident wave attenuation and the upstream reflection coefficient of perforated resonators for stationary bench test conditions. The application of the four-microphone wave decomposition method was also extensively described in a paper by Davies, Harrison and Collins [2.16]. They

used the method to validate the linear acoustic models of multiple path silencers with random excitation and mean flow. Holland and Davies [4.1] suggested some further refinements to the signal processing for the method which is adopted for this study.

The wave component spectra are determined from the auto spectra, cross spectra and transfer functions between two pairs of microphones placed at the inlet and outlet side of the silencer component. With reference to Figure 4.1 below, at each frequency the wave components $P^{\pm}$ at the inlet and outlet side are calculated from the corresponding spectral pressure measurements (P_1, P_2, P_3 and P_4) to characterise the acoustic performance of the system. These include pressure ratios, reflection coefficients, acoustic impedance, attenuation and power flux spectra, as defined in Chapter 3, Section 3.3.1.

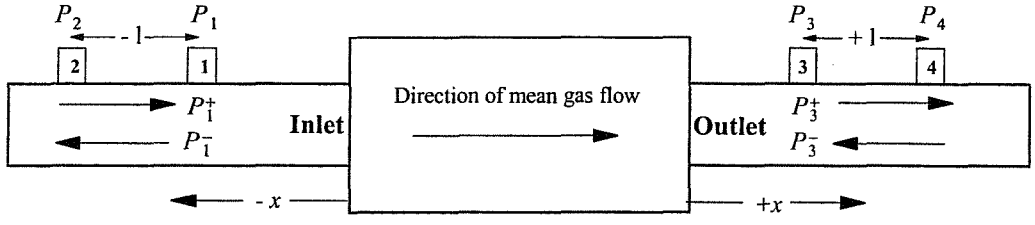

Figure 4.1 Four-microphone wave decomposition set-up.

At the inlet side of the system, the acoustic pressure at any plane can be related to the wave components at station #1.

Thus, with one-dimensional waves,

$$\hat{P}_x(\omega,x) = \hat{P}_1^+ e^{-i\hat{k}^+ x} + \hat{P}_1^- e^{i\hat{k}^- x}. \qquad (4.1)$$

The symbol $\hat{}$ over a quantity indicates that it is complex; and the distance x is determined relative to station #1.

Hence, $\hat{P}_1(\omega,x) = \hat{P}_1^+ + \hat{P}_1^-$ for $x = 0$, (4.2)

and $\hat{P}_2(\omega,x)=\hat{P}_1^+e^{-i\hat{k}^+l}+\hat{P}_1^-e^{i\hat{k}^-l}$ for $x=l.$ (4.3)

The complex wave number $\hat{k}$ is defined by

$$\hat{k}=\frac{\omega}{c}-ia;\quad \hat{k}^+=\frac{\hat{k}}{(1+M)},\quad \hat{k}^-=\frac{\hat{k}}{(1-M)}, \tag{4.4a, b, c}$$

where M is the mean flow Mach number, a is the visco-thermal attenuation coefficient [2.13] and c is the speed of sound. The physical variables and fluid properties that depend on the exhaust gas temperature are described in Appendix 4.1.

The auto spectrum $C_{1,1}$ at station #1 is defined by

$$C_{1,1}=(\hat{P}_1^++\hat{P}_1^-)(\hat{P}_1^++\hat{P}_1^-)^*, \tag{4.5}$$

where * represents the complex conjugate.

The cross-spectrum $C_{2,1}$ between stations #2 and #1 is defined by

$$\hat{C}_{2,1}=(\hat{P}_1^+e^{-i\hat{k}^+l}+\hat{P}_1^-e^{i\hat{k}^-l})(\hat{P}_1^++\hat{P}_1^-)^*, \tag{4.6}$$

and the reflection coefficient at the inlet side is expressed by

$$\hat{R}_1=\frac{\hat{P}_1^-}{\hat{P}_1^+}. \tag{4.7}$$

Hence, $$\frac{\hat{C}_{2,1}}{C_{1,1}}=\frac{e^{-i\hat{k}^+l}+\hat{R}_1e^{i\hat{k}^-l}}{1+\hat{R}_1}, \tag{4.8}$$

$$\hat{R}_1=-\left(\frac{\hat{C}_{2,1}-C_{1,1}e^{-i\hat{k}^+l}}{\hat{C}_{2,1}-C_{1,1}e^{i\hat{k}^-l}}\right), \tag{4.9}$$

$$\hat{R}_1 = -\left(\frac{\hat{H}_{2,1} - e^{-i\hat{k}^+ l}}{\hat{H}_{2,1} - e^{i\hat{k}^- l}}\right), \tag{4.10}$$

where $\hat{H}_{2,1} = \dfrac{\hat{P}_2}{\hat{P}_1}$ is the transfer function between the signals at stations #2 and #1.

From equation (4.5),

$$C_{1,1} = (P_1^+)^2(1+\hat{R}_1)(1+\hat{R}_1)^*. \tag{4.11}$$

Therefore it follows that the modulus of the incident wave component at station #1 is

$$\hat{P}_1^+ = \frac{\sqrt{C_{1,1}}}{|(1+\hat{R}_1)|}, \tag{4.12}$$

and the complex reflected wave component at station #1 is defined by

$$\hat{P}_1^- = \hat{R}_1 \cdot \hat{P}_1^+ . \tag{4.13}$$

If one notes that the phase of P_1^+ is chosen to be zero, equation (4.12) also gives the modulus of P_1^+.

The same procedure is followed to determine the wave components at the outlet side of the silencer component (stations #3 and #4), using station #3 as the reference.

Hence, the reflection coefficient at station #3 is

$$\hat{R}_3 = -\left(\frac{\hat{H}_{4,3} - e^{-i\hat{k}^+ l}}{\hat{H}_{4,3} - e^{i\hat{k}^- l}}\right). \tag{4.14}$$

The phase relationship between stations #3 and #1 relative to station #1 can be estimated from the cross spectrum $\hat{C}_{3,1}$ between stations #3 and #1 [4.1] to determine the complex value of P_3^+:

$$\hat{P}_3^+ = P_3^+ \left(\frac{\hat{C}_{3,1}}{(\hat{P}_3^+ + \hat{P}_3^-)(\hat{P}_1^+ + \hat{P}_1^-)^*} \right). \tag{4.15}$$

The acoustic behaviour of silencer elements is normally highly reactive. Therefore, as expressed by equation (A3.1.7) on page 63, the interference between incident and reflected waves results in an acoustic field consisting of both standing and progressive waves [2.13]. Furthermore, the fluid motion generally includes other disturbances convecting with the flow. These are represented by turbulence and vortical motion generated at the duct boundary with wakes and separating shear layers [1.5]. The reliability of the estimation of $P^{\pm}$ depends on the extent to which the spectral estimates of $\hat{H}_{2,1}$ and $\hat{H}_{4,3}$ are contaminated by the flow-induced pressure fluctuations and other background noise [1.11]. Such conditions may result in poor signal-to-noise ratios at a specific frequency, particularly when pressure minima occur at one of the transducer positions [1.1]. Thus, for the estimation of $P^{\pm}$ in the presence of mean flow, effective procedures are required that improve the signal-to-noise ratio. These are described in Section 4.5.

Unreliable results can also be expected when the acoustic pressure signals at the pairs of transducers are almost identical. This condition occurs when the spacing between the microphones l is close to multiples of the half wavelength, $kl = n\pi$, with $n = 1, 2, 3, etc$ [1.11]. Appendix 4.2 provides a detailed discussion on the subsequent error that is introduced into the calculations and how it can be overcome by selecting a suitable transducer array.

4.3 BENCH TEST SET-UP

The silencer component and tubes containing the pressure transducer holders were placed inside a semi-anechoic chamber. Acoustic excitation was provided by means of a compression driver and the excitation signal was generated using a sweep functional generator. Air flow was controlled by an adjustable valve connected to a 6 bar line pressure and air velocity was estimated using a pitot tube. The rig was also provided with a water trap and a preliminary silencer to attenuate noise caused by the flow before it reached the system being tested. The bench test set-up is set out in Figure 4.2 below.

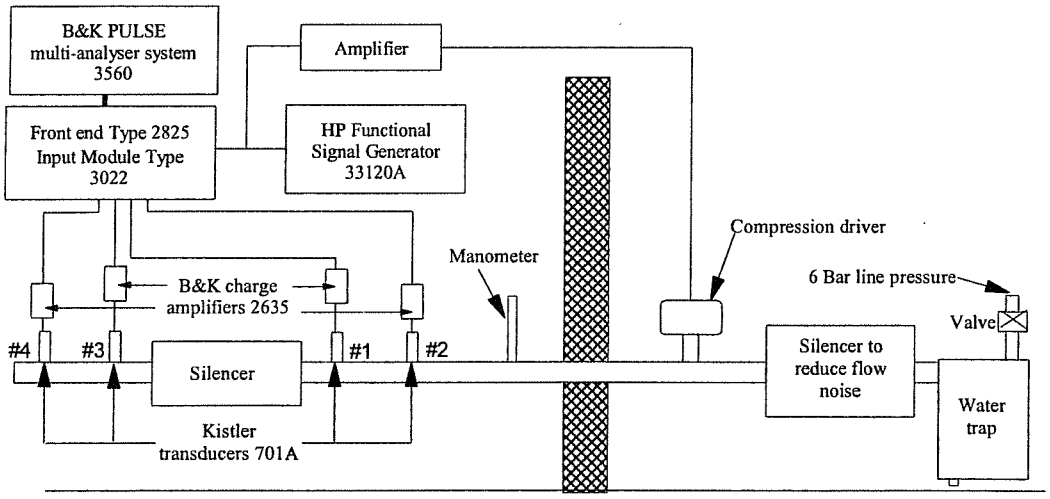

Figure 4.2 Experimental set-up to assess the acoustic properties of a silencer component on a cold flow bench.

The sound pressure time-history was measured using Kistler (Type 701A) quartz pressure transducers. The wide dynamic range (0 to 250 bar) and high sensitivity (80 *pC/bar*) of the transducers make them suitable for these dynamic pressure measurements. The transducers were mounted flush behind a 2 mm hole in the pipes to reduce the effect of flow-induced noise, as is shown in Figure 4.3 on page 74. Charge amplifiers were used to produce a voltage output signal proportional to the input charge of the transducers.

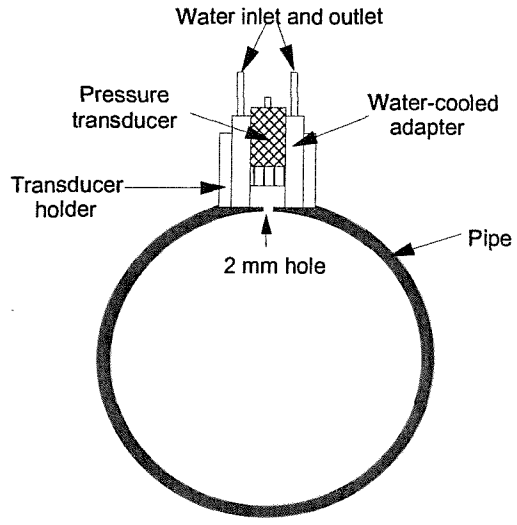

Figure 4.3 Pressure transducer installation.

4.4. ORDER ANALYSIS TECHNIQUES

The application of the measurement procedure involves the choice of a number of vital parameters. In contrast to normal stationary signal analysis, one should take into account that one has non-stationary signal records. The basic engine cycle frequency as well as the mass flow and temperature all change systematically in time, at a sweep-rate which is also never quite stationary. As was noted earlier, the idea is to extract the spectral characteristics of the time-varying signal at specific engine speed intervals to describe the acoustic quantities. Order analysis is a standard measurement technique tailored to extract the harmonic component information of a measurement from an acoustic-mechanical system under periodic loading [4.2]. It is ideally suited to capturing the exhaust noise harmonic pressure information at the four pressure transducer stations during a run-up or run-down of the engine. Order analysis methods are commonly divided into two basic groups: fixed sampling rate methods and order tracking methods [4.3].

4.4.1 Fixed sampling rate method

The fixed sampling rate method uses a fixed sampling rate and the Fast Fourier transform (FFT) of each record gives the corresponding frequency spectrum. The FFT algorithm describes a fast and efficient calculation of the Discrete Fourier Transform (DFT). The forward DFT is described by

$$G(f_k) = \frac{1}{N} \sum_{n=0}^{N-1} g(n) e^{-j \frac{2\pi kn}{N}}, \tag{4.16}$$

and the inverse transform is described by

$$g(t_n) = \sum_{k=0}^{N-1} G(k) e^{j \frac{2\pi kn}{N}}, \tag{4.17}$$

where $G(f_k)$ denotes the complex frequency spectrum and $g(t_n)$ denotes the time signal. Because the DFT applies to a discrete and periodic time signal and frequency spectrum, only a finite number of samples N are involved in the transform [4.4]. The DFT first performs a blockwise analysis of the time signal consisting of N samples from zero to T, the record length. For a sampling frequency of f_s, the sampling interval $\Delta t = 1/f_s$ and the block of N samples corresponds to a record length $T = N \cdot \Delta t$, where Δt is the time interval. The DFT assumes that the block of data is one period of an artificial infinitely long periodic signal. The frequency spectrum also consists of N evenly spaced samples from zero to the sampling frequency f_s. The interval of the frequency samples is also referred to as the frequency resolution $\Delta f = f_s/N$ [4.5]. Hence, the frequency resolution Δf of the analysis is the inverse of the record length T and it is, according to Randall [4.6] equal to

$$\Delta f = \frac{1}{T} = \frac{1}{N \cdot \Delta t} = \frac{f_s}{N}. \tag{4.18}$$

When the time function $g(t_n)$ is a real-value time function (for example, a physical time signal), then the frequency spectrum $G(f_k)$ becomes a conjugate even function, in other words, $G(f_k) = G^*(-f_k)$, where the symbol * refers to the complex conjugate. The positive frequencies $+f_k$ and the negative frequencies $-f_k$ have the same amplitudes and opposite phase. The instantaneous power of the time signal $g(t_n)$ is equal to $[g(t_n)]^2$ [4.6].

In order to avoid aliasing of the frequency components, an anti-aliasing filter is used with a cut-off frequency $f_c = f_s/2$. In a commercial analyser, N equals a number that is a power of 2. So, for example, 1K bytes of memory relates to $2^{10} = 1024$ frequency lines, of which only 512 are independent and not influenced by aliasing. In practice, only 400 lines are displayed, hence the ratio between the frequency range f_{max} and the sampling frequency f_s is $f_s/f_{max} = 1024/400 = 2.56$ [4.4].

To limit the number of samples in the time function, the sampled time signal is multiplied by a time window [4.4]. Subsequently, the sampled time signal is truncated at the beginning and end of the time-window, introducing ripples or sidelobes into the frequency spectrum. One should note that the characteristics of the ripples are determined by the Fourier transform of the particular window function. With a DFT the continuous time signal is not monitored; instead it is sampled and time-limited. When the original time signal contains discrete frequency components influenced by the window function, one might not observe the correct maximum value, but only the lower value on the slopes of the peak [4.4]. When a time signal contains an integer number of periods in the time record T, the frequency peak coincides with an analysis line and all other samples fall at the zeros between the sidelobes. On the other hand, with a non-integer number of periods in the record length T, the peak falls somewhere between the two analysis lines and the sidelobes are sampled at their maximum. This effect is referred to as leakage, because power from discrete frequencies components is leaked into adjacent analysis bands [4.7].

In order to limit the effect of leakage and obtain a better selectivity, a smooth time window function is preferred, for example, the Hanning window. This time window function is simply one period of a sinusoid with a length equal to the time record T [4.8]:

$$w(t) = 2 \cdot \sin^2\left(\frac{2\pi t}{T}\right) \qquad \text{for} \qquad 0 \le t < T. \qquad (4.19)$$

The use of the Hanning window decreases the amplitude of the time signal to zero at the beginning and end of the record length. The Hanning window gives a much better selectivity than a rectangular window, since the main sidelobe is 20dB lower and the rate of fall of the sidelobes is higher. The ripple characteristics of the Hannning window give a maximum amplitude error of 1.42dB, compared to 3.9dB for the rectangular window [4.8]. The effect of leakage is demonstrated in Section 4.5.

For the fixed sampling rate method, an FFT of the time signal is obtained at appropriate fixed steps in the rotation speed of the engine during a run-up or run-down of the engine. The measurements are triggered by a tachometer signal that is connected to the instantaneous speed of the engine. The result gives the well-known Campbell diagram (see Figure 1.1 on page 3), where the signature spectra are plotted against engine speed. The harmonic components appear as radial straight lines and system resonances appear as fluctuations in amplitude along almost vertical straight lines. The spectral amplitudes may be indicated using a colour scale.

Averaging of the data is required to suppress the pressure fluctuations of the background noise at frequencies where the signal-to-noise ratio is low [4.1]. Exponential averaging is preferred when one needs to analyse continuously varying signals [4.6]. The contribution of each sample towards the average is weighted using an exponentially decaying curve with a time constant equal to the number of samples, with the emphasis on the last sample. Exponential averaging is a continuous process and useful for analysing a continuous non-stationary signal [4.9]. With linear

averaging, equal emphasis is placed on all the samples. Therefore, the averaging process is stopped after reaching a specific number of averages and not when the measurement is completed. Therefore linear averaging is not suitable for the analysis of variable signals.

Overlap analysis is also preferred. This process involves the re-use of data in one or more previous time records for the following reasons: firstly, to avoid loss of data, secondly, to obtain better amplitude accuracy and thirdly, to get a flat overall weighting of the data [4.9]. Effective analysis time T_a depends on the record length T, the number of averages N_a and the fractional overlap OL. For a linear sweep-rate, the effective analysis time should be smaller than the time needed to sweep a measurement interval Δr:

$$T + [(T \cdot (1 - OL) \cdot (N_a - 1)] < \frac{\Delta f_K}{S_K} \quad ; \quad K = 1, 2, etc., \qquad (4.20)$$

S_K = Sweep-rate of order K (Hz/s),

Δf_K = Frequency range covered by order K during the measurement interval Δr (Hz).

Smearing of the higher order components is, however, a natural consequence of fixed rate sampling. Each record is acquired for the same fixed time interval, while the corresponding sweep-rate of individual harmonics (orders) increases with the order number over that time interval, so that the energy of the order is smeared over a number of analysis lines [1.1, 4.3]. The effect of smearing is demonstrated in Section 4.5.

4.4.2 Order tracking method

Order tracking is preferred when one is primarily interested in the behaviour of harmonic orders. In this method, the sampling frequency of the analysis is synchronised with the rotation speed of the engine. A tachometer is normally used to

measure the rotation speed; and the fundamental frequency is represented by a number of pulses per shaft revolution [4.10]. For order tracking, the signal is sampled a certain number of times for each revolution, rather than at a fixed sampling rate, as described in Section 4.4.1. The basic principle of order tracking is demonstrated in Figure 4.4 below:

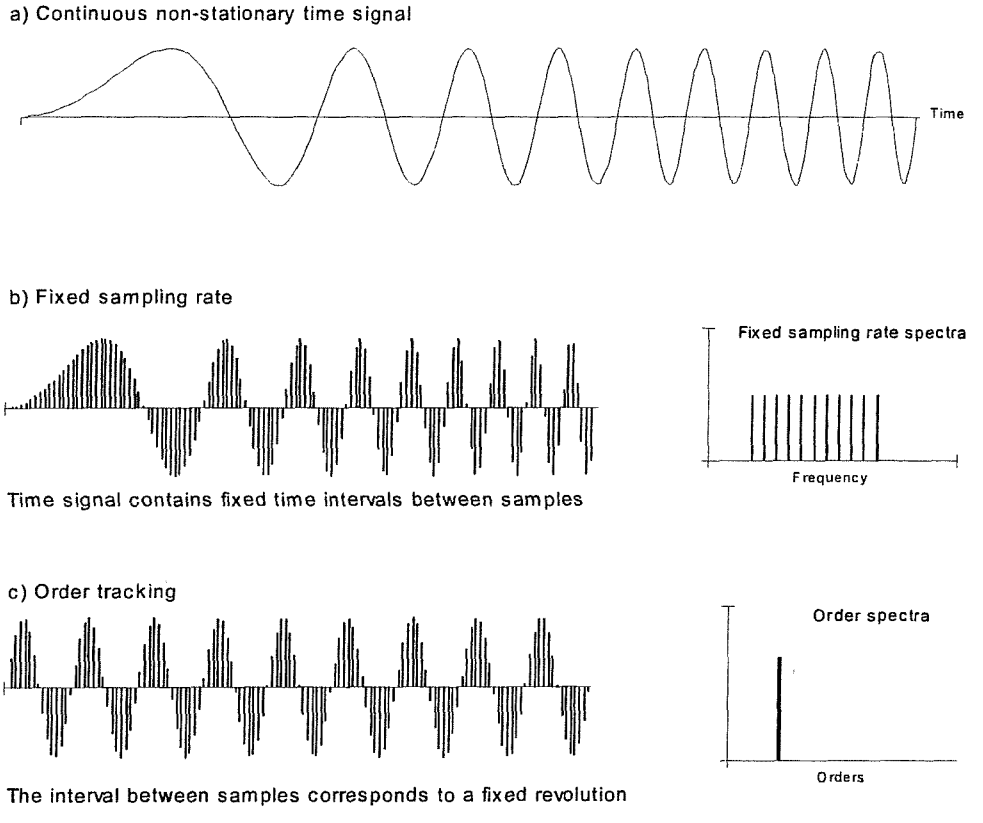

Figure 4.4 Basic principle of fixed sampling rate order analysis and order tracking.

a) Physical continuous varying time signal.

b) Time record and frequency spectrum analysed using a fixed time interval Δt.

c) Time record and frequency spectrum analysed using a fixed revolution interval Δrev.

Graph a) shows a continuous time-varying physical signal. Its fixed sampled time record is displayed in Graph b). In this case, the time interval Δt is fixed for the

sampled record and the FFT of the record gives the frequency spectrum. The spectral peaks are smeared over a number of analysis lines corresponding to the speed change along the record, illustrated by the frequency spectrum in Graph b) [4.6]. For order tracking, the interval between the samples corresponds to a fixed revolution interval Δrev [4.11]; hence the component is sampled a fixed number of times for each period. The varying sampling rate has changed the varying sine-wave (fundamental order) into a stationary fixed sine-wave [4.12]. The FFT of this record gives the order spectrum and the fundamental sweeping frequency is now located in one frequency line. The result is a high resolution order spectrum where the power of each harmonic component is concentrated in an individual line independent of speed variations; thus smearing is avoided [4.11].

Interpolation of the tacho signal is used in the resampling of the time signal along the record to convert it to revolutions [4.12]. The time record is measured in revolutions rather than seconds and the corresponding FFT spectrum is measured in orders rather than frequency [4.11]. The order resolution Δn is equal to the inverse of the number of revolutions per record $1/revs$. The time-frequency relationship for order tracking is given by $N = K \cdot revs$, where N is the number of analysis lines, K is the number of orders and $revs$ is the number of revolutions per record [4.11]. The number of analysis lines N and the number of orders K are also a function of the order resolution Δn, expressed by

$$\Delta n = \frac{1}{revs} = \frac{K}{N}. \tag{4.21}$$

When the ratio N/K is an integer, in other words, an integer number of revolutions per record, leakage is avoided for the order components and a rectangular window may be used without any amplitude error (see Section 4.4.1). However, if one is also interested in the non-order related components, a Hanning window is preferred, because it will reduce the amplitude error for the non-orders [4.8].

For order tracking the maximum frequency of the analysis f_{max} is continuously updated proportionally to the fundamental frequency F_1, expressed by

$$f_{max} = K \cdot F_1. \tag{4.22}$$

In order to avoid aliasing, the sampling frequency f_s is also continuously adjusted relative to the fundamental frequency F_1, expressed by

$$f_s = K \cdot F_1 \cdot 2.56. \tag{4.23}$$

This corresponds to a sampling interval Δrev in the record that is equal to $revs/(N \cdot 2.56)$, where $revs$ is the number of revolutions in the record and N is the number of analysis lines.

The relationship between order tracking and FFT analysis can be expressed by

$$\Delta f = \frac{1}{T} = \Delta n \cdot F_1, \tag{4.24}$$

and

$$\Delta t = \frac{1}{f_s} = \frac{\Delta rev}{revs \cdot \Delta n \cdot F_1}, \tag{4.25}$$

where:
- Δf = Frequency resolution (Hz), proportional to engine speed,
- T = Record length (seconds), inversely proportional to engine speed,
- Δn = Order resolution, (orders), constant,
- F_1 = Fundamental frequency (Hz), proportional to engine speed,
- Δt = Time interval (seconds), proportional to engine speed,
- f_s = Sampling frequency, proportional to engine speed,
- Δrev = Revolution interval (revolutions), constant,
- $revs$ = Number of revolutions in the record (revolutions), constant.

One notes that Δf and Δt are continuously updated relative to the fundamental component F_1 during the sweep. On the other hand, Δn, Δrev and $revs$ remain

constant during the analysis due to the resampling of the time signal. Consequently the analysis of a swept periodic signal of constant amplitude will produce exactly the same order spectra and records along the sweep as indicated in Figure 4.4 c) on page 79. However, the optimum order tracking parameters depend on the required sweep rate and signal-to-noise ratios. The experimental procedures to determine the most effective order analysis parameters are discussed in Section 4.5.

4.5 ORDER ANALYSIS OPTIMISATION

The analysis was performed using a Bruel & Kjaer Pulse multi-analysis system 3560 (see Figure 4.2 on page 73) [4.9]. The main aim of the measurement technique was to capture the harmonic sound pressure information inside the exhaust system during the constant acceleration of a vehicle. For this purpose the order analysis methods described in Section 4.4 were applied. It was essential to optimise the analysis parameters for measurements in the presence of mean flow which can give rise to very poor signal-to-noise ratios. For this reason, experimental measurements were first performed on a test bench to identify the most effective procedures.

Although the order tracking method is superior to the fixed sampling rate method because leakage and smearing are avoided, the fixed sampling rate method is preferable when one only wants to track the fundamental harmonic over a wide frequency span. For order tracking the frequency resolution might be too low at high frequencies to separate the harmonic components from flow-induced background noise. So, for example, an order resolution of $\Delta n = 0.025$ relates to a frequency resolution Δf of 30 Hz at 1200 Hz (see equation (4.24) on page 81). With the fixed sampling rate method, the analysis of the fundamental order can be performed with the appropriate fixed frequency resolution. Holland and Davies [4.1] described such a procedure. However, the maximum fundamental frequency associated with internal combustion engines is considerably lower. So, for example, for a four-stroke four-cylinder engine it is 200 Hz at 6000 r.p.m.. This gives a maximum frequency resolution of $\Delta f = 5$ Hz for an order resolution $\Delta n = 0.025$.

4.5.1 Fixed sampling rate method

This section highlights some of the significant effects that are related to the fixed sampling rate method (for example, leakage and smearing). Leakage occurs when the time period of the harmonic component is not an integer of the record length T. The rippled appearance of some of the order components in Figure 4.5 below clearly demonstrates the effect of leakage. The measurement shows the sound pressure order components recorded in front of the silencer (station #1) on the test bench with swept ramp excitation (see Figure 4.2 on page 73). For this measurement, fixed sampling rate spectra were captured for $\Delta r = 1$ Hz of the fundamental frequency from 50 to 200 Hz. The analysis was performed with a frequency resolution $\Delta f = 4$ Hz, which corresponded to a record length of $T = 1/4 = 0.25$ seconds. Maximum amplitude error occurred when the time signal for that particular interval had a half integer number of periods in the record length T. The analysis was performed using a Hanning window. The maximum amplitude error was 1.42dB [4.8]. One may note that leakage was avoided for the 4th order because the number of periods in the record length T was an integer for all the measurement intervals.

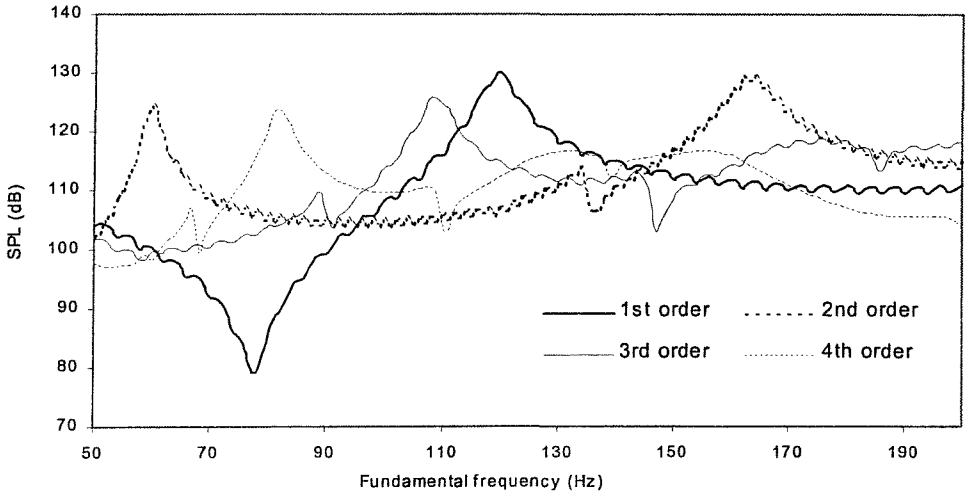

Figure 4.5 Sound pressure orders recorded in front of the silencer component on the test bench with periodic excitation. The rippled appearance of the 1st, 2nd and 3rd order was caused by leakage.

The error that is caused by leakage is eliminated for the acoustic quantities (equations (3.1) to (3.9)). These quantities are the result of some ratios and both the numerator and denominator are subject to the same amount of amplitude error. In general, leakage is only of concern for the fixed sampling rate method when absolute sound pressure order amplitudes are to be considered.

One problem associated with the capture of variable harmonic excitation is the smearing of data. The higher order components cover an increasing frequency span during the sweep; hence the acoustic power is spread over several analysis lines during the analysis time. The effect of smearing is demonstrated in Figure 4.6 below and in Figure 4.7 on page 85, showing the sound pressure recorded in front of the silencer (station #1) on the bench test (see Figure 4.2 on page 73).

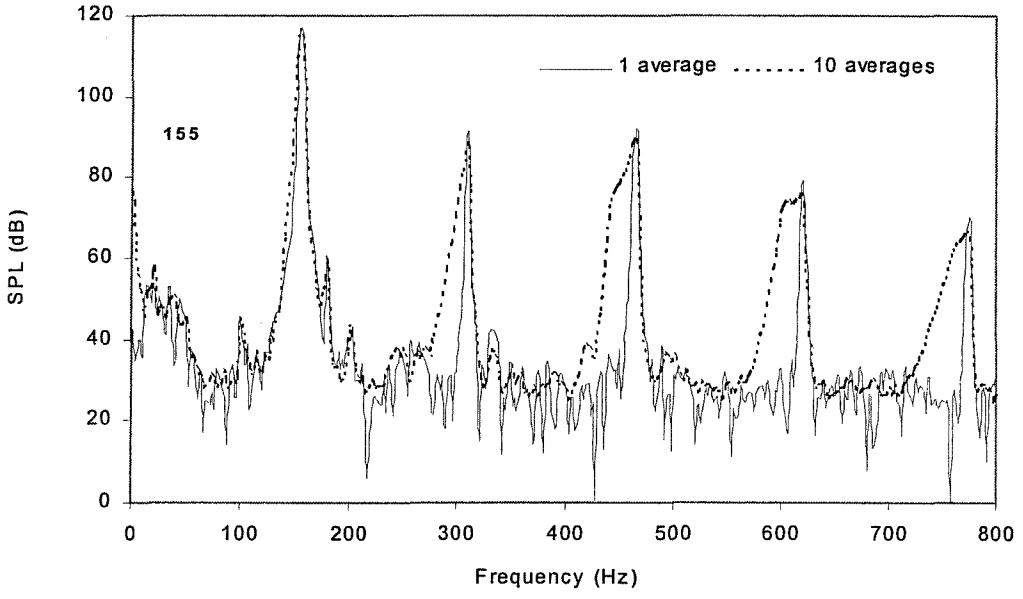

Figure 4.6 Sound pressure spectra recorded at the inlet of the silencer component (station #1) on the bench test with variable periodic excitation. The spectrum was captured at a fundamental frequency of 155 Hz. The analysis was performed with one average (solid curve) and ten averages (dash curve) to demonstrate spectral smearing.

Swept harmonic excitation (0.5 Hz/s) was used with a fundamental frequency range from 50 to 200 Hz. Figure 4.6 on page 84 shows the frequency spectrum that was captured at a fundamental frequency of 155 Hz with one average and ten averages. One notes that when the analysis time was increased (ten averages), the maximum component amplitudes were reduced due to smearing. It can also be observed that the amount of smearing is proportional to the sweep-rate of the particular order component, in other words, the amount of smearing increases with the order number *K*.

Smearing was reduced with one average, because the order components covered a much smaller frequency span during the analysis time. The difference in levels for the 4th order, analysed with one and ten averages, is shown in Figure 4.7 below.

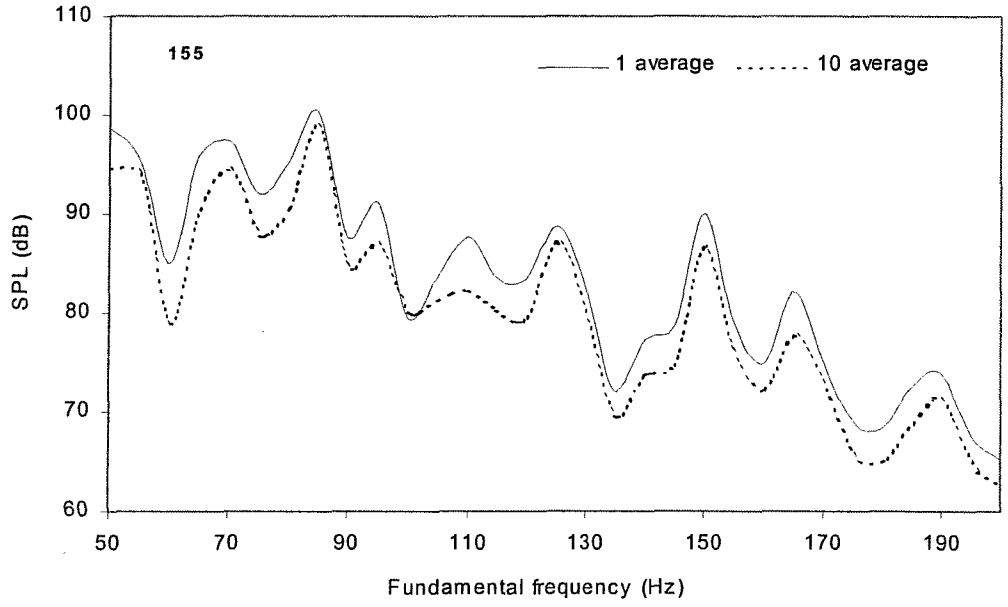

Figure 4.7 Sound pressure levels recorded at the inlet of the silencer component (station #1) on the test bench for the 4th order (8E), analysed with one average and ten averages. One notes that an increase in averages resulted in a reduction of levels due to smearing.

4.5.2 Order tracking method

The optimisation of the order tracking was performed on the test bench (see Figure 4.2 on page 73) with a practically representative constant exhaust mass flow of 0.07 kg/s that is typical for a small four-cylinder engine at high engine speed. This gave a Mach number $M = 0.1$ at 20^o Celsius. The acoustic excitation for a four-cylinder four-stroke engine was simulated between 1500 and 6000 r.p.m., giving a fundamental frequency range from 50 to 200 Hz. A linear sweep-rate of 0.5 Hz/s (15 r.p.m./s) was used for the fundamental frequency that represents a realistic run-up of an engine. The system was excited with a swept ramp period signal.

Signal-to-noise ratios are reduced when measurements are performed in the presence of mean flow, due to the increase in the flow-induced broad-band background noise. Hence it is more difficult to obtain reliable measurements [1.1, 4.1]. To illustrate the effect of order resolution and averaging, the real part of the transfer function $H_{4,3}$ in the outlet pipe shown in Figure 4.8 below was evaluated.

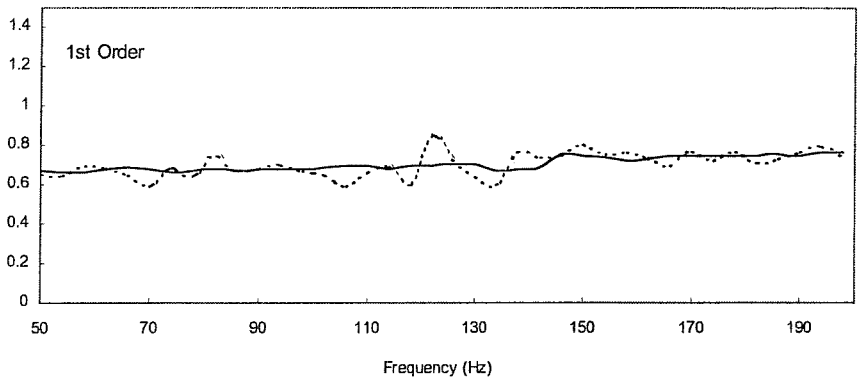

Figure 4.8 Real part of the transfer function $H_{4,3}$ for the 1st order (2E) recorded on the test bench for a Mach number $M = 0.1$. A smoother curve was produced with $\Delta n = 0.025$ orders and ten averages (solid curve) compared to the spiky appearance analysed with $\Delta n = 0.2$ orders and one average (dash curve).

The theoretical transfer function $H_{4,3}$ produced a smooth horizontal curve for the first order component due to the absence of acoustic resonance. This was the case when the analysis was performed with an order resolution $\Delta n = 0.025$ orders and ten averages, compared to the spiky appearance of the lower 0.2 orders resolution and one average.

The coherence between the transducers at stations #3 and #4 and the signal-to-noise ratio were also improved when the order tracking analysis was performed with the higher order resolution and increased averages. The results are compared in Figure 4.9 below and in Figure 4.10 on page 88 respectively. The higher order resolution concentrated the acoustic energy of the order components in a narrower band and the averaging process then tended to suppress any random fluctuations of the harmonic components by reducing the relative levels of the broad-band noise contributions. The signal-to-noise ratio was estimated from the ratio of the acoustic pressure with and without acoustic excitation in the presence of mean flow, Mach number $M = 0.1$.

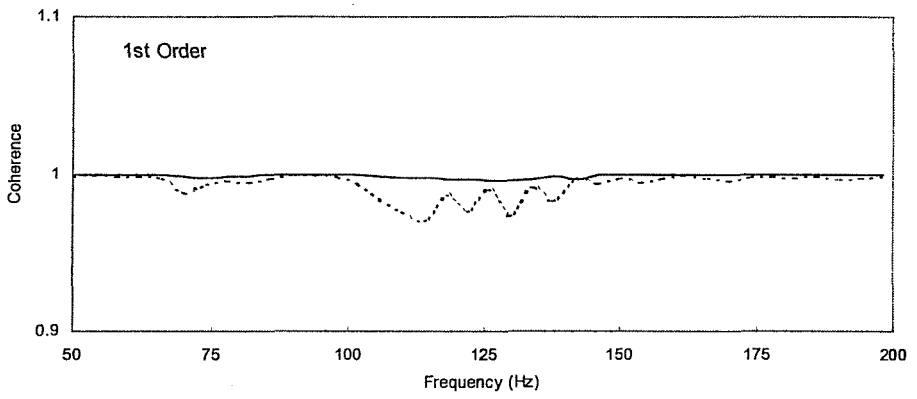

Figure 4.9 Coherence between stations #4 and #3 for the 1st order (2E) recorded on the test bench for a Mach number $M = 0.1$. The coherence was closer to 1 when the analysis was performed with an order resolution of $\Delta n = 0.025$ orders and ten averages (solid curve) compared to $\Delta n = 0.2$ orders and one average (dashed curve).

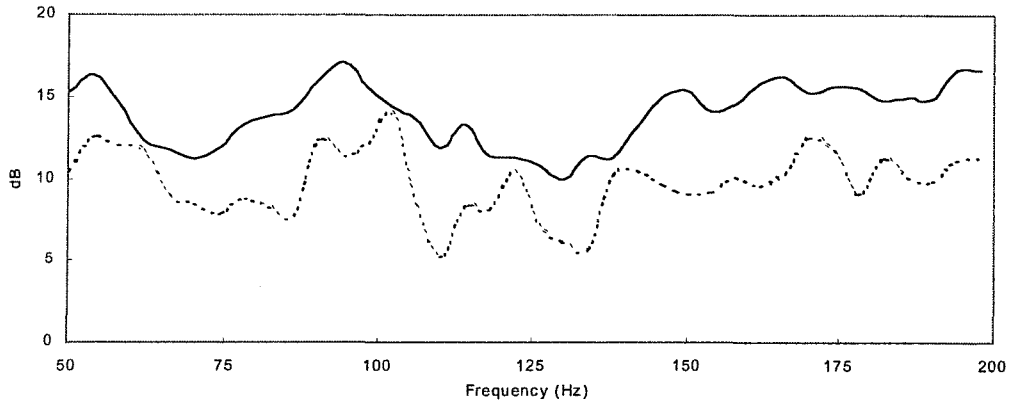

Figure 4.10 Signal-to-noise ratio at station #3 for the 1st order (2E) recorded on the test bench for a Mach number $M = 0.1$. The signal-to-noise ratio was improved when the analysis was performed with an order resolution of $\Delta n = 0.025$ orders and ten averages (solid curve) compared to $\Delta n = 0.2$ orders and one average (dashed curve).

It can also be observed from Figure 4.11 below that the signal-to-noise ratios were generally higher in the inlet pipe (station #1), compared to the outlet pipe (station #3). This is due to the attenuation of the harmonic components by the expansion chamber in combination with the flow-induced noise at the outlet of the expansion chamber.

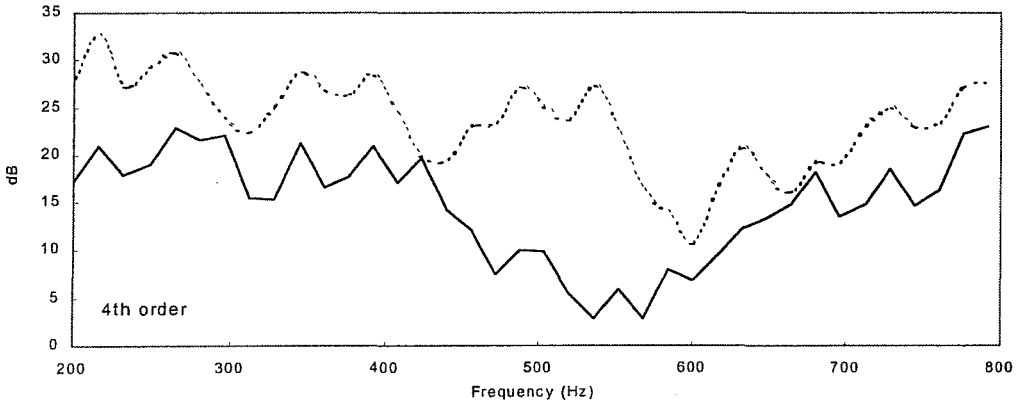

Figure 4.11 Signal-to-noise ratio at station #1 (dashed curve) and station #3 (solid curve) for the 4th order (8E) analysed with an order resolution of $\Delta n = 0.025$ orders and ten averages recorded.

As has already been mentioned, one problem associated with harmonic excitation is the increasing sweep-rate required at the higher harmonics and the possibility of smearing. With order tracking, spectral smearing is eliminated, as illustrated in Section 4.4.2. However, amplitude smearing may occur when the effective analysis time is too long relative to the rate of change in the signal [4.13], in other words, the amplitude of the harmonic component is represented by the average value within the analysis time. This may result in a loss of data and phase distortion for cross-spectra as the harmonic component amplitude may not be represented by its actual strength. The effect of increasing the analysis time is demonstrated in Figure 4.12 below. This was achieved by increasing the averages from ten to twenty. The graph shows the sound pressure data for the 4th order component (8E) recorded at station #1.

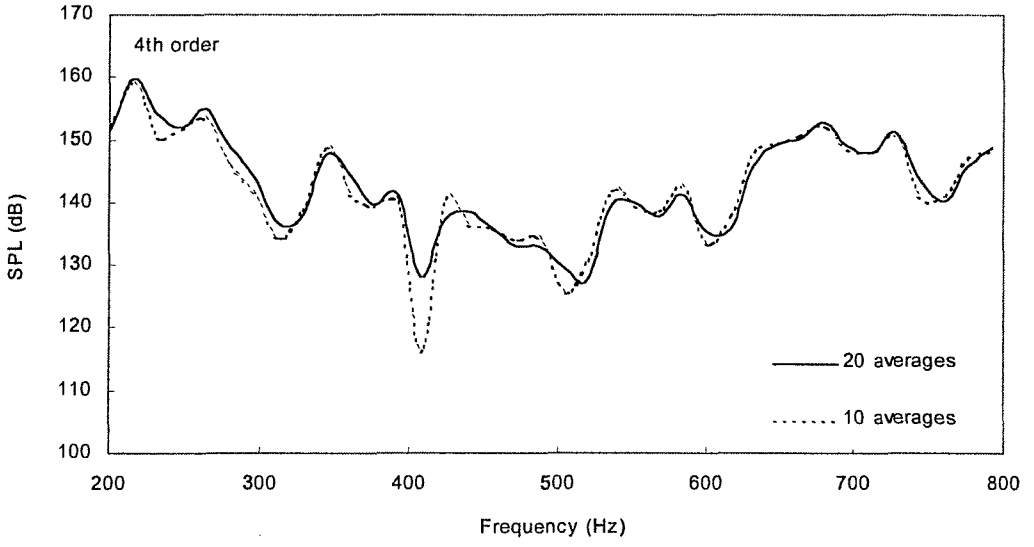

Figure 4.12 Sound pressure for the 4th order (8E) component measured at station #1, analysed with ten averages (dash curve) and 20 averages (solid curve). The effect of amplitude smearing was most evident at 400 Hz, due to a too long analysis time with the 20 averages.

For this measurement, the analysis was performed with an order resolution of $\Delta n = 0.025$ orders; 75 % overlap and order spectra were updated at Δr =4 Hz. With a linear sweep-rate of 0.5 Hz/sec, each interval was 2 seconds long. The corresponding analysis time is obtained with 37 averages (see equation (4.20) on page 78) at the start of the measurement ($F_1 = 50$ Hz). However, experimentation indicated that amplitude smearing was avoided for averages of less than ten that correspond to an analysis time of 1.3 seconds, during which time the 4th order (8E) covers a frequency range of 5.2 Hz. One may observe from Figure 4.12 on page 89 that amplitude smearing occurred when the analysis time was increased (20 averages). This was most significant at 400 Hz where the rate of change in the sound pressure signal appeared to be the largest.

It is also essential to capture information at regular intervals to acquire sufficient data to describe the narrow-band characteristics of the silencer component. This is particularly applicable to the higher order components that cover an increasing frequency range Δf_K during the measurement interval Δr. Although the analysis time of 1.3 seconds (75% overlap, $\Delta n = 0.025$ orders and 10 averages) allowed a smaller value for Δr (2.6 Hz or 78 r.p.m.), the number of measurement intervals was restricted by the digital signal processing resources of the measurement system. Subsequently, measurements were captured for $\Delta r = 4$ Hz that corresponded to a frequency range $\Delta f_4 = 16$ Hz for the 4th order (8E). This was found to be adequate to describe the acoustic performance of the expansion chamber and provided a good compromise between measurement resolution and order resolution.

This was one of the main limitations of the measurements performed by Temple [1.9] and Yaseen [1.10]. They captured information only at five engine speed intervals that were insufficient to describe the acoustic performance adequately. Figure 4.13 on page 91 demonstrates the loss of data for the 4th order (8E) when the measurement interval Δr was increased from 4 Hz to 8 Hz.

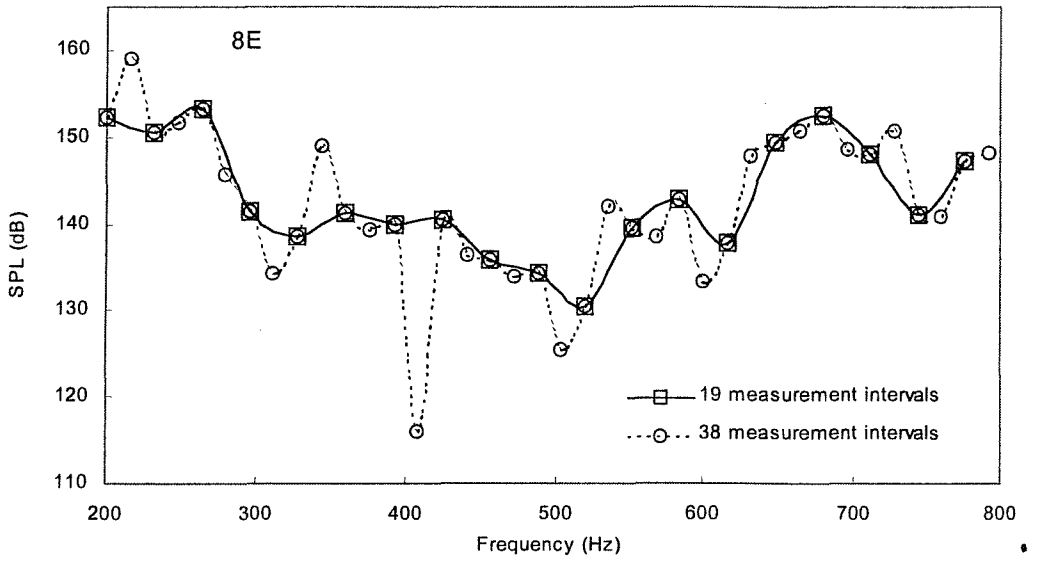

Figure 4.13 Sound pressure levels for the 4th order (8E) captured at a fundamental frequency interval $\Delta r = 4$ Hz that corresponds to a frequency range $\Delta f_4 = 16$ Hz (dash curve with circle) and $\Delta r = 8$ Hz that corresponds to a frequency range $\Delta f_4 = 32$ Hz (solid curve with square). The decrease in measurement intervals from 38 to 19 resulted in a loss of data.

4.6 CALIBRATION PROCEDURE

The acoustic field inside a mechanical silencer component is highly reactive. The acoustic power flux for a certain position and frequencies may be very close to zero due to the small difference between the forward travelling wave amplitude P^+ and the reflected wave amplitude P^- [1.11]. Therefore a precise relative calibration of the pressure transducers is critical for the success of the measurement technique [4.1]. The relative calibration was performed by exposing the pressure transducers to the same pressure field and the relative calibration factors were estimated using the following transfer functions:

$$\hat{R}_{n,1} = \frac{\hat{P}_n \cdot \hat{P}_1^*}{P_{1,1}} \quad ; \quad n = 1, 2, 3, etc., \qquad (4.26)$$

$\hat{P}_n \cdot \hat{P}_1^*$ = Cross-spectrum,

$\hat{P}_{1,1}$ = Auto-spectrum,

$*$ = Complex conjugate,

$\widehat{\ }$ = Complex value.

A detailed description of the calibration procedure is set out in Appendix 4.3.

4.7 BENCH TEST MEASUREMENTS AND PREDICTIONS

The most effective procedures that were established in Section 4.5 were used to measure the acoustic performance of a simple expansion chamber. The prediction of the acoustic performance of the silencer components was performed using APEX (see Chapter 3, Section 3.3.1). Constant mass flow and temperature conditions existed for the measurements on the bench: that is, the harmonic components at each measurement interval were subjected to the same conditions. Therefore it was possible to use the programme in its standard format to calculate the acoustic performance for each order separately, with the appropriate frequency range and measurement resolution Δf_K. Measurements were compared to predictions to validate the experimental technique.

A software programme was developed to calculate the wave components $P^{\pm}$ from the measured acoustic quantities, and the measured temperature and mass flow. The wave components $P^{\pm}$ were estimated according to the theoretical procedures outlined in Section 4.2 and Appendix 4.1. Figure 4.14 on page 93 also provides a flow diagram of this specially developed Labview computer programme.

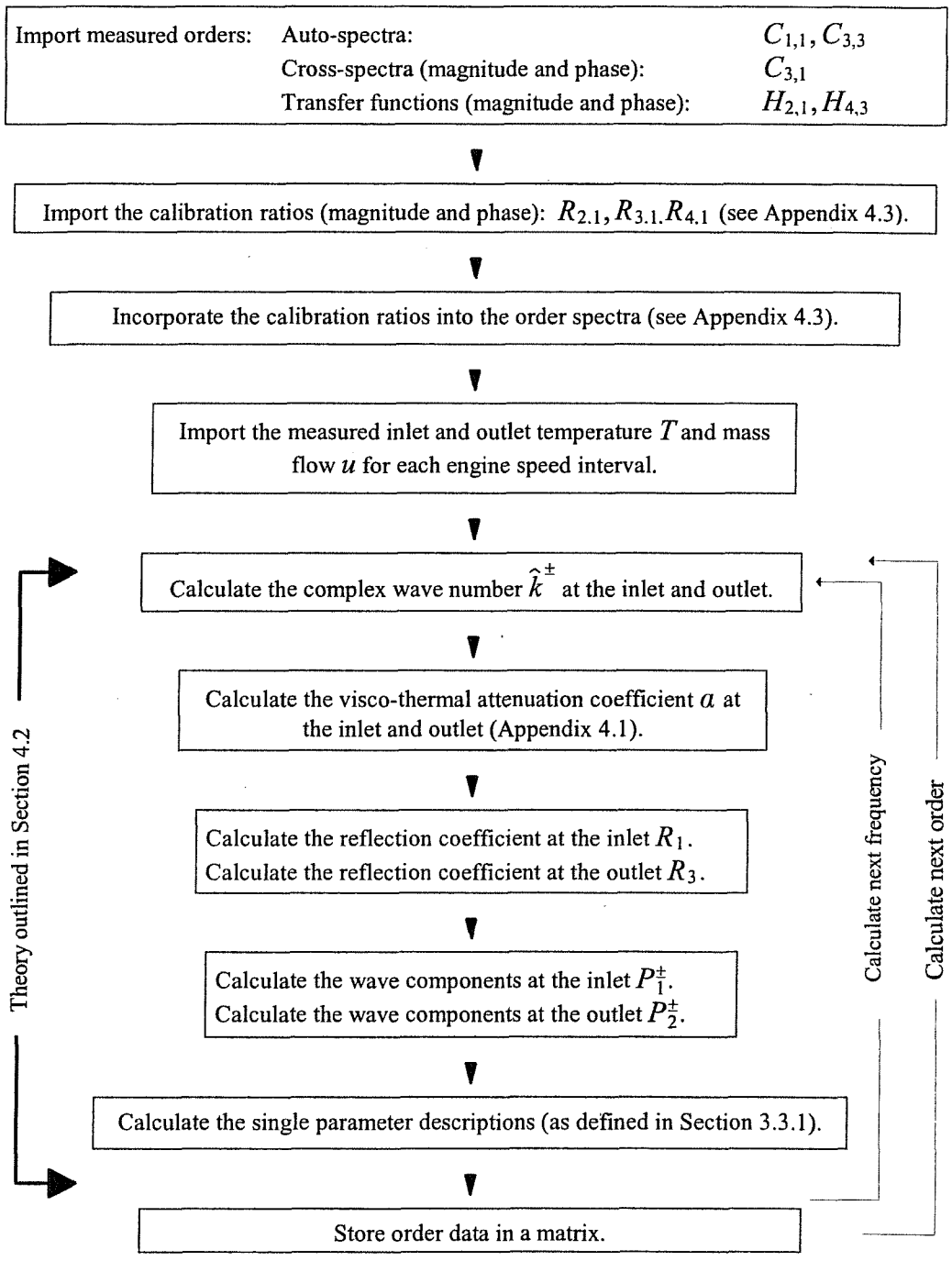

Figure 4.14 Flow diagram of the Labview software programme that was specifically developed to calculate the wave components $P^{\pm}$ from the measured acoustic quantities.

4.7.1 Fixed sampling rate method

As has already been mentioned, the fixed sampling rate method is preferred when one only wants to track the fundamental order over a wide frequency range (see Section 4.5). Accordingly, a brief discussion of the results is provided because the main aim of the work is to capture the harmonic information of exhaust noise. However, this method holds some merit for the assessment of the acoustic performance of a silencer component on a test bench [1.11, 4.1], for example, the validation of silencer components presented in Appendix 4.4. Originally it was planned to assess the acoustic performance of an elliptical section triflow silencer, because the commercial application of this type of silencer is very popular. [2.14, 2.16]. Validation measurements presented in Appendix 4.4 indicated that the APEX code did not provide realistic modelling of the elliptical section reverse flow chambers that form component elements of a triflow silencer, but only of circular ones [2.16]. For this reason, expansion chambers were reconsidered.

The simple expansion chamber in Figure 4.15 on page 95 was evaluated. The expansion chamber consisted of a 2 mm thick shell with 1.5 mm end caps, while the inlet and outlet pipes had a wall thickness of 2 mm. The expansion chamber radius was 49 mm, giving an area expansion ratio between the pipe and the chamber of 7.01, which produced an estimated maximum attenuation of *20 Log* 7.01 or 16.9dB. The first circumferential mode propagated when the Helmholtz number *ka* exceeded the value of 1.84 [2.16]; and so the lowest higher order modes could only propagate in the chamber at frequencies above 2000 Hz.

The experimental set-up displayed in Figure 4.2 on page 73 was used and the measurements were performed for zero flow $M = 0$. The system was excited using a swept-sine signal with a linear sweep-rate of 4 Hz/s from 50 Hz to 1194 Hz to gave a total measurement time of 4.8 minutes. The excitation signal from the generator was used to trigger the predetermined measurement intervals. In order to avoid the error magnification factor at high frequencies, a transducer separation distance of 70 mm was used (see Appendix 4.2).

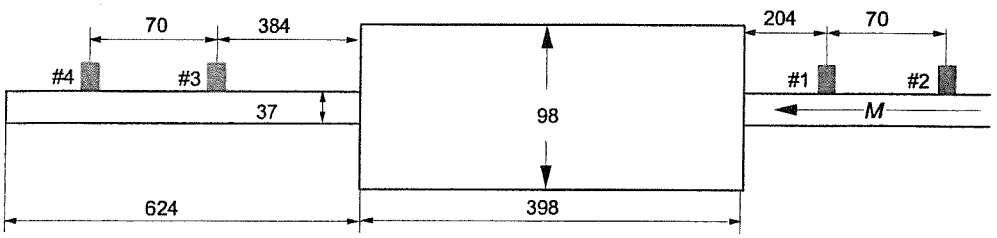

Figure 4.15 Details of the simple expansion chamber used for the fixed sampling rate measurements on the bench test (all dimensions are in millimetres).

The analysis was performed using a frequency resolution of Δf = 8 Hz, 75% overlap, a Hanning window and 30 exponential averages. Spectra were captured at Δr =8 Hz intervals from 50 to 1194 Hz that related to 143 measurement intervals. These parameters gave an effective analysis time of one second during which time the fundamental order swept 4 Hz (sweep-rate = 4 Hz/sec). This was adequate to avoid smearing. Figures 4.16 and 4.17 on page 96 compare the measured and predicted transfer function $H_{3,1}$ and attenuation $AL_{1,3}$. In both cases good agreement was obtained (±2 to 3dB or better).

4.7.2 Order tracking method

The most effective procedures established for the order tracking method in Section 4.5 were used to measure the acoustic performance of a simple expansion chamber for simulated exhaust noise conditions. The main aim of the technique was to assess the acoustic performance of a silencer component on a running vehicle (covered in Chapter 5). For this reason, a more detailed description of the bench test order tracking results is provided. The analysis was performed using a Hanning window, 75 % overlap, ten exponential averages and an order resolution of Δn = 0.025 orders. Order spectra were captured at Δr = 4 Hz of the fundamental or firing frequency. The fundamental harmonic of the excitation signal was used as a tachometer signal and the first four order components were extracted.

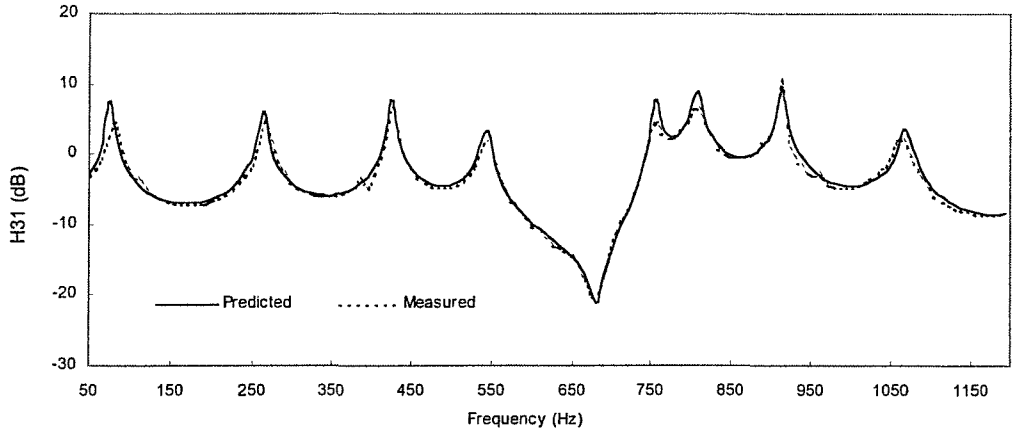

Figure 4.16 Measured and predicted magnitude of the transfer function $H_{3,1}$ with zero flow. The measurement was analysed using a fixed sampling rate.

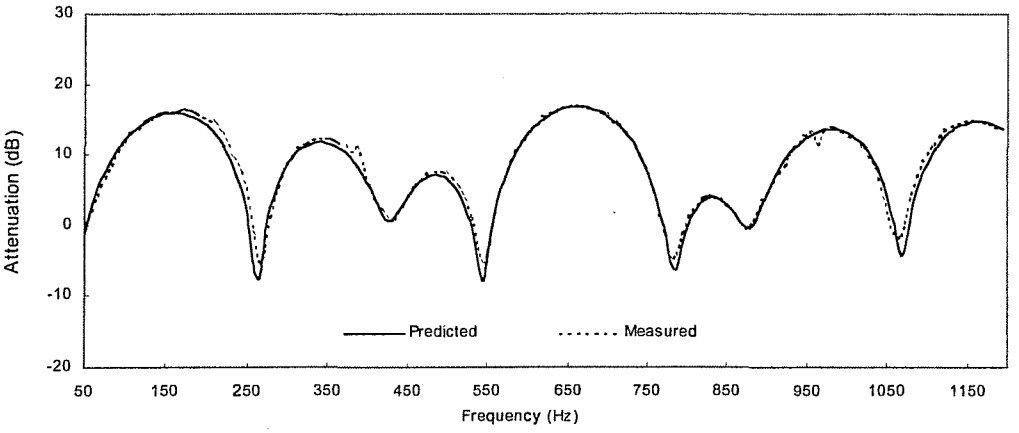

Figure 4.17 Measured and predicted magnitude of the attenuation $AL_{1,3}$ with zero flow. The measurement was analysed using a fixed sampling rate.

On the test bench, the exhaust noise harmonics can either be simulated using a sweep-ramp signal and analysed simultaneously, or each harmonic order can be individually simulated using a sine-sweep signal. Sine-sweep excitation was preferred because higher excitation levels could be achieved with lower amplification. This improved the signal-to-noise ratio and enhanced the durability of the compression driver. The acoustic excitation for a four-cylinder four-stroke engine was simulated between 1500 and 5940 r.p.m., which corresponded to a fundamental

harmonic (2E) from 50 to 198 Hz. A linear sweep-rate of 0.5 Hz/s (15 r.p.m./s) was used for the fundamental frequency. Linear engine sweep-rates between 15 to 30 r.p.m./s (0.5 to 1 Hz/s for the fundamental frequency for a four-cylinder four-stroke engine) are realistic for a practical run-up of an engine.

The simple expansion chamber displayed in Figure 4.18 below was used for the measurements. The construction was the same as the one shown in Figure 4.15 on page 95. The expansion chamber radius was 62.5 mm, giving an area expansion ratio between the pipe and the chamber of 7.38 that produced an estimated maximum attenuation of *20 Log* 7.38 or 17.3dB. The first circumferential mode propagates when the Helmholtz number *ka* exceeds the value of 1.84 [2.16], and so the lowest higher order mode can only propagate in the chamber at frequencies above 1600 Hz. For this measurement a separation distance of 100 mm was used, since the maximum frequency of interest was lower (800 Hz) compared to the previous measurement (1200 Hz) and still avoided a significant error magnification factor (see Appendix 4.2). The measurements were performed using a constant exhaust mass flow of 0.07 kg/s, which is typical for a small four-cylinder engine at high engine speed.

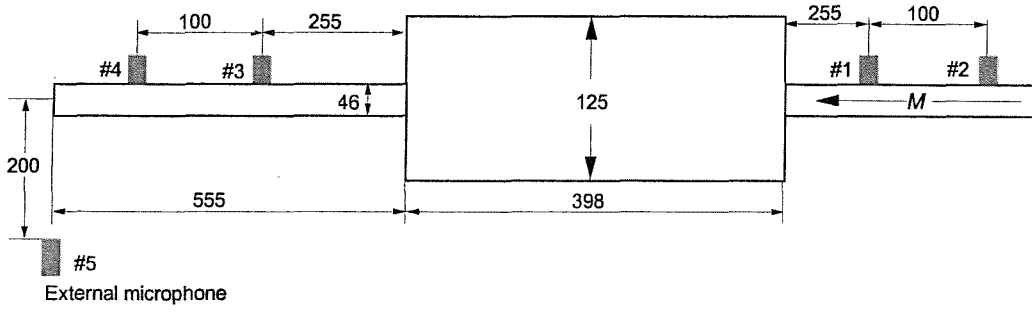

Figure 4.18 Details of the simple expansion chamber used for the order tracking measurements on the bench test (all dimensions are in millimetres).

Measurements of transfer functions, system attenuation, normalised acoustic power flux and normalised radiated power were compared to predictions to validate the technique. The magnitude and phase of the transfer functions $H_{2,1}$ and $H_{4,3}$ are set out in Figures 4.19 to 4.22 (pages 98 and 100) respectively. The magnitude of the

transfer functions across the silencer $H_{3,1}$ and $H_{1,5}$ are displayed respectively in Figures 4.23 and 4.24 on page 100 and 101. The external microphone for $H_{1,5}$ was positioned perpendicular and 200 mm from the centre of the tail-pipe outlet (see Figure 4.18 on page 97). These were all measured for a Mach number $M = 0.1$. The magnitude of the transfer functions was estimated by

$$H_{A,B} = 10 \cdot \log \left| \frac{P_A^+ + P_A^-}{P_B^+ + P_B^-} \right| \text{ (dB)}, \tag{4.27}$$

where A refers to the response position and B is the reference position. Alternatively, one can estimate the transfer function directly from the measured quantities using the following expression [4.6]:

$$H_{A,B} = 10 \cdot \log \left| \frac{C_{A,B}}{C_{A,A}} \right| \text{ (dB)}, \tag{4.28}$$

where $C_{A,B}$ is the cross-spectrum between response position A and reference position B, and $C_{A,A}$ is the auto-spectrum at position A.

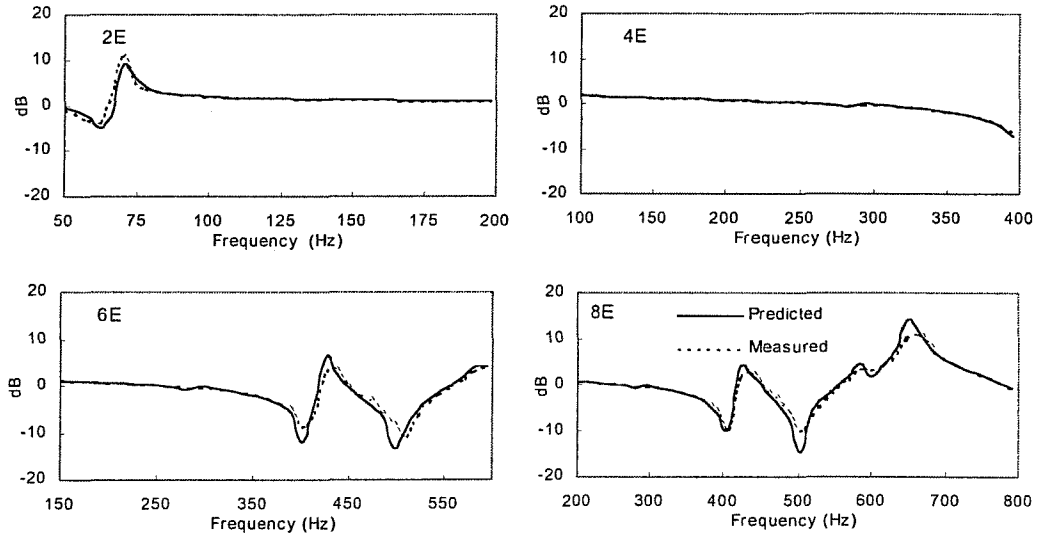

Figure 4.19 Measured (dash) and predicted (solid) magnitude of the transfer function $H_{2,1}$ with a Mach number $M = 0.1$. The measurement was analysed using order tracking.

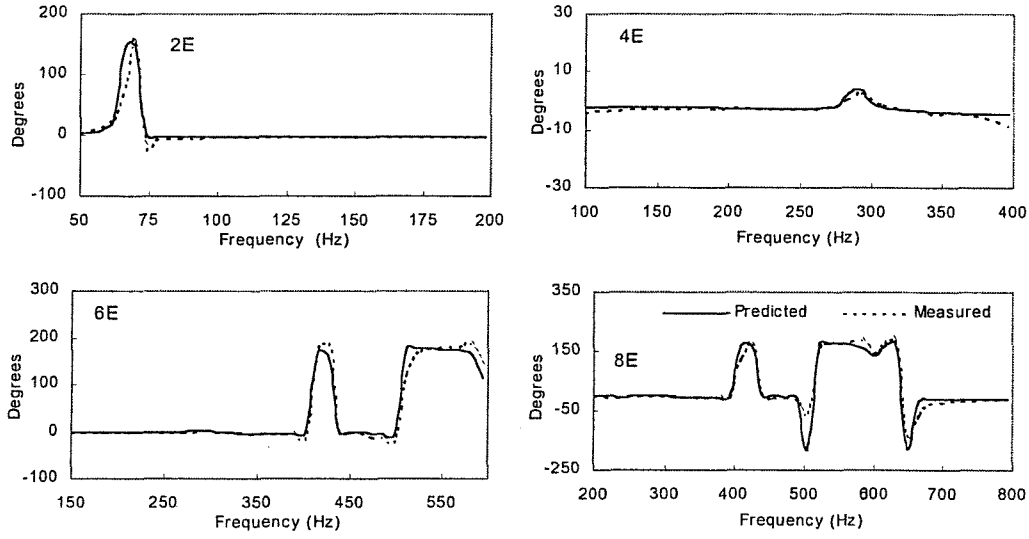

Figure 4.20 Measured (dash) and predicted (solid) phase of the transfer function $H_{2,1}$ with a Mach number $M = 0.1$. The measurement was analysed with using tracking.

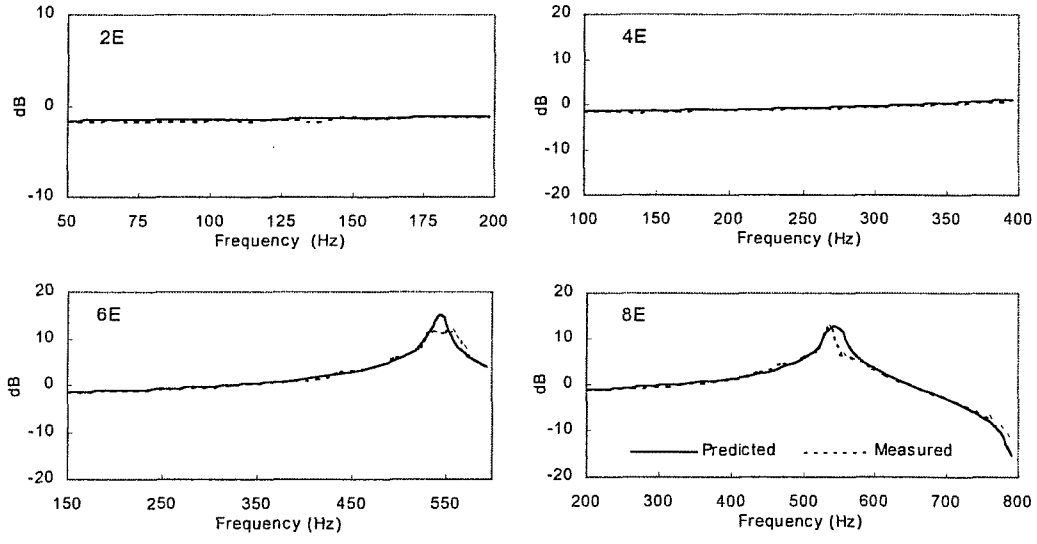

Figure 4.21 Measured (dash) and predicted (solid) magnitude of the transfer function $H_{4,3}$ with a Mach number $M = 0.1$ The measurement was analysed using order tracking.

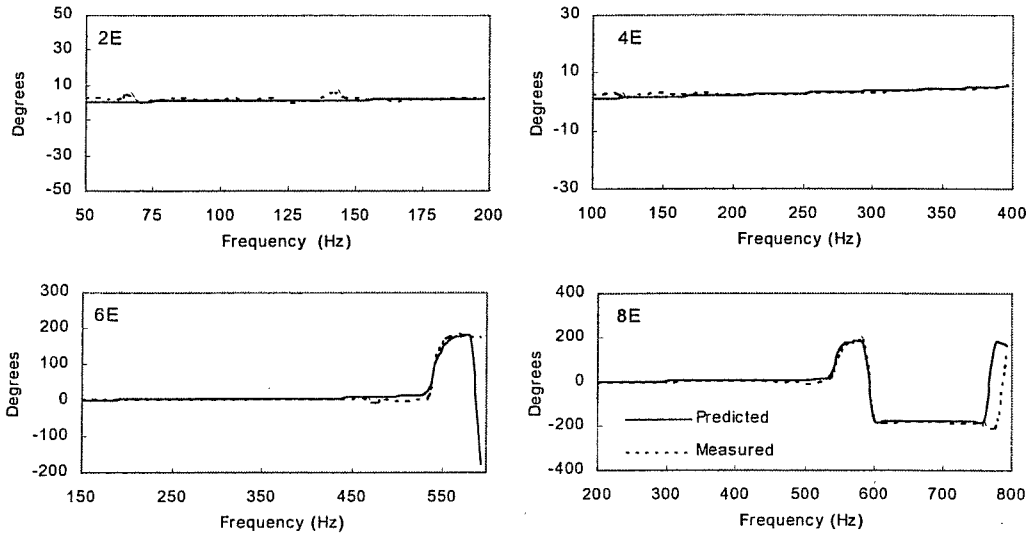

Figure 4.22 Measured (dash) and predicted (solid) phase of the transfer function $H_{4,3}$ with a Mach number $M = 0.1$. The measurement was analysed using order tracking.

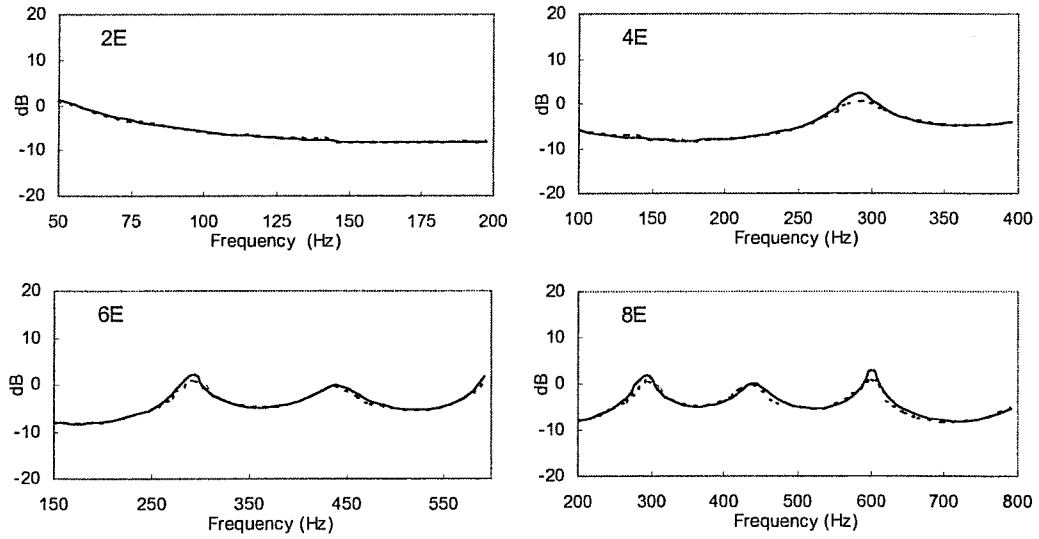

Figure 4.23 Measured (dash) and predicted (solid) magnitude of the transfer function $H_{3,1}$ with a Mach number $M = 0.1$. The measurement was analysed using order tracking.

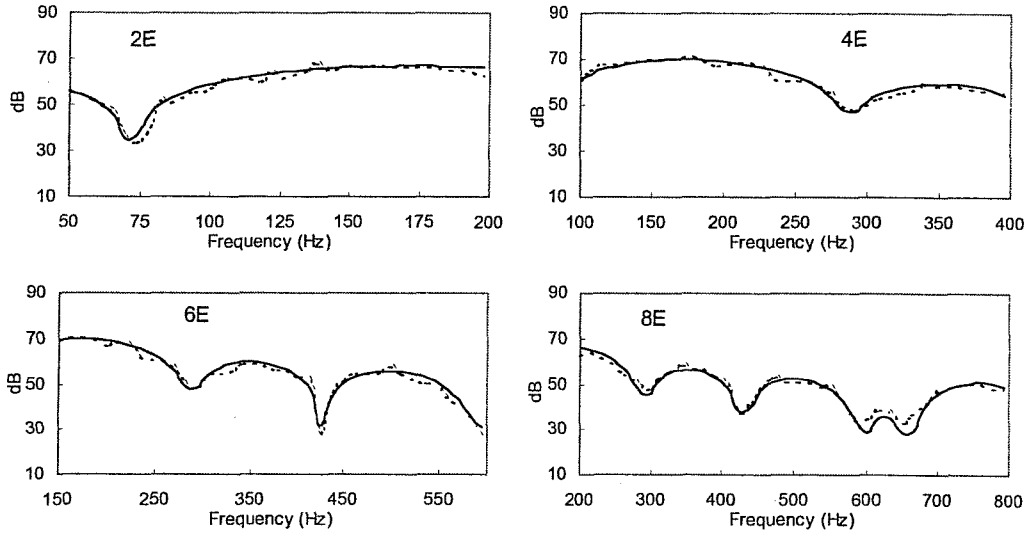

Figure 4.24 Measured (dash) and predicted (solid) magnitude of the transfer function $H_{1,5}$ with a Mach number $M = 0.1$. The measurement was analysed using order tracking.

The attenuation was estimated from the incident wave components at the inlet (station #1) and outlet of the expansion chamber (station #3), so that:

$$AL_{1,3} = 20Log\left|\frac{P_1^+}{P_3^+}\right| \text{ (dB)}. \tag{4.29}$$

Figure 4.25 on page 102 shows a comparison between the predicted and measured system attenuation for the first four order components with a Mach number $M = 0.1$.

The acoustic power flux in the outlet pipe was determined from the acoustic intensity I [2.13] and the corresponding pipe area. Thus, for example, at station #3

$$W_3 = \frac{1}{\rho_3 c_3}(|P_3^+|^2(1+M_3)^2 - |P_3^-|^2(1-M_3)^2). \tag{4.30}$$

This was normalised to the incident acoustic intensity I_1^+ at the inlet of the expansion chamber, where $I_1^+ = |P_1^+|^2(1+M_1)^2/\rho_1 c_1$, to obtain the relative acoustic power flux

$W_{3,1}$, as both pipe areas are the same. Figure 4.26 below shows the results for the normalised acoustic power flux in the outlet pipe for the first four order components with a Mach number $M = 0.1$.

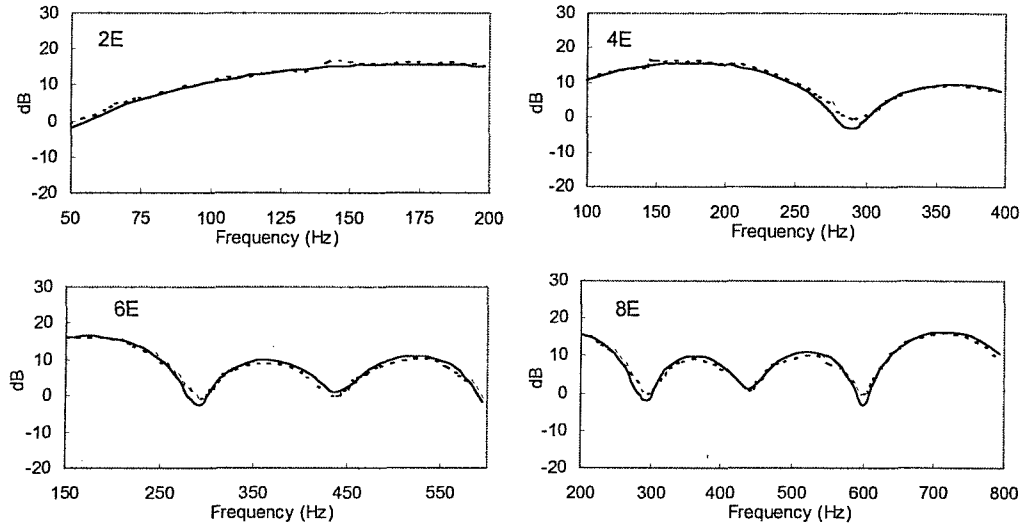

Figure 4.25 Measured (dash) and predicted (solid) system attenuation $AL_{1,3}$ with a Mach number $M = 0.1$. The measurement was analysed using order tracking.

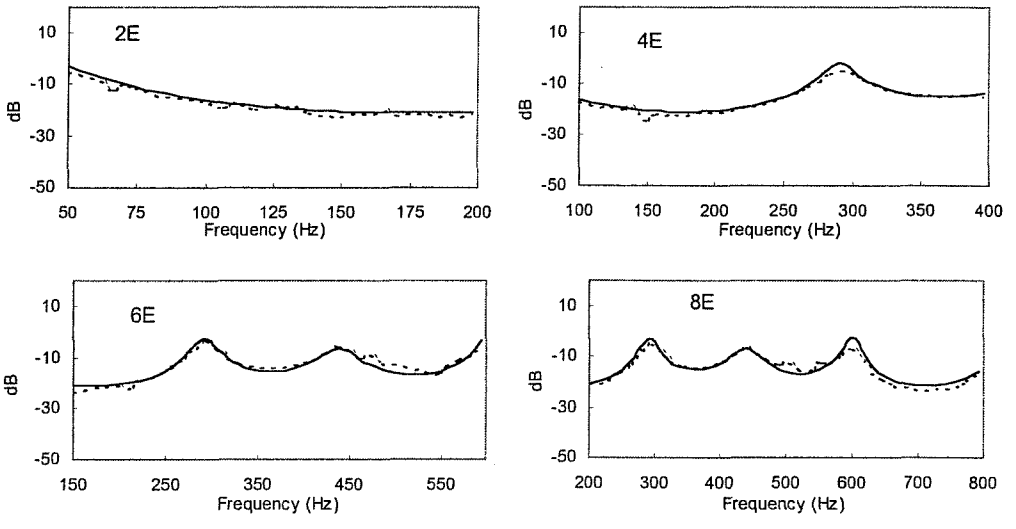

Figure 4.26 Measured (dash) and predicted (solid) normalised acoustic power flux in the outlet pipe $W_{3,1}$ with a Mach number $M = 0.1$. The measurement was analysed using order tracking.

The acoustic radiated power was estimated from the following equation [2.10]:

$$W_r = \frac{4\pi r^2 \, |G_{5,5}|^2}{\rho_0 c_0}, \tag{4.31}$$

where r is the microphone radius, $G_{5,5}$ is the auto-spectrum at station #5, c_0 is the ambient speed of sound and ρ_0 is the ambient density of air. The acoustic radiated power was also normalised to the acoustic power flux at the inlet of the expansion chamber to obtain the relative acoustic radiated power. Figure 4.27 below shows the predicted and measured radiated power for the first four order components with a Mach number $M = 0.1$.

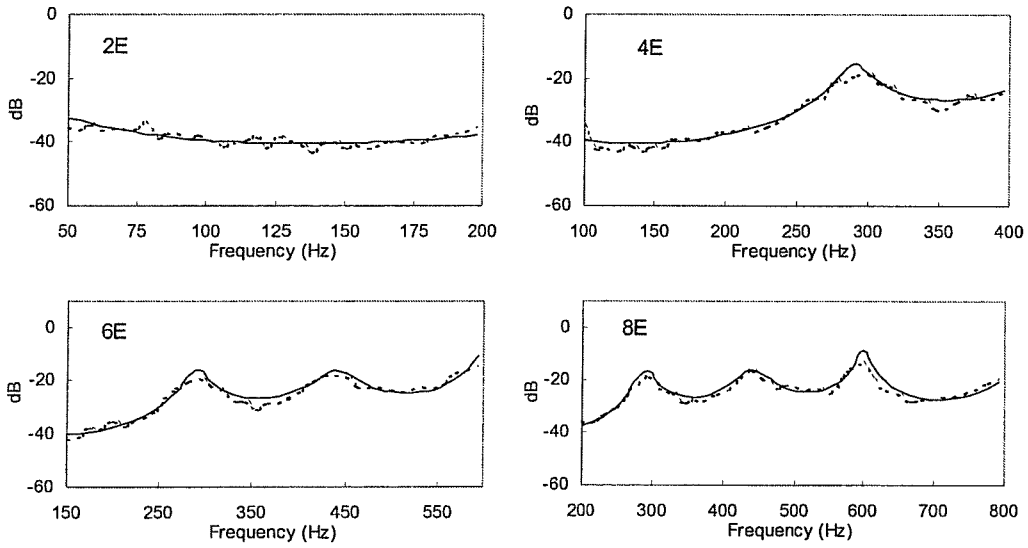

Figure 4.27 Measured (dash) and predicted (solid) normalised acoustic radiated power $W_{5,1}$ with a Mach number $M = 0.1$. The measurement was analysed using order tracking.

A fairly large measurement error due to contamination by non-acoustic pressure fluctuations can be tolerated in the resulting transfer function estimates as the results were directly estimated from the magnitude of the measured acoustic spectral pressure ratios [4.1]. This is illustrated by the good agreement (±2 to 3dB or better)

between the measured and predicted results for the transfer function $H_{3,1}$ (see Figure 4.23 on page 100) even at frequencies where the signal-to-noise ratios were relatively low for the 8E component between 500 and 600 Hz at station #3 (see Figure 4.11 on page 88). On the other hand, the system attenuation and acoustic power flux measurements were determined from the wave components $P^{\pm}$. Precise estimates of the transfer functions at the inlet $H_{2,1}$ (see Figures 4.19 on page 98 and 4.20 on page 99) and outlet $H_{4,3}$ (see Figures 4.21 on page 99 and 4.22 on page 100) of the silencer component are essential to yield reliable results for the wave component evaluation. The raggedness of the system attenuation and acoustic power flux measurements between 500 and 600 Hz for the 6E and 8E components (see Figures 4.25 and 4.26 on page 102) were caused by the lower signal-to-noise ratios, where the measured quantities were not sufficiently precise. The raggedness of the transfer function $H_{1,5}$ (see Figure 4.24 on page 101) and the acoustic radiated power (see Figure 4.27 on page 103) are partly due to room effects [4.1] as an external microphone is required for these measurements.

Close inspection of the results reveals that, as one would expect, the levels of the four orders for each individual measurement are the same where the frequency span of the orders overlap. The reason for this is that all the measured and predicted order components are subjected to the same mass flow and temperature conditions for the complete sweep. In addition, the results are either relative or normalised. However, it is important to realise that the frequency range, sweep-rate and frequency interval Δf_K for each order must be different at all the overlapping frequencies.

4.8 CONCLUSION

The bench test results showed that order analysis techniques can be used to capture transient harmonic pressure data to evaluate the acoustic performance of a silencer component. The successful application of the measurement technique required close attention to various theoretical and practical factors to ensure reliable results in the presence of mean flow. These factors are summarised below:

- careful selection of the order analysis signal processing parameters to achieve the optimum signal-to-noise ratios for a particular sweep rate and fundamental frequency;

- the design of a suitable transducer array to avoid the theoretical error in the four-microphone wave decomposition calculations (Appendix 4.2);

- a precise relative calibration of the pressure transducers, which is essential to compensate for the amplitude and phase differences that may exist in the four measurement channels (Appendix 4.3), and is crucial in obtaining realistic estimates of the very small proportion of the total fluctuating wave energy that is propagated through highly reactive exhaust systems;

- the precise incorporation of the gas properties in the calculation of the visco-thermal coefficient α and Mach number M (Appendix 4.1); knowledge of these properties is essential for a reliable estimation of the wave components $P^{\pm}$; and is particularly crucial for the measurements on a running vehicle where the gas properties change systematically, depending on the engine load and speed;

- the determination of the most favourable position of the pairs of pressure transducers at the inlet and outlet of the silencer component to obtain the optimum signal-to-noise ratios across the frequency range of interest.

The fixed sampling rate method is preferred when one only wants to capture the fundamental order for a wide frequency range. Careful selection of the signal processing parameters, including the record length, overlap and number of averages is essential to limit smearing and avoid leakage for a particular sweep-rate and measurement interval. On the other hand, order tracking is preferred to capture variable harmonic excitation because leakage and spectral smearing are avoided.

The order tracking method was used to evaluate the acoustic performance of a silencer component for partly simulated exhaust noise conditions. This was accomplished using variable harmonic excitation in the presence of mean flow on a test bench. The signal-to-noise ratio and the coherence were improved when the analysis was performed using a higher order resolution and an increased number of averages. It was essential to optimise the analysis time to avoid amplitude smearing. This was achieved by establishing the maximum number of averages that could be used for a given sweep-rate to prevent loss of data and phase distortion.

Good agreement (within ±2 to 3dB or better) was found between predicted and measured acoustic transfer functions, system attenuation, acoustic power flux and acoustic radiated power for the first four order components, which served to validate the measurement technique and opened up the possibility of measuring the acoustic performance of a silencer component on a running vehicle.

The rapid assessment of a silencer component acoustic behaviour for the normal operating conditions of a vehicle is demonstrated in the next chapter, applying the order tracking method. Measurements of the acoustic performance of an expansion chamber was compared to predictions to ascertain whether linear acoustic theory remains valid in the exhaust system of a running vehicle.

APPENDIX 4.1

TEMPERATURE-RELATED VARIABLES

The physical variables and fluid properties such as density ρ, pressure P, velocity u, kinematic viscosity ν, thermal conductivity k_T and ratio of specific heat γ, all depend on the local absolute temperature T of the flow. The acoustic behaviour of the exhaust system or its elements depend on the local sound propagation speed $c(1 \pm M)$, where c is the local speed of sound and M is the Mach number [1.4]. Thus, any assessment of the exhaust system acoustic performance requires a knowledge of the mass flow and temperature distribution throughout the system for the speed range of the engine.

The visco-thermal coefficient a for plane wave propagation in a circular duct can be expressed as [2.13]:

$$a = \left(\frac{1}{r \cdot c}\right) \cdot \sqrt{\frac{2\nu\pi f}{2}} \cdot \left(1 + (\gamma - 1) \cdot \sqrt{\frac{1}{Pr}}\right), \qquad \text{(A4.1.1)}$$

r = Pipe radius,
ν = Kinematic viscosity,
f = Frequency,
γ = Ratio of specific heat,
Pr = Prandtl number,
c = Speed of sound.

The wave propagation speed or speed of sound is defined by

$$c = c_o \cdot \sqrt{\frac{T_k}{273}} \cdot \left(\frac{\gamma}{\gamma_o}\right), \qquad \text{(A4.1.2)}$$

where T_k is the exhaust gas temperature in Kelvin and γ_o is the ratio of specific heat at 0^oC ($c_o = 331.5$ m/s).

According to Mayhew and Rodgers [4.14] the ratio of specific heat γ in terms of the temperature is expressed by

$$\gamma = 1.4033 - \left[0.024 \cdot ln\left(1 + \left(\frac{T_k}{504}^4\right)\right)\right], \qquad \text{(A4.1.3)}$$

and the ratio of specific heat γ_o at 0^oC is given by

$$\gamma_o = 1.401 \cdot \left(\frac{c_o}{331.5}\right)^2. \qquad \text{(A4.1.4)}$$

The following empirical expressions give the kinematic viscosity v for different temperature conditions [4.14]:

$$v = 1.33E-5 \cdot \left(\frac{T_k}{273}\right)^{1.71} \quad \text{for} \quad T_k < 800 \text{ and} \qquad \text{(A4.1.5)}$$

$$v = 1.802E-5 \cdot \left(\frac{T_k}{300}\right)^{1.565} \quad \text{for} \quad T_k > 800. \qquad \text{(A4.1.6)}$$

Exhaust gas velocity u is described by

$$u = \frac{m}{\rho \cdot S}, \qquad \text{(A4.1.7)}$$

where m is the mass flow, ρ is the gas density and S is the cross-sectional area.

The exhaust mass flow m is described by

$$m = m_{inlet} \cdot 1.071, \qquad \text{(A4.1.8)}$$

where m_{inlet} is the measured inlet mass flow. The exhaust mass flow m was estimated from the product of the inlet mass flow m_{inlet} and the assumed stochiometric air fuel mixture of 14.1 to 1 that increases the exhaust mass flow by a factor of 7.1%.

The exhaust gas density ρ is defined by

$$\rho = 1.2926 \cdot \left(\frac{273}{T_K}\right), \tag{A4.1.9}$$

and the Mach number is expressed by

$$M = \frac{u}{c}. \tag{A4.1.10}$$

APPENDIX 4.2

WAVE DECOMPOSITION ERROR MAGNIFICATION FACTOR

This appendix describes the error that occurs in the calculation of $P^{\pm}$ when the spacing between the microphones is close to a multiple of the half wavelength spacing, in other words, $kl = n\pi$, with $n = 1, 2, 3, etc.$ The effect of the error on the four-microphone wave decomposition measurements is demonstrated and a procedure to design a suitable transducer array is described.

First, an alternative approach is described to define the wave components $P^{\pm}$ from the pressure measurements P_1 and P_2 at station #1, as indicated in Figure A4.2.1 below [1.9].

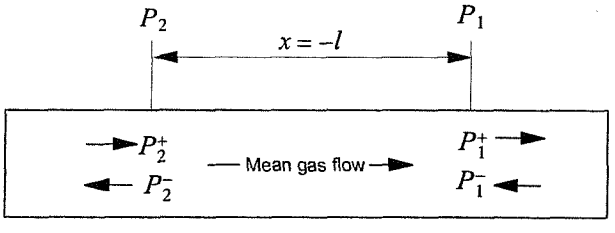

Figure A4.2.1 Two-microphone wave decomposition set-up.

With one-dimensional waves the acoustic pressure at stations #1 and #2 can be expressed in the frequency domain as the complex sum of the wave components at station #1:

$$P_1 = P_1^+ + P_1^-. \tag{A4.2.1}$$

$$P_2 = P_1^+ e^{-ik^+ l} + P_1^- e^{ik^- l}. \tag{A4.2.2}$$

Subtracting equation (A4.2.1) from (A4.2.2) gives

$$P_1 - P_2 = P_1^+ - P_1^+ e^{-ik^+ l} + P_1^- - P_1^- e^{ik^- l}. \qquad \text{(A4.2.3)}$$

Continuity of pressure at station #1 gives

$$P_1 = P_1^+ + P_1^- \quad \text{and} \quad P_1^+ = P_1 - P_1^-. \qquad \text{(A4.2.4a, b)}$$

It follows that

$$P_2 = P_1^+(e^{-ik^+ l} - e^{ik^- l}) + P_1 e^{ik^- l}. \qquad \text{(A4.2.5)}$$

Rearranging equation (A4.2.5) gives

$$P_1^+ = \frac{P_2 - P_1 e^{ik^- l}}{(e^{-ik^+ l} - e^{ik^- l})}, \qquad \text{(A4.2.6)}$$

and the modulus of the incident wave component is

$$|P_1^+| = \left| \frac{P_2 - P_1 e^{ik^- l}}{(e^{-ik^+ l} - e^{ik^- l})} \right|. \qquad \text{(A4.2.7)}$$

The reflected wave component is given by

$$P_1^- = -\left[\frac{P_2 - P_1 e^{-ik^+ l}}{(e^{-ik^+ l} - e^{ik^- l})} \right], \qquad \text{(A4.2.8)}$$

and the modulus of the reflected wave component is

$$|P_1^-| = \left| \frac{P_2 - P_1 e^{-ik^+ l}}{(e^{ik^- l} - e^{-ik^+ l})} \right|. \qquad \text{(A4.2.9)}$$

The calculated values for the wave components $|P_1^{\pm}|$ approach infinity when the denominator of equations (A4.2.7) and (A4.2.9) approaches zero. This condition occurs when $kl = n\pi$, with $n = 1, 2, 3, etc..$

One can show that equation (4.12) is equal to equation (A4.2.7). The modulus of equation (4.12) is equal to

$$|P_1^+| = \left| \frac{\sqrt{C_{1,1}}}{(1+R_1)} \right|. \tag{A4.2.10}$$

$$|P_1^+| = \left| \frac{\sqrt{C_{1,1}}}{1-\left(\frac{C_{2,1}-C_{1,1}e^{-ik^+l}}{C_{2,1}-C_{1,1}e^{ik^-l}}\right)} \right|. \tag{A4.2.11}$$

$$|P_1^+| = \left| \frac{\sqrt{(P_1P_1^*)}}{1-\left(\frac{(P_2P_1^*)-(P_1P_1^*)e^{-ik^+l}}{(P_2P_1^*)-(P_1P_1^*)e^{ik^-l}}\right)} \right|. \tag{A4.2.12}$$

$$|P_1^+| = \left| \frac{P_1}{1-\left(\frac{P_2-P_1e^{-ik^+l}}{P_2-P_1e^{ik^-l}}\right)} \right|. \tag{A4.2.13}$$

$$|P_1^+| = \left| \frac{P_1}{\frac{P_1e^{-ik^+l}-P_1e^{ik^-l}}{P_2-P_1e^{ik^-l}}} \right|. \tag{A4.2.14}$$

$$|P_1^+| = \left| \frac{P_2-P_1e^{ik^-l}}{e^{-ik^+l}-e^{ik^-l}} \right|. \tag{A4.2.15}$$

Therefore, equation (4.12) is also subjected to contamination caused by the error magnification factor.

It follows that one needs to make a detailed analysis of the error magnification factor $(e^{-ik^+l} - e^{ik^-l})^{-1}$ to determine the appropriate transducer arrays for a specified frequency range. The modulus of the denominator in equation (A4.2.15) can, according to Greenberg [4.15], also be defined by

$$\text{Denominator} = |e^{-ik^+l} - e^{ik^-l}|, \tag{A4.2.16}$$

$$= \sqrt{[cos(k^+l) - cos(k^-l)]^2 - i[sin(k^+l) - sin(k^-l)]^2}, \tag{A4.2.17}$$

$$= \sqrt{2(1 - cos(k^+l + k^-l)}, \tag{A4.2.18}$$

and the modulus of the error magnification factor $|E|$ is defined by

$$|E| = \frac{1}{\sqrt{2(1 - cos(k^+l + k^-l)}}, \tag{A4.2.19}$$

where $$k^+l + k^-l = \frac{2\pi fl}{C(1+M)} + \frac{2\pi fl}{C(1-M)} = \frac{4\pi fl}{C(1-M^2)}. \tag{A4.2.20}$$

When $\sqrt{2(1 - cos\left(\frac{4\pi fl}{C(1-M^2)}\right)} = 0$ and $cos\left(\frac{4\pi fl}{C(1-M^2)}\right) = 1$, the magnification error approaches ∞ so that discrepancies are introduced into the calculations.

The frequencies of these discrepancies occur at

$$f = n\left(\frac{C(1-M^2)}{2l}\right) \quad ; \quad l = 0, 1, 2, etc.. \tag{A4.2.21}$$

The error magnification is avoided when

$$\sqrt{2(1 - cos\left(\frac{4\pi fl}{C(1-M^2)}\right)} > 1 \quad \text{and} \quad cos\left(\frac{4\pi fl}{C(1-M^2)}\right) < 0.5.$$

Thus, for a single pair of transducers separated by an axial distance l, reliable estimates of the wave components can be expected when

$$\frac{(6n+1)\pi}{3} \leq \left(\frac{4\pi fl}{C(1-M^2)}\right) \leq \frac{(6n+5)\pi}{3} \quad ; \quad n = 0, 1, 2, etc.. \qquad \text{(A4.2.21)}$$

To demonstrate the characteristics of the error magnification factor, the variation of $\sqrt{2(1-cos\left(\frac{4\pi fl}{C(1-M^2)}\right)}$ as a function of $\left(\frac{4\pi fl}{C(1-M^2)}\right)$ is displayed in Figure A4.2.2 below. One notes that it displays a cyclical nature.

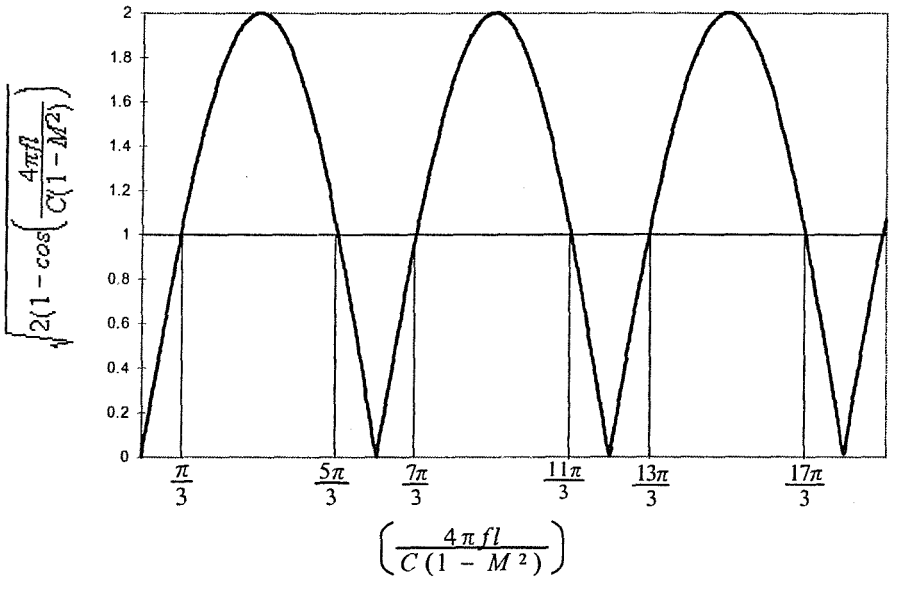

Figure A.4.2.2 Frequency characteristics of the error magnification factor.

Therefore, a single transducer separation provides a number of frequency bands where the measurements are not contaminated. Experience suggests that the first band provides more reliable estimates than the others. When the frequency range to be analysed exceeds the band provided by a single pair of transducers, additional pairs of transducer arrays are required [4.16]. The procedure to determine the number of transducer arrays is specified below.

The minimum frequency for the first band is

$$\frac{4\pi fl}{C(1-M^2)} = \frac{\pi}{3}, \tag{A4.2.22}$$

$$f_{min} = \frac{C(1-M^2)}{12l}, \tag{A4.2.23}$$

and the maximum frequency for the first band is

$$\frac{4\pi fl}{C(1-M^2)} = \frac{5\pi}{3}, \tag{A4.2.24}$$

$$f_{max} = \frac{5 * C(1-M^2)}{12l}. \tag{A4.2.25}$$

The ratio R between f_{max} and f_{min} should therefore be less than 5 to avoid the error indicated by

$$R = \frac{f_{max}}{f_{min}} = \frac{5 * C(1-M^2)}{C(1-M^2)} < 5, \tag{A4.2.26}$$

$$R < 5. \tag{A4.2.27}$$

The number of transducer arrays for a specific frequency band is expressed by

$$n = log_5\left(\frac{f_{final}}{f_{initial}}\right) \text{ (rounder to + infinity)}, \tag{A4.2.28}$$

n	=	Number of transducer arrays,
f_{final}	=	Final frequency,
$f_{initial}$	=	Initial frequency.

A computer programme was developed to design the appropriate transducer arrays for a specific frequency band, based on the above theory. So, for example, four microphone separation distances of 950 mm, 285 mm, 95 mm and 35 mm were required to cover a frequency band from 20 Hz to 4 kHz. These are displayed in Figure A4.2.3 below, showing the overlapping frequency bands of the four transducer arrays where the value of the error magnification factor falls below the value of one.

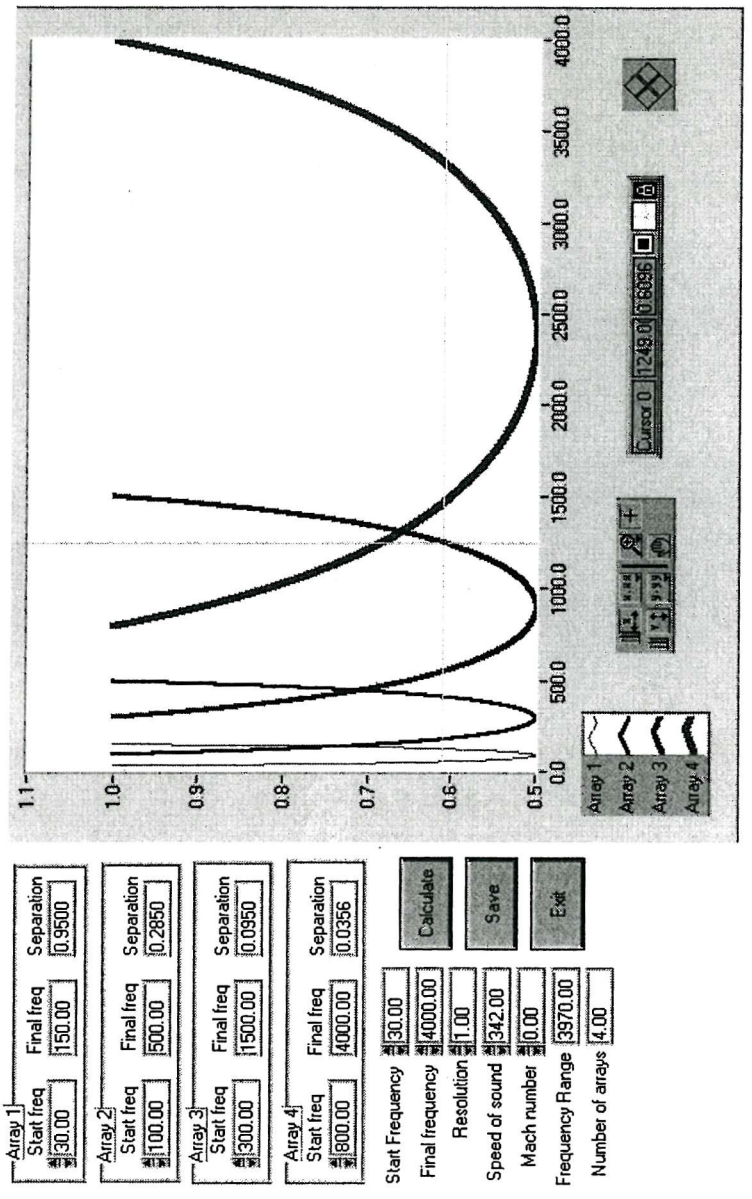

Figure A4.2.3 Front panel of the computer programme that was developed to optimise the transducer arrays for a specified frequency range.

To demonstrate the influence of the error magnification factor, the acoustic performance of the simple expansion chamber displayed in Figure A4.2.4 below was measured on a test bench with zero flow. The system was excited with broad-band noise by means of a loudspeaker. The pressure time signals were analysed with an FFT analyser to obtain the required auto, cross and transfer function spectra. These quantities were used to estimate the wave components $P^{\pm}$ at the inlet and outlet of the silencer according to the procedures outlined in Section 4.2. The acoustic predictions were performed using APEX.

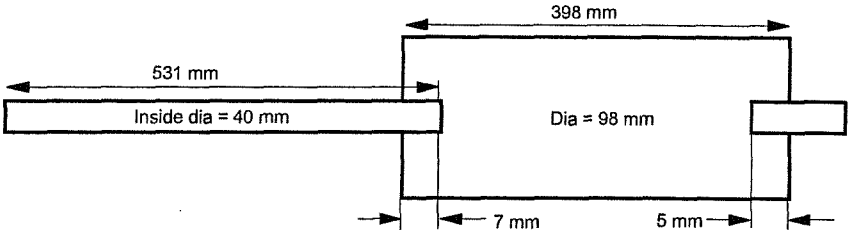

Figure A4.2.4 Geometric detail of the simple expansion chamber for which the acoustic performance was measured on the test bench using broad-band excitation.

Figures A4.2.5 and A4.2.6 (on pages 118 and 119) show the measured system attenuation for six different microphone separation distances, from 50 mm to 350 mm. The predicted system attenuation and error magnification factor are also displayed. The microphone positions are indicated in Figure A4.2.7 on page 120.

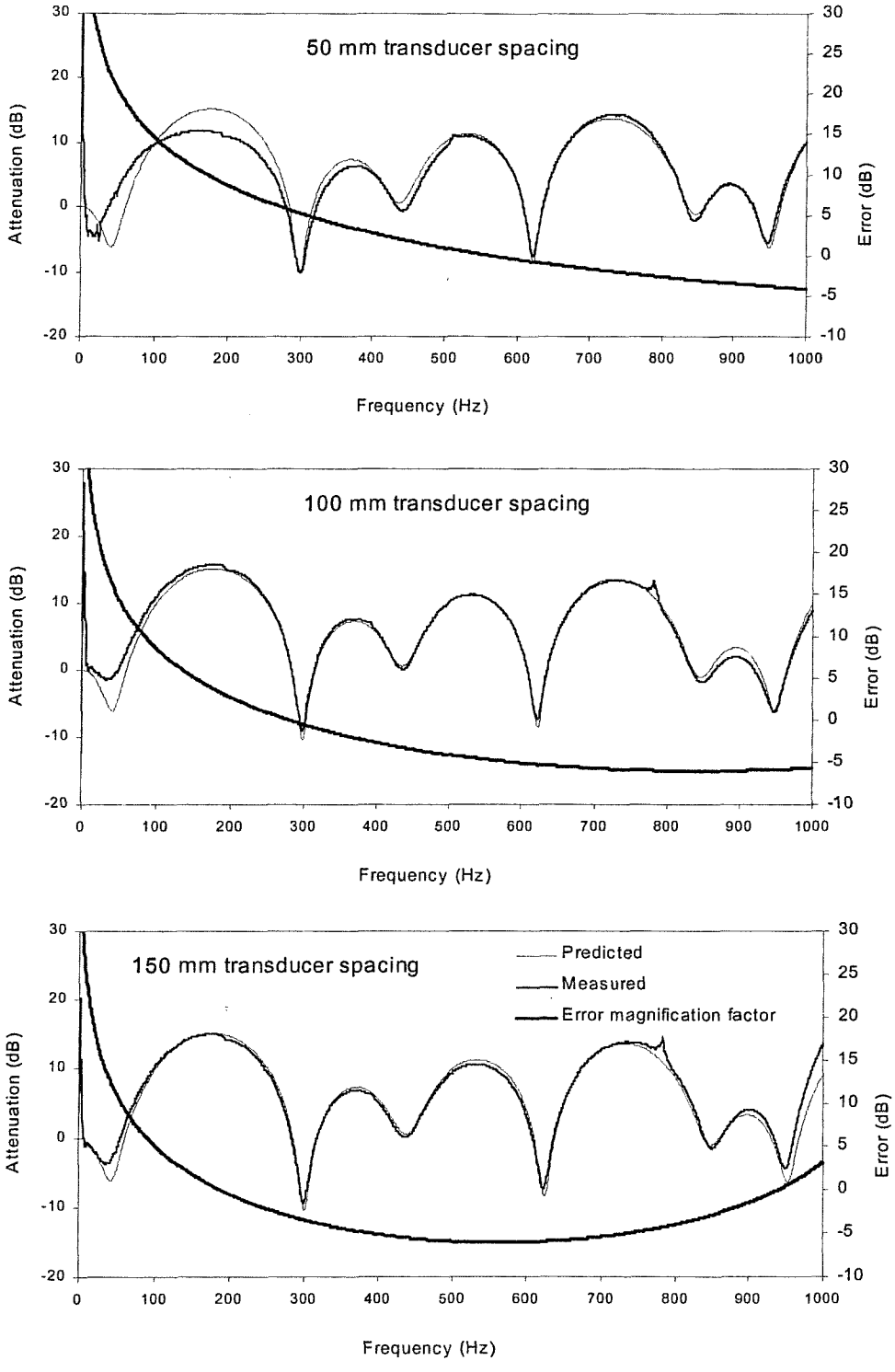

Figure A4.2.5 Measured and predicted system attenuation for separation distances of 50 mm, 100 mm and 150 mm, measured on the test bench using random excitation and zero flow.

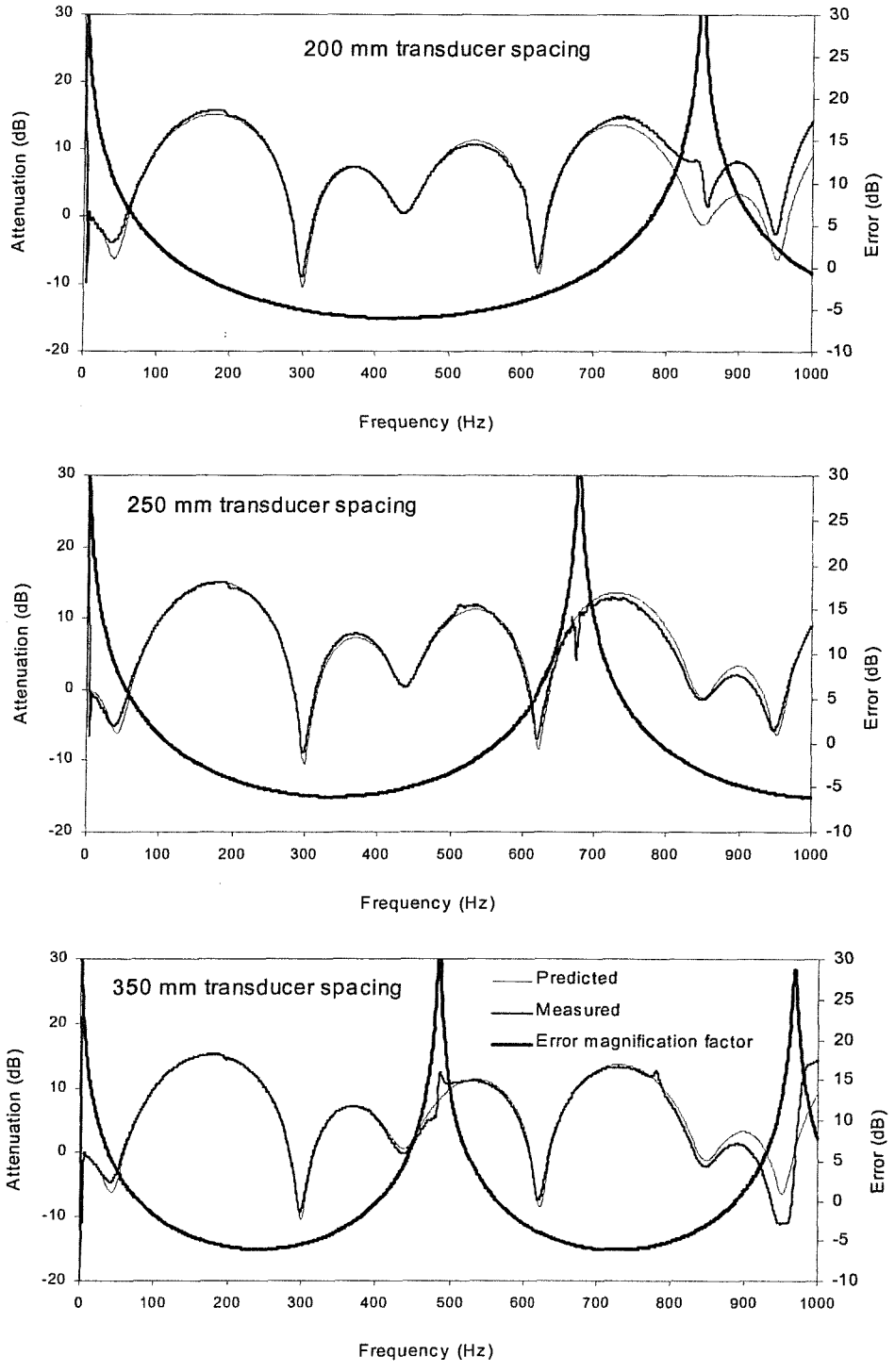

Figure A4.2.6 Measured and predicted system attenuation for separation distances of 200 mm, 250 mm and 350 mm, measured on the test bench using random excitation and zero flow.

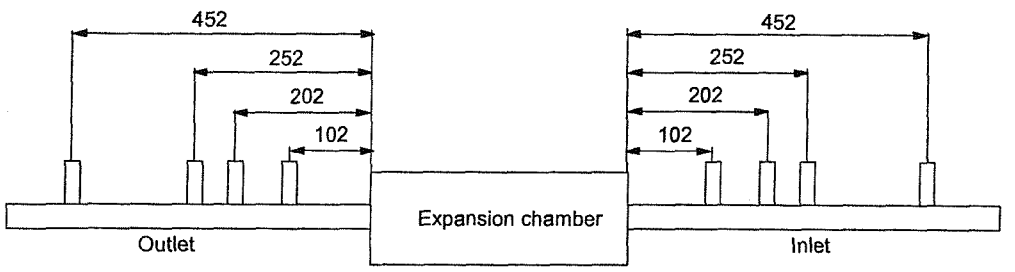

Figure A4.2.7 Microphone positions at the inlet and outlet of the expansion chamber that were used to demonstrate the effect of the error magnification factor.

Good agreement was obtained between the measured and predicted results at frequencies where the magnification error was less than zero dB (1). The small discrepancy at 784 Hz for the separation distances of 100 mm, 150 mm and 350 mm was related to low signal-to-noise ratios. One notes that large discrepancies occurred when the transducer spacing was close to multiples of a half wavelength. Therefore, one can conclude that an appropriate transducer array to obtain reliable results for a specified frequency range, as outlined above, needs to be designed.

APPENDIX 4.3

WAVE DECOMPOSITION CALIBRATION PROCEDURE

A relative calibration of the transducers was required to compensate for the amplitude and phase differences that may exist in the four measurement channels. This can be accomplished by mounting the pressure transducers on the same axial section of a duct (see Figure A4.3.1 below) and exposing them to the same pressure field P_0.

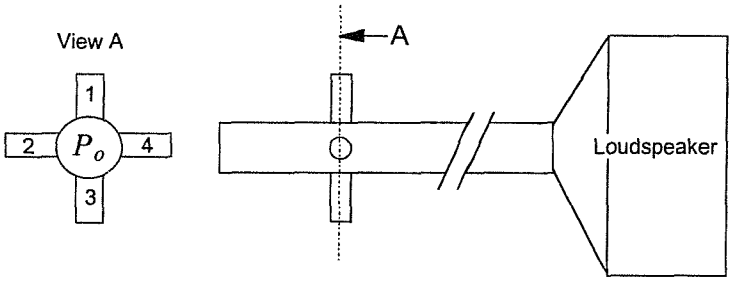

Figure A4.3.1 Position of microphones mounted on the same axial plane for relative calibration measurements.

An absolute calibration of the microphone mounted at station #1 was first performed when absolute sound pressure levels were required. The pressure transducers were then positioned in the tube at the same axial position and subjected to a pure tone (500 Hz). The gain factor for each measurement channel was adjusted to give exactly the same amplitude as that measured for channel #1. Because all the pressure transducers are subjected to the same acoustic field P_0, the absolute calibrated pressure $\overline{P}_n$ for a particular measurement channel n and frequency are expressed by

$$\overline{P}_n = \frac{V_n}{S_{va}} * G_n \qquad ; \qquad n = 1,2,3,etc., \qquad \text{(A4.3.1)}$$

$\overline{P_n}$ = Absolute calibrated pressure,
V_n = Channel signal (Volts),
S_{va} = Pressure transducer sensitivity (mV/Pa),
G_n = Channel gain factor.

Next, a relative calibration was performed to correct the frequency response of the pressure transducers relative to the frequency response of the pressure transducer mounted at station #1 (see Figure A4.3.1 on page 121). Generally, the relative calibration factors $\hat{R}_n$ may be estimated by means of the following equations:

$$\hat{R}_{n,1} = \frac{\hat{P}_n}{\hat{P}_1} \qquad ; \qquad n = 1,2,3,etc., \qquad \text{(A4.3.2)}$$

$\hat{P}_n$ = Pressure transducer n,
$\hat{P}_1$ = Pressure transducer #1,
$\hat{}$ = Complex value.

Alternatively, the measured relative calibration factors can be defined by means of a transfer function $\hat{R}_{n,1}$:

$$\hat{R}_{n,1} = \frac{\hat{P}_n \cdot \hat{P}_1^*}{P_{1,1}} \qquad ; \qquad n = 1,2,3,etc., \qquad \text{(A4.3.3)}$$

$\hat{P}_n \cdot \hat{P}_1^*$ = Cross-spectrum,
$\hat{P}_{1,1}$ = Auto-spectrum,
$*$ = Complex conjugate.

As outlined in Section 4.2, the following spectral functions are required to extract $P^{\pm}$ from the four pressure measurement:

$C_{1,1}$ = Auto-spectrum at station #1 (real value),

$C_{3,3}$ = Auto-spectrum at station #3 (real value),

$\hat{C}_{3.1}$ = Cross-spectra between station #3 and #1 (complex value),

$\hat{H}_{2.1}$ = Transfer function between stations #2 and #1 (complex value),

$\hat{H}_{4,3}$ = Transfer function between stations #4 and #3 (complex value).

These are then incorporated into the relative calibration ratios $\tilde{R}_{n,1}$ to obtain the relative calibrated functions by means of the following ratios:

$$C_{1,1} = \frac{C_{1,1}}{R_{1,1}} = \frac{C_{1,1}}{1} = C_{1,1}. \qquad \text{(A4.3.4)}$$

$$\tilde{C}_{3,3} = \frac{C_{3,3}}{\hat{R}_{3,1}}. \qquad \text{(A4.3.5)}$$

$$\tilde{C}_{3,1} = \frac{\hat{C}_{3,1}}{\hat{R}_{3,1}}. \qquad \text{(A4.3.6)}$$

$$\tilde{H}_{2,1} = \frac{\hat{H}_{2,1}}{\hat{R}_{2,1}}. \qquad \text{(A4.3.7)}$$

$$\tilde{H}_{4,3} = \frac{\hat{H}_{4,3}}{(\hat{R}_{4,1}/\hat{R}_{3,1})} = \frac{\hat{H}_{4,3}}{\hat{R}_{4,3}}. \qquad \text{(A4.3.8)}$$

Where $\tilde{}$ refers to relative calibrated function.

An alternative method was also evaluated by mounting the pressure transducers on the same axial position, but parallel to the duct, as illustrated in Figure A4.3.2 below. The holder was machined out of aluminium and provided with four holes to accommodate the transducers. A small edge at the end of the holes ensured that the microphones were all positioned on the same plane. The potential advantage of this method is that the position of the holder inside the pipe can be optimised to avoid pressure minima.

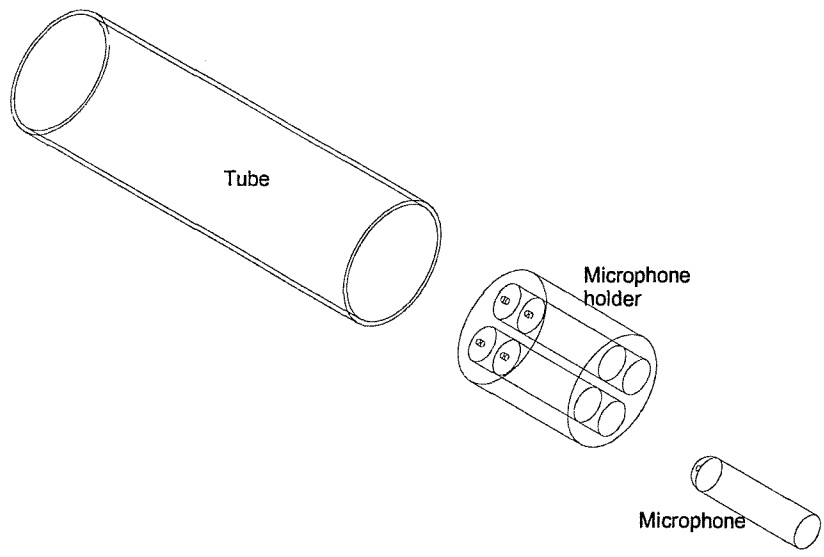

Figure A4.3.2 Alternative method to mount pressure transducers for the calibration procedure.

The magnitude and phase of $\hat{R}_{2,1}$, $\hat{R}_{3,1}$ and $\hat{R}_{4,1}$ for the first four harmonics are displayed in Figures A4.3.3 to A4.3.6 on pages 125 and 126 respectively. The results show magnitudes close to one and phase angles close to zero, which is an indication that the frequency response of the measurement channels is similar. However, the higher frequencies (6E and 8E) showed greater variation than the lower frequencies (2E and 4E).

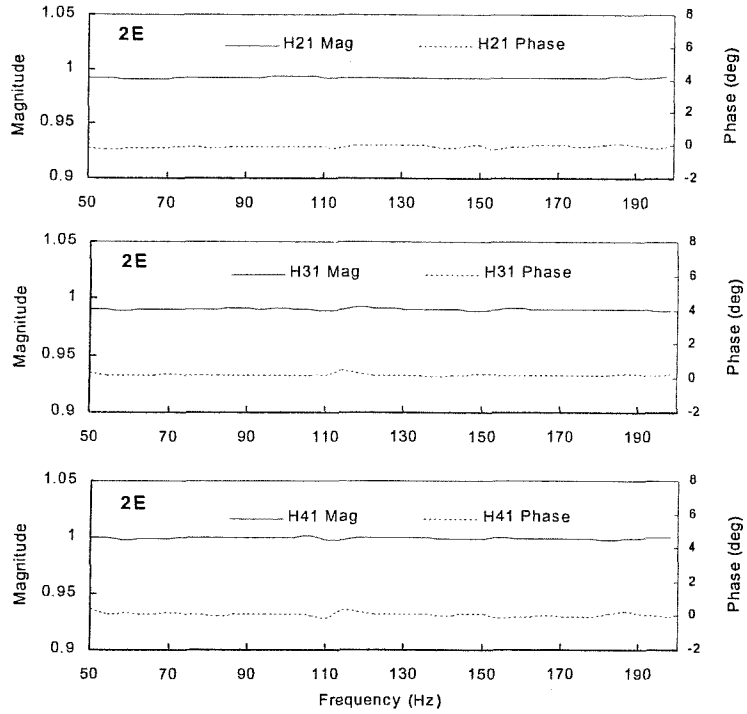

Figure A4.3.3 Relative calibration ratios $\hat{R}_{2,1}$, $\hat{R}_{3,1}$ and $\hat{R}_{4,1}$ (magnitude and phase) estimated for the 1st harmonic (2E).

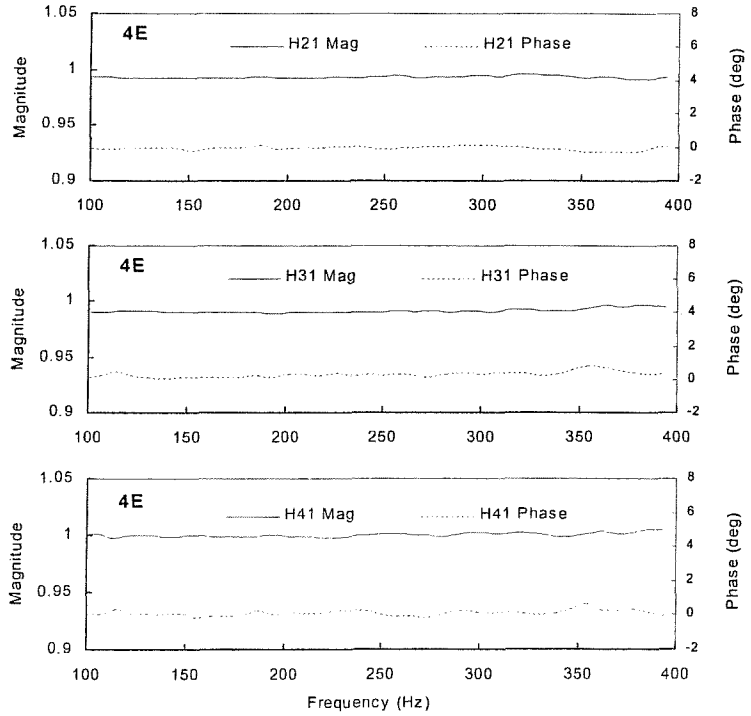

Figure A4.3.4 Relative calibration ratios $\hat{R}_{2,1}$, $\hat{R}_{3,1}$ and $\hat{R}_{4,1}$ (magnitude and phase) estimated for the 2nd harmonic (4E).

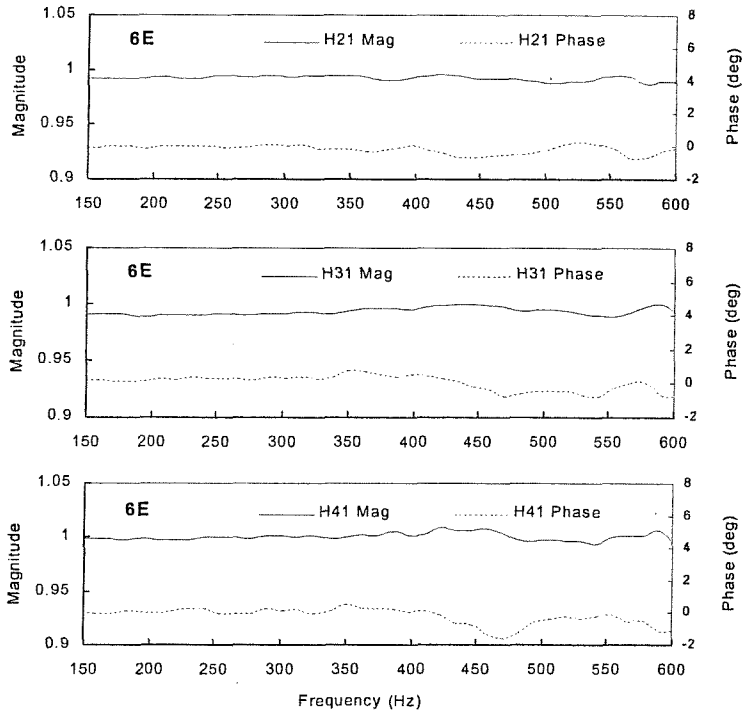

Figure A4.3.5 Relative calibration ratios $\hat{R}_{2,1}$, $\hat{R}_{3,1}$ and $\hat{R}_{4,1}$ (magnitude and phase) estimated for the 3rd harmonic (6E).

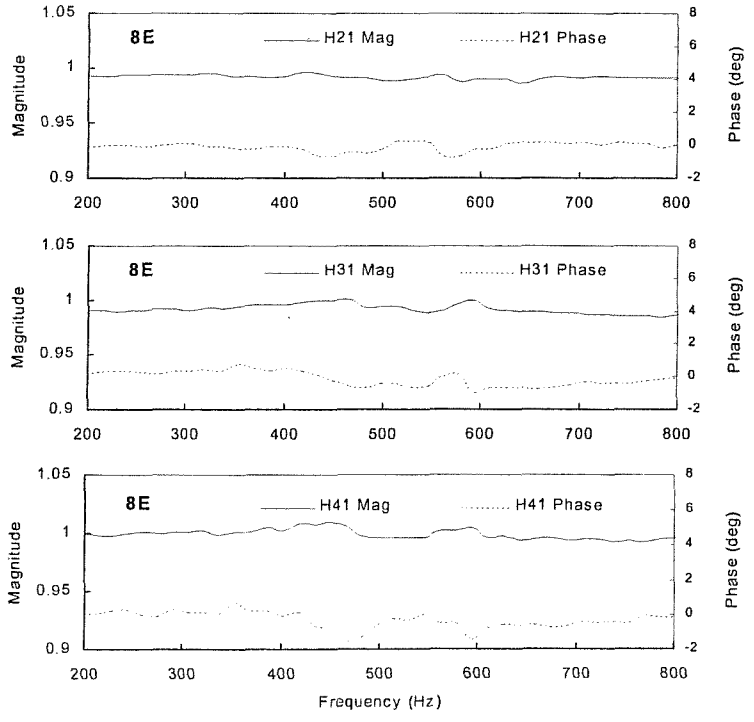

Figure A4.3.6 Relative calibration ratios $\hat{R}_{2,1}$, $\hat{R}_{3,1}$ and $\hat{R}_{4,1}$ (magnitude and phase) estimated for the 4th harmonic (8E).

APPENDIX 4.4

ACOUSTIC VALIDATION OF ELLIPTICAL SECTION REVERSE FLOW SILENCER ELEMENTS

To validate the APEX prediction of elliptical section reverse flow chambers, the fixed sampling rate method described in Section 4.7.1 was adopted. The geometric details of the reverse flow elements considered for this study are displayed in Figures A4.4.1 to A4.4.3 on pages 127 and 128. One notes that the elliptical section, and the inlet and outlet pipe configuration were kept the same for all three silencers, while the length of each chamber was different.

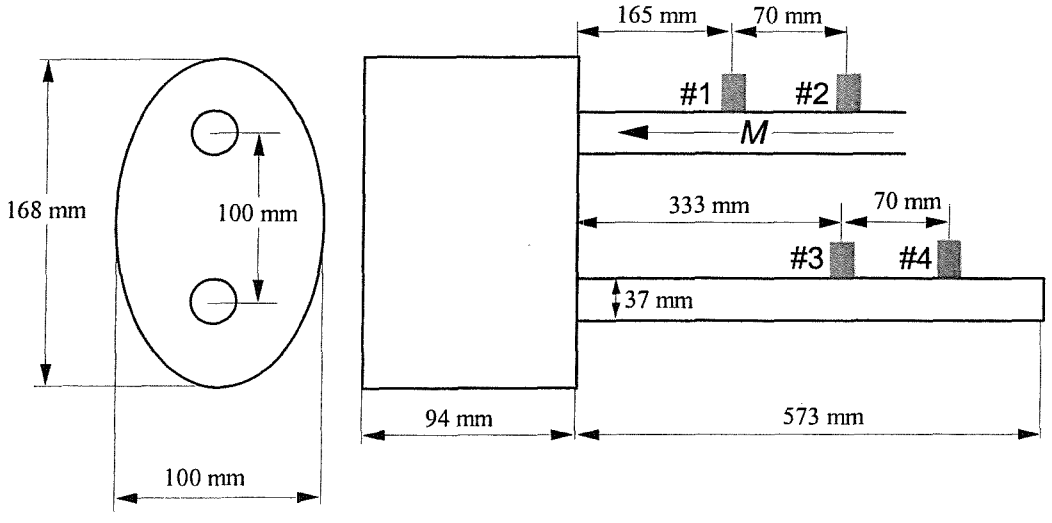

Figure A4.4.1 Reverse flow element #1.

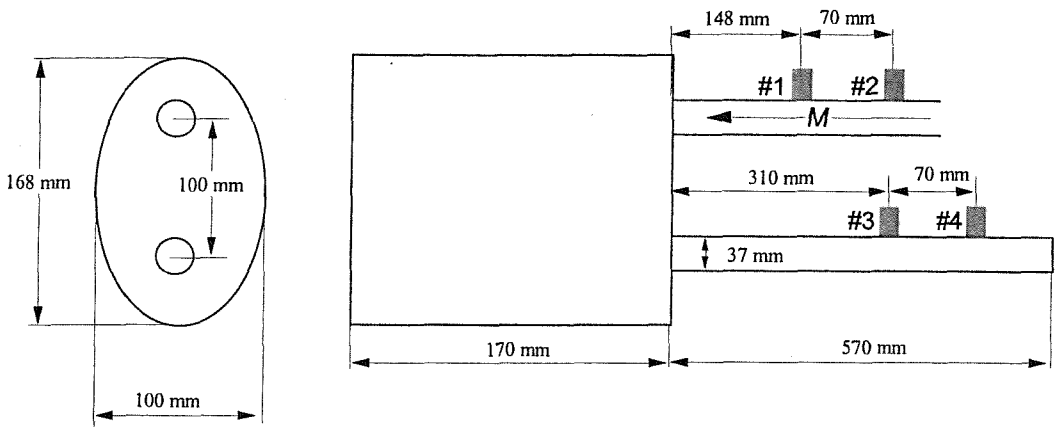

Figure A4.4.2 Reverse flow element #2.

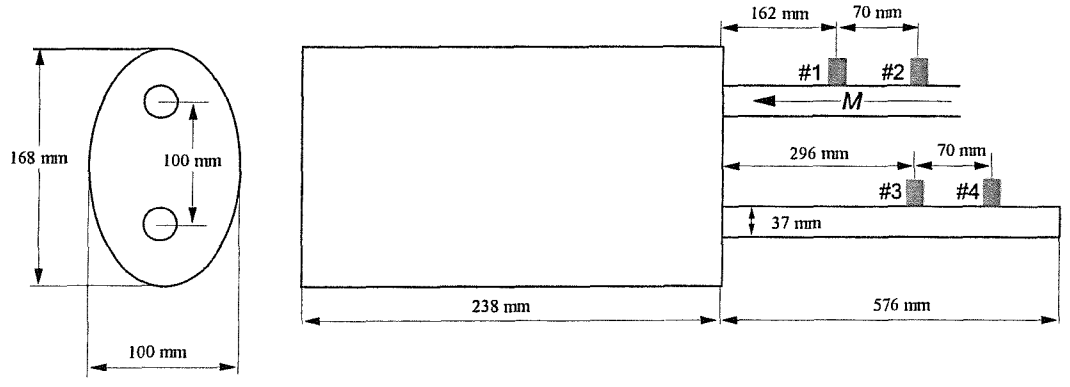

Figure A4.4.3 Reverse flow element #3.

The predicted and measured attenuation $AL_{1,3}$ of the three reverse flow elements are displayed in Figure A4.4.4 (Reverse flow element #1), Figure A4.4.5 (Reverse flow element #2) and Figure A4.4.6 (Reverse flow element #3).

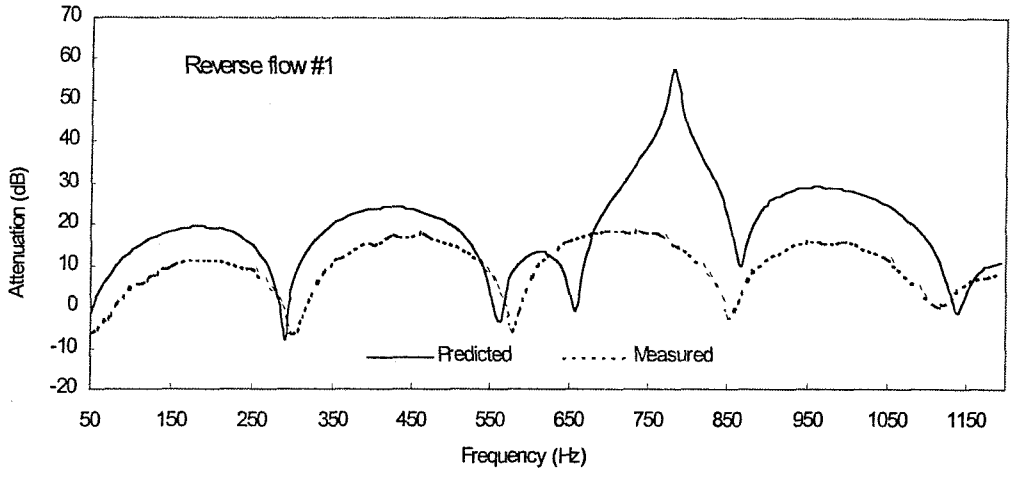

Figure A4.4.4 Predicted and measured attenuation $AL_{1,3}$ for reverse flow element #1.

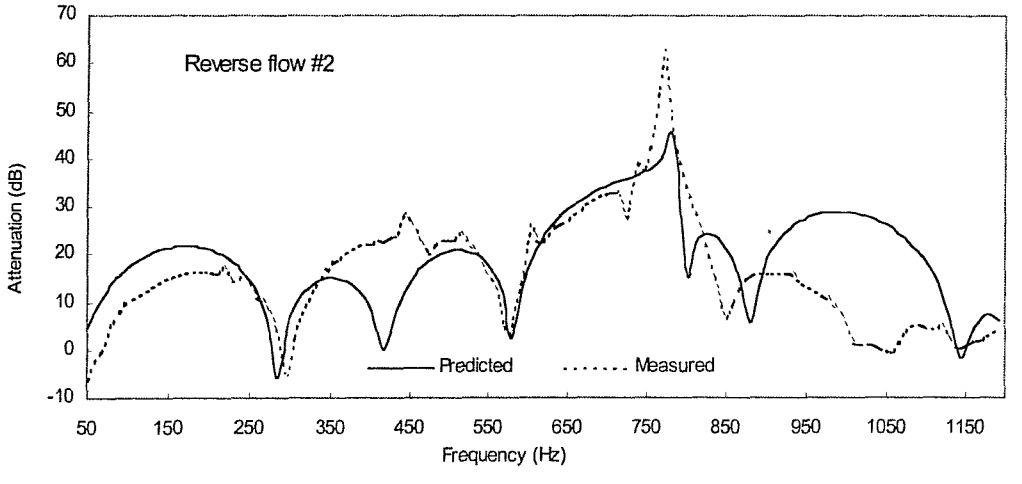

Figure A4.4.5 Predicted and measured attenuation $AL_{1,3}$ for reverse flow element #2.

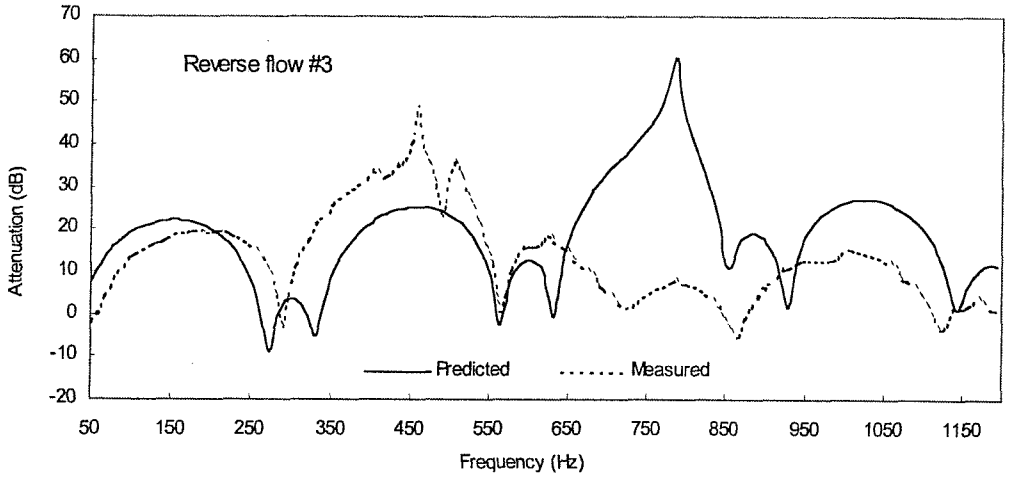

Figure A4.4.6 Predicted and measured attenuation $AL_{1,3}$ for reverse flow element #3.

One notes that the predicted and measured system attenuation $AL_{1,3}$ generally showed poor agreement for all three elements. This was the case for both the tail-pipe resonance troughs and attenuation levels. The predicted results showed peak attenuation levels for all three chambers just below 800 Hz. It appears that this peak is related to some branch volume that acts as a side branch tube which depends on the distance between the inlet and outlet pipe (100 mm). By contrast, the side branch frequency for the measured results was reduced when the chamber length was increased. In fact, the side branch resonance could not be observed for the shortest chamber length (reverse flow element #1). These results clearly indicate the need for further research to improve the APEX acoustic modelling of elliptical section reverse flow silencers. With other measurements Davies, Harrison and Collins [2.16] suggested that models that assume one-dimensional wave propagation may often be inadequate with flow reversal geometry.

Young and Crocker [4.17] used a numerical approach based on a finite element method to predict the transmission loss characteristics of elliptical section reverse flow mufflers. Predictions and measurements showed fair agreement for a number of inlet and outlet configurations up to 1800 Hz.

Denia, Albelda and Fuenmayor [4.18] recently published a paper on the acoustic behaviour of elliptical chamber mufflers. The solution of the wave equation in elliptic co-ordinates was expressed in terms of Mathieu functions which was used to obtain the natural frequencies and mode shapes. The model superposition technique and point source method were applied to obtain the transmission loss of a number of elliptical sections, including flow reversal chambers. The analytical results were compared to finite element calculations and measurements. However, the above authors preferred the new analytical method, due to the long computation time required by finite element methods at high frequencies to obtain sufficient accuracy. Polynomial fitting curves were also evaluated to predict the cut-off frequency, since the plane wave model is valid only below the frequency which corresponds to the first transversal mode. The multi-dimensional analytical transmission loss results agreed well with both the finite element calculation and measurements up to 3000 Hz.

Bench testing provides an alternative experimental method for developing predictive models [2.11, 2.26, 4.19]. This may be accomplished by the experimental evaluation of the wave components $P^{\pm}$ at the inlet and outlet of a silencer element or a sequence of elements to describe their acoustic transfer characteristics by means of the four elements of the scattering matrix T [4.19]. The complex values of the four elements of the scattering matrix are a function of the geometry of the element or system, density ρ, speed of sound c, frequency of excitation f and Mach number M, but remain independent of the acoustic impedance at the termination Z. The transmission coefficients $T_i = P_1^+/P_2^+$ and $T_r = P_1^-/P_2^-$, together with the reflection coefficient $r = P_2^-/P_1^-$, may then be used to determine the four elements of the scattering matrix T outlined in [4.19]. The results would require appropriate scaling for successful application in practical predictive modelling.

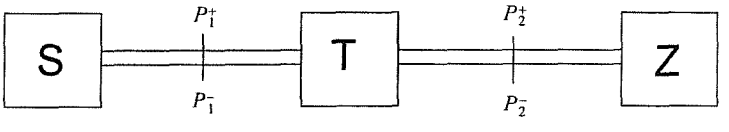

Figure A4.4.7 Plane wave acoustic transmission across an element.

CHAPTER 5

ACOUSTIC ASSESSMENT OF A SILENCER COMPONENT ON A RUNNING VEHICLE

5.1 INTRODUCTION

The primary aim of the transient measurement technique developed in the previous chapter was to assess the acoustic behaviour of a silencer component, together with all the variable factors for the transient operating conditions of a running engine. Subsequently, it was applied to assess the acoustic performance of an expansion chamber fitted to the exhaust system of a Honda 1.5 litre, four-stroke four-cylinder engine for an acceleration run-up. Although the basic approach for the bench test and vehicle measurements are similar, the engine acceleration, instead of the acoustic excitation, is now the controlled variable. In addition, the engine frequency, sound pressure, exhaust mass flow and exhaust gas temperature all change systematically over time, depending on the engine sweep-rate and engine load conditions. Precise measurement of these variables is required at regular engine speed intervals to estimate the acoustic performance. Furthermore, the transient operation of the vehicle on the chassis dynamometer was restricted by the overheating of the engine, and so appropriate changes to the experimental and data processing procedures were required [1.1, 1.11].

Section 5.2 presents the experimental set-up of the vehicle, the details of the exhaust system and the equipment that was used to measure the mass flow, temperature and pressure. Section 5.3 describes a procedure to estimate the signal-to-noise ratios from the measured harmonic spectra to evaluate the reliability of the measurements, as it was not possible to measure them. Section 5.4 covers the acoustic predictions. This is

followed by the acoustic assessment of the expansion chamber for the practical operating conditions of the vehicle in Section 5.5. Measurements were also performed for constant engine speed conditions to demonstrate the advantages of the new transient approach in Section 5.6. Other applications are illustrated in Appendix 5.1

5.2 EXPERIMENTAL SET-UP

The vehicle was operated in third gear on a chassis dynamometer inside a semi-anechoic chamber. The acceleration rate of the vehicle was controlled by means of a computer connected to an eddy current brake. The silencer component was mounted next to the vehicle to allow access to the equipment, as set out in Figure 5.1 below. A packed perforated silencer was mounted at the front to reduce flow noise. A flexible coupling was used to reduce vibration levels.

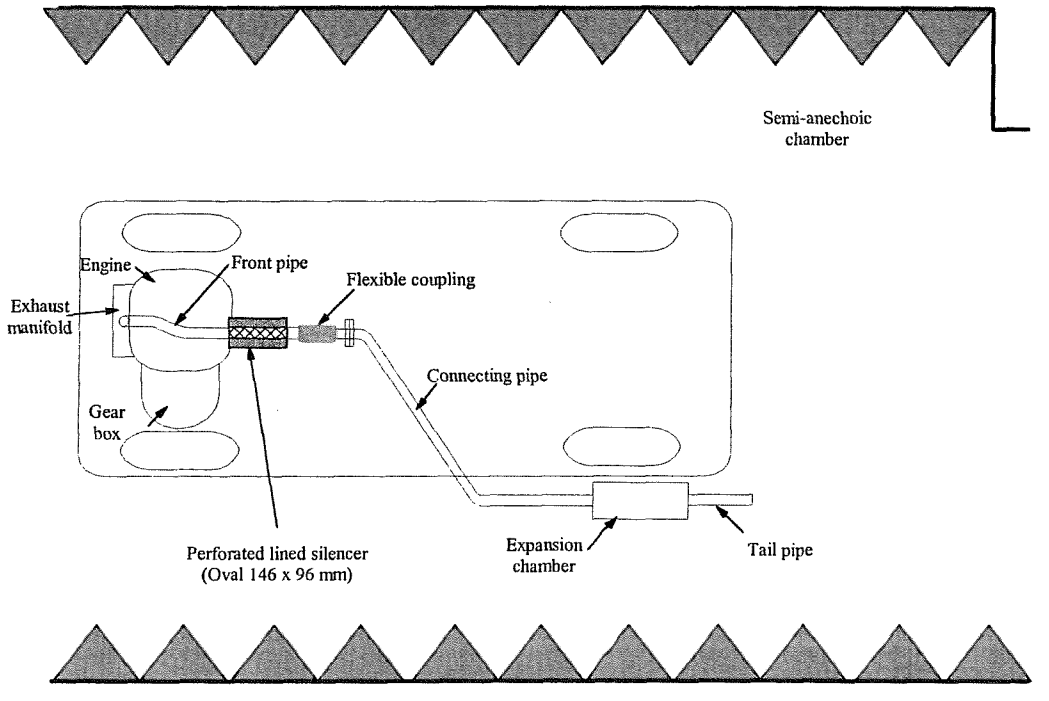

Figure 5.1 Schematic representation of the vehicle set-up, showing the position of the vehicle inside the semi-anechoic chamber. The silencer component was positioned next to the vehicle so that it was possible to access the pressure transducers and thermocouples.

The experimental set-up is shown in Figure 5.2 below. One notes that it is similar to that used for the bench test measurements described in Section 4.3, except that the tracking of the fundamental frequency was measured using a tachometer connected to the ignition coil of the engine. The Kistler (Type 701A) quartz pressure transducers used on the bench test were also used for the measurements on the vehicle. The installation of the transducers is displayed in Figure 4.3 on page 74. It was necessary to connect the transducers to a cooling system due to the high exhaust gas temperature (300 to 700 ^{o}C). The pressure transducers were mounted inside water-cooled adapters and water was circulated through the adapters at ambient temperature. The effect of engine vibration on the sound pressure measurements was limited by the very low acceleration sensitivity of the transducers (<0.001 bar/g).

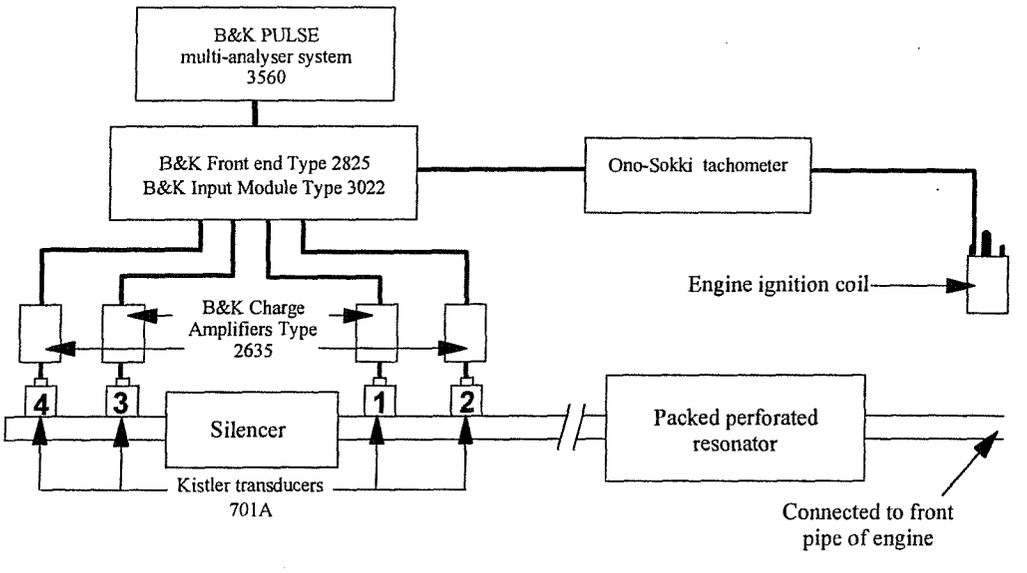

Figure 5.2 Experimental set-up to measure the acoustic properties of a silencer component during engine acceleration.

The exhaust system layout and the geometric detail of the expansion chamber are set out in Figure 5.3 below. The simple expansion chamber was similar in construction to those used for the bench test measurements. Comparison with Figure 4.18 on page 97 shows that the expansion ratio has been increased from 7.38 to 9, but the lengths of the expansion chambers are almost the same. The transducer separation distance was increased for the measurements on the vehicle, compared to the separation distance used on the bench test because of the higher exhaust gas temperatures and the corresponding increase in wave lengths. The error magnification factor was avoided for frequencies below 800 Hz with a transducer separation distance of 180 mm (see Appendix 4.2). The external microphone was positioned perpendicular and 200 mm from the centre of the tail-pipe outlet.

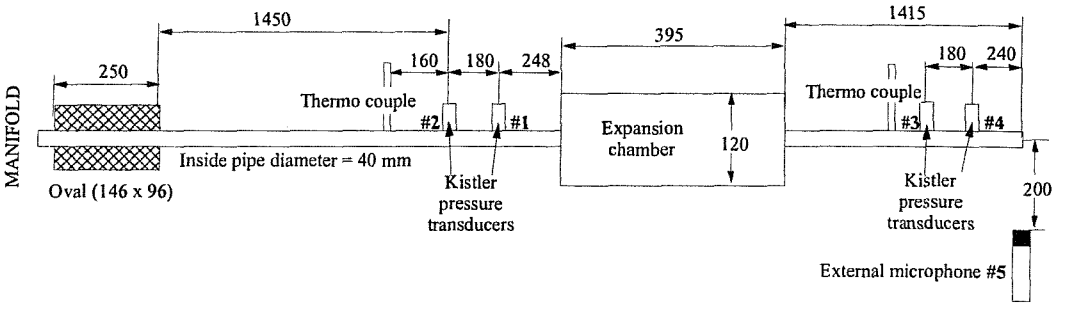

Figure 5.3 Schematic representation of the exhaust system layout and the geometric detail of the expansion chamber fitted to the Honda 1.5 litre (all dimensions are in millimetres).

The intake mass flow was measured using a hot wire probe that was connected to the inlet duct of the carburettor, mounted inside a 2 metre long pipe to obtain a smooth flow, as is shown in Figure 5.4 on page 136. The analogue output of the probe was connected to a data acquisition system. The mass flow calibration was performed on a flow rig with a water manometer. The mass flow and the analogue output voltage of the probe was recorded at forty positions between 0 and 0.1 kg/s. on a cold flow bench for calibration purposes.

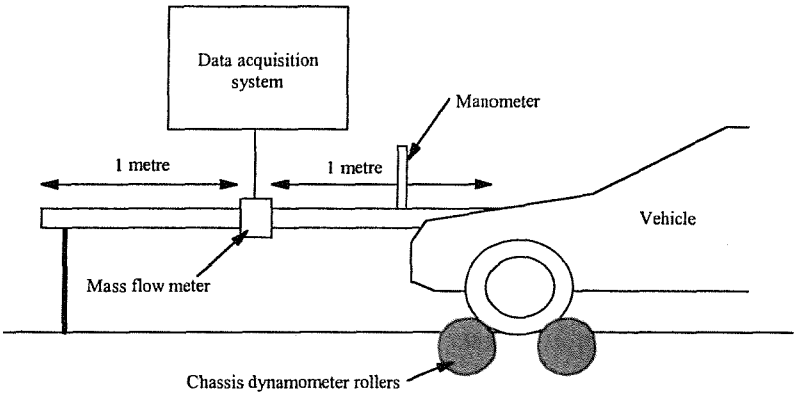

Figure 5.4 Equipment set-up to measure the intake mass flow of the engine while operating the vehicle on the chassis dynamometer.

The exhaust gas temperature was measured with type K-thermocouples. An open hot junction with a 0.8 mm wire was used to obtain a fast response time. The wire was mounted inside a ceramic sleeve to insulate it from the skin temperature of the exhaust system. The thermocouple set-up is presented in Figure 5.5 below. The open junction was mounted in the middle of the pipe to capture the gas temperature. The thermocouples were calibrated with a small industrial precision oven. The linear response of the analogue output was corrected to the absolute temperature by introducing a slope and offset in the software of the data acquisition system.

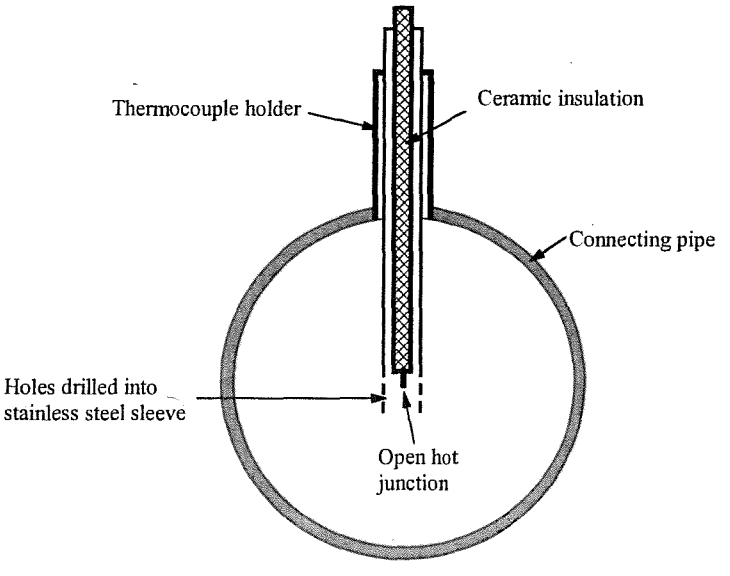

Figure 5.5 Schematic representation of the thermocouple installation.

A data acquisition system was used to record the intake mass flow (*kg/s*), exhaust gas temperatures (^{o}C), dynamometer speed (*km/h*), engine speed (r.p.m.) and wheel tracktive effort (*Newton*) at the same predetermined engine speed intervals anticipated as those for the acoustic measurements.

5.3 ACOUSTIC PREDICTIONS

The variable mass flow and temperature gradients generated during the transient operating conditions of the engine have a controlling influence on the system acoustic performance. In order to incorporate these affects into the calculation process, the APEX code was adapted to simulate the changing temperature and flow conditions during engine acceleration [1.1]. A detail description of the appropriate additions and adjustments made to the APEX prediction code is provided in Chapter 3, Section 3.4. In essence, the programme calculates the wave components $P^{\pm}$ at appropriate positions along the exhaust system for each harmonic frequency at the specified speed intervals with the corresponding measured mass flow and temperature. The calculated harmonic spectra matrix was then manipulated to present the acoustic quantity and single parameter description results in harmonic format (order components).

5.4 ESTIMATION OF THE SIGNAL-TO-NOISE RATIO FOR MEASUREMENTS ON THE VEHICLE

One problem associated with acoustic measurements on running engines is that it is not possible to measure the signal-to-noise ratio directly, because the combined cyclic operation of the pistons and valves generates both the primary source and secondary sources of exhaust noise. It was not possible to measure the flow-induced noise inside the system separately in the absence of the harmonic excitation generated by the pulsating flow. Nevertheless, it was important to establish an alternative method to estimate the signal-to-noise ratios for later explanation of certain recorded measurement errors and discrepancies. The approach was to estimate the amplitudes

of the signal and of the noise independently from the order spectra [1.1]. The basic principle of the approach is illustrated in Figure 5.6 below, showing an order spectrum recorded in the tail-pipe at 5100 r.p.m. during a full throttle run-up. It can be observed from Graph a) that the peak levels of the harmonic components occurred at integers of the fundamental frequency, 1st order, 2nd order, 3rd order and 4th order (2E, 4E, 6E and 8E). Furthermore, the acoustic energy of the order components were concentrated in a band of 0.1 orders, as is indicated in Graph b).

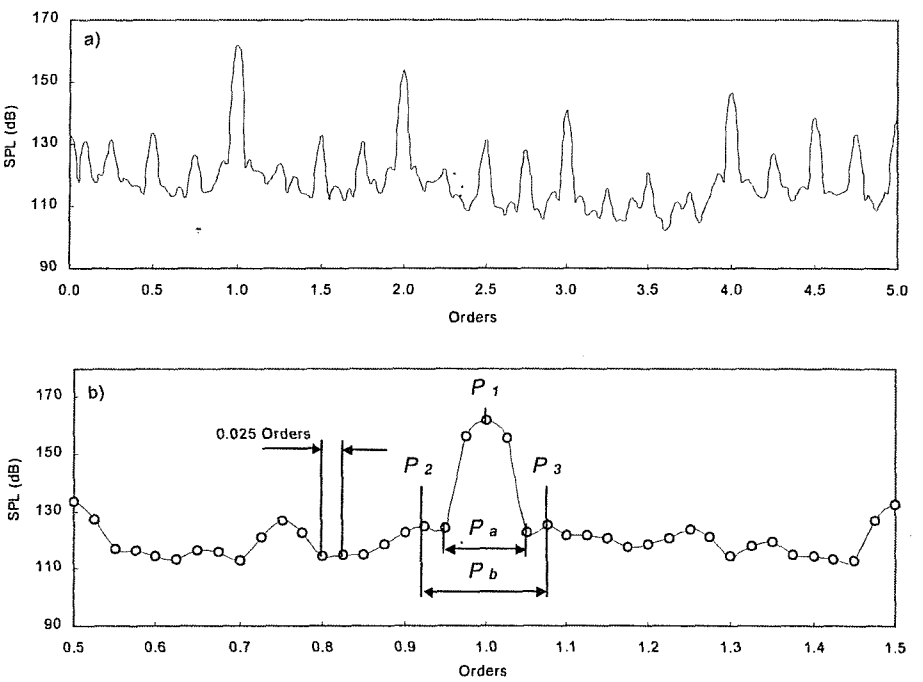

Figure 5.6 a) An order spectrum recorded inside the tail-pipe at 5100 r.p.m. during a full throttle run-up of the vehicle on the chassis dynamometer.

b) The order spectrum between 0.5 and 1.5 orders, indicating the order parameters used in equations (5.1) and (5.2) to estimate the signal-to-noise ratio.

Two methods were used to estimate the signal-to-noise ratio from the order spectra. The first method extracted the sum of the acoustic energy from two different order-bands centred around the harmonic components. Thus, referring to Figure 5.6 on page 138, the signal-to-noise ratio is expressed by

$$\text{Signal-to-noise ratio} = \frac{P_a}{P_b - P_a}, \tag{5.1}$$

where P_a represents the order-band from which the pressure for the signal is estimated and $(P_b - P_a)$ is the order-band from which the pressure for the noise is estimated. The order-band for P_a was 0.1 orders and for P_b it was 0.15 orders.

The second method extracted the sound pressure at the harmonic component and at either side of the harmonic peak. The signal-to-noise ratio could then be estimated using the following equation:

$$\text{Signal-to-noise ratio} = \frac{P_1 \cdot 2}{P_2 + P_3}, \tag{5.2}$$

where P_1 represents the peak sound pressure at the harmonic component, P_2 is the sound pressure to the left of the peak and P_3 the sound pressure to the right of the peak. $(P_2 + P_3)/2$ gives the average of the noise around the peak.

The same procedure was followed to estimate the signal-to-noise ratio at the other orders for all the measurement intervals. However, the first method was preferred as it was possible to calculate the signal-to-noise ratios during the analysis by means of an external software programme.

The two methods were then validated by comparing the estimated signal-to-noise ratios as described above to actual measured signal-to-noise ratios. Figure 5.7 below shows the actual and estimated signal-to-noise ratios in the outlet pipe of the expansion chamber for a Mach number $M = 0.1$. These measurements were performed on the test bench displayed in Figure 4.2 on page 73. The agreement seems sufficiently close (± 3 to 4dB or better) to validate the effectiveness of the proposed methods to estimate the signal-to-noise ratios from the measured order spectra.

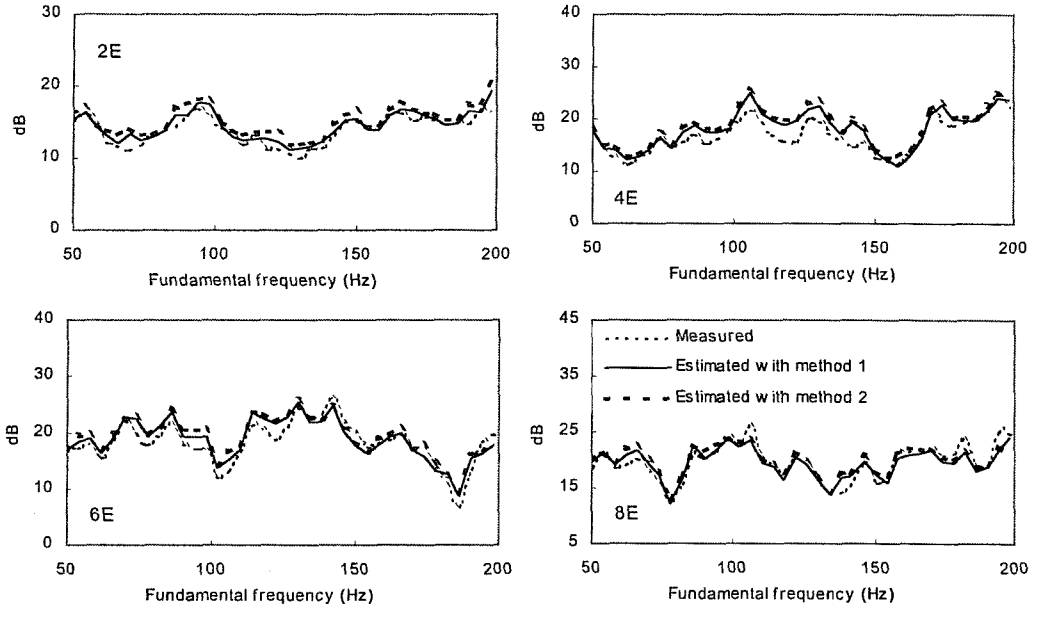

Figure 5.7 Comparison of measured and estimated signal-to-noise ratios on a cold test bench for a Mach number $M = 0.1$. The measured signal-to-noise ratios were calculated from the ratio of the acoustic pressure with and without acoustic excitation. The estimated signal-to-noise ratios for method 1 were defined by equation (5.1), and those for method 2 by equation (5.2).

5.5 ACOUSTIC ASSESSMENT OF AN EXPANSION CHAMBER FOR TRANSIENT OPERATING CONDITIONS

5.5.1 Measurement method

The objective was to assess the acoustic performance of the expansion chamber for various conditions that represent the normal operation of the vehicle. Practically, this entailed constant acceleration run-ups for the speed range of the engine, while avoiding overheating of the engine. This was achieved for a sweep-rate of 30 r.p.m./sec (1 Hz/sec for the fundamental harmonic (2E)) in third gear from 1500 r.p.m. to 5400 r.p.m.. Measurements performed at a slower sweep-rate (15 r.p.m./sec) required a cooling fan to avoid engine overheating. The same order tracking parameters used for the bench test were also applied for the measurements on the vehicle, namely $\Delta n = 0.025$ orders, 75% overlap and a Hanning window (an equivalent sweep-rate of 15 r.p.m./sec was used for the bench test measurements with ten averages). However, only five averages could be achieved due to the faster sweep-rate. Order spectra were captured at 120 r.p.m. intervals that related to 33 measurement intervals ($\Delta r = 4$ Hz).

The procedure described in Chapter 4, Section 4.2 was again adopted for the wave decomposition calculations. The specially developed Labview software programme (see Figure 4.14 on page 93) was used to estimate the wave components $P^{\pm}$ from the measured harmonic pressure and the corresponding measured variable mass flow and temperature. Table 5.1 on page 142 and Table 5.2 on page 143 show the fluid properties at the inlet and outlet of the expansion chamber respectively. These were calculated from the measured mass flow and temperatures at stations #1 and #3 as recorded during a full throttle run-up of the vehicle on the chassis dynamometer. In contrast to bench test measurements where the temperature and mass flow conditions were stationary, one notes that the fluid properties were now related to the distribution of the variable mass flow and temperature.

Engine speed (r.p.m.)	Density ρ_1 (kg/m^3)	Viscosity ν_1 ($m^2/\sec$)	Ratio of specific heat γ_1	Inlet temperature T_1 (^oC)	Flow velocity u_1 ($m/\sec$)	Speed of sound c_1 (m/s)	Mass flow m_1 (kg/s)	Mach number M_1
1503	0.60	4.87E-05	1.38	311	33	477	0.025	0.069
1623	0.60	4.98E-05	1.38	318	35	479	0.026	0.073
1752	0.59	5.09E-05	1.38	326	37	483	0.027	0.077
1883	0.58	5.19E-05	1.38	332	40	485	0.029	0.082
1989	0.58	5.31E-05	1.38	340	43	488	0.031	0.089
2111	0.57	5.39E-05	1.37	346	46	490	0.033	0.095
2225	0.56	5.51E-05	1.37	354	49	493	0.035	0.1
2356	0.56	5.63E-05	1.37	362	52	495	0.036	0.105
2472	0.55	5.72E-05	1.37	368	55	497	0.038	0.11
2590	0.54	5.86E-05	1.37	377	58	501	0.039	0.115
2713	0.54	6.00E-05	1.37	386	62	504	0.041	0.122
2823	0.53	6.16E-05	1.37	396	65	507	0.043	0.129
2960	0.52	6.31E-05	1.37	406	69	511	0.045	0.135
3077	0.51	6.47E-05	1.37	416	72	514	0.046	0.14
3200	0.50	6.64E-05	1.37	426	76	517	0.048	0.147
3310	0.50	6.80E-05	1.37	436	80	520	0.05	0.154
3436	0.49	6.98E-05	1.36	447	84	524	0.052	0.16
3568	0.48	7.14E-05	1.36	456	87	527	0.053	0.166
3680	0.48	7.29E-05	1.36	466	91	530	0.055	0.172
3782	0.47	7.46E-05	1.36	475	93	533	0.055	0.175
3921	0.47	7.64E-05	1.36	486	96	536	0.056	0.179
4039	0.46	7.83E-05	1.36	497	101	540	0.058	0.186
4161	0.45	7.98E-05	1.36	506	105	542	0.06	0.193
4281	0.45	8.17E-05	1.36	517	107	546	0.06	0.197
4410	0.44	8.11E-05	1.36	528	110	549	0.061	0.201
4514	0.44	8.29E-05	1.35	538	114	552	0.062	0.207
4646	0.43	8.42E-05	1.35	546	118	555	0.064	0.212
4767	0.43	8.58E-05	1.35	555	121	557	0.065	0.218
4872	0.42	8.79E-05	1.35	567	125	561	0.066	0.223
4996	0.42	8.92E-05	1.35	575	129	563	0.067	0.228
5113	0.41	9.06E-05	1.35	583	133	565	0.069	0.235
5246	0.41	9.21E-05	1.35	591	137	568	0.07	0.241
5357	0.40	9.35E-05	1.35	599	141	570	0.072	0.247

Table 5.1 Fluid properties at the inlet of the expansion chamber (station #1) estimated from the measured mass flow and temperature captured at regular engine speed intervals (120 r.p.m.) during a full throttle run-up of the vehicle on the chassis dynamometer.

Engine speed (r.p.m.)	Density ρ_3 (kg/m^3)	Viscosity ν_3 ($m^2/\sec$)	Ratio of specific heat γ_3	Outlet temperature T_3 (^oC)	Flow velocity u_3 ($m/\sec$)	Speed of sound c_3 (m/s)	Mass flow m_3 (kg/s)	Mach number M_3
1503	0.68	3.94E-05	1.39	242	29	450	0.025	0.064
1623	0.68	4.01E-05	1.39	248	31	453	0.026	0.068
1752	0.67	4.08E-05	1.38	253	32	455	0.027	0.071
1883	0.66	4.15E-05	1.38	258	35	457	0.029	0.077
1989	0.66	4.22E-05	1.38	264	38	459	0.031	0.083
2111	0.65	4.27E-05	1.38	267	41	460	0.033	0.088
2225	0.65	4.36E-05	1.38	273	43	463	0.035	0.093
2356	0.64	4.44E-05	1.38	279	45	465	0.036	0.097
2472	0.63	4.53E-05	1.38	286	48	468	0.038	0.102
2590	0.62	4.62E-05	1.38	293	50	470	0.039	0.107
2713	0.62	4.72E-05	1.38	300	54	473	0.041	0.113
2823	0.61	4.82E-05	1.38	307	56	475	0.043	0.119
2960	0.60	4.92E-05	1.38	313	60	478	0.045	0.125
3077	0.59	5.02E-05	1.38	321	62	481	0.046	0.129
3200	0.59	5.16E-05	1.38	330	66	484	0.048	0.136
3310	0.58	5.26E-05	1.38	337	69	487	0.05	0.141
3436	0.57	5.38E-05	1.37	345	72	489	0.052	0.147
3568	0.56	5.51E-05	1.37	354	75	493	0.053	0.153
3680	0.56	5.63E-05	1.37	362	78	495	0.055	0.158
3782	0.55	5.78E-05	1.37	371	80	499	0.055	0.161
3921	0.54	5.92E-05	1.37	380	83	502	0.056	0.165
4039	0.53	6.04E-05	1.37	389	86	505	0.058	0.171
4161	0.53	6.17E-05	1.37	397	90	507	0.06	0.178
4281	0.52	6.33E-05	1.37	407	92	511	0.06	0.181
4410	0.51	6.47E-05	1.37	416	95	514	0.061	0.184
4514	0.51	6.63E-05	1.37	425	98	517	0.062	0.19
4646	0.50	6.76E-05	1.37	434	102	520	0.064	0.195
4767	0.49	6.90E-05	1.36	442	105	522	0.065	0.2
4872	0.49	7.05E-05	1.36	451	108	525	0.066	0.205
4996	0.48	7.16E-05	1.36	458	111	528	0.067	0.21
5113	0.48	7.34E-05	1.36	468	115	531	0.069	0.217
5246	0.47	7.52E-05	1.36	479	119	534	0.07	0.223
5357	0.46	7.71E-05	1.36	490	123	538	0.072	0.229

Table 5.2 Fluid properties at the outlet of the expansion chamber (station #3) estimated from the measured mass flow and temperature captured at regular engine speed intervals (120 r.p.m.) during a full throttle run-up of the vehicle on the chassis dynamometer.

5.5.2 Results and discussion for a full throttle run-up

The acoustic pressure field inside the exhaust system was contaminated by shear layer turbulence and flow noise due to the high flow velocities generated during the normal operating conditions of an engine. This presents a formidable challenge to the performance of reliable measurements of the acoustic behaviour of the exhaust system elements [1.1, 4.1]. Figure 5.8 below (also see Tables 5.1 and 5.2) shows the mass flow, Mach number and temperature recorded at the inlet and outlet of the expansion chamber for a full throttle constant acceleration run-up (30 r.p.m./s). The mass flow at maximum engine speed (0.07 kg/s) was the same as that used on the bench test. However, the increase in temperature and corresponding decrease in air density resulted in much higher flow velocities; hence, the maximum Mach number was increased by a factor of more than two ($M = 0.247$).

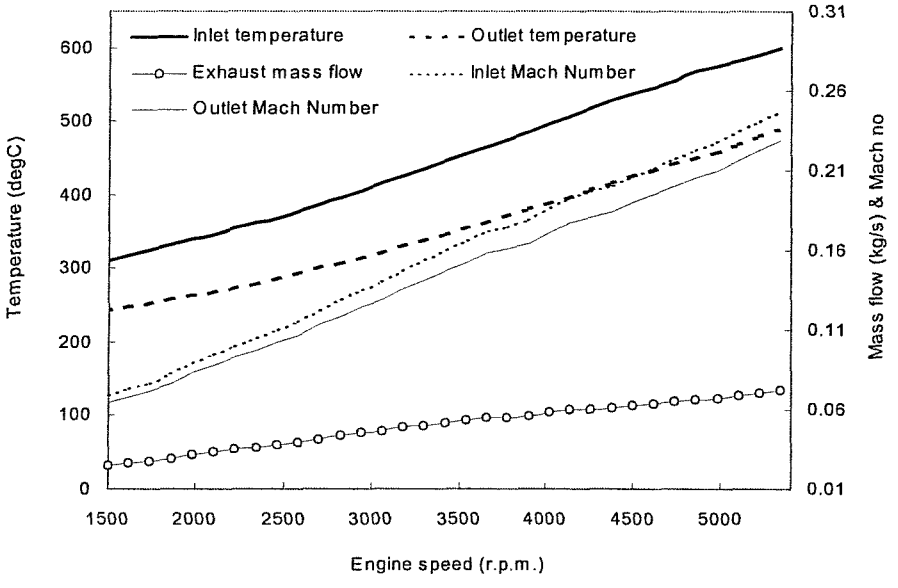

Figure 5.8 Mass flow, Mach number and exhaust gas temperature at the inlet (station #1) and outlet (station #3) of the expansion chamber recorded for a full throttle run-up of the vehicle on the chassis dynamometer.

The order contour plot in Figure 5.9 below, measured at station #3, gives an overview of the acoustic pressure field, showing both the harmonic order information and random flow-induced noise. The Y-axis represents engine speed and the X-axis represents the order number. The amplitude of the sound pressure is represented by the grey colour scale in decibels. Order 1 refers to the 2E component and order 2 refers to the 4E component etc.. Low signal-to-noise areas can be identified where the harmonic orders approach the flow noise. The resonance frequencies of the tail-pipe can be distinguished by the excitation of the order components and random flow noise around the hyperbolic curves.

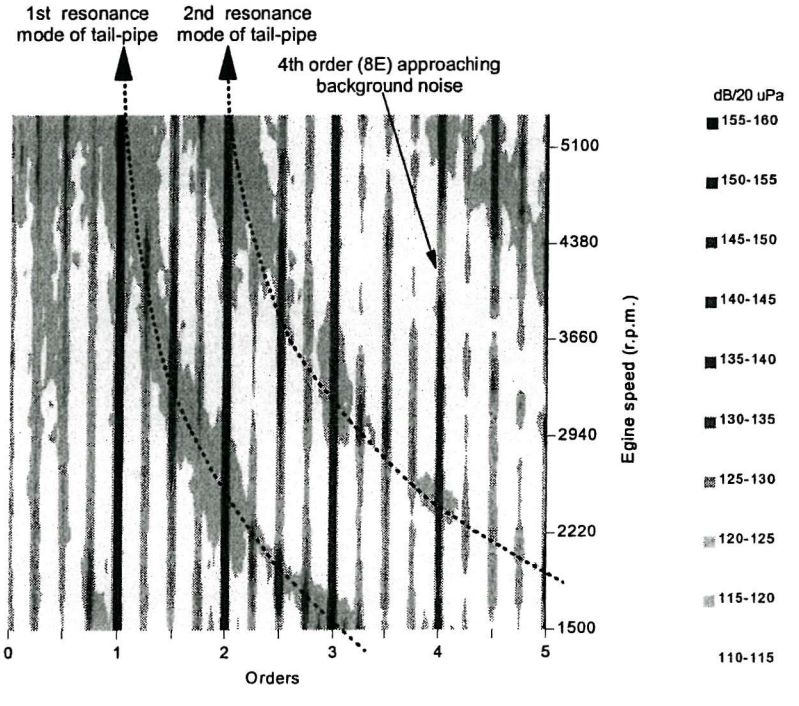

Figure 5.9 Order contour plot of the sound pressure recorded in the tail-pipe (station #3) for a full throttle run-up of the vehicle on the chassis dynamometer. Orders 1 (2E), 2 (4E), 3 (6E), and 4 (8E) represent the harmonic components of the pulsating gas flow. The excitation of levels around the hyperbolic lines represents the acoustic resonances of the tail-pipe.

The sound pressure order components measured at station #1 were also extracted from the order plot and are displayed in Figure 5.10 below. All the orders reached maximum levels above 165dB (3556 Pa).

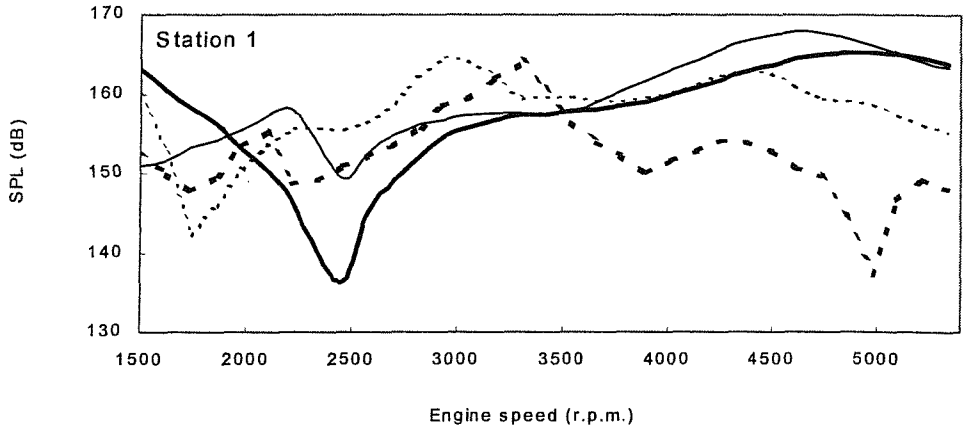

Figure 5.10 Sound pressure orders recorded at the inlet of the expansion chamber (station #1) for a full throttle run-up of the vehicle on the chassis dynamometer, 2E (thick solid), 4E (thin solid), 6E (thin dash), 8E (thick dash).

The reliability of the measurements depends on the sufficiently precise estimation of the transfer functions at the inlet $H_{2,1}$ and the outlet $H_{4,3}$ of the silencer component [4.1]. A sequence of measurements was performed over a period of time and it was found that measurement error was, in most cases, related to the low signal-to-noise ratio at the outlet side of the silencer. This resulted from the acoustic attenuation of the silencer in combination with the flow-induced pressure fluctuations at the outlet of the silencer (as noted earlier with the flow bench). In order to improve the reliability of the measurements, it was necessary to optimise the position of the transducers at the outlet side to increase the signal-to-noise ratios [1.1]. To illustrate such an example, the measured transfer function $H_{4,3}$ for the 4E component in Figure 5.11 on page 147 shows an apparently spurious spike at 4050 r.p.m. with the transducers mounted close to the silencer outlet. Good agreement between measured and predicted values was obtained, as is shown in Figure 5.12 on page 147, when the transducers were moved to a position close to the tail-pipe outlet, as is indicated in

Figure 5.3 on page 135. Note the significant change in both the measured and predicted spectral distribution at the two positions along the same pipe.

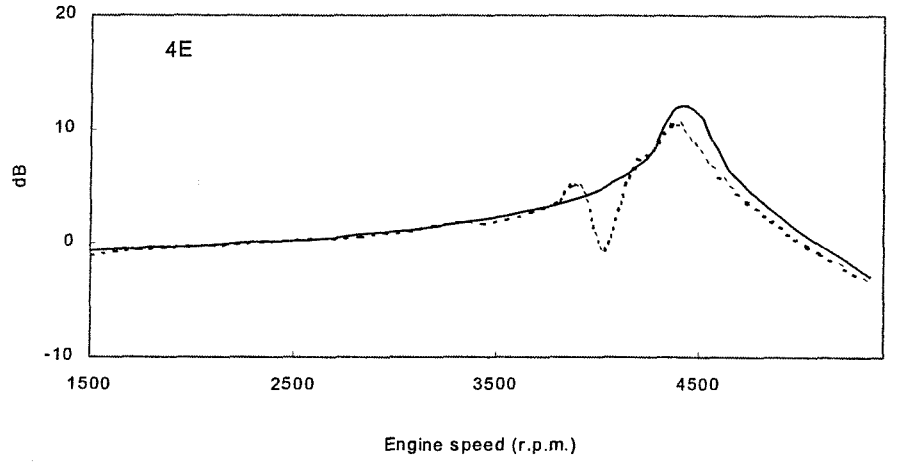

Figure 5.11 Measured (dash) and predicted (solid) transfer function (magnitude) $H_{4,3}$ for the 4E component with the transducers mounted close to the outlet side of the silencer.

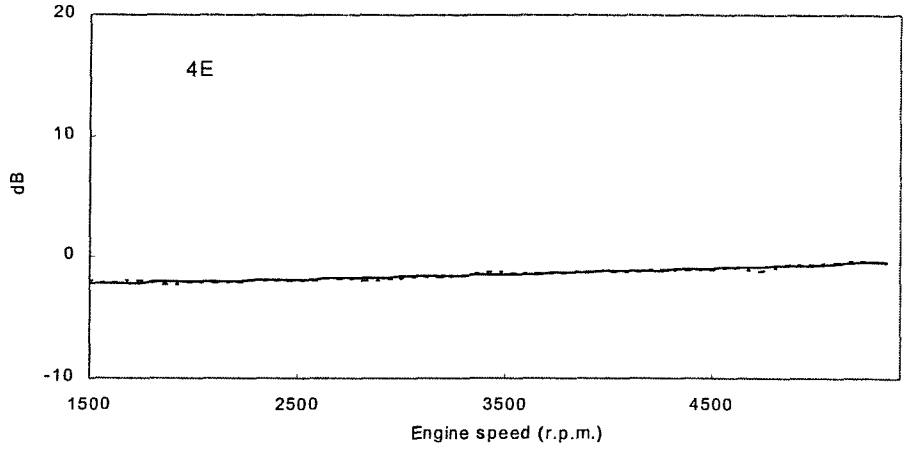

Figure 5.12 Measured (dash) and predicted (solid) transfer function (magnitude) $H_{4,3}$ for the 4E component with the transducers mounted close to the tail-pipe outlet.

The results in Figure 5.13 below clearly indicate that the measurement error resulted from low signal-to-noise ratios. These were below those found to yield acceptably realistic estimates of acoustic attenuation or acoustic power flux.

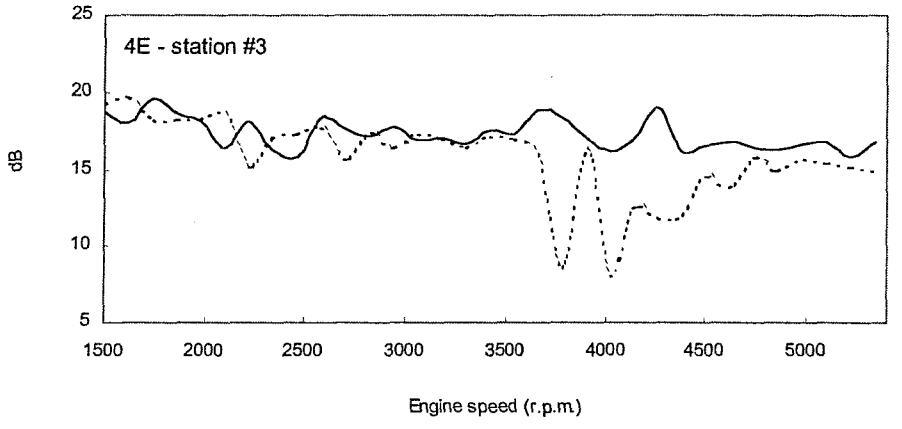

Figure 5.13 Signal-to-noise ratios estimated at station #3 for the 4E component with the pressure transducers mounted close to the outlet of the silencer (dash) and close to the tail-pipe outlet (solid).

The predicted and measured acoustic performance of the expansion chamber after such precautions were adopted is shown in Figures 5.14 to 5.18. Generally good agreement was obtained between measured and predicted magnitude of the transfer functions at the inlet $H_{2,1}$ and the outlet pipe $H_{4,3}$ of the expansion chamber, as is shown in Figures 5.14 and Figure 5.15 on page 149 respectively. Excellent agreement (within ±1dB) was found for all the order components except for the 8E component at 4000 r.p.m. for $H_{2,1}$ and at 4400 r.p.m. for $H_{4,3}$, where agreement was ±6dB. These discrepancies were directly related to reduced signal-to-noise ratios.

The measured and predicted transfer function across the expansion chamber $H_{3,1}$ in Figure 5.16 on page 150 showed good agreement (±3dB or better).

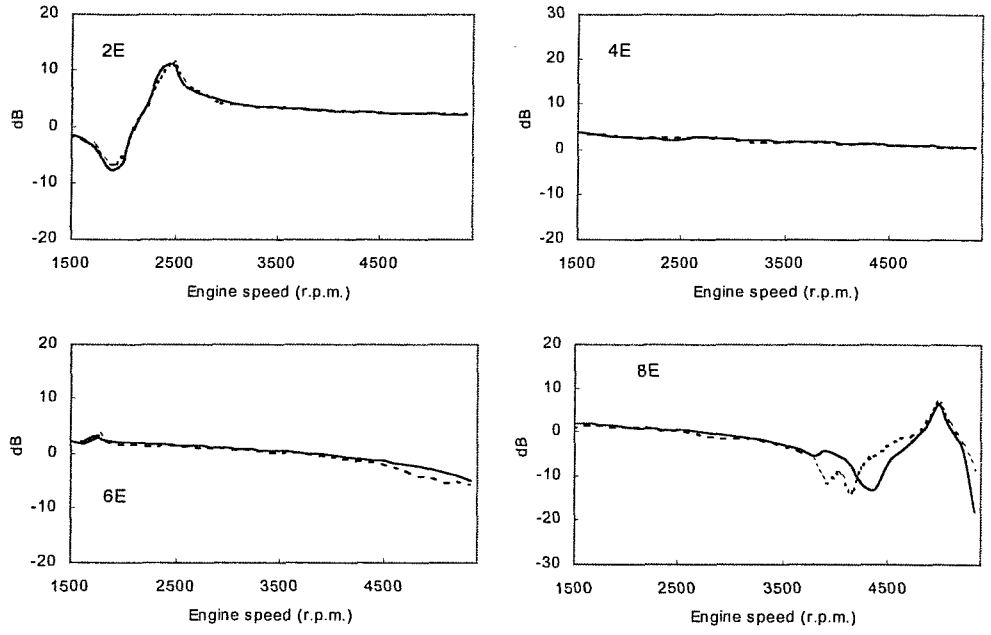

Figure 5.14 Measured (dash) and predicted (solid) magnitude of the transfer function $H_{2,1}$ for a full throttle run-up of the vehicle on the chassis dynamometer.

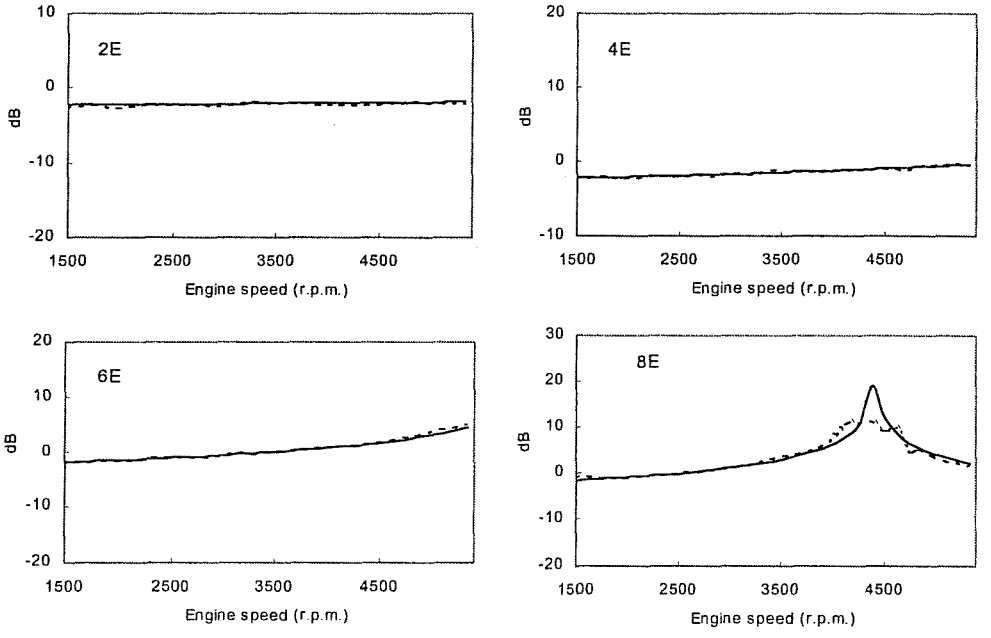

Figure 5.15 Measured (dash) and predicted (solid) magnitude of the transfer function $H_{4,3}$ for a full throttle run-up of the vehicle on the chassis dynamometer.

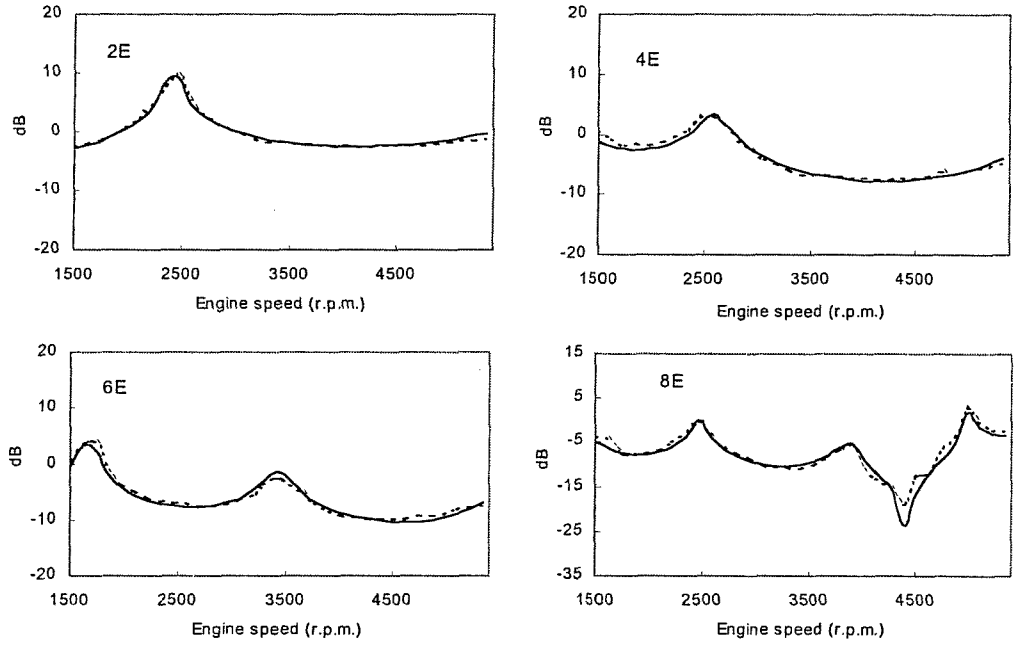

Figure 5.16 Measured (dash) and predicted (solid) magnitude of the transfer function $H_{3,1}$ for a full throttle run-up of the vehicle on the chassis dynamometer.

Measured system attenuation $AL_{1,3}$ in Figure 5.17 on page 151 showed in general close agreement (within ±4dB or better) with predictions. As indicated in Chapter 3, Section 3.3.3, the assessment of the attenuation $AL_{1,3}$ enables the identification of the acoustic characteristics of the expansion chamber, as indicated in Figure 5.17. For ease of analysis, the corresponding frequency range for each order component is shown at the top of each graph.

The attenuation was estimated from

$$AL_{1,3} = 20Log\left|\frac{P_1^+}{P_3^+}\right| \text{ (dB).} \qquad (5.3)$$

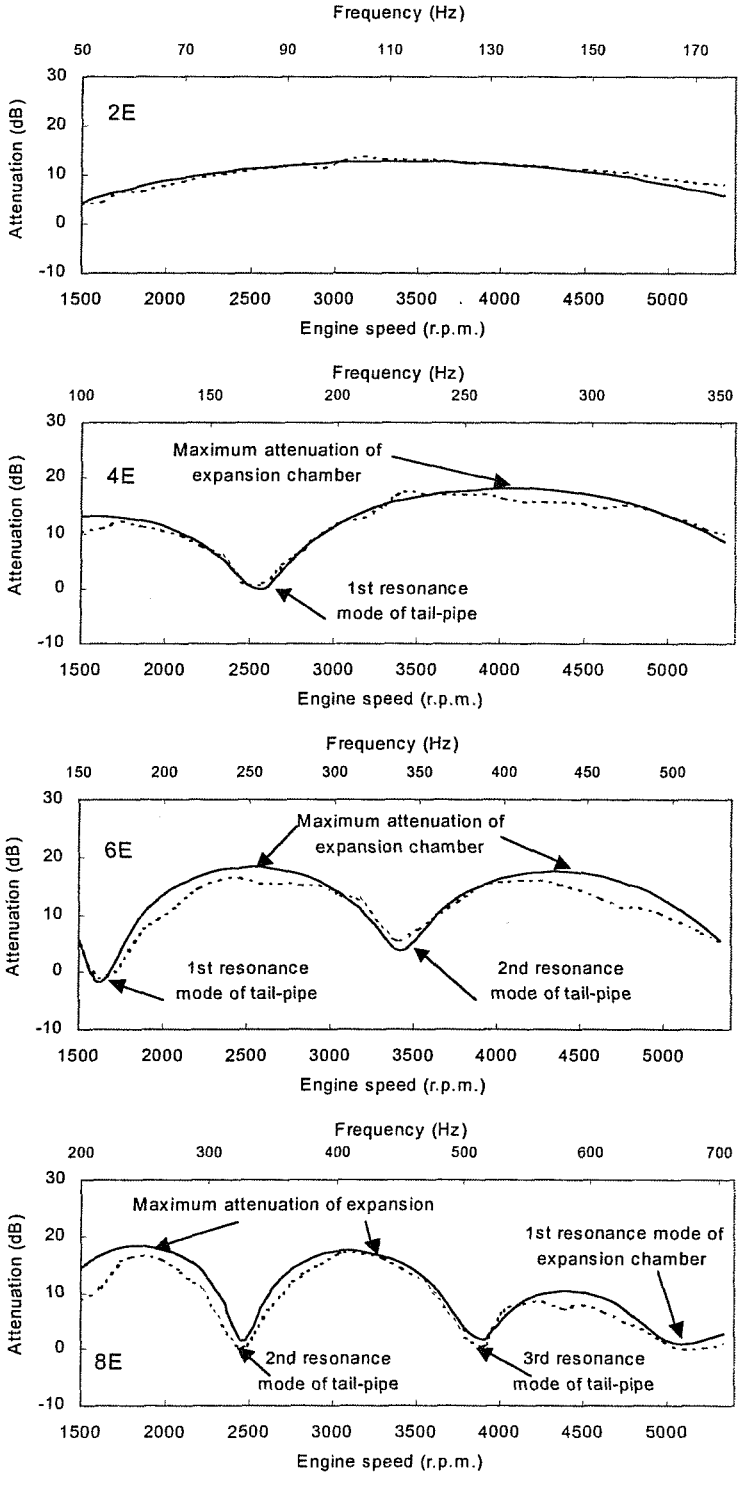

Figure 5.17 Measured (dash) and predicted (solid) system attenuation $AL_{1,3}$ for a full throttle run-up of the vehicle on the chassis dynamometer. The acoustic behaviour of the expansion chamber is indicated in the graphs.

The variable mass flow and temperature for the engine run-up on the chassis dynamometer resulted in an amplitude variation and a frequency shift of the orders at corresponding frequencies [1.1]. For example, in Figure 5.17 on page 151, one can see that the first half wavelength resonance of the tail-pipe was excited at 2580 r.p.m. (172 Hz, 1.1dB) for the 4E component and at 1620 r.p.m. (162 Hz, -0.84dB) for the 6E component. In most cases the small differences that existed between measured and predicted results corresponded to the lower estimates of the measured magnitudes at frequencies where maximum attenuation occurs. Perhaps this was related to the resulting increase of the relative contamination by flow noise or some other factors (such as yielding of the silencer shell, which was not correctly anticipated in the theoretical models). However, in most cases, close agreement was found between measured and predicted results; in particular, there was close agreement at resonant frequencies that are obviously of much more practical significance in terms of the overall acoustic performance of the silencer component in service [1.1, 1.2]. As is discussed later (Chapter 6), such resonances normally correspond to maximum sound energy transmission.

The acoustic power flux in the tail-pipe (station #3) normalised to the incident acoustic power at the inlet (station #1) was estimated from

$$W_{3,1} = 10Log\left[\frac{\rho_1 c_1(|P_3^+|^2(1+M_3)^2 - |P_3^-|^2(1-M_3)^2)}{\rho_3 c_3(|P_1^+|^2(1+M_1)^2)}\right] \text{dB.} \qquad (5.4)$$

Note that the cross-sectional area for the inlet pipe (station #1) and outlet pipe (station #3) are the same and has therefore been eliminated for equation (5.4).

The measured and predicted normalised acoustic power flux in the tail-pipe $W_{3,1}$ is shown in Figure 5.18 on page 153. Although the measured curve appeared to be more spiky, close agreement (±4dB or better) was obtained. Differences between measured and predicted net power flux may indicate the presence of flow-induced noise sources or sinks. Such an example is covered in Appendix 5.1. Comparison between Figure 5.17 and Figure 5.18 also indicates that the power flux in the tail-pipe

corresponds closely to the inverse of the attenuation $AL_{1,3}$. For this reason, one may use estimates of net power flux as an alternative to describe the acoustic behaviour of the exhaust system, as was demonstrated in Chapter 3.

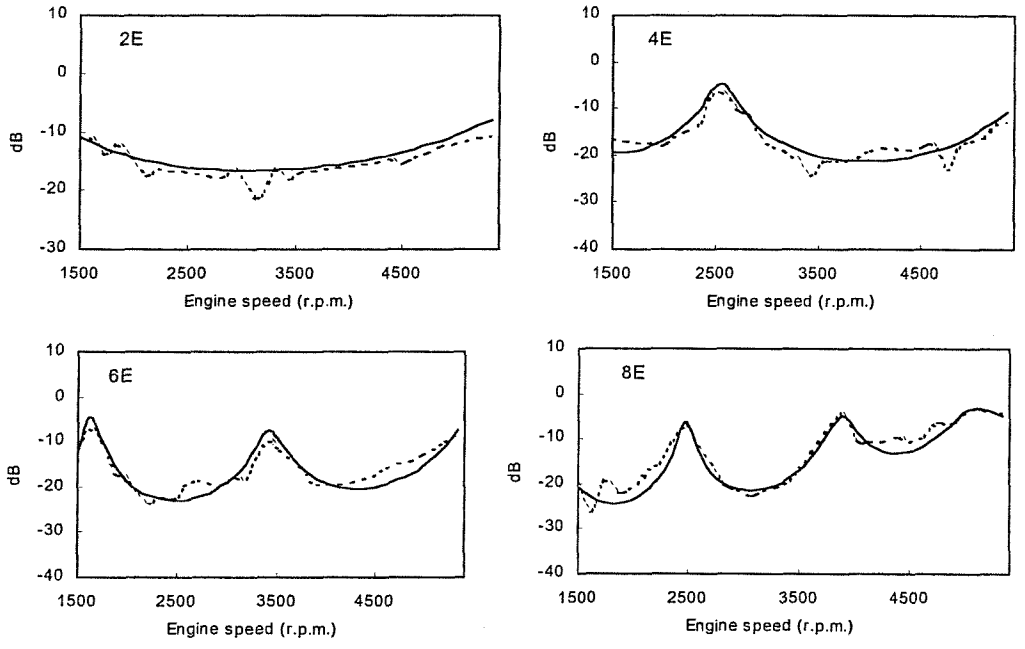

Figure 5.18 Measured (dash) and predicted (solid) normalised acoustic power flux in the outlet pipe (Station #3) $W_{3,1}$ for a full throttle run-up of the vehicle on the chassis dynamometer.

5.5.3 Results and discussion for a half throttle run-up

During the course of the project a series of assessments was performed, not only to improve the reliability of the measurements, but also to evaluate the acoustic behaviour of the expansion chamber for different operating conditions of the vehicle. These included alternative sweep-rates and engine load conditions. Assessments at slower sweep-rates (15 r.p.m./sec) showed an increase in exhaust gas temperature due to the longer duration of the measurement. Although the number of exponential averages could be increased, these operating conditions were not deemed realistic, because a cooling fan was required.

To demonstrate the effect of engine load on the acoustic behaviour of the expansion chamber, results are also presented for a half throttle run-up performed at the same sweep-rate (30 r.p.m./sec) as the full throttle run-up. The measured and predicted system attenuation $AL_{1,3}$ for the half throttle run-up is displayed in Figure 5.19 below. Close agreement was found (within ±4dB or better), similar to that for the full throttle run-up presented in Section 5.5.2.

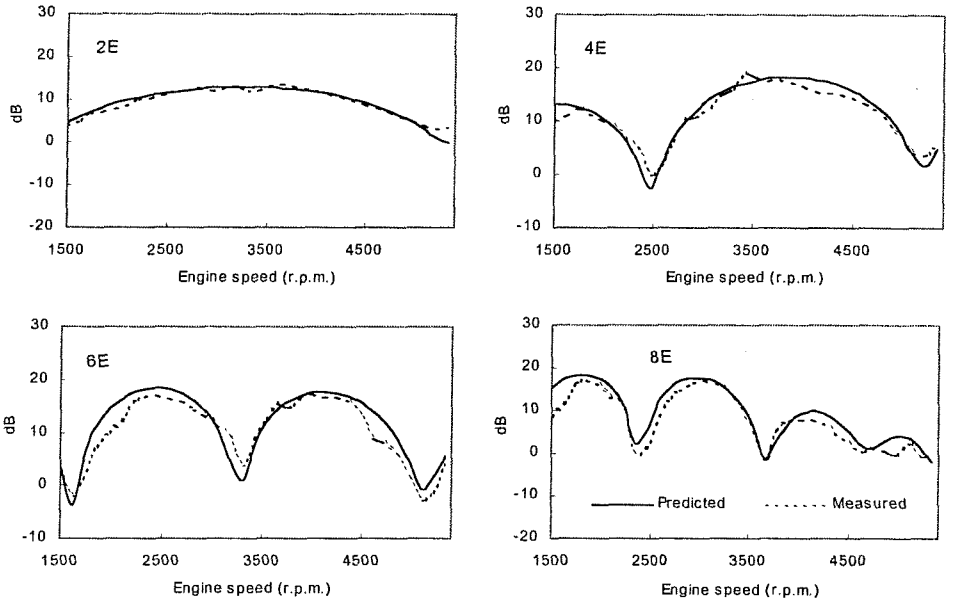

Figure 5.19 Measured (dash) and predicted (solid) system attenuation $AL_{1,3}$ for a half throttle run-up of the vehicle on the chassis dynamometer.

The inlet temperature (station #1), outlet temperature (station #3) and mass flow for the full throttle and half throttle run-up are compared in Figure 5.20 on page 155. One notes the temperature difference between the full throttle and half throttle run-up increased with engine speed; this was the case for both the inlet and outlet temperatures. As one would expect, the mass flow for the full throttle run-up was higher, compared to the half throttle run-up, due to the throttle position.

The measured system attenuation $AL_{1,3}$ for the full throttle and half throttle run-up is also compared in Figure 5.21 on page 156. One notes similar acoustic behaviour at low engine speeds where the temperatures were nearly the same. Corresponding

resonances were separated further at higher engine speeds due to increasing difference in temperature. Notably, the first half wavelength resonance of the tail-pipe occurred at 5220 r.p.m. for the 2E component for the half throttle measurement, which was not the case for the full throttle measurement. For the 8E component, the third half wavelength resonance of the tail-pipe occurred at 3650 r.p.m. for the half throttle run-up, and at 4000 r.p.m. for the full throttle run-up.

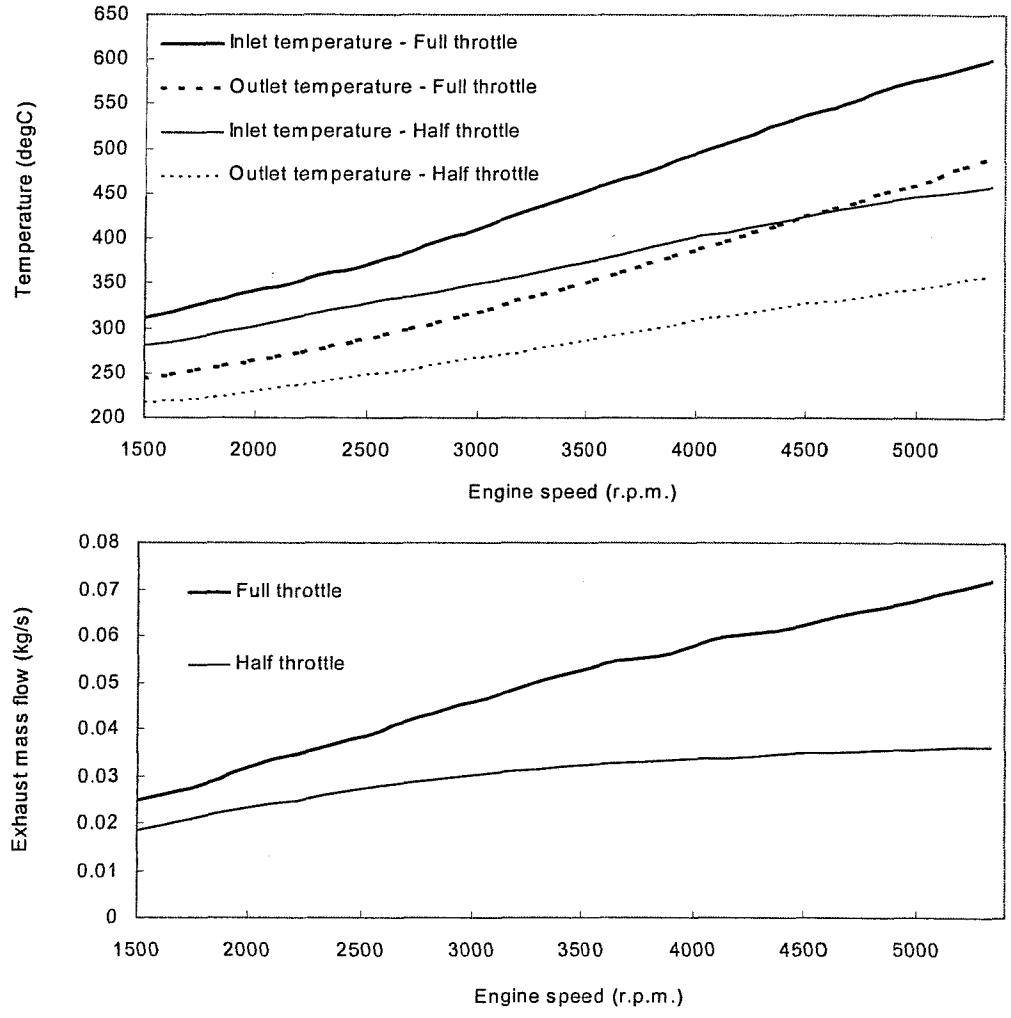

Figure 5.20 Inlet temperature, outlet temperature and mass flow recorded for a full throttle run-up and a half throttle run-up.

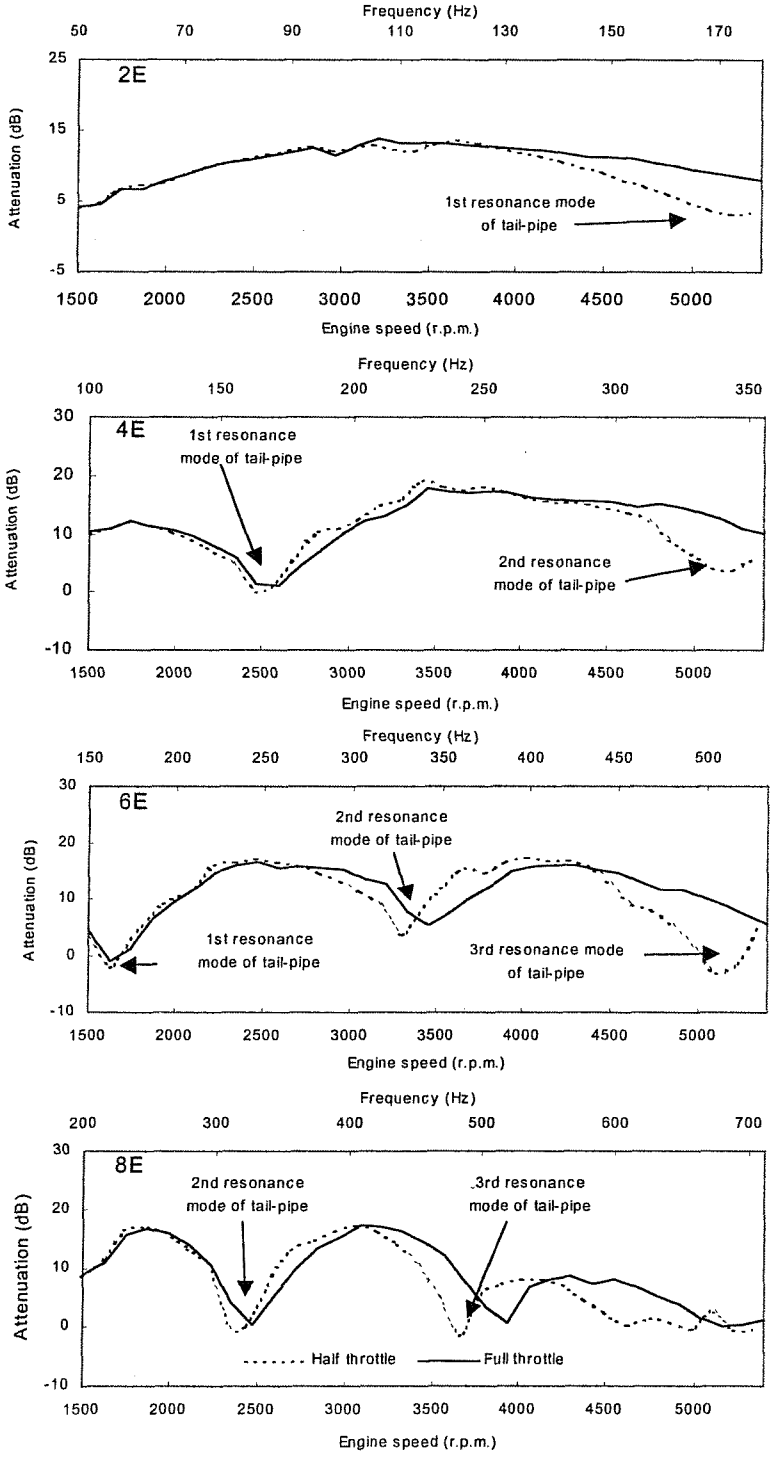

Figure 5.21 Measured acoustic attenuation $AL_{1,3}$ of the expansion chamber for a half throttle run-up (dash curve) and full throttle run-up (solid curve) of the vehicle on the chassis dynamometer. Note the difference in acoustic performance that was related to the exhaust gas temperature gradient associated with each load condition.

5.6 ACOUSTIC ASSESSMENT OF AN EXPANSION CHAMBER FOR STATIONARY ENGINE CONDITIONS

Stationary measurements (described in Chapter 2) were performed to demonstrate the advantages of the new transient measurement approach. These measurements were performed at constant engine speed intervals after the exhaust gas temperature had stabilised. The same vehicle, equipment set-up (Figure 5.2 on page 134) and exhaust system (Figure 5.3 on page 135) were used for these measurements. External cooling of the engine and the dynamometer brake was required to obtain a maximum of 8 measurement intervals. The spectra were captured every 480 r.p.m. (Δr = 16 Hz) between 1500 and 4860 r.p.m.. The total measurement duration was 33.87 minutes.

This procedure was extremely time-consuming. For this reason, the output signal of the pressure transducers was recorded for subsequent analysis optimisation rather than performing them concurrently. In contrast to the variable signals for the transient measurement, the signals were constant. The analysis was performed with the fixed sampling rate method because smearing of the order components was not a problem here. The recorded signals for each measurement interval were played back individually and analysed using a fixed frequency resolution Δf = 4 Hz, 50 linear averages and a Hanning window up to 800 Hz. Next, the order information was manually extracted from each spectrum to calculate the wave components $P^{\pm}$ as outlined in Section 4.2.

The eight spectra recorded at station #1 are combined in Figure 5.22 on page 158. In this graph it is difficult to identify the characteristics of the order components due to the restricted number of measurement intervals. Comparison of this graph to the spectral map in Figure 3.2 on page 40 (33 measurement intervals) illustrates the inadequate description of the exhaust noise signature. This is further demonstrated by the measured and predicted attenuation $AL_{1,3}$ in Figure 5.23 on page 159 for eight constant engine speed measurement intervals. The predicted acoustic behaviour of the expansion chamber was also performed using 33 measurement intervals (dash

line in Figure 5.23) to illustrate the insufficient description of only eight intervals. The inadequate descriptions are particularly evident at the resonance troughs for the 4E, 6E and 8E components. One notes that only the 2E component was adequately described, due to its limited frequency range (50 to162 Hz).

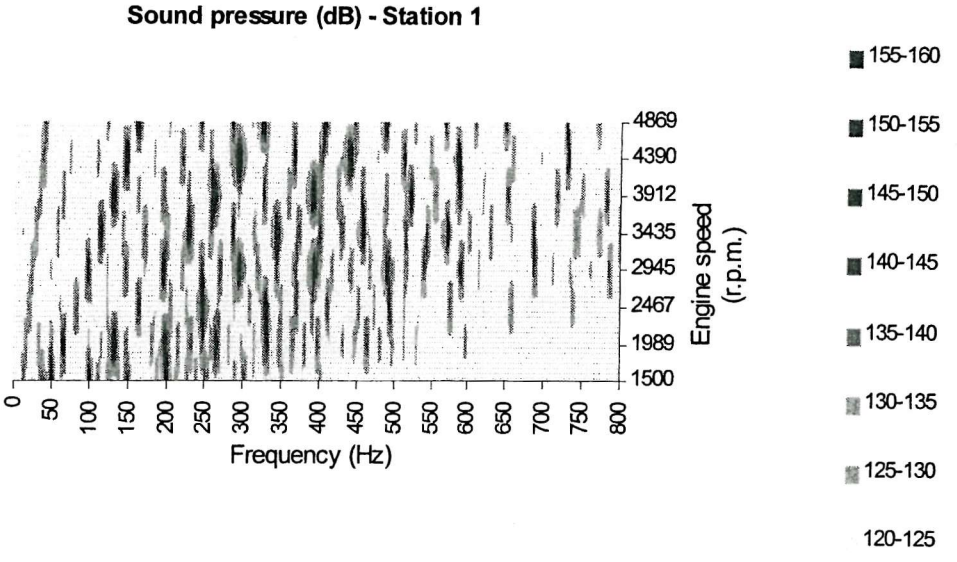

Figure 5.22 Spectral map recorded at station #1 for the constant engine speed conditions. The map represents the narrow-band spectra captured at the eight measurement intervals between 1500 r.p.m. and 4680 r.p.m..

Temple [1.9] and Yaseen [1.10] followed a similar approach to assess the acoustic behaviour of silencer components on a running engine. They reported discrepancies between the measured and the predicted results, probably caused by equipment constraints and undetermined measurement errors. By contrast, the close agreement between measured and predicted results (see Figure 5.23 on page 159) in the current study validates the precision of the new measurement procedure. Nevertheless, acoustic description of the expansion chamber performance was inadequate for guiding design optimisation due to the restricted number of measurement intervals.

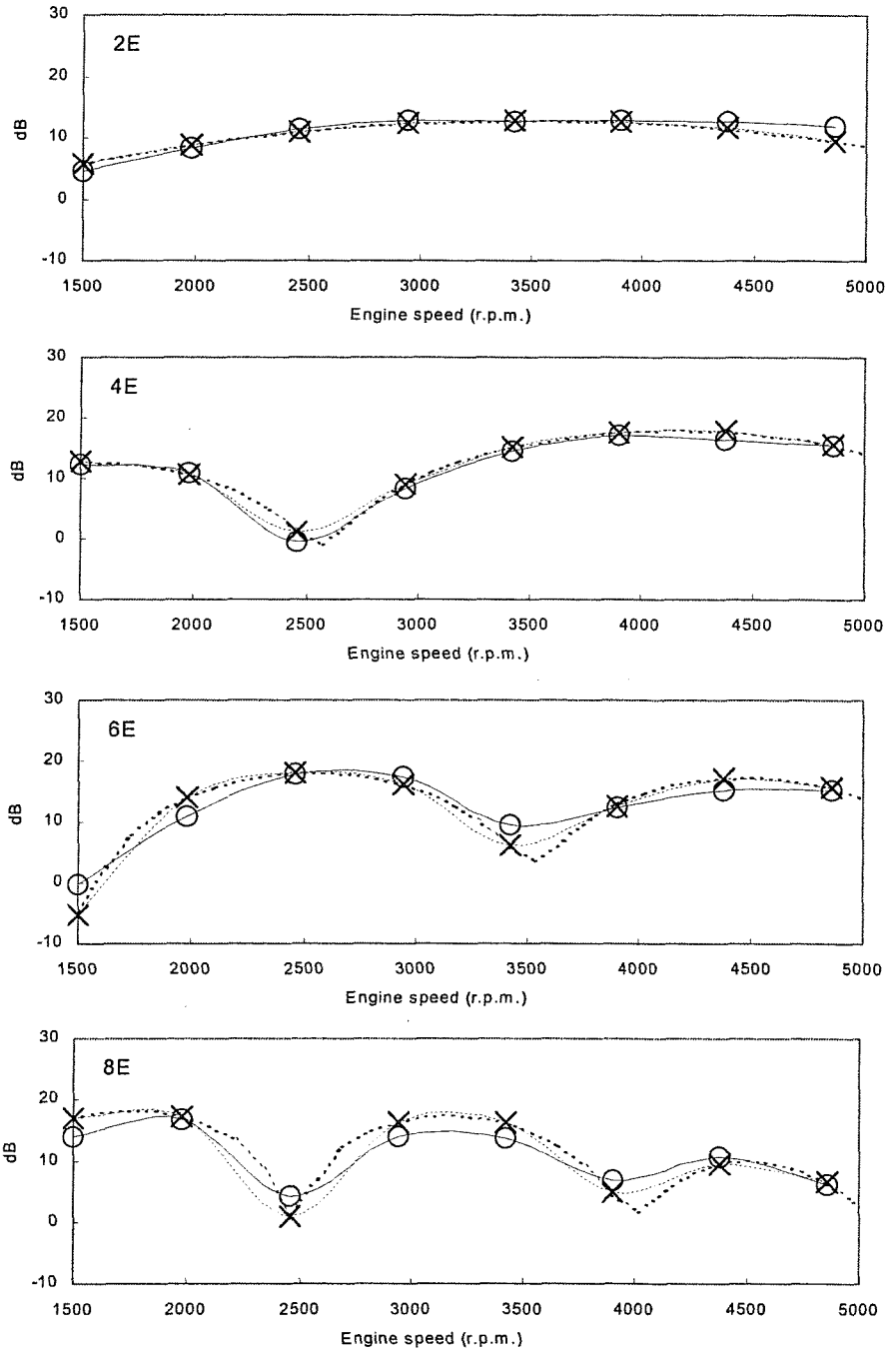

Figure 5.23 Measured (solid curve with circle) and predicted (dash curve cross) attenuation $AL_{1,3}$ for eight constant speed measurement intervals. The predicted attenuation $AL_{1,3}$ was also performed at 33 measurement intervals (dash line) to highlight the inadequate description of the eight measurement intervals most evident at the resonance troughs.

5.6.1 Advantages of transient measurements compared to constant engine speed measurements

Figure 5.24 below shows the inlet temperature recorded at station #1 for constant engine speed and transient operating conditions. The difference in the temperature gradients had a controlling influence on the observed acoustic behaviour of the expansion chamber. Comparison between Figure 5.17 on page 151 and Figure 5.23 on page 159 clearly illustrates this. For example, the first half wavelength resonance of the tail-pipe occurred at 1600 r.p.m. for the 6E component for the transient measurement, and was below 1500 r.p.m. for the constant engine speed measurement. Also, the third half wavelength resonance of the tail-pipe for the 8E component occurred at 3800 r.p.m. for the transient measurement, and at 4000 r.p.m. for the constant engine speed measurements. Based on these results, it appears that the constant engine speed conditions may not normally represent the practical operating conditions of the vehicle, due to the increased temperature.

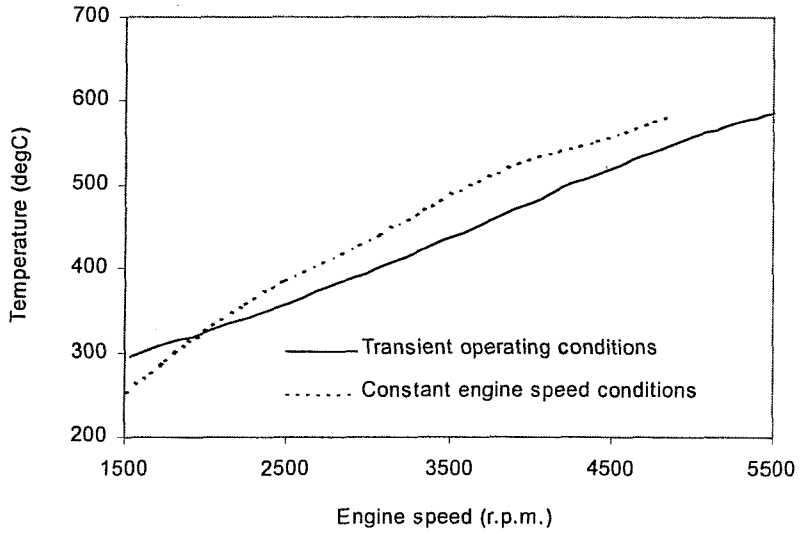

Figure 5.24 Inlet temperature (station #1) recorded for the transient and constant engine speed conditions while operating the vehicle at full throttle on the chassis dynamometer.

Figure 5.25 below shows the measurement duration and number of intervals for the transient and constant engine speed conditions. The interval duration (Y-axis) is represented on a logarithmic scale due to the extensive difference between the total duration of these measurements. The total measurement duration was 2.12 minutes for the transient measurement and 33.87 minutes for the constant engine speed measurements. The transient measurement was performed at constant time intervals and the constant engine speed measurement intervals constantly decreased in time as the engine reached a stable temperature more quickly with an increase in engine speed. In comparison with the results of acceleration tests, these results demonstrated that constant speed tests are excessively time-consuming, and the restricted number of measurement intervals may not describe the acoustic behaviour adequately.

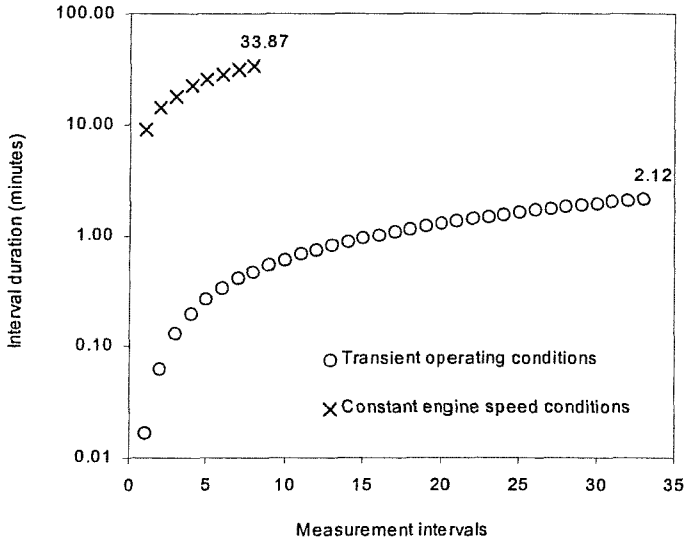

Figure 5.25 Measurement duration for the transient (circle) and constant engine speed (cross) conditions. The Y-axis is represented on a logarithmic scale due to the extensive difference in measurement duration. These results demonstrate the advantages of the transient procedure to obtain a comprehensive set of rapid results.

5.7 CONCLUSION

In this chapter the transient measurement technique was applied to assess the acoustic behaviour of an expansion chamber on a running vehicle. The practical operating conditions of the vehicle were represented by a constant acceleration run-up at a rate that avoided overheating of the engine but avoided resorting to external cooling. The slowest acceleration that achieved these preconditions was found to be 30 r.p.m./sec. The variable temperature and mass flow were recorded at regular engine speed intervals (120 r.p.m. yielded 33 intervals) during the run-up undertaken to obtain the four pressure time-histories needed to perform the wave decomposition calculations and acoustic predictions.

As has been mentioned in Chapter 4, the successful application of the transient experimental technique depends on the precise relative calibration of the pressure transducers, a thorough understanding of order analysis measurement techniques, the design of a suitable transducer array and a method to determine the optimum position of the pressure transducers. In addition, the following special precautions were required for the successful application of the measurement technique during the transient operation of the vehicle on the chassis dynamometer:

- Water-cooled adapters were required to protect the pressure transducers against the very high exhaust gas temperatures ($700^0 C$) generated during the transient operation of the vehicle.

- Special thermocouples with a fast enough response time were required to capture the changing temperatures during a realistic run-up of the vehicle.

- In order to evaluate the quality of the measurements and to explain certain recorded measurement errors and discrepancies, the signal-to-noise ratios were estimated from the order spectra, as it was not possible to measure them directly. In order to improve the reliability of the measurements, the best position for the

pressure transducers was found by recording the estimated signal-to-noise ratios for the order components as a function of transducer position. Results showed that low signal-to-noise ratios in the tail-pipe corresponded to doubtful measured data.

- It was essential to capture the precise variable intake mass flow and exhaust gas temperature at the same predetermined intervals as those selected for the acoustic measurements. This data is required to obtain reliable estimates of the wave components $P^{\pm}$.

After the interpretation of the acoustic behaviour of the expansion chamber for a run-up of the vehicle on the chassis dynamometer, the following observations were made:

- The peak sound power transmission in the exhaust system was dominated by the system resonances, including the half wavelength modes of the tail-pipe and expansion chamber.

- The variable exhaust gas temperature had a strong influence on the spectral distribution of corresponding resonances for different order components.

- Changes in throttle position (full throttle and half throttle) resulted in a significant difference in the spectral distribution of resonances.

- The change in mass flow associated with different throttle positions resulted in a smaller influence for peak resonance levels.

- Clearly the system resonances are of much more practical significance in terms of the acoustic performance of the complete exhaust system. The primary aim during any design strategy is the manipulation of these resonances by means of geometric modification to reduce sound power transmission along the system to

the terminating orifice where the noise is emitted. The other essential design consideration is the acoustic interaction between elements. In this chapter only one element (the expansion chamber) was considered and therefore excluded the interaction between elements. These aspects are covered in Chapter 6.

Measured and predicted transfer functions, acoustic attenuation and acoustic power flux in the tail-pipe showed close agreement (±3 to 4dB or better) for a full throttle run-up. In contrast to the bench test results, the order components with overlapping frequencies for a particular acoustic quantity (for example, acoustic attenuation) showed amplitude variation and frequency shift caused by the variable mass flow and temperature. Close agreement was also obtained between the measured and predicted attenuation for a half throttle run-up. As one might expect, the acoustic behaviour for the full throttle and half throttle run-ups did not correspond at similar engine speeds, due to the difference in exhaust gas properties associated with each engine load condition.

Despite the close agreement (± 3dB or better) between measured and predicted results for constant engine speed and load conditions, this experimental procedure proved to be considerably more time-consuming compared with the transient (run-up) measurement technique. The prolonged measurement duration (16 times longer than the transient method) and overheating of the engine yielded an incomplete description of the acoustic behaviour of the exhaust system components due to the restricted number of measurement intervals (eight intervals). The clear difference in acoustic behaviour recorded for the transient and constant engine speed measurements suggests that constant engine speed measurements did not reflect the realistic operating conditions of the vehicle because of the unrealistic temperature distribution. One may conclude that the new transient procedure provides a more reliable and rapid method to obtain a comprehensive set of data to assess the acoustic performance of an exhaust system under the normal operating conditions of the vehicle.

The agreement between measurements and predictions calculated using the extended version of APEX suggests that linear acoustic theory remains sufficiently valid for guiding system refinement in the exhaust system of a running engines for high sound pressures up to 3500 Pa (165dB). This implies that wave steepening was not a significant factor in the present case [1.11, 2.21]. This provides some justification for the adoption of appropriate hybrid methods [2.10] to predict the exhaust tail-pipe sound emission rather than predictions based on non-linear gas dynamic calculations [1.3] throughout the exhaust system. Moreover, the validated linear acoustic code adapted for transient operating conditions can be employed as an effective design tool to facilitate rapid acoustic optimisation of an exhaust system. The advantage of this approach, compared to the assessment of tail-pipe radiation noise, is discussed in the Chapter 6, Section 6.4.

APPENDIX 5.1

IDENTIFICATION OF FLOW-INDUCED NOISE SOURCES BY MEANS OF POWER FLUX MEASUREMENT

One essential consideration in exhaust system design is the prediction and control of flow generated noise. It seems that the relevant predictive software is not yet available [1.4], so empirical methods are currently adopted. The measurement technique described in this thesis may be used to identify flow-induced acoustic sources along the exhaust system. For example, this can be accomplished by means of precise measurement of net power flux at either side of suspected flow noise sources. Alternatively, any significant differences between measured power flux and that predicted by linear acoustic code may be attributed to the presence of flow-induced sources or sinks [5.1]. These originate from the non-linear transfer between flow energy and sound energy [1.4, 1.5, 3.9-3.12, 5.2] often associated with vortex excitation of an expansion chamber/tail-pipe combination. This can then lead to flow noise generation or to amplification/attenuation of incident sound.

Such an example is demonstrated in Figure A5.1.1 on page 167, displaying the measured and predicted normalised power flux for the 6E and 8E components at the outlet of the expansion chamber in Figure A5.1.2 on page 168 (normalised to the incident power flux at the inlet of the expansion chamber). The measurement was performed for a full throttle run-up of the vehicle on the chassis dynamometer. The construction of the expansion chamber was the same as the one in Figure 5.3 on page 135, but the tail-pipe length was reduced from 1415 mm to 966 mm. The power flux amplitudes in Figure A5.1.1 are represented for critical analysis in a linear scale. One notes a significant difference between the predicted and measured peaks in power flux at the tail-pipe resonances.

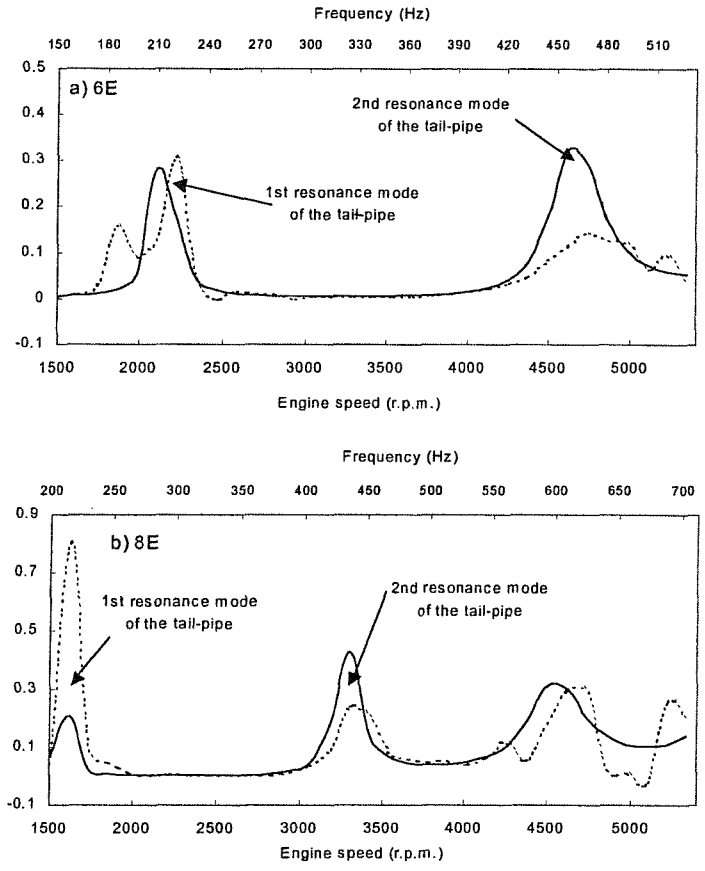

Figure A5.1.1 Measured (dash) and predicted (solid) normalised acoustic power flux in the tail-pipe for the 6E component (Graph a)) and 8E component (Graph b)).

For the 6E component the first resonance mode of the tail-pipe occurred at 2100 r.p.m. (210 Hz) and the second resonance mode of the tail-pipe occurred at 4620 r.p.m. (462 Hz). For the 8E component the first resonance mode of the tail-pipe occurred at 1620 r.p.m. (216 Hz) and the second resonance mode of the tail-pipe occurred at 3300 r.p.m. (440 Hz). It appears that the discrepancies between the measured and the predicted power flux arise from the flow noise generation at the chamber outlet/tail-pipe junction at frequencies corresponding to the acoustic resonances of the tail-pipe [1.5, 3.10, 3.11]. The increase in measured power flux amplitudes at the first resonance mode of the tail-pipe may be interpreted as the presence of a flow noise source. By contrast, the reduction in measured power flux amplitudes at the second resonances mode of the tail-pipe may be attributed to the

presence of a flow noise sink. These features remained constant for successive measurements. The measured discrepancies for the 8E component above 4500 r.p.m. seemed to be correlated with low signal-to-noise ratios (see Figure A5.1.3 on page 168), when measurements became less reliable.

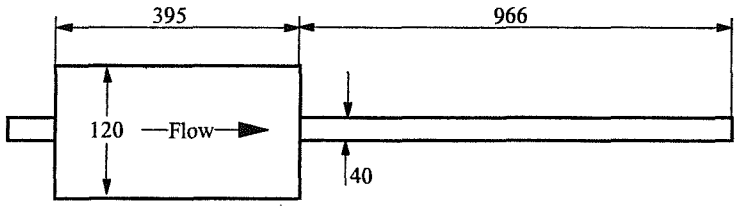

Figure A5.1.2 Details of the simple expansion chamber and tail-pipe (all dimensions in millimetres).

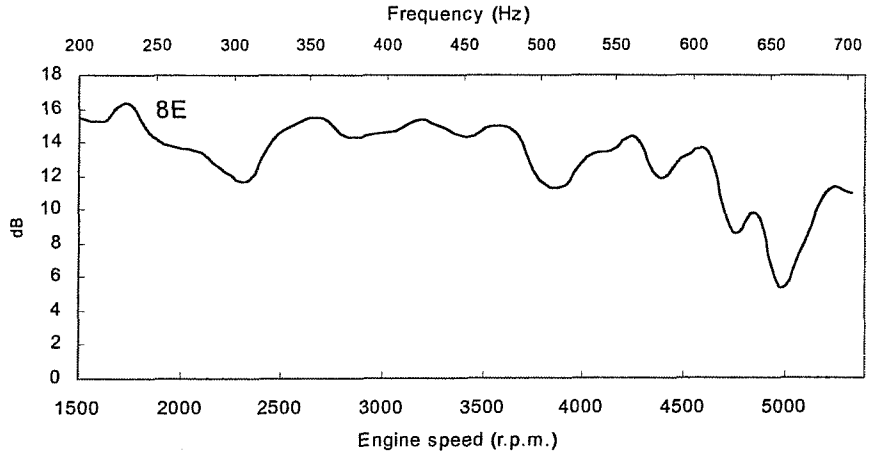

Figure A5.1.3 Estimated signal-to-noise ratios in the tail-pipe for the 8E component.

CHAPTER 6

ACOUSTIC ASSESSMENT AND OPTIMISATION OF A SIMPLE EXHAUST SYSTEM

6.1 INTRODUCTION

The close agreement (within ±3 to 4dB or better) found between the measured and predicted results in the previous chapter showed that realistic descriptions of the acoustic behaviour of an exhaust silencer element can be achieved on a running vehicle. The predictions were based on one-dimensional linear acoustic modelling with sound pressure amplitudes as high as 3.5 kPa (165dB), while the influence of acoustic resonances still dominates both the acoustic excitation and the peak sound power transmission in the exhaust system [6.1]. The calculations should be open to clear interpretation and identification of the individual contribution of each element to the overall acoustic performance under realistic operational conditions [1.1, 1.2]. These proceedings should allow the rapid optimisation of the acoustic performance of the exhaust system by means of geometric modifications.

To demonstrate these underlying principles, this chapter describes the acoustic assessment of a simple exhaust system, based on realistic predictive modelling of the acoustic, gas dynamic and operational conditions for a practical run-up of the vehicle. The potential advantage of this approach for the rapid optimisation of the exhaust system, over one restricted to the evaluation of tail-pipe orifice noise emission measurements is demonstrated. The assessment and optimisation of the exhaust system presented in this chapter are based on the rational design strategy described in Chapter 3.

Section 6.2 presents the experimental procedures and the layout of the simple exhaust system used. Section 6.3 describes the acoustic assessment of this exhaust system by means of tail-pipe orifice noise emission measurements and realistic predictive modelling. The rapid acoustic optimisation of the exhaust system is described in Section 6.4.

6.2 EXPERIMENTAL PROCEDURES

As before, a Honda Ballade vehicle, fitted with a 1.5 litre, four-stroke four-cylinder engine, was used for the experimental work. The vehicle was operated in third gear on a chassis dynamometer installed inside a semi-anechoic chamber. The exhaust system was mounted in front of the vehicle to enhance accessibility during the optimisation process, as set out in Figure 6.1 below.

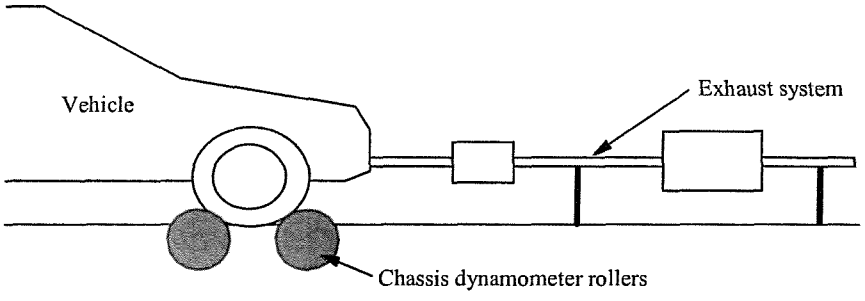

Figure 6.1 Schematic representation of the vehicle positioned on the chassis dynamometer with the exhaust system mounted in front of the vehicle.

The layout of the exhaust system and the geometric dimensions of the elements are set out in Figure 6.2 on page 171. They are representative of a small passenger vehicle. The sketch also depicts the acoustic model of the system, consisting of three elements. The inlet and outlet of each element are numbered from 1 to 4, starting at the tail-pipe outlet. An external microphone was placed at a distance of 0.5 metres at 45 degrees from the exhaust outlet, indicated by position 5. Both the front and rear silencers are simple expansion chambers with the dimensions indicated in Figure 6.2 on page 171.

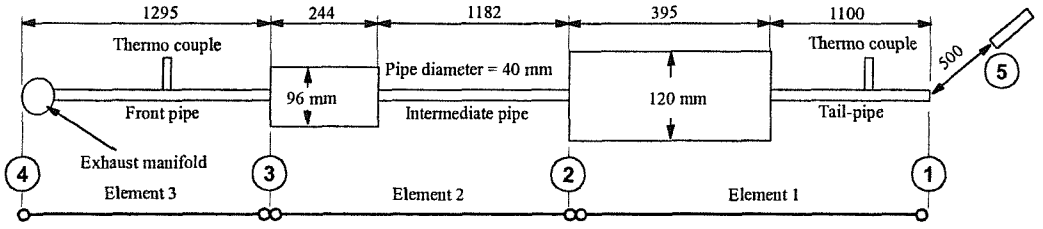

Figure 6.2 Exhaust system layout, displaying the geometric details of the three elements (all dimensions are in millimetres).

The order tracking procedure adopted previously was again applied for the tail-pipe noise measurements. The vehicle was accelerated at a controlled sweep-rate of 30 r.p.m./sec and order spectra were captured every 120 r.p.m. between 1200 r.p.m. and 5400 r.p.m.. The order tracking analysis was performed with an order resolution of $\Delta n = 0.025$ orders, 75 % overlap using a Hanning window and five exponential averages. The tracking of the fundamental frequency was measured using a tachometer connected to the ignition coil of the engine. The mass flow, inlet temperature and outlet temperature (see Figure 6.3 below) were recorded at predetermined engine speed intervals to provide the additional data required for the corresponding predictions.

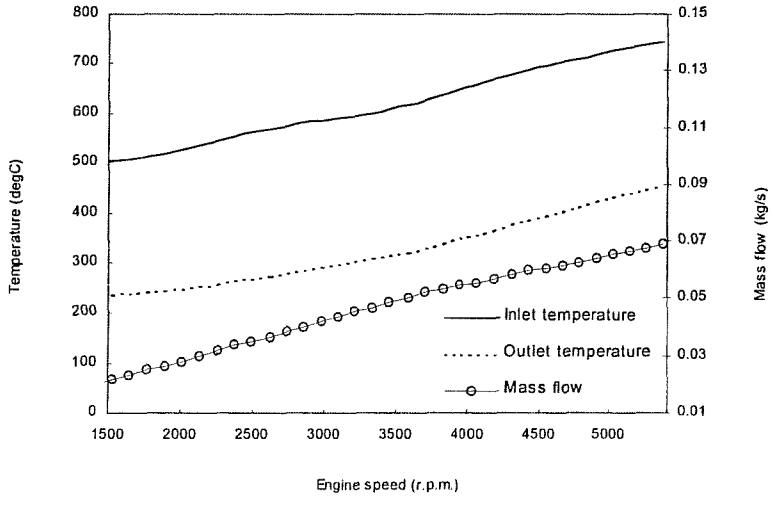

Figure 6.3 Mass flow and exhaust gas temperatures recorded for the full throttle run-up of the vehicle on the chassis dynamometer.

6.3 ACOUSTIC ASSESSMENT OF A SIMPLE EXHAUST SYSTEM

As was discussed in Chapter 3, the acoustic behaviour of the exhaust system is normally governed by system resonances. These resonances are related to the length of the wave path through each element, together with their respective boundary conditions [1.2]. The spectral behaviour of these resonances depends on the resonances of individual elements as well as the variable temperature and mass flow distribution generated during the normal operating conditions of the vehicle. Clear interpretation and identification of the acoustic contribution of each individual element to the overall acoustic performance of the exhaust system, together with the controlling influence of the variable gas properties, are essential to guide appropriate geometric modifications for rapid optimisation [1.2, 1.4].

6.3.1 Tail-pipe orifice noise emission assessment

Although measurements or predictions of tail-pipe orifice noise emission provide a useful evaluation of the overall performance of an exhaust system, they do not generally provide an adequate description to guide the optimisation process. This is demonstrated in Figure 6.4 on page 173, showing the radiated tail-pipe orifice noise emission measurement of the exhaust system in Figure 6.2 on page 171 for a full throttle run-up of the vehicle. The microphone was placed at a distance of 0.5 metres at 45 degrees from the exhaust outlet and the levels were A-weighted (the standard evaluation procedure in the automotive industry). The first four order components (2E, 4E, 6E and 8E) were displayed as was the overall noise.

One notes that the order components and the overall noise were dominated by a sequence of peaks associated with the resonances of the exhaust system. These included tail-pipe and connecting pipe resonances, cavity resonances and expansion chamber resonances (as described in Chapter 3, Section 3.3.2). Clearly, the manual identification of these resonances is a time-consuming task if one takes into account the variable mass flow and axial temperature distribution over the engine speed range

(see Figure 6.3), even for this simple system. For example, a particular resonance may occur at a low engine speed for one order component and at a high engine speed for another order component: corresponding resonances are thus subjected to different temperature conditions. It is also not possible to identify the acoustic behaviour of individual elements and their mutual interaction from tail-pipe noise measurements. To achieve this, $P^{\pm}$ must be estimated at appropriate positions along the exhaust system from pressure measurements, or base the design procedure on realistic predictive acoustic modelling of the individual elements.

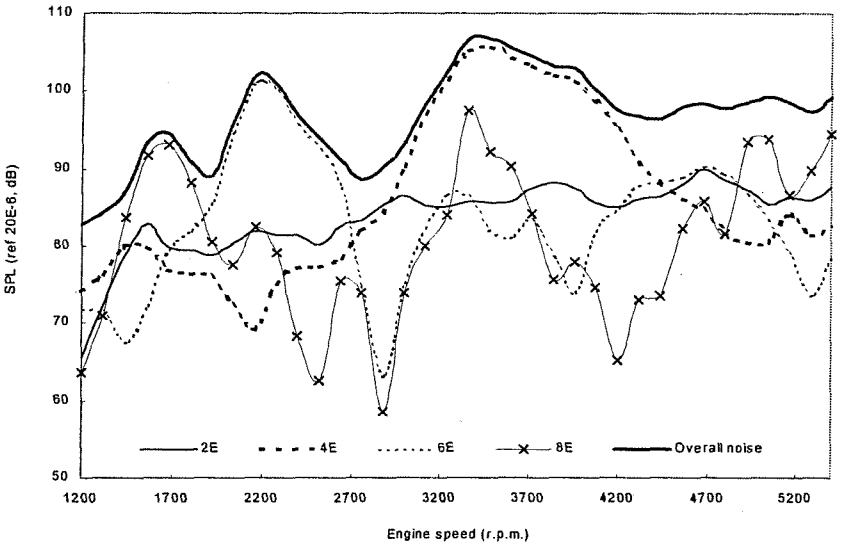

Figure 6.4 Tail-pipe orifice noise emission measurement of the exhaust system in Figure 6.2 on page 171 for a full throttle run-up of the vehicle on the chassis dynamometer. The graph shows the first four order components (2E, 4E, 6E and 8E) and the overall levels.

6.3.2 Predictive acoustic modelling assessment

The positive experimental results obtained on the running engine in Chapter 5 validate the use of linear acoustic theory for the transient operating conditions of the vehicle, at least for the examples described so far. This opens up the possibility of predicting the acoustic contribution of each individual element to the overall acoustic performance of an exhaust system during engine acceleration to facilitate rapid assessment.

The new APEX code adapted for transient conditions was applied to identify the acoustic behaviour of the exhaust system for the run-up. The acoustic modelling of the exhaust system was based on the three elements represented in Figure 6.2 on page 171, consisting of the exhaust manifold, front silencer and rear silencer with their respective connecting pipes. Although the acoustic modelling of the exhaust manifold might not be fully realistic, due to non-linear wave propagation and other behaviour that normally exists close to the valves [2.23, 6.2], the manifold was incorporated into the prediction model to identify the resonant behaviour which has been shown to correspond closely to the acoustic behaviour of the front pipe. The original manifold was replaced by a simple plenum chamber connected to the exhaust valve ports by short pipes. Therefore, it was possible to model it as a simple expansion chamber. The run-up was simulated by incorporating the measured mass flow and exhaust gas temperature gradients into the calculations. These were performed at the corresponding engine speed intervals contemplated for the tail-pipe orifice noise emission measurement.

As was discussed in Chapter 3, one may use either acoustic attenuation or normalised power flux to identify the acoustic behaviour of the exhaust system. Figure 6.5 on page 175 shows the attenuation of each element ($AL_{2,1}$, $AL_{3,2}$ and $AL_{4,3}$) for the first four order components (2E, 4E, 6E and 8E). The exhaust system resonances are represented by the troughs and distinguished by a symbol 1a, 1b, etc., where the number represents the element and the character the specific resonance (as indicated in Table 6.1 on page 177). The transmitted power across each element $W_{1,2}$ (element #1), $W_{2,3}$ (element #2) and $W_{3,4}$ (element #3) for the 2E, 4E, 6E and 8E components are displayed in Figure 6.6 on page 176; here the system resonances are represented by the peaks. One may note that the normalised power flux for each element corresponds closely to the inverse of the attenuation.

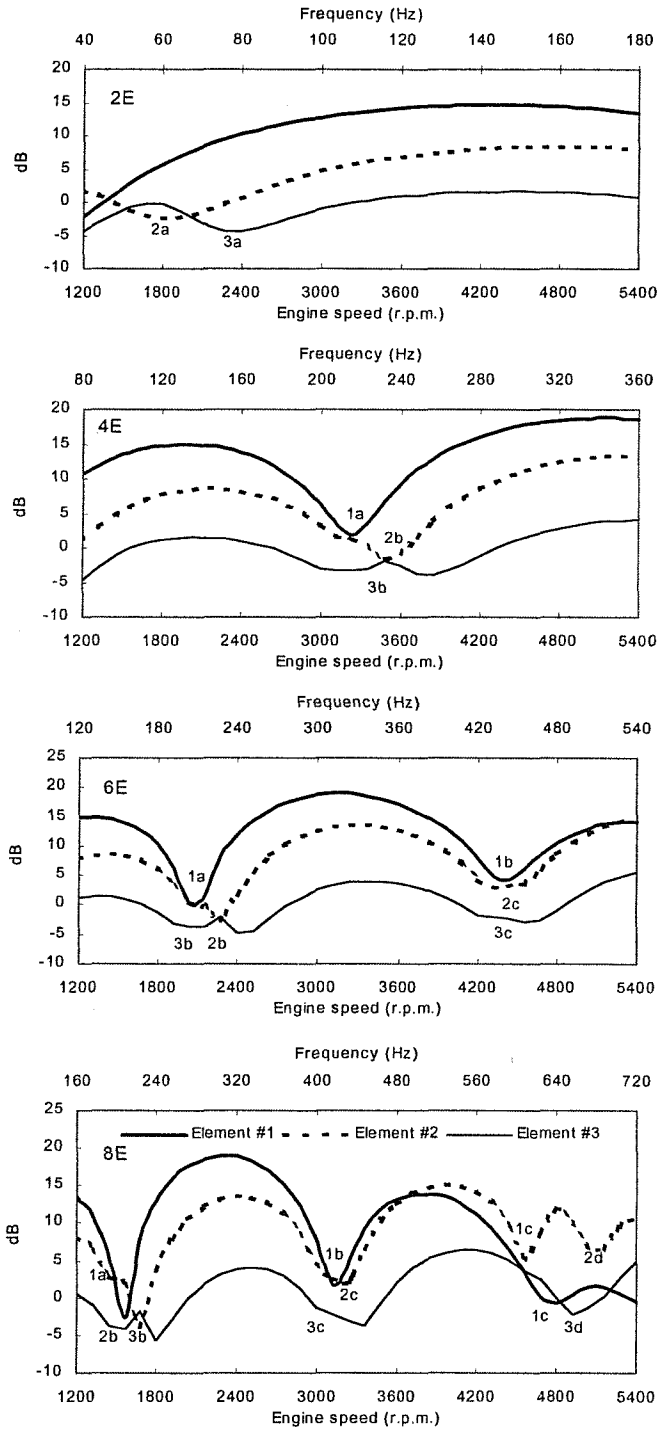

Figure 6.5 Predicted attenuation of element #1 $AL_{2,1}$ (thick solid line), element #2 $AL_{3,2}$ (dash line) and element #3 $AL_{4,3}$ (thin solid line) for the 2E, 4E, 6E and 8E order components for a simulated run-up. The resonances are indicated by the symbols 1a, 1b, etc. (described in Table 6.1 on page 177).

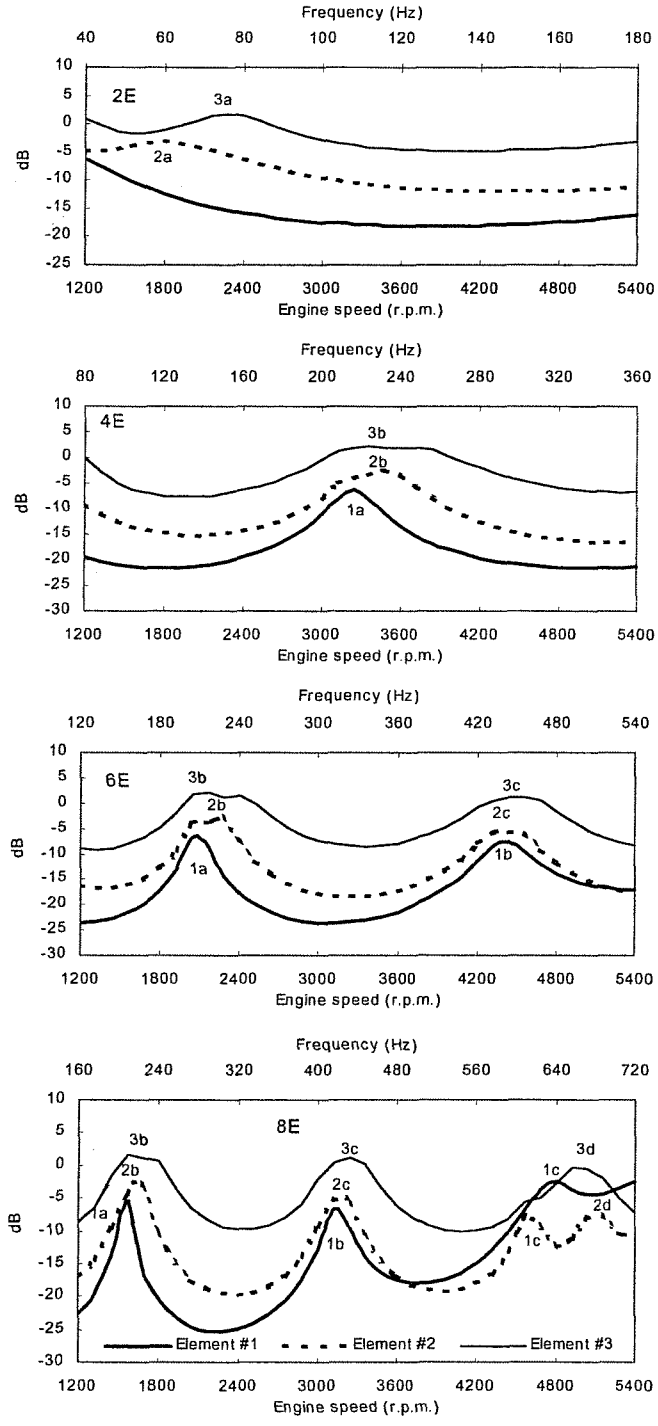

Figure 6.6 Predicted normalised power flux of element #1 $W_{1,2}$ (thick solid line), element #2 $W_{2,3}$ (dash line) and element #3 $W_{3,4}$ (thin solid line) for the 2E, 4E, 6E and 8E order components for a simulated run-up. The resonances are indicated by the symbols 1a, 1b, etc. (described in Table 6.1 on page 177).

Description of resonance	Symbol	Order
Cavity resonance of element #2	2a	2E
Cavity resonance of element #3	3a	2E
1st half wavelength mode of tail-pipe	1a	4E, 6E, 8E
2nd half wavelength mode of tail-pipe	1b	4E, 6E, 8E
1st half wavelength mode of rear expansion chamber	1c	8E
1st half wavelength mode of intermediate pipe	2b	4E, 6E, 8E
2nd half wavelength mode of intermediate pipe	2c	6E, 8E
3rd half wavelength mode of intermediate pipe	2d	8E
1st half wavelength mode of front pipe	3b	4E, 6E, 8E
2nd half wavelength mode of front pipe	3c	6E, 8E
3rd half wavelength mode of front pipe	3d	8E

Table 6.1 Description of the resonances for the simple exhaust system in Figure 6.2 on page 171. The resonant behaviour of the order components and the associated symbols are also indicated in Figures 6.5 and 6.6 on pages 175 and 176 respectively.

One notes that the cavity resonances 2a and 3a in Figures 6.5 and 6.6 on pages 175 and 176 appeared only for the 2E component, while it was below 40 Hz (1200 r.p.m.) for element #1. The frequency of these resonances was associated with the chamber volume and connecting pipe dimensions (see equation (3.12)) and normally occurred below 100 Hz (3000 r.p.m.) for conventional automotive exhaust systems.

The assessment also indicated that the first and second half wavelength modes of the tail-pipe, intermediate-pipe and front-pipe occurred at similar frequencies for the 4E, 6E and 8E components, as demonstrated in Figures 6.5 and 6.6 on pages 175 and 176 respectively. It can also be observed that the resonances that occurred for element #3 $AL_{4,3}$ could not clearly be identified, due to the dynamic interaction with the resonances of element #1 and element #2. So, for example, the modification of the 8E component at 608 Hz for element #2 ($AL_{3,2}$, $W_{2,3}$) demonstrated the dynamic interaction between elements. This resonance was related to element #1 and was associated with the first half wavelength mode of the expansion chamber for element #1 (1c).

Now that the resonances of the exhaust system have been clearly identified and interpreted, one may combine the results to acquire the system attenuation $AL_{4,1}$ as displayed in Figure 6.7 below. The result describes the overall acoustic performance of the exhaust system and incorporates the acoustic contribution of each individual element. A detailed description of the resonances is provided in Table 6.2 on page 179. One notes that the predicted system resonant frequencies (troughs) in Figures 6.5 and 6.7 (acoustic attenuation) and the peaks in Figure 6.6 (transmitted normalised power flux) with Tables 6.1 and 6.2 corresponded closely to those inferred from the tail-pipe orifice noise emission in Figure 6.4 on page 173.

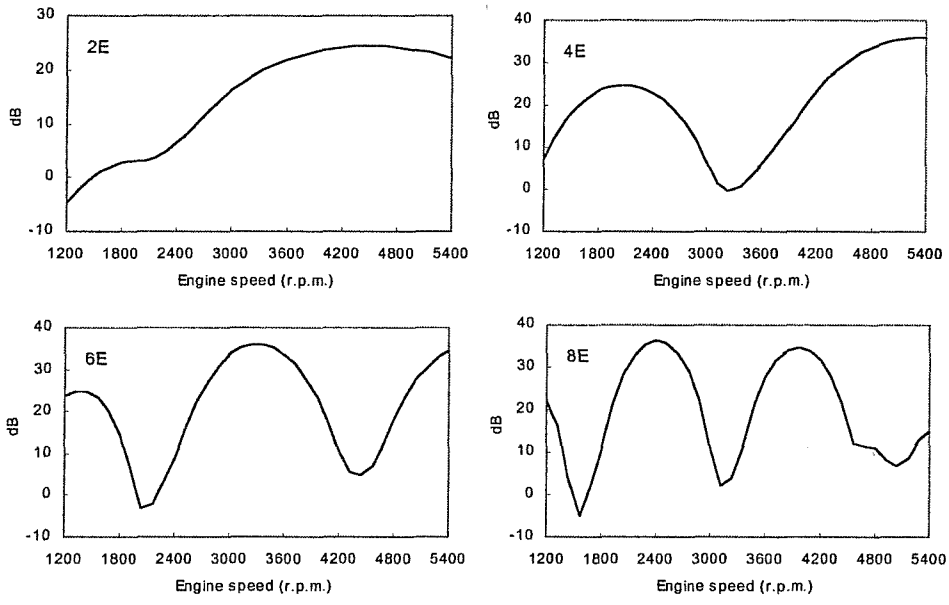

Figure 6.7 Predicted system attenuation $AL_{4,1}$ for the exhaust system in Figure 6.2 on page 171 for a full throttle run-up. Note that the minima (troughs) identify the system resonances that corresponded closely with the measured tail-pipe peaks.

6.4 ACOUSTIC OPTIMISATION OF THE EXHAUST SYSTEM

Returning to Figure 6.4 on page 173, one notes that the overall levels were dominated by the resonances at 1560 r.p.m. (8E), 2160 r.p.m. (6E) and 3300 r.p.m (4E) (as described in Figure 6.7 above and Table 6.2 on page 179). In order to optimise the

acoustic performance of the original exhaust system (Figure 6.2 on page 171) these resonances had to be eliminated or damped. Alternatively, the length of the connecting pipes could be tuned so that the resonances were sufficiently separated to avoid the strong coincidence reported in Table 6.2. To demonstrate the effective tuning of the system, the existing expansion chambers and overall length of the system were kept the same.

Order	Engine speed (r.p.m.)	Label	Description of resonance
2E	2,160	2a	Cavity resonance of element #2
		3a	Cavity resonance of element #3
4E	3,240	1a	1st half wavelength mode of tail-pipe
		2b	1st half wavelength mode of intermediate pipe
		3b	1st half wavelength mode of front pipe
6E	2,160	1a	1st half wavelength mode of tail-pipe
		2b	1st half wavelength mode of intermediate pipe
		3b	1st half wavelength mode of front pipe
6E	4,440	1b	2nd half wavelength mode of tail-pipe
		2c	2nd half wavelength mode of intermediat pipe
		3c	2nd half wavelength mode of front pipe
8E	1,560	1a	1st half wavelength mode of tail-pipe
		2b	1st half wavelength mode of intermediate pipe
		3b	1st half wavelength mode of front pipe
8E	3,120	1b	2nd half wavelength mode of tail-pipe
		2c	2nd half wavelength mode of intermediate pipe
		3c	2nd half wavelength mode of front pipe
8E	4,560 to 5040	1c	1st half wavelength mode of rear expansion chamber
		2d	3rd half wavelength mode of intermediate pipe

Table 6.2 Description of the resonances for the predicted system attenuation $AL_{4,1}$ (see Figure 6.7 on page 178) for the original exhaust system in Figure 6.2 on page 171.

The objective was to refine the acoustic performance of the system by means of geometric modifications. A sequence of attenuation predictions was performed for the first four order components to determine the appropriate connecting pipe lengths; the objective was to ensure that the system resonances were well separated. It took approximately 1.5 seconds to calculate each interval and less than a minute to calculate the 36 intervals to simulate the run-up. Therefore it was possible to evaluate a number of different system configurations in a short period to ensure rapid acoustic

optimisation of the exhaust system. The geometric details of the optimised exhaust system are shown in Figure 6.8 below; the length of the tail-pipe was shortened by 200 mm and the length of the front pipe was increased by 200 mm; the rest of the system was left unchanged and the overall length was kept the same.

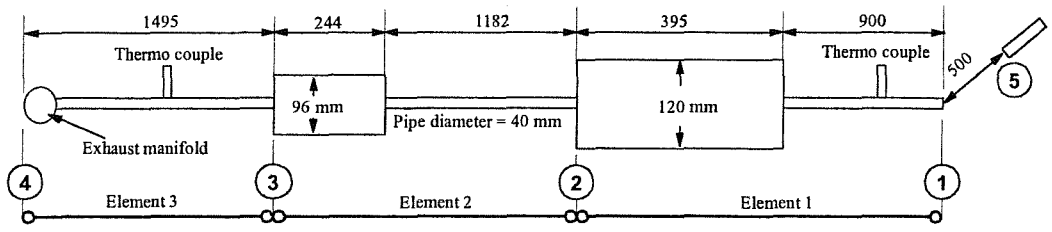

Figure 6.8 Layout of the optimised exhaust system (all dimensions are in millimetres).

The predicted attenuation for the three elements ($AL_{2,1}$, $AL_{3,2}$ and $AL_{4,3}$) is shown in Figure 6.9 on page 181 for the first four order components (2E, 4E, 6E and 8E). When this is compared to Figure 6.5 on page 175, one notes that the resonant modes of the intermediate pipe occurred at the same frequencies, since the pipe length was kept the same (1182 mm). Conversely, the acoustic modes of the tail-pipe occurred at higher frequencies and those for the front pipe at lower frequencies which are related to a decrease and increase in pipe length respectively. The separation of the resonances resulted in a more equal distribution of the resonances over the engine speed range. This is clearly illustrated by the system attenuation $AL_{4,1}$ and radiated power $W_{1,5}$ in Figures 6.10 and 6.11 on page 182, comparing the original and the optimised system overall acoustic performance. These comparisons clearly demonstrate the improvement in the predicted overall acoustic performance of the optimised system where the resonance levels were reduced by 10 to 15dB.

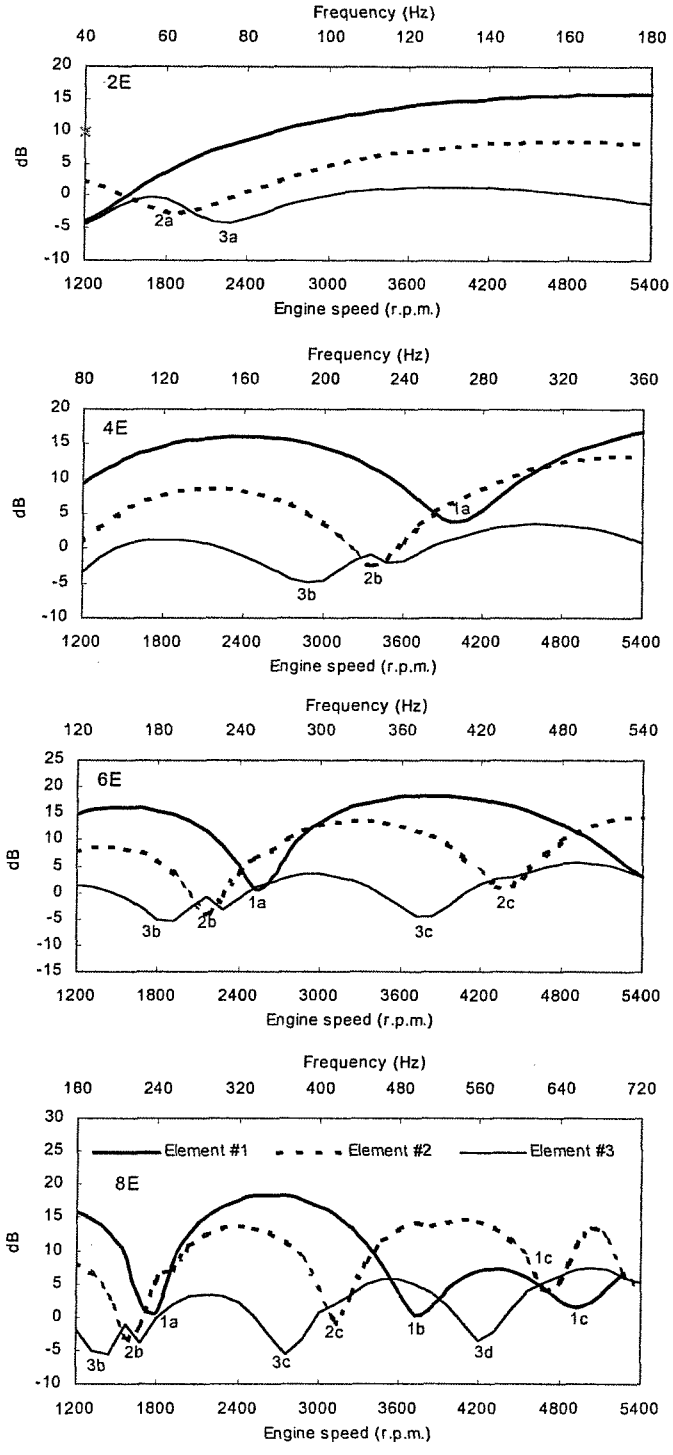

Figure 6.9 Predicted attenuation of element #1 $AL_{2,1}$ (thick solid line), element #2 $AL_{3,2}$ (dash line) and element #3 $AL_{4,3}$ (thin solid line) for the optimised exhaust system (see Figure 6.8 on page 180) for a simulated run-up. The resonances are indicated by the symbols 1a, 1b, etc. (described in Table 6.1 on page 177).

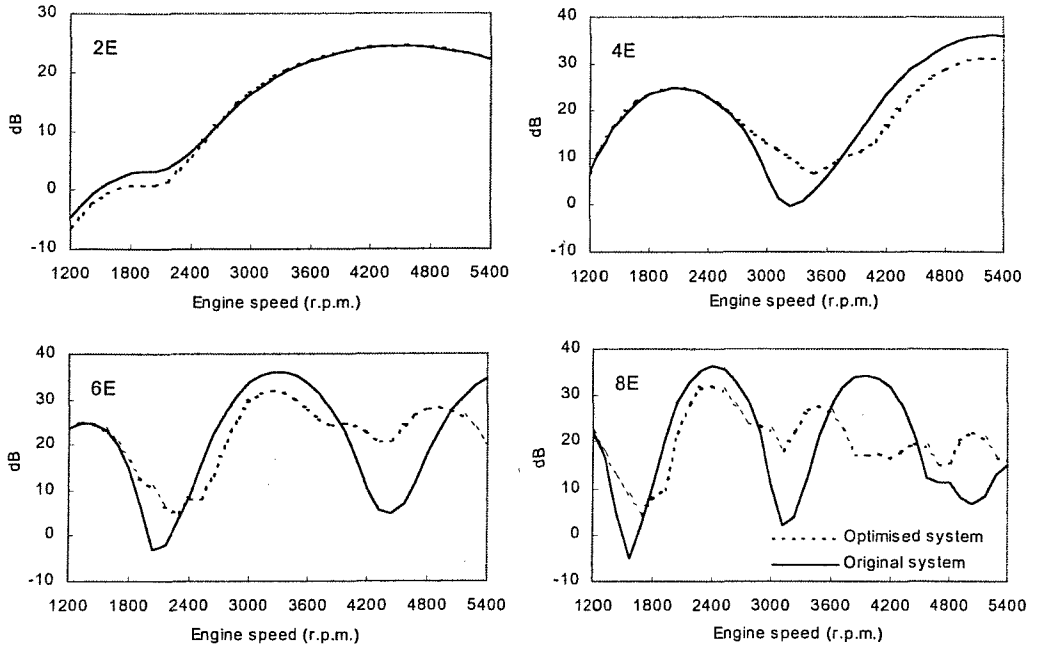

Figure 6.10 Predicted system attenuation $AL_{4,1}$ for the original system (solid curve) and the optimised system (dash curve) for a full throttle run-up.

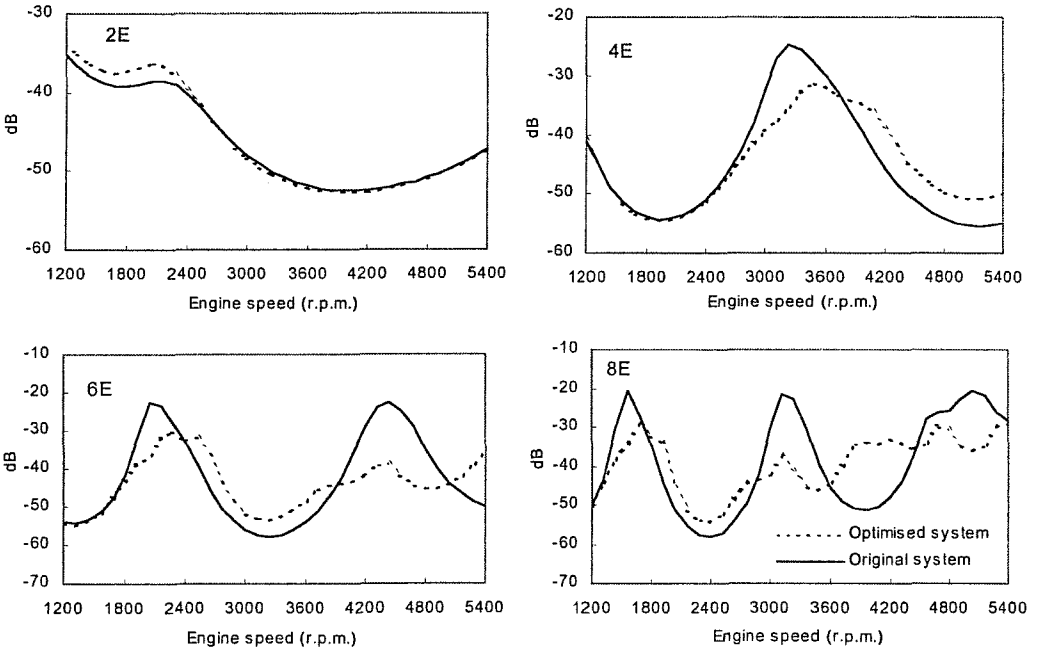

Figure 6.11 Predicted radiated power $W_{1,5}$ for the original system (solid curve) and the optimised system (dash curve) for a full throttle run-up.

The optimised exhaust system was fitted to the vehicle and the tail-pipe orifice noise emission was measured according to the same procedure as that adopted for the original system. The results for the first four order components were compared to the tail-pipe noise for the original system in Figure 6.12 below. Similar tail-pipe levels were recorded for the first order (2E) because the acoustic behaviour of both systems was similar at low frequencies. The optimised system showed a small increase in levels at low engine speeds and a small decrease in levels at high engine speeds associated with the increased cavity resonance frequency of element #1 since the tail-pipe was shorter. Although some of the order components of the optimised system showed an increase in levels (for example, at 3000 r.p.m. for the 6E component and at 4200 r.p.m. for the 8E component), a significant reduction of levels was achieved at the engine speeds where the resonances for the original system occurred.

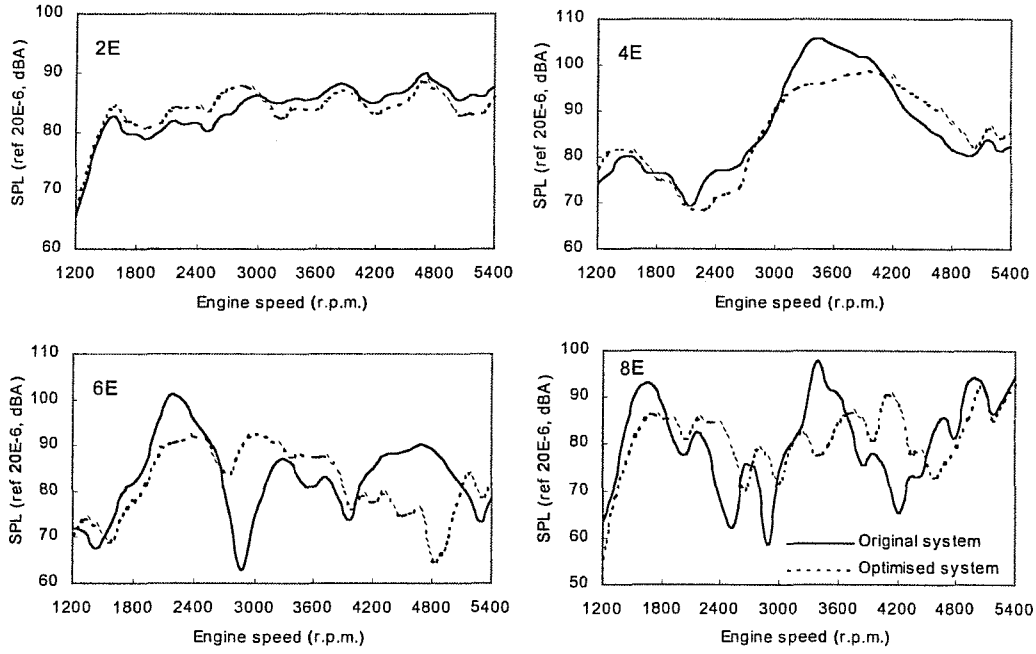

Figure 6.12 Comparison between tail-pipe orifice noise emission recorded for the original system (solid curve) and the optimised system (dash curve) for a full throttle run-up.

The comparison presented in Figures 6.10 (system attenuation $AL_{4,1}$), 6.11 (radiated power $W_{1,5}$) and 6.12 (measured tail-pipe orifice noise emission) not only demonstrates the acoustic performance improvement that can be obtained by means of a careful tuning of the components, but also the close correlation between the predictions and the measured tail-pipe orifice noise emission. These results illustrate the practical value of the appropriate use of linear acoustic modelling as part of a rational design strategy.

The significant improvement that was achieved with the optimised system is further demonstrated in Figure 6.13 below, comparing the overall tail-pipe levels (dBA) of the original and optimised systems. This was particularly evident for the peaks at 1560 r.p.m., 2160 r.p.m. and 3300 r.p.m., where the levels were reduced by 5dB, 10dB and 8dB respectively. A small increase in levels was recorded for the optimised system above 4500 r.p.m.. The increase was related to the first half wavelength mode of the expansion chamber. The peak at 4680 r.p.m. was associated with the acoustic interaction between element #1 and element #2 and the peak at 5040 r.p.m. was associated with element #1 (see Figure 6.9 on page 181).

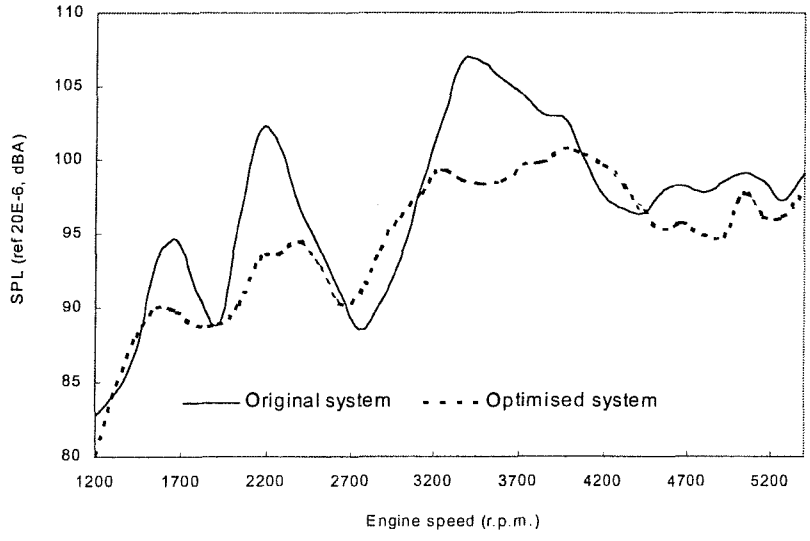

Figure 6.13 Comparison between overall tail-pipe orifice noise emission recorded for the original system (solid curve) and the optimised system (dash curve) for a full throttle run-up of the vehicle.

6.5 CONCLUSION

This chapter described the assessment and optimisation of a simple exhaust system. The evaluation of radiated tail-pipe orifice noise emission recorded for a full throttle run-up showed that the overall noise was dominated by a sequence of peaks associated with the resonances of the first four order components. Although this was a convenient method to assess the overall acoustic performance of the exhaust system, the spectral information did not provide sufficiently detailed information to indicate the appropriate changes to each specific element required to optimise the acoustic performance of the complete exhaust system. Furthermore, the variable mass flow and temperature gradients complicated the interpretation of the results.

Predictions performed with the new APEX code adapted for transient conditions provided a clear identification and interpretation of the acoustic behaviour of the exhaust system by simulating the operational conditions for a full throttle run-up. Attenuation and normalised power flux results quantified the system resonances of each element and the acoustic interaction between the elements. The assessment indicated that the peak levels recorded for the tail-pipe orifice noise emission were caused by the coincidence of several individual system resonances associated with the connecting pipes and expansion chambers.

The insight obtained with the predictive assessment and the short calculation time allowed the rapid acoustic optimisation of the exhaust system within the same overall space. The peak order component levels of the original system were reduced by tuning the connecting pipe lengths so that the system resonances were well separated. This produced a significant improvement in the overall tail-pipe orifice noise emission by eliminating the resonance peaks. The acoustic optimisation of the simple exhaust system by means of a minor geometric modification illustrated the significance of the location of the silencers in terms of the initial overall layout of vehicle.

Finally, as shown in Figures 6.10 to 6.12 comparison between the predicted results (system attenuation and normalised power flux) and measured tail-pipe orifice noise emission correlated closely. This validates the use of linear acoustic modelling as part of a rational design strategy. Nevertheless, modelling of the physical variables and fluid properties to simulate the operational conditions of the engine is essential to obtain a realistic description and identification of the acoustic behaviour of the exhaust system concerned.

CHAPTER 7

FINDING AND RECOMMENDATIONS

7.1 SUMMARY

The work presented in this thesis describes the establishment of new experimental and computation procedures to evaluate the acoustic properties of an exhaust system for the practical operating conditions of a vehicle. The aim of the study was to facilitate the rapid acoustic optimisation of an exhaust system by guiding appropriate geometric modification to the system. This required the development and validation of new advanced measurement technology that quantifies the acoustic performance of individual silencer elements during transient operating conditions. It also involved the development of prediction software to model the acoustic and gas dynamic behaviour of an exhaust system under transient operational conditions. The objective of these procedures was to overcome the limitation of tail-pipe orifice noise emission assessments that are currently employed as a design strategy because, on their own, they provide insufficient spectral information to guide the optimisation process.

A review of the relevant literature (Chapter 2) showed that previous experimental methods on running engines have been restricted to constant operating conditions. In some instances both the impedance tube and wave decomposition methods have been employed to estimate the wave components $P^{\pm}$ at appropriate positions along the system to validate linear acoustic theory at constant engine speed intervals. However, in practice, the time needed to obtain stable acoustic and temperature conditions restricted the number of measurement intervals. This approach proved to be time-consuming and practical application was often limited, because a restricted

number of measurement intervals was insufficient to identify all the significant details of the acoustic behaviour of the exhaust system.

Tail-pipe radiation noise and in-duct pressure measurements recorded at low stationary engine speeds have been used to validate non-linear gas dynamic and hybrid models. Such results are restricted to descriptions of the overall acoustic performance of the exhaust system and provide insufficient spectral information to identify the acoustic behaviour of individual elements.

One can conclude that, although these experimental methods provide sufficient procedures to validate theoretical models, they often fail to indicate the appropriate changes to individual elements to guide the design process under the normal operational conditions of the vehicle. A review of the relevant literature suggested that linear acoustic theory could provide the most effective approach to the acoustic modelling of the exhaust system when one needs to facilitate rapid optimisation of acoustic performance.

Experience has indicated (Chapter 3) that the acoustic behaviour of an exhaust system is determined by its geometry, while the spectral distribution of the orifice noise emission, amongst other factors, depends on the local speed of sound c and Mach number M. Each element contributes to the overall acoustic performance and the elements interact dynamically with each other. It is essential to identify the acoustic contribution of each individual element to the overall performance under the normal operating conditions of the vehicle to obtain a clear understanding of the acoustic behaviour of the whole exhaust system. In order to achieve this, appropriate additions and adjustments were made to existing validated linear acoustic code (APEX) to model the changing temperature and flow conditions during engine acceleration. Preliminary attenuation predictions performed with the new prediction code for a simple exhaust system clearly demonstrated the controlling influence of the variable temperatures and mass flow on the acoustic behaviour of the exhaust system for a constant acceleration run-up. The variable gas dynamic conditions

resulted in an amplitude variation and frequency shift of the harmonic components at corresponding frequencies.

Experimental results on the test bench (Chapter 4) showed that order analysis techniques can be used to capture transient harmonic pressure data to evaluate the acoustic performance of each silencer component under simulated engine operating conditions. The wave components $P^{\pm}$ were estimated from the complex transfer function order spectra measured simultaneously at the inlet and outlet of a silencer component. The fixed sampling rate method was preferred to capture only the fundamental harmonic for a wide frequency range (1000 Hz). Otherwise, with order tracking, the sampling rate might have been too low at high frequencies to separate the harmonic components from flow-induced background noise, since the frequency resolution would then be synchronised with the fundamental frequency. However, careful selection of the record length, overlap and number of averages was required to optimise the analysis time for the fixed sampling rate method to limit smearing and avoid leakage for a particular sweep-rate.

Order tracking is to be preferred when one sets out to capture the acoustic behaviour with variable harmonic excitation, since leakage and spectral smearing are avoided. The maximum fundamental frequency associated with internal combustion engine orifice noise emission signature is sufficiently low (200 Hz to 300 Hz) for the sampling rate to be sufficiently high to separate the harmonic information from the flow-induced noise at high engine speeds. The experiments described in Chapter 4 demonstrated that the signal-to-noise ratio and the coherence improved when the analysis was performed with a higher order resolution and an increased number of averages. It was essential to optimise the analysis time to avoid amplitude smearing that could have resulted in a loss of data and in phase distortion. The appropriate analysis time was achieved by establishing the maximum number of averages that could be used for a given sweep-rate. After such procedures had been adopted, the results showed that the experimental technique provided precise and reliable results to identify the small proportion of the total fluctuating energy propagated through

highly reactive exhaust systems. Good agreement (± 2 to 3dB or better) was found between predicted and measured acoustic transfer functions, system attenuation, normalised acoustic power flux and normalised acoustic radiated power for the first four order components, which served to validate the measurement technique.

The transient measurement technique was then applied in Chapter 5 to assess the acoustic behaviour of an expansion chamber on a running vehicle. The signal-to-noise ratios were estimated from the order spectra, since it was not possible to measure them directly. This was required to evaluate the quality of the measurements and to optimise the position of the pressure transducers for reliable measurements. Measured and predicted transfer functions, acoustic attenuation and acoustic power flux in the tail-pipe showed close agreement (±3 to 4dB or better) for a full throttle run-up. Close agreement was also obtained between measured and predicted attenuation for a half throttle run-up. These measurements demonstrated the controlling influence of the temperature and mass flow on the acoustic behaviour of the expansion chamber for different load conditions. One can conclude that the transient measurement procedure yielded precise and reliable results that identified the acoustic behaviour of an exhaust system on a running engine.

Although the records captured at constant engine speed and load conditions agreed closely with predictions, the procedure was time-consuming. The procedure also produced an incomplete description of the acoustic behaviour of the exhaust system components since the number of measurement intervals was restricted by the overheating of the engine. Comparison to transient results also indicated that constant engine conditions do not really reflect the realistic operating conditions of the vehicle. This finding was directly related to the unrealistic temperature distribution. One can conclude that the new transient procedure provides a robust method for the rapid acoustic assessment of exhaust systems under the practical operating conditions of a vehicle.

The agreement between measurements and predictions calculated with the extended version of APEX indicates that linear acoustic theory is sufficiently valid for predicting wave propagation in the exhaust system of a running engine for high sound pressures up to 3500 Pa (165dB). This provides some justification for the adoption of appropriate hybrid methods for predicting exhaust tail-pipe sound emission rather than methods based on non-linear gas dynamic calculations.

The new prediction code was then applied in Chapter 6 to assess and optimise the acoustic performance of a simple exhaust system for a full throttle run-up of the vehicle on a chassis dynamometer. Modelling of the acoustic, gas dynamic and operational conditions provided a clear description and interpretation of the acoustic contribution of each individual element and the dynamic interaction between them. Acoustic attenuation and normalised acoustic power flux predictions clearly identified the acoustic behaviour that contributed to system resonances. The assessment indicated that the peak tail-pipe noise levels were caused by the coincidence of several individual system resonances. The acoustic performance of the exhaust system was optimised by tuning the connecting pipes so that the resonances were well separated. A significant improvement in acoustic performance was confirmed by tail-pipe noise measurements. Although the evaluation of tail-pipe noise measurements offered a convenient method to assess the overall performance of the exhaust system quickly, the harmonic component information was usually insufficient in itself to identify the acoustic behaviour of the exhaust system clearly. For this reason, the evaluation of tail-pipe noise measurements was found to be inadequate to guide the optimisation process. The insight acquired by means of the predictive assessment and the much shorter calculation time provided by adapting linear theory, facilitated the rapid optimisation of the exhaust system acoustic performance.

Comparison revealed close correlation between acoustic predictions and measured tail-pipe orifice noise emission. This validates and demonstrates the potential advantages of the effective use of linear acoustic modelling as part of a rational

design strategy. A direct comparison between linear acoustic predictions and tail-pipe noise measurements was, however, not feasible in the current investigation, because the predicted results were expressed as relative quantities. The linear acoustic predictive assessment demonstrated the potential advantage for the design procedure, facilitating the rapid optimisation of the acoustic performance of an exhaust system compared to tail-pipe orifice noise emission measurements. However, it is essential to model the gas dynamic and operational performance for the practical operating conditions of the vehicle to obtain realistic predictions, as has been demonstrated in this thesis.

7.2 FINDINGS

The primary aim was the development of new technology to facilitate the rapid optimisation of exhaust system acoustic performance. This included the development of a robust experimental technique for the precise estimation of the wave components $P^{\pm}$ at appropriate locations along an exhaust system. Optimised procedures and special equipment were employed to capture sound pressure levels as high as 3.5 kPa (165dB) in the presence of mean flow with Mach numbers up to $M = 0.25$ and temperature gradients between 300^0C to 700^0C. This task was even more challenging when one considered that all the data had to be recorded during transient operating conditions (run-up) of the vehicle. Appropriate order analysis procedures had to be developed for the isolation of the acoustic contribution of the harmonic components from the flow-induced pressure fluctuations. This was essential to obtain the required signal-to-noise ratios for reliable results at representative sweep-rates of the engine (30 r.p.m./sec). The new technology also included the extension of existing linear acoustic code for transient conditions. Although the adaptation was straightforward, the presentation of the relative acoustic performance in order component format proved to be a more useful illustration than is currently used in the literature.

The new contribution to knowledge arising from the application of the new technology in identifying the acoustic behaviour of an exhaust system for the transient operation of a vehicle included the following:

- the identification of the acoustic contribution of each individual element to the overall exhaust system acoustic performance;
- the identification of the acoustic interaction between elements;
- the clear interpretation and identification of system resonances;
- the interpretation of the acoustic interaction between system resonances;
- the spectral modification of the system resonances associated with throttle position.
- the overall acoustic behaviour of the exhaust system is controlled by system resonances;
- the influence of the variable exhaust gas temperature on the spectral distribution of the resonances;
- the identification of flow-induced sources and sinks by means of power flux measurements (according to the author's knowledge such measurements for a running engine have not yet been published in the literature).

All the above results were described by means of order component amplitudes versus engine speed. According to the author's knowledge this representation of the data for a running engine has not yet been published in the literature.

Application of the new technology also demonstrated the following advantages compared to existing methods:

- The new measurement technology provided a much faster method for the evaluation of the relative acoustic performance of an exhaust system, compared to the impedance tube technique method and to the wave decomposition method for constant engine speed conditions. Reliable results may be obtained with the new measurement technology in less than three minutes, depending on the required sweep rate of the engine.

- Tail-pipe orifice noise emission measurements are extensively used in the automotive industry for the evaluation of the acoustic performance of the exhaust system. Although it is possible to measure the order components rapidly, the resultant assessment is restricted to the overall acoustic performance of the exhaust system. This spectral data is insufficient to guide the appropriate geometric modification to the individual elements of the exhaust system required for rapid acoustic optimisation. Consequently, the optimisation process with this data is based on a systematic trial and error approach [7.1]. By contrast, the new technology presented in this thesis enables the identification and interpretation of the contribution to the acoustic behaviour by each individual element of an exhaust system, as outlined on page 193, which then facilitates rapid acoustic optimisation.

- Another practical application of the new prediction technology is the potential for manipulation of the order content of the exhaust noise signature to produce, for example, a more 'sporty' sound. [7.1, 7.2]. This can be accomplished by means of a sequence of geometric changes to the exhaust system for a simulated run-up of the engine. Attenuation or power flux predictions for the lower order components and sub-order components can be assessed to guide the geometric changes needed to obtain the required harmonic filtering characteristics. These predictions can be performed in less than a minute for each geometric change.

Other potential applications of the new technology are described in Section 7.3.

7.3 FUTURE APPLICATIONS OF THE WORK

Hybrid predictions and experimental validation results [2.10, 2,11, 2.12] are currently performed at a constant engine speed. For design purposes, a comprehensive record of the exhaust noise signature for the speed range of the vehicle is required. A realistic assessment should include the practical operating conditions of the vehicle in the form of a run-up and run-down of the engine. The hybrid method offers a considerable reduction in computation time, compared to calculations made in real time. Therefore it is foreseen that it will be possible to perform predictions throughout the speed range of the engine with acceptably short computation times. The experimental procedure presented in this thesis could serve as a basis for establishing a measurement technique to validate hybrid prediction code for transient operating conditions.

The increase in exhaust gas flow velocities due to the continuous improvement in engine performance enhances the generation of flow-induced or aerodynamic noise at contractions and expansions and other discontinuities inside the exhaust system. This implies that there is an urgent need for research to obtain a better understanding of the aeroacoustics associated with exhaust systems. As a starting point, the power flux measurement procedure described in this thesis may be applied to identify flow-induced noise sources and sinks (Appendix 5.1).

The main application of the work in this thesis is related to the rational exhaust design strategy set out in Figure 3.1. The transient measurement technique and software provide new advanced technology to facilitate the rapid acoustic assessment and refinement of exhaust systems. These design tools may be applied to evaluate the acoustic performance of the exhaust system during engine acceleration. This is the standard test procedure in the automotive industry. To the author's knowledge, the

acoustic assessment of an exhaust system under transient conditions was not previously possible. As a first step, acoustic predictions may be performed in conjunction with tail-pipe orifice noise emission measurements, as set out in Chapter 6, to evaluate a baseline exhaust system, taking into account specific requirements in terms of available space, layout and back pressure specifications. This may be followed by a systematic tuning of the component geometry to refine the acoustic performance of the exhaust system. The study (Chapter 6) has demonstrated that calculations for a run-up can be performed with the newly developed software in less than a minute on a desk-top computer. When adequate acoustic models are not available for more complicated silencer elements or systems, the new experimental order tracking procedure (as described in Chapter 4 and 5) may be applied to identify component resonances by direct measurement on the vehicle. It has been demonstrated that data may be captured in two to three minutes in real time for practical engine sweep-rates. Alternatively, the fixed sampling rate method described in Chapter 4 may be applied to identify the basic acoustic performance of silencer elements or systems on a bench test that can be re-scaled by appropriate non-dimensional adjustment to temperature and flow.

The acoustic optimisation of the exhaust system described in Chapter 6 was based on the clear interpretation and identification of the individual contribution of each element to the overall acoustic performance. The prediction and measurement techniques described in this thesis may be applied in conjunction with existing or new design optimisation methods for rapid results. However this subject falls outside the scope of this thesis and is recommended for future research.

It is anticipated that the positive linear acoustic predictive results obtained for simulated engine acceleration conditions (at least for the simple exhaust systems examined in this thesis) will serve as an incentive for continued research to improve linear acoustic modelling of more complicated silencer components such as elliptical multi path triflow silencers.

REFERENCES

1.1 D.C. van der Walt
Journal of Sound and Vibration 243 (5), 797-821 (2001)
Measurement technique to assess the acoustic properties of a silencer component for transient engine conditions

1.2 P.O.A.L. Davies
Journal of Sound and Vibration 190 (4), 677-712 (1996)
Piston engine intake and exhaust system design

1.3 A. Onorati
SAE paper 951755 (1997)
Numerical simulation of exhaust flows and tail-pipe noise of a small single cylinder diesel engine

1.4 P.O.A.L. Davies and K.R. Holland
Journal of Sound and Vibration 223 (3), 425-444 (1999)
I.C. engine intake and exhaust noise assessment

1.5 P.O.A.L. Davies and K.R. Holland
Journal of Sound and Vibration, 239 (4), 695-708 (2001)
The observed aeroacoustic behaviour of some flow excited expansion chambers

1.6 R.J. Alfredson
PhD Thesis University of Southampton (1970)
The design and optimisation of exhaust silencers

1.7 R.J. Alfredson and P.O.A.L. Davies
Journal of Sound and Vibration 15, 175-196 (1971)
Performance of exhaust silencer components

1.8 D.D. Davis Jr, G.M. Stokes, D. Moore and G.L. Stevens Jr
NACA 1192 (1954)
Theoretical and experimental investigation of mufflers with comments on engine exhaust muffler design

1.9 J.E. Temple
MSc Dissertation University of Southampton (1980)
An investigation into the source region characteristics of internal combustion engine exhaust systems

1.10 E.A. Yaseen
MSc Dissertation University of Southampton (1982)
Analysis of an exhaust system on a test bed

1.11 K.R. Holland, P.O.A.L. Davies and D.C. van der Walt
ISVR technical report No. 291 (2000)
Sound power flux measurements in strongly excited flow ducts

2.1 R.M. Munt
Journal of Sound and Vibration 142 (3), 413 - 436 (1990)
Acoustic transmission properties of a jet pipe with subsonic jet flow: I. The cold jet reflection coefficient

2.2 H. Levine and J. Schwinger
Physical review 73, 383-486 (1948)
On radiation of sound from an unflanged circular pipe

2.3 M. Bhattacharya
PhD Thesis University of Southampton (1979)
I.C. engine exhaust noise source characteristics – an analysis and evaluation of experimental techniques

2.4 M.G. Prasad and M.J. Crocker
Journal of Sound and Vibration 90 (4), 479-490 (1983)
Acoustical source characterisation studies on a multi-cylinder engine exhaust system

2.5 M.G. Prasad and M.J. Crocker
Journal of Sound and Vibration 90 (4), 491-508 (1983)
Studies of acoustical performance of a multi-cylinder engine exhaust muffler system

2.6 L. Desmonds, J. Hardy and Y. Auregan
Journal of Sound and Vibration 179 (5), 869-878 (1995)
Determination of the acoustical source characteristics of an internal combustion engine by using several calibrated loads

2.7 S.M. Sapsford, V.C.M. Richards, D.R. Amlee, T. Morel and M.T. Chappell
SAE paper 920686 (1992)
Exhaust system evaluation and design by non-linear modelling

2.8 G. Ferrari and A. Onorati
SAE paper 945135 (1994)
Determination of silencer performances and radiated noise spectrum by 1-D gas dynamic modelling

2.9 F. Payri, A.J. Torregrosa and M.D. Chust
Journal of Sound and Vibration 195 (5), 757-773 (1996)
Application of MacCormack schemes to I.C. engine exhaust noise prediction

2.10 P.O.A.L. Davies and M. F. Harrison
Journal of Sound and Vibration 202 (2), 249-274 (1997)
Predictive acoustic modelling applied to the control of intake/exhaust noise of internal combustion engines

2.11 F. Payri, J.M. Desantes and A.J. Torregrosa
Journal of Sound and Vibration 188 (1), 85-110 (1995)
Acoustic boundary condition for unsteady one-dimensional flow calculations

2.12 J.M. Desantes, A.J. Torregrosa and A. Broatch
SAE paper 950545 (1995)
Hybrid linear/non-linear method for exhaust noise predictions

2.13 P.O.A.L. Davies
Journal of Sound and Vibration 124, 91-115 (1988)
Practical flow duct acoustics

2.14 G.D. Gallow and K.S. Peat
IMechE C19/88 (1988)
Insertion loss of engine intake and exhaust silencers

2.15 L.J. Erikcsson and P.T. Thawani
SAE paper 850989 (1985)
Theory and practice in exhaust system design

2.16 P.O.A.L. Davies, M.F. Harrison and H.J. Collins
Journal of Sound and Vibration 200 (2), 195-225 (1997)
Acoustic modelling of multiple path silencers with experimental validation

2.17 J.L. Bento Coelho
PhD Thesis University of Southampton (1983)
Acoustic characteristics of perforate liners in expansion chambers

2.18 L.J. Eriksson
JASA Vol. 68 (2), 545-550 (1980)
Higher order mode effects in circular ducts and expansion chambers

2.19 K.S. Peat
Journal of Sound and Vibration 123 (1), 43-53 (1988)
The transfer matrix of a uniform duct with a linear temperature gradient

2.20 P.O.A.L. Davies
Journal of Sound and Vibration 122 (2), 389-392 (1988)
Plane acoustic wave propagation in hot gas flow

2.21 M.F. Harrison and P.O.A.L. Davies
IMechE C487/019, 183-189 (1994)
Rapid prediction of vehicle intake/exhaust radiated noise

2.22 A. Onorati
Noise Control Engineering Journal 45 (1), 35-51 (1997)
Non-linear fluid dynamic model of reactive silencers involving extended inlet/outlet perforated ducts

2.23 A. Onorati, contribution to D.E. Winterbone and R.J. Pearson
Professional engineering publishing limited, London UK, Chapter 6,
267-340, Numerical simulation of unsteady flows in internal combustion
engine silencers and the prediction of tail-pipe noise (1999)
Design techniques for engine manifolds

2.24 N.S. Dickey, A. Selamet and J.M. Novak
Journal of Sound and Vibration 211 (3), 435-448 (1998)
Multi-pass perforated tube silencers: A computational approach

2.25 D.A Jones, W. K. van Moorhem and R.T. Voland
Noise Control Engineering Journal 26 (2), 74-80 (1986)
Is the full non-linear method necessary for the prediction of radiated engine
exhaust noise

2.26. F. Payri, A.J. Torregrosa and R. Payri
Applied Acoustics 60, 489-504 (2000)
Evaluation through pressure and mass velocity distributions of the linear
acoustic description of I.C. engine exhaust systems

3.1 P.H. Smith and J.C. Morrison
Robert Bentley, Cambridge, Massachusetts, 3rd edition (1971)
Scientific design of exhaust and intake systems

3.2 A. Plimom, P. Bartsch and A. Ennemoser
SAE paper 971443 (1997)
Application of computer simulation in the development process

3.3 D.C. van der Walt
Noise and vibration conference, Pretoria, R.S.A. (1993)
Experimental study and solution of the interior boom noise of a small pick-up truck

3.4 D.C. van der Walt
Noise and vibration conference, Pretoria, R.S.A. (1995)
Standing waves in automotive exhaust systems

3.5 K.S. Peat, G.D. Callow and P.A. Bannister
IMechE C420/021, 119-127 (1990)
Improving the acoustic performance of an intake system

3.6 S.M. Sapford
IMechE C420/036, 113-117 (1990)
Exhaust noise synthesis - an essential component of engine concept design

3.7 R. Stone
Society of automotive engineers, Warrendale (1993)
Introduction to internal combustion engines

3.8 M.L. Munjal
John Wiley and Sons, New York (1987)
Acoustics of ducts and mufflers

3.9 P.O.A.L. Davies
Journal of Sound and Vibration 190 (3), 345-362 (1996)
Aeroacoustics and time varying systems

3.10 M. Nakano
Inter-noise 91, Sydney, Australia, 545-548 (1991)
Self-sustained flow oscillations in a silencer with a single expansion chamber

3.11 N. Kojima and B. Z. Liu
Inter-noise 94, Yokohama, Japan, 1623-1627 (1994)
A study on the interaction between acoustic resonance and turbulence in mufflers

3.12 P.O.A.L. Davies
Journal of Sound and Vibration 77 (2), 191-209 (1981)
Flow-acoustic coupling in ducts

3.13 P.O.A.L. Davies, K.R. Holland and D.C. van der Walt
Noise and vibration seminar, S682, IMechE HQ, 39-50 (1999)
Sound power flux measurements in exhaust systems

3.14 L. L. Beranek
McGraw Hill, USA (1988)
Noise and vibration control

3.15 W.W. Seto
McGraw Hill USA (1971)
Acoustics

3.16 P. Steenackers
Bosal International Belgium
Discussion on the capability of acoustic prediction software

4.1 K.R. Holland and P.O.A.L. Davies
Journal of Sound and Vibration 230 (4), 915-932 (2000)
The measurement of sound power flux in flow ducts

4.2 S. Gade, H. Herlufsen, H. Konstantin-Hansen and H. Vold
Brüel & Kjaer Technical review No 2 (1995)
Characteristics of the Vold-Kalman order tracking filter

4.3 D.K. Bandhopadhyay and D. Griffiths
SAE paper 951273 (1996)
Methods for analysing order spectra

4.4 N. Thrane
Brüel & Kjaer Technical Review No 1 (1997)
Discrete Fourier Transform and FFT analysers

4.5 N. Thrane
Brüel & Kjaer Technical Review No 2 (1980)
Zoom FFT

4.6 R.B. Randall
K. Larsen & Son, 3rd edition (1987)
Frequency analysis

4.7 S. Gade and H. Herlufsen
Brüel & Kjaer Technical Review No 4 (1987)
Windows to FFT analysis (Part 2)

4.8 S. Gade and H. Herlufsen
Brüel & Kjaer Technical Review No 4 (1987)
Windows to FFT analysis (Part 1)

4.9 Brüel & Kjaer
User Manual
Technical documentation PULSE, Multi-analyzer system, Type 3560

4.10 H. Herlufsen
Brüel & Kjaer application notes 021 (1981)
Order analysis using zoom FFT

4.11 S. Gade, H. Herlufsen, H. Konstantin-Hansen and N.J. Wismer
Brüel & Kjaer Technical review No 2 (1995)
Order tracking analysis

4.12 S. Gade
Brüel & Kjaer lecture notes, BA 7606-15
Order analysis

4.13 H. Herlufsen
Brüel & Kjaer, Denmark
Discussion on order tracking

4.14 Arranged by Y.R. Mayhew and G.F.C. Rodgers
Oxford, Blackwell and Matt, 2nd edition (1972)
Thermodynamics and transport properties of fluids

4.15 M.D. Greenberg
Prentice-Hall (1988)
Advanced engineering mathematics

4.16 P.O.A.L. Davies
Journal of Sound and Vibration 72 (4), 539-542 (1980)
Measurement of plane wave acoustic fields in flow ducts

4.17 C.J. Young and M.J. Crocker
JASA Vol. 60 (5), 1111-1118 (1976)
Acoustic analysis, testing, and design of flow-reversing muffler chambers

4.18 F.D. Denia, J. Albelda and F.J. Fuenmayor
Journal of Sound and Vibration 241 (3), 401-421 (2001)
Acoustic behaviour of elliptical chamber mufflers

4.19 P.O.A.L. Davies
Journal of Sound and Vibration 151 (2), 333-338 (1991)
Transmission matrix representation of exhaust system acoustic characteristics

5.1 P.O.A.L. Davies, K.R. Holland and D.C. van der Walt
Submitted to JASA (2002)
Sound power flux measurements in ducts with flow

5.2 P.O.A.L. Davies, K.R. Holland and D.C. van der Walt
17th ICA, Rome, 2-8 September (2001)
Measurement and control of flow generated noise

6.1 P.O.A.L. Davies, K.R. Holland and D.C. van der Walt
European conference on vehicle noise and vibration at IMechE HQ, 11-12 June, C605/024/2002, 193-204 (2002)
The experimental assessment of flow generated noise emissions from intake and exhaust systems

6.2 E.A.A. Yaseen and P.O.A.L. Davies
Journal of Sound and Vibration 124 (3), 586-590 (1988)
Finite interfering waves in continuously excited pipes

7.1 S. Naylor and R. Willats
Proceeding of the IMechE conference, C577/002/2000, 369-377 (2000)
The development of a 'sport' tail pipe noise with the predictions of its effect on interior vehicle sound quality

7.2 A. Jackson and I. Arbuckle
Proceeding of the IMechE conference, C605/006/2002, 95-107 (2002)
Exhaust system optimization for drive by noise